PET Film Artificial Weathering: The Action of Degradation Agents on Bulk and Surface Properties

by

DAVID THOMAS BELL

A Thesis submitted to the University of Birmingham for the degree of DOCTOR OF ENGINEERING

School of Chemical Engineering
College of Engineering and Physical Sciences
University of Birmingham
September 2015

ABSTRACT

Polyethylene terephthalate (PET) films can be advantageously utilised to replace both glass and metal in photovoltaic (PV) devices. However, there remain aspects of their performance in outdoor applications which may be improved upon to meet PV device requirements more efficiently. DuPont Teijin Films (DTF) employ artificial weathering techniques to investigate PET film degradation processes, such as UV degradation and hydrolysis, which occur during the outdoor application of PET films.

In this Thesis, a thorough investigation into the modification of PET film properties with exposure to various artificial weathering techniques has been conducted. Techniques including infra-red spectroscopy, gel permeation chromatography, atomic force microscopy and nano-indentation have been employed to improve the understanding of the effects of artificial weathering on PET films. The effects of exposure to high intensity simulated solar radiation have also been investigated and compared with those of the combined degradation agents present during ISO standard accelerated environmental weathering. Surface modifications have been compared with those of the bulk, in particular, surface roughening and microcracking have been investigated in much greater detail than previously in the literature. Finally, the stabilising effects of including an organic ultraviolet absorber on weathered PET film bulk and surface properties have also been assessed.

ACKNOWLEDGEMENTS

In writing this Thesis I have received invaluable input from many people, without whom, it would surely not be present in its current form today. As such, I would like to acknowledge those people here.

Thanks first to my academic supervisors Richard Greenwood and Jon Preece, and my industrial supervisors Karl Rakos and Mark Hodgson, for believing in me at the beginning, and for helping me make it to the end.

Thanks to Paul Marsh of Intertek MSG, Steve Holding of Smithers RAPRA, Niklas Nordgren of SP Technical Research Institute of Sweden, and James Bowen of the University of Birmingham, for conducting the specialist analysis projects which helped to bring aspects of the research presented in this Thesis to the leading edge of analytical science.

Thanks to my family and friends who have been there for me before, during, and continue to be after the EngD, and have helped to keep me on the path to completion, whether they realised it or not. Thanks also to all those not mentioned who I met over the course of the EngD, without whom, the EngD experience would have been a far lesser version of the great experience it turned out to be.

And a final, special thanks must go to my fiancée Louise, who has done more for me in the time that I've known her, than I can ever hope to thank her for in so few words. This Thesis represents the sum of much of my efforts over the last four years, but the more valuable thing I attained in that time is the story which she and I are still writing together.

TABLE OF CONTENTS

LISTS OF FIGURES, TABLES AND EQUATIONS

List of Figures

List of Tables

List of Equations

LIST OF ACRONYMS

AFM	Atomic Force Microscope/Microscopy
ATR	Attenuated Total Reflection
$BaSO_4$	Barium Sulphate
DHO	Damp Heat Oven
DLO	Diffusion Limited Oxidation
DMA	Dynamic Mechanical Analysis
DSC	Differential Scanning Calorimetry
DTF	DuPont Teijin Films UK Ltd
EDX	Elemental Dispersive X-ray (spectroscopy)
EngD	Doctor of engineering/Engineering doctorate
eV	Electron Volts
FOV	Field Of View
FTIR	Fourier Transform Infra-Red (Spectroscopy)
GPa	Gigapascal
GPC	Gel Permeation Chromatography
GU	Gloss Units
GW	GigaWatt
HFIP	Hexafluoroisopropanol
HISS	High Intensity Solar Simulator
ICI	Imperial Chemical Industries PLC
IR	Infra-red
IIT	Instrumented (nano-) Indentation
LDPE	Low Density Polyethylene

mm	Millimetre
MEG	Mono Ethylene Glycol
MLF	Multi Layered Film
MWD	Molecular Weight Distribution
nm	Nanometre
OTR	Oxygen Transmission Rate
PBT	Polybutylene Terephthalate
PC	Polycarbonate
PE	Polyethylene
PEBE	1,4-Bis(2-(3,4-ethylenedioxy)thienyl)benzene
PECT	poly(ethylene-co-1,4-cyclohexanedimethylene terephthalate)
PEN	Polyethylene Naphthalate
PET	Polyethylene Terephthalate
PFQNM	Peak-Force Quantitative Nano-Mechanical (mode/analysis)
PHBV	Poly(3-hydroxybutyrate-co-3-hydroxyalverate)
PMMA	Poly(methyl methacrylate)
PP	Polypropylene
ppm	Parts Per Million
PS	Polystyrene
PSA	Pressure Sensitive Adhesive
PSI	Phase Shifting Interferometry
PTFE	Poly(tetrafluoroethylene)
PV	Photovoltaic
PVME	Poly(vinyl methyl ether)

PVC	Polyvinyl Chloride
Ra	Average Roughness
RH	Relative Humidity
Rq	Root Mean Squared Roughness
RST	Relative Spectral Transmittance
Rz	Maximum Roughness
SBR	Styrene Butadiene Rubber
SEM	Scanning Electron Microscope/Microscopy
SPM	Scanning Probe Microscope/Microscopy
TA	Terephthalic Acid
TiO_2	Titanium Dioxide
T_g	Glass Transition Temperature
TLT	Total Luminous Transmittance
TM-AFM	Tapping Mode Atomic Force Microscopy
UV	Ultraviolet (radiation)
UVA	Ultraviolet Absorber
UV-Vis	Ultraviolet-Visible (spectroscopy)
VSI	Vertical Scanning Interferometry
WCA	Water Contact Angle
WLI	White Light Interferometer/Interferometry
WOM	Weather-o-meter
WVTR	Water Vapour Transmission Rate
µm	Micrometre

INTRODUCTION

1.1 Project background

In recent years, there has been increasing pressure put upon Governments and industries to improve their green credentials by increasing the proportion of energy they utilise from renewable sources, such as wind, hydro-electric and solar power. Such action is one means for Governments to better meet ever more stringent international criteria for global fossil fuel emission reductions.

In order to stimulate the growth of renewable energy industries and allow them to compete with the already well established fossil fuel energy industries, Government green subsidies called feed-in tariffs have been widely implemented, which effectively pay suppliers relatively higher rates for energy generated from renewable sources. This has allowed many renewable energy industries to develop with sustainable growth, which in turn has provided increasing global demand for the raw materials used to produce renewable technologies, such as photovoltaic (PV) modules (Prismark, 2014).

As part of the progression PV technology, devices are evolving to become thinner, lighter, flexible, portable, more robust and producible by high throughput manufacturing methods (roll-to-roll) (Brabec, 2004). Many of these improvements can be imparted to PV devices by utilising polymer films, such as polyethylene terephthalate (PET), instead of more traditional metal and glass as substrate and encapsulation materials (Spanggaard and Krebs, 2004, Jorgensen *et al*., 2006). A simplified PV module schematic is shown in Fig. 1.1, which highlights the various PV device layers potentially substitutable by PET films.

Figure 1.1: Simplified schematic layout of a PV module

The drive for ever more advanced PV devices presents an excellent opportunity for polymer film manufacturers such as the sponsoring company DuPont Teijin Films (DTF). DTF are a global polyester films business producing PET and polyethylene naphthalate (PEN) films for a variety of markets including capacitors, flexible electronics, specialist packaging as well as the PV market. In 2012 DTF had a global volume of approximately 250,000 tonnes of polyester films, with sales yielding a global turnover of approximately $1.5 billion (2013). In 2014 it is estimated that 49 GigaWatts (GW) of PV modules were produced globally (Prismark, 2014). This represents a potential market for approximately 83,000 tonnes of differentiated PET films as module backsheet materials alone (Peevor, 2015). Further, PV module supply, the number of modules being produced globally per year, is predicted to increase by 10-15 % year-on-year, making the PV market an increasingly attractive market space for differentiated film producers like DTF.

However, substituting glass and metal with polymer films is not without drawbacks, in particular, worse O_2/moisture barrier performance and long term environmental stability (Kempe, 2006, Andrady, 2007, Grossiord *et al*., 2012, Gardette *et al*., 2014). These are often critical performance properties of devices intended for use in hot and humid environments, where PV devices usually perform best. Hence, to increase the

uptake of polymer films by PV device manufacturers and allow the technology to continue to progress, a great deal of research and development (R&D) is being performed by polymer film producers such as DTF, which allows them to better understand and mitigate these drawbacks, and thus, produce differentiated film products to suit the evolving PV market needs. For example, PET film new product developments for outdoor applications often contain stabilisers, included to protect the films against the effects of degradation agents (Andrady *et al*., 1998, Billingham, 2000, Fechine *et al*., 2004) and thereby extend PET film outdoor service lifetimes in line with the rest of the PV device components - a minimum of 25 years (Celina, 2013). Further innovations in this area will eventually enable the use of PET films as PV module front sheet and substrate materials, allowing for greater market penetration and greater returns on investment spends for DTF and other differentiated film manufacturers.

1.2 Project overview

This Thesis forms one aspect of DTF's R&D efforts, wherein the modification of the performance properties of basic PET films with artificial weathering has been carefully analysed using the latest analytical equipment. These modifications have been related to the degradation processes known to occur during exposure to environmental degradation agents, such as heat, moisture and ultraviolet (UV) radiation. Decades of research suggests that UV radiation is the main agent limiting PET film performance in PV suitable environments (Stephenson *et al*., 1961c, Day and Wiles, 1972a, Edge *et al*., 1991, Fechine *et al*., 2002b, Yadav *et al*., 2011).

To better understand its individual role during environmental exposure, the high intensity solar simulator (HISS) was acquired for the project and incorporated into DTFs weathering facilities. This allowed for UV to be isolated from the other PET environmental degradation agents - heat and moisture - and its effects in isolation compared with those in conjunction with heat and moisture during ISO standard accelerated environmental weathering.

Of particular interest to DTF was the phenomenon of surface microcracking, which occurs after extended sample exposure to UV weathering and represents a significant failure criteria in the outdoor application of PET films (Deblieck *et al*., 2011, Kimball and Munir, 1978). One aim of the project was to utilise DTFs advanced surface metrology facilities to investigate this and other PET degradation phenomena at the film surface, as well as more broadly, to investigate the physical effects of environmental degradation processes on the film surface compared with the film bulk and how this difference in material surroundings affects them.

Finally, the investigation was extended to incorporate a film which included an ultraviolet absorber (UVA) in its film formulation, to assess the impact of the UVA on the modifications being characterised, which can be thought of as the efficacy of UV stabilisation. This Thesis complements new product development work, which forms the majority of DTFs R&D efforts in this field. It provides more fundamental information, which can be utilised when developing and testing experimental films in an empirical manner.

1.3 Thesis Aims

In brief, the aims of this Thesis are as follows:

- To investigate the degradation of PET films caused by prolonged exposure to accelerated UV weathering.
- To comprehensively characterise this degradation in novel ways using techniques including atomic force microscopy (AFM), infra-red spectroscopy and nano-indentation (IIT).
- To develop the limited understanding of the relationship between chemical degradation and surface modification.
- Ultimately, to attempt to use this new knowledge to inform existing techniques for preventing UV degradation from occurring in outdoor applications of PET film.

1.4 Academic impact

The research conducted during this Thesis has developed the understanding of several aspects of the artificial weathering of PET films. It has revealed the effects of isolated high intensity simulated solar radiation on PET film properties, which enabled the comparison of individual and synergistic effects of UV radiation with humidity, heat and direct water contact. It has also shown the stabilising effects of UVAs against PET degradation processes, in particular against photo-crosslinking and surface roughening, which it now appears play more significant roles in macroscopic film modifications than previously thought.

1.5 Commercial impact

DTF R&D efforts are aimed at improving productivity, in order to manufacture films at increasingly competitive prices, and improving differentiated PET film solutions, to better meet dynamic customer requirements. The research conducted during this Thesis has contributed to the latter aspect in several key ways. It has improved the understanding of how PET films respond to various degradation agents and the interplay between said degradation agents during accelerated environmental weathering. It has highlighted the importance of good hygiene during film weather testing, which was previously of little concern to DTF, but has been shown to contribute to reduced test lifetimes. It has improved the understanding of the micro and nanostructures of various DTF PET film grade surfaces, and how surface topography affects micromechanical properties. And finally, by hosting the EngD researcher at their R&D headquarters, DTF have benefited from an in-house AFM custodian able to conduct all AFM measurement requirements which arose over the 4 year duration of the EngD. This has resulted in a large body of surface analysis work, which positively contributed to many different DTF research projects and customer feedback issues.

1.6 Thesis layout

This Thesis consists of 7 Chapters which document the research conducted as part of the EngD in Formulation Engineering with the University of Birmingham and DuPont Teijin Films. Chapter 1 introduces the Thesis and includes background information and the motivations for conducting the research project. Chapter 2 is a review of the literature most relevant to the Thesis, which demonstrates the state-of-

the-art in the characterisation of UV degradation and areas of interest in which further work may be conducted. Chapter 3 describes the materials and methods employed in this Thesis, including the artificial weathering and film characterisation techniques used. Chapter 4 presents the results related to PET film *bulk* modifications due to various artificial weathering methods, while Chapter 5 contains the results related to PET film *surface* modifications. In Chapter 6, the most informative methods utilised in the previous two results Chapters have been applied to a UV stabilised film grade in order to assess the efficacy of the stabiliser in preventing the observed modifications in unstabilised PET film. Finally, Chapter 7 concludes the Thesis and presents suggestions for future work, followed by the appendices and references.

LITERATURE REVIEW

2.1 Introduction

In this Chapter the published scientific literature relevant to this Thesis has been critically reviewed. This includes literature in the field of PET and polyester degradation, but also many papers within the more general subject of polymer degradation and environmental weathering, where a technique or phenomena common in polyester degradation has been identified. Finally, the methodologies within these fields used to study surface degradation, particularly utilising AFM, have also been reviewed. By the end of this Chapter the reader will be familiar with the processes and considerations of polymer accelerated environmental weathering relevant to this Thesis, as well as the development and state-of-the-art in the study of polyester and polymer surface degradation.

2.2 Polyester degradation agents and mechanisms

PET is sensitive to environmental degradation agents, which over time can cause the deterioration of the optical and material performance properties which give PET much of its market value. The most important of these with respect to PV applications are UV radiation and humidity. These are discussed below, along with the degradation reactions that they invoke in polyesters. However, since UV radiation is the degradation agent of greatest interest to this Thesis, only a very brief review of PET hydrolysis is presented.

2.2.1 Ultraviolet radiation

Ultraviolet radiation is light which has wavelength between 10 and 400 nm. In polymer UV degradation studies however, the relevant range of study is more commonly between 100 and 400 nm. Where environmental degradation is of interest, the most relevant range is known as terrestrial UV, with wavelength between 290 and 400 nm, as the Earth's atmosphere prevents light with wavelengths less than 290 nm from reaching its surface (Blumthaler, 1993).

2.2.1.1 Photolysis of polyesters

Research into UV degradation of PET was first published by Osborn (1959) and was of great interest at the time, as unlike many newly discovered polymers of the mid 20^{th} century, PET absorbed UV radiation not due to the presence of impurities (typically carbonyl groups and peroxides), but due to intrinsic aromatic carbonyl ester chromophore groups linked by C=C conjugation. By measurement of 1% solution viscosities, it was calculated that due to exposure to laboratory light sources and the subsequent absorbance of UV wavelengths, the polymer molecular weight (see Appendix 2) of UV exposed PET samples was reduced as a function of exposure time and intensity. A quantum yield (the number of polymer bonds ruptured per photon absorbed) of 5×10^{-4} was calculated, which was then compared with the documented quantum yields of other UV absorbing polymers and shown to be significantly lower, *i.e.* that PET was more UV stable.

Soon after, Stephenson and co-workers investigated the UV irradiation of several plastics, including PET in the form of Mylar® C, a then DuPont grade. In their first paper, Stephenson *et al.* (1961a) demonstrated variable deterioration of the

mechanical properties of the polymers due to exposure to narrow bandwidths of radiation (centred at 244, 314 and 369 nm) from high pressure mercury arc lamps. Samples were exposed in a nitrogen atmosphere and additionally for the shortest waveband under vacuum. It was shown that PET tensile mechanical properties deteriorated faster when samples were exposed to shorter wavelengths, and when exposed in nitrogen rather than under vacuum. This variable degradation due to exposure to different wavebands was likened to the process of random chain scission due to thermal oxidation and hydrolysis, but was explained by introducing the concept of a damage index - the change in mechanical properties per unit irradiance. By extrapolating their data to zero irradiance and plotting against photon energy they concluded that degradation should only occur if samples were exposed to photons with energy approximately greater than or equal to that of a carbon-carbon bond, approximately 3.4 eV.

The second and third papers of the series attempted to develop the understanding of the degradation mechanisms of polymers exposed to UV radiation in vacuum and nitrogen atmosphere (Stephenson *et al*., 1961b, Stephenson *et al*., 1961c). General photolysis reaction pathways were suggested to account for the observed reaction products (low molecular weight material, gels and gases) evolved due to UV exposure. Then in the final publication of the series, Stephenson and Wilcox (1963) introduced polymer UV exposure in an oxygen atmosphere and showed this to be the most detrimental exposure condition to polymer mechanical properties yet. These many contributions were later summarised in an early review of PET degradation agents by Buxbaum (1968), however, the significance of this final result was not fully

appreciated until several years later when Day and Wiles published their highly influential series of papers on the photochemical degradation of PET.

2.2.1.2 Photo-oxidation of polyesters

In their first paper, Day and Wiles (1972a) investigated the variable effects of xenon and carbon arc exposure on PET films due to their differing spectral distributions. Transmission and attenuated total reflection (ATR) Infra-red (IR) spectroscopy was used to monitor the levels of carboxylic acid end groups in the bulk and at the surface, which they proposed were produced in their samples as a result of random chain scissions. To do this, the absorbance band of IR radiation centred at wavenumber 3290 cm^{-1}, assigned to the carboxylic O-H stretching vibration, was measured and normalised using the C-H vibration centred at 2970 cm^{-1}, which is assumed to change negligibly with exposure time due to the extremely large number of these bonds present and hence very strong absorbance, in any PET sample (assignments from Manley and Williams (1969)). The ratio of 3290 cm^{-1}/2970 cm^{-1} was termed the carboxyl index and was considered a normalised measure of the extent of photo-scission in a UV degraded PET sample. By normalising in this way the CI accounts for sample to sample variations in optical density resulting from variable contact between sample and the ATR crystal, but more crucially allows for direct comparisons to be made between ATR and transmission IR measurements (surface and bulk respectively). The CI results obtained indicated differing numbers of chain scissions caused by the two radiation sources, which was attributed to their differing spectral outputs.

Day and Wiles (1972b) then investigated PET film degradation in the presence and absence of oxygen. Crucially, they observed that in non-oxidative conditions photo-yellowing and crosslinking were the most prevalent modifications, whereas in the presence of oxygen, the formation of carboxylic acid end groups and blue-green fluorescing species were most prevalent. They proposed an aromatic radical-radical recombination mechanism to account for the observed photo-crosslinking and a mono-hydroxylation process to account for the blue-green fluorescence. A review of further research regarding aromatic hydroxylation is presented in section 2.2.1.4.

In the third paper of the series Day and Wiles (1972c) proposed further reaction mechanisms to account for all the observed PET photolysis (Norrish type 1) and photo-oxidation products (Norrish type 2), presenting well reasoned explanations for their main observations as well as those of prior PET photo-degradation publications.

The works of Day and Wiles remain to this day arguably the most influential publications in the field of PET photo-degradation and the mechanisms put forward therein form the basis of understanding for the majority of works on the subject thereafter. A short summary of some of the key findings from their work on polymer degradation can be found in a later publication (Wiles, 1973).

More recently, Rivaton (1993a) utilised IR spectroscopy to identify and explain the formation of photolysis products and photo-oxidation products (Rivaton, 1993b) in weathered polybutylene terephthalate (PBT) films, demonstrating that the polyester degrades with UV exposure in a very similar manner to PET, which is reasonable when one considers the minor differences between their molecular structures (2 additional methylene groups per repeat unit in PBT). Again photolysis reactions were proposed to proceed via Norrish type 1 and 2 reactions, however, the photo-oxidation

reactions were proposed to proceed via a hydroperoxide intermediate followed by beta-scission or a cage reaction. These photo-oxidation mechanisms for PBT presented by Rivaton represent the most probable ways in which the photo-oxidation of PET takes place and are presented in Figure 2.1.

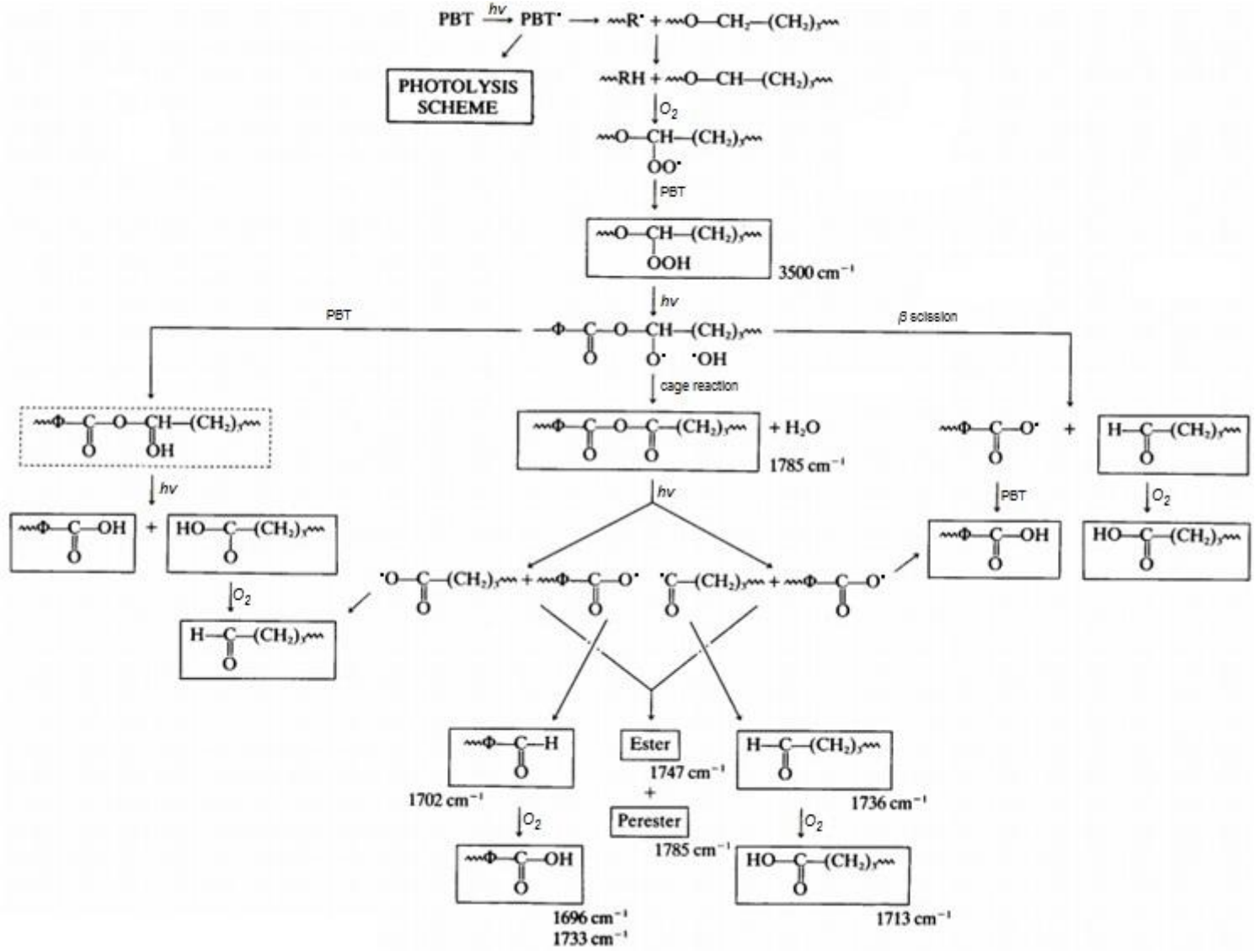

Figure 2.1: Photo-oxidation scheme for PBT (adapted from Rivaton (1993b))

Wang *et al.* (1999) studied the kinetics of PET photo-oxidation and proposed a two-step photo-degradation process to explain the non-linear molecular weight changes that they observed with UV exposure. This comprised an initially quicker degradation step, followed by a slower step for the remainder of their observation period, which they explained by introducing the concept of “weak links”, used previously to explain some thermo-oxidative polymer reaction kinetics (Vink, 1963). These weak links are proposed to be more susceptible to UV degradation, and thus degrade more rapidly, then once they are exhausted the polymer degrades at a reduced rate. This is not the only possible explanation for such non-linear degradation kinetics, diffusion limited oxidation or 2^{nd} order reaction kinetics for example, however no such alternatives were considered by the authors.

Perhaps most notable of the PET UV degradation works of the last decade or so are those of Fechine and co-workers. Their works have focussed mainly upon characterising the UV degradation of PET formulations with and without ultra violet stabilisers, included to inhibit UV degradation processes. This reflects the general shift in the emphasis of many more recent polymer degradation studies to the prevention of degradation and efficacy of stabilisers, important themes within today’s polymer industries. In their first work on this subject Fechine *et al.* (2002a) studied the stabilising effect of a mixture of inorganic additives (TiO_2 and $BaSO_4$), carbon black and the organic ultraviolet absorber (UVA) Tinuvin 1577, and concluded that the UVA was the best stabiliser for use in PET due to the large reduction in carboxyl index observed and coupled with the low impact on other performance properties. They then carried out a more detailed study of the degradation of PET with and without UVAs in the formulation, in which they observed that the inclusion of a UVA

reduced the number of chain scissions taking place (by carboxyl index measurement) and inhibited degradation most for the rear surface due to its UV screening properties (Fechine *et al.*, 2004). Next they utilised the same methodologies to compare the degradation of PET to that of multilayer PET copolymers and found the copolymers to be more sensitive to degradation, suggesting reaction pathways to account for the species observed by FTIR spectroscopy (Fechine *et al.*, 2007). Finally they demonstrated a rapid method of testing UVA efficacy involving the continuous detection of CO_2 produced from films degraded over a few hours in a specifically designed cell (Fechine *et al.*, 2009), pioneered by Fernando *et al.* (2007) two years earlier. Fechine and co-workers found that the presence of UVA markedly reduced the amount of CO_2 being produced under UV irradiation, and thus the amount of degradation taking place.

A complete treatment of the UV stabilisation of polymers is beyond the scope of this review, however there are several excellent reviews on the subject to which the reader is referred for a more complete discussion (Wiles and Carlsson, 1980, Zweifel, 1999, Andrady, 2007).

2.2.1.3 Photo-crosslinking of polyesters

As well as chain scission reactions, it has been proposed in various PET UV degradation studies that during photo-reactions radicalised PET molecules may recombine to form crosslinked networks. Marcotte *et al.* (1967) and Campbell and Turner (1968) detected aromatic radicals using electron spin resonance spectroscopy and thus explained the presence of insoluble gels by proposing crosslinking of the aromatic nuclei of PET due to phenyl hydrogen abstraction

followed by radical-radical recombination. Such insoluble gels have also been detected in the more recent work by Allen *et al.* (2002) with photo-crosslinking again proposed as the mechanism of their formation. Most recently Gardette *et al.* (2014) proposed photo-crosslinking via the mechanism shown in Fig. 2.2, to explain their findings of increased surface hardness and reduced OTR of UV degraded PET, more will be said about this last and other similar studies in section 2.3.4 Surface and heterogeneous modification of polymers.

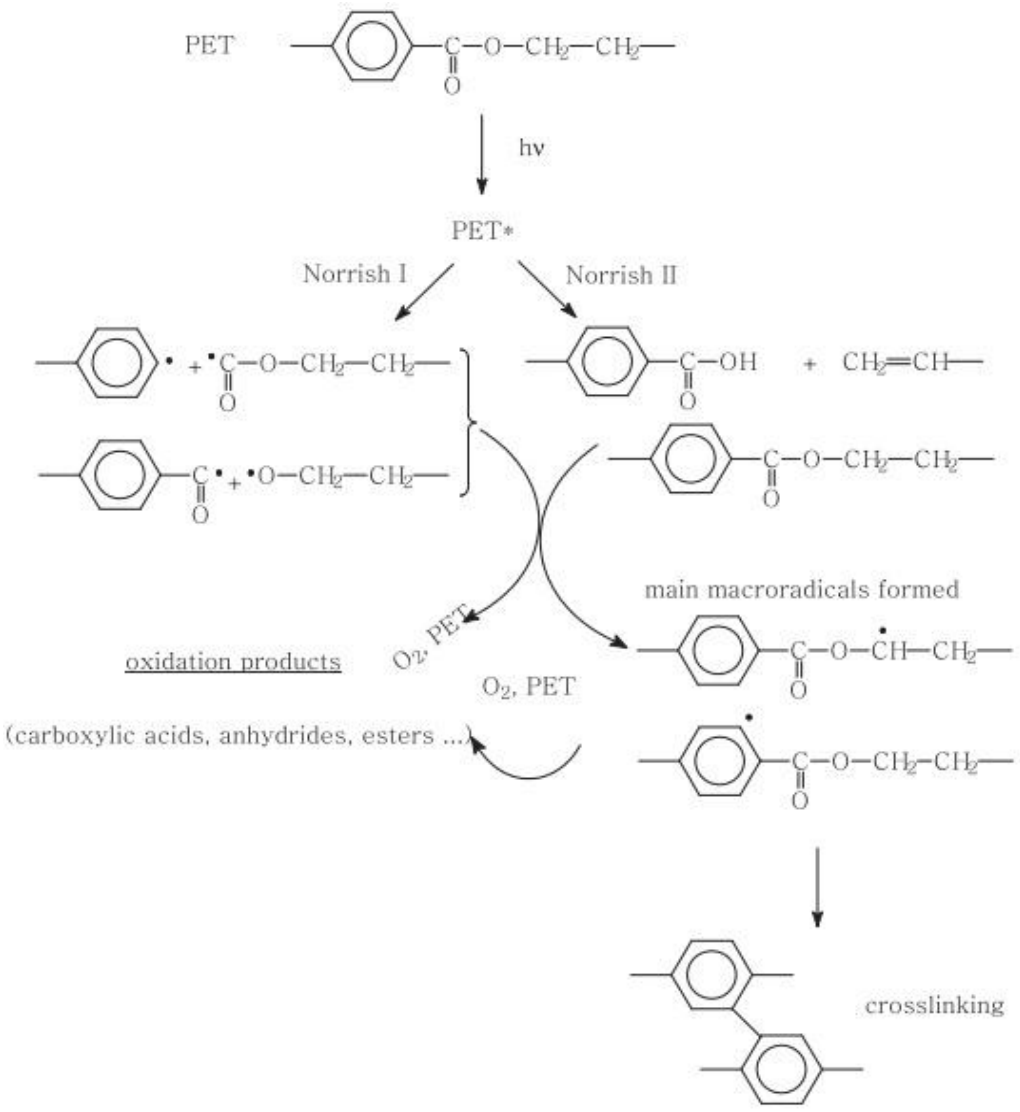

Figure 2.2: PET photo-crosslinking mechanism as proposed by Gardete *et al.* (2014)

2.2.1.4 Hydroxylation of polyester aromatic nuclei

First observed by Pacifici and Straley (1969), the modified photo-luminescence of PET photo-degraded in air was attributed to newly produced hydroxylated aromatic species by observing similarities between the fluorescent emission spectra of photo-degraded PET and those of model compounds containing hydroxylated aromatic species. UV exposure of PET in the presence of oxygen has been shown to promote the growth of a new spectral absorbance peak centred around 330 nm, while in the absence of oxygen it has been shown to promote the growth of a broad shoulder reaching beyond 400 nm (Day and Wiles, 1972b). The growth of the absorbance peak observed after exposure to photo-oxidative conditions has also been explained by production of hydroxylated aromatic species as their fluorescent emission is excited by 340 nm radiation. Fluorescing hydroxylated aromatic species, formed by direct hydroxylation or via a hydroperoxy intermediate, are also proposed to be responsible for the photo-yellowing of PBT (Tabankia and Gardette, 1986, Rivaton, 1993b), block copoly(ether-ester) elastomers (PEBE) (Tabankia and Gardette, 1987) and the PET copolymer poly(ethylene-co-1,4-cyclohexanedimethylene terephthalate) (PECT) (Allen *et al.*, 2000, Grossetête *et al.*, 2000). Polymer yellowing will be discussed in more detail in section 2.3.1.

2.2.2 Humidity

As PET is produced in a condensation reaction, it is sensitive to water, which is present in the atmosphere at varying levels, depending upon the air temperature and the availability of water. At elevated temperatures and humidities PET is increasingly susceptible to hydrolysis.

2.2.2.1 PET hydrolysis

PET hydrolysis is known to occur at the ester linkages in a reaction between the linkage and a water molecule which reduces the molecular weight of the polymer molecule. McMahon (1959) first investigated the effects of heat and water on PET, showing PET to among the most resistant organic polymers of the time to hydrolysis. However, hydrolysis itself was shown to proceed at a faster rate than thermal and oxidative reactions suggesting it may still be a significant concern for PET film outdoor applications. PET hydrolysis was shown to be associated with a loss of mechanical properties and its rate to be independent of small variations in pH.

Much more recently, Picket and Coyle (2013) showed PET hydrolysis to be a second order reaction, proposing that a second water molecule is required to catalyse the hydrolysis reaction. Donelli *et al.* (2010) investigated PET hydrolysis at the film surface, demonstrating that water contact angle and surface crystallinity could be modified by hydrolysis, in addition to polymer molecular weight.

2.3 Characteristic effects of polyester degradation agents

It is helpful at this point to shift the focus of this review to the various characteristic physical observations made of PET as a result of exposure to polyester degradation agents, as further research relevant to the project can be most easily categorised in this way. As well as research focussed on the degradation of PET, the findings from research conducted on other polymers, particularly other polyesters such as PBT, are also relevant as many polymers undergo very similar changes to PET when exposed to weathering experiments.

2.3.1 Polymer yellowing

Yellowing is a very important consequence of environmental exposure for engineering polymers as colour change (or a lack thereof) can be critical to the long term success of an application. In many polyester degradation studies, yellowing has been characterised by monitoring changes to spectral absorbance or transmittance. Increased absorbance (decreased transmittance) in the 310-500 nm range, characteristic of yellowing, can occur as a result of several different factors. The hydroxylated aromatic species formed upon degradation, absorb in this range and therefore contribute to the yellowing of polyesters (Tabankia and Gardette, 1987). Further evidence for this has been presented in a study of the thermal yellowing of PET, where good agreement was found between the spectral fluorescence of model compounds containing mono- and di-hydroxylated aromatic species and those of thermally oxidised PET (Edge *et al.*, 1995). In this case however, quinone and dimer species were proposed to contribute more greatly to the yellowness of degraded samples, which are unlikely to be of relevance to this work, as these samples were generated by exposure to temperatures exceeding 280 degrees C, well above what would commonly be experienced by polyester films during their service life. A more recent study also investigated the effect of titanium vs. antimony based production catalysts on the degree of yellowing (due to hydroxylation) of thermally oxidised PET, found that film synthesised using titanium based catalysts suffered greater yellowing than film synthesised using antimony (Yang *et al.*, 2010).

2.3.2 Morphological modifications

There have been several publications in the field of PET degradation where the role of polymer morphology in degradation has been investigated. Typically, oriented PET has a semi-crystalline morphology, meaning that it is composed of crystalline and amorphous phases, in varying proportions (Dinelli *et al*., 2000, MacDonald, 2002). This semi-crystalline morphology affects many of PETs physical properties and thus, variation in these proportions can affect the ability of PET to perform well throughout its service lifetime.

An initially lower level of crystallinity has been associated with greater levels of hydrolytic and thermal degradation (Edge *et al.*, 1991). This finding was explained by considering that oxygen and water permeability are inversely proportional to polymer crystallinity and thus, degradation should occur to a greater extent in samples of lower crystallinity where there should be a greater permeability to and hence availability of oxygen and water to react with the polymer.

Several groups have also shown that degradation agents can cause an increase in polyester crystallinity to occur. Termed chemi-crystallisation, this process is proposed to occur due to the scission of tie molecules in the inter-phase region. This is thought to generate molecular fragments which can then associate with the crystalline phase, thus increasing the crystal size and crystalline proportion of the sample. Chemi-crystallisation of PET has thought to have been observed in samples exposed to hydrolytic conditions (Ballara and Verdu, 1989, Sammon *et al.*, 2000), samples hydrolysed by alkali and cutinase (Donelli *et al.*, 2010) and samples exposed to accelerated environmental weathering (Fechine *et al.*, 2002b). Chemi-crystallisation of PET was initially thought to be a process which should only be able to occur with

degradation above the glass transition temperature (T_g), however the plasticising effect of moisture has been proposed to explain the ability of molecules to rearrange below T_g (Allen *et al.*, 1991).

2.3.3 Modification of polymer bulk mechanical properties

Since mechanical properties are often critical to polymer performance it is unsurprising that their evolution with degradation has been studied extensively over the years. The predominant method for evaluating the mechanical properties of polymer films in degradation studies is by destructive tensile testing, usually conforming to the ASTM standard test method D882-12 (2012b) which acts to ensure that observed differences between obtained and previous results are not due to unwanted tensile test method variance. Some studies utilise bend tests which can vary by which direction the bend is made in (towards or away from the exposed surface in UV studies), or how it is carried out (by hand or in a test machine). Table 2.1 lists several polymer degradation studies which have included mechanical testing in their degradation analysis. Mechanically tested polymers will generally exhibit either ductile or brittle failure, depending on a number of factors, including but not limited to: molecular weight properties, crystalline structure, T_g, crosslink density and presence of microcracks. The transition point between ductile and brittle failure is a common failure criteria for weather tested materials.

Table 2.1: Polymer degradation studies including bulk mechanical testing

Material	Degradation agent	Paper(s)
PET	UVB/C radiation	(Stephenson *et al*., 1961c, Day and Wiles, 1972b)
PE, PP	Acc. weathering	(Raab *et al*., 1982)
PET, PEN	Heat and humidity	(Edge *et al*., 1994)
LDPE	Acc. weathering	(Liu *et al*., 1995)
PP	Acc. Weathering	(Schoolenberg and Meijer, 1991)

Of far greater relevance to this Thesis is surface mechanical property modification, which has been investigated by various authors and is discussed in the next section.

2.3.4 Surface and heterogeneous modification of polymers

Surface modification is a commonly investigated phenomenon in polymer degradation studies for several reasons. Firstly, the surface differs from the bulk material as it forms the interface between the material and the degradation agents to which it is being exposed. This makes it a logical place to investigate for characteristic effects of degradation and also where possible, to then compare these surface effects with bulk observations which can often help to explain interesting disparities. Surface properties can also play an important role in determining the performance properties of a material, this is particularly true for products with high a surface area to volume ratio, such as polymer films. The surface is also generally

accessible for investigation without complex sample preparation and a wealth of analytical techniques have been developed to study its many different aspects.

Surface techniques can be defined in terms of their surface sensitivity, effectively how far into the bulk from the surface the technique investigates. Some like attenuated total reflection Fourier transform infra-red spectroscopy (ATR-FTIR) have a surface sensitivity of up to 2 microns (Harrick and du Pré, 1966), while others such as AFM based techniques have surface sensitivities in the nanometre range (Binnig and Quate, 1986). This distinction is very important as it may be that the properties of the top few nanometres of a material differ dramatically from the top few microns and yet they may both be considered as “the surface” when interpreting results. The following sections explore the many different aspects of polymer surface degradation, heterogeneity in surface and bulk degradation and the relevant learning gained from its study.

2.3.4.1 Surface microcracking

In early polymer degradation studies the desire to further understand the underlying causes of macroscopic observations of materials in the advanced stages of degradation (such as embrittlement, increased haziness and gloss loss), prompted the introduction of optical and electron microscopy to researcher’s analytical toolkits, allowing them to take a closer look at the resultant effects of chemical degradation.

Microcracking is one such microscopic feature which has macroscopic consequences, and which is commonly observed on highly weathered engineering polymer surfaces. In polymer research it has been characterised with varying amounts of rigour over the years due to the difficult nature of quantitatively

quantifying it. Using SEM prior to mechanical testing, Schoolenberg and Vink (1991) observed that microcracking of UV weathered polypropylene (PP) was related to the embrittlement of the material and that microcrack density was proportional to exposure time, however they made no attempt to quantify this relationship, instead focussing on sample production differences (injection vs. compression moulding) which they reasoned should have affected crack orientation. Wang *et al.* (1998) noted that UV exposure alone was not able to microcrack thin PET films, and went on to suggest that the application of an external force is required to initiate microcracking. By weathering thin films in a multilayered stack they observed more severe embrittlement of the upper layers and thus proposed an A-B model to explain the typical brittle failure behaviour of weathered thicker films in tensile tests. Therein they proposed that microcracks initiated at the degraded surface (A) would propagate under tension into the undegraded material below (B) causing brittle failure to occur earlier than might have been expected for a material degraded primarily at and near the surface.

Microcracking perpendicular to the direction of tensile testing was observed by Nichols and Peters (2002) on UV weathered polycarbonate (PC) surfaces showing that external forces play an important role in microcrack propagation as well as initiation. Zhao and Li (2006) observed on UV weathered PP samples, the appearance of microcracks on the surface, which were finer when the polymer included UVAs. Importantly though they also observed cracks which had propagated in the exposure direction (into the undegraded material) on tensile fractured surfaces, supporting the A-B failure model of Wang and co-workers. Larche *et al.* (2010) showed that microcracking could be initiated on UV degraded crosslinked acrylic

coatings by immersion in hot water (10 degrees < T_g) for 2 hours and that the extent of UV degradation was then reflected in the severity of the cracking (viewed by optical microscopy). Thus they also concluded that stress, due to the absorption and desorption of water, was necessary to initiate microcracking, but that UV exposure caused the increase in crosslink density which primed the sample for failure.

Further general understanding of microcrack nucleation and propagation was provided by Poulingue *et al.* (1999). They studied multilayered oxides deposited on an aluminium substrate polluted with fine diamond particles and subjected these to tension within an SEM. The particles were shown to create stress nucleation points at the surface which affected microcrack growth in the oxide, best illustrated by their own images (see Figure 2.3). To the authors knowledge they have also demonstrated the most comprehensive quantification methods of microcracks within scientific literature relating microcrack density to sample strain. The microcracking of PET due to UV weathering is a subject which has received little attention in academia but is often one failure criteria for DTF when evaluating new product developments.

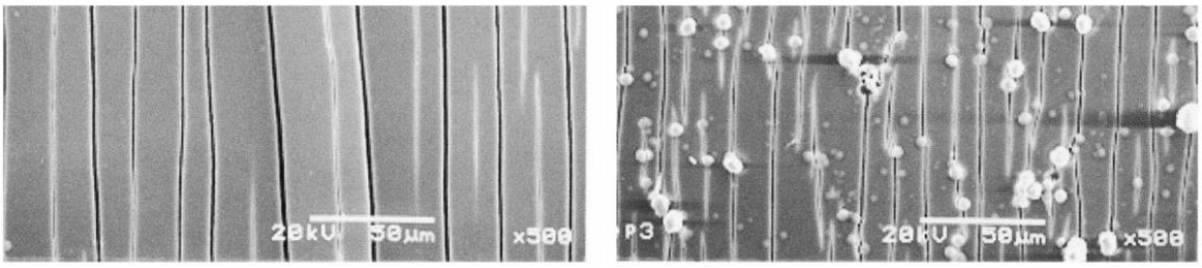

Figure 2.3: Strained sample without particle induced stress points (left) and with (right)

2.3.4.2 Topographic modifications

There are many examples in the literature of researchers including topographic analysis when investigating weathering and degradation. Using SEM, Kimball and Munir (1978) observed differing structures at the fracture surfaces of weathered and unweathered PET samples and related this to the observed change in mechanical failure mode from ductile to brittle. Terselius *et al.* (1982) used SEM to characterise surface features which appeared on the internal surface of high density polyethylene (HDPE) pipes subjected to thermally oxidising conditions, which they proposed were formed due to the biaxial stresses imparted on the sample at production. Edge *et al.* (1991) presented light microscope images of their weathered PET containing samples which helped them to illustrate some of the physical changes occurring due to observed chemical modifications, this link, however, was not well defined.

In more recent years, since its development into a routine research tool, AFM has been utilised (with varying degrees of success) to monitor the evolution of polymer surfaces due to the action of various degradation agents, with many studies attempting to relate observed topographic and chemical modifications. Surface roughening is a commonly observed phenomenon in degradation studies utilising AFM and some prominent examples have been summarised in Table 2.2. Not all of these examples utilise AFM data well however, with some presenting little more than select images which may or may not be representative of the sample surface as a whole.

Table 2.2: Polymer degradation studies utilising AFM to monitor surface roughness

Material	**Degradation agent**	**Paper(s)**
PSA	Alkaline solution	(Shakesheff *et al.*, 1995)
PHBV	Bacterial culture	(Bourban *et al.*, 1998)
PS/PVME blend	Acc. weathering	(Mailhot *et al.*, 2000)
PET	RF Plasma	(Gupta *et al.*, 2000)
Acrylic melamine coating	Simulated solar UV	(VanLandingham *et al.*, 2001)
Polyester resin	Alkaline solution	(Gu *et al.*, 2001)
Polyester/melamine paint	Acc. weathering	(Biggs *et al.*, 2001)
PP	Outdoor exposure (tropical)	(Bedia *et al.*, 2003)
Polyurethane coating	Acc. weathering	(Johnson and Cote, 2003)
PET	UV/O_3 irradiation	(Jang and Jeong, 2006)
Amine-cured epoxy	Outdoor exposure	(Gu *et al.*, 2008)
PET	Oxygen ion beam	(Awasthi *et al.*, 2010)
Acrylic coatings	Acc. weathering	(Osterhold and Glöckner, 2001, Nguyen *et al.*, 2012)

Of the studies summarised in Table 2.2, some have also made interesting observations in addition to surface roughening worthy of further discussion. Mailhot

et al. (2000) observed the generation of new surface peaks, which they proposed to be degraded material that had phase separated and migrated to the surface. Other surface features described as pits and craters have been formed and observed to grow with exposure time in several different polymer degradation studies (VanLandingham *et al.*, 2001, Gu *et al.*, 2001, Biggs *et al.*, 2001, Gu *et al.*, 2008, Nguyen *et al.*, 2012). Such heterogeneous degradation of the surface appears to be relatively common though it is difficult to determine in some cases whether it is due to heterogeneity in the exposed sample (stress concentrations, local flaws, weak points *etc*), or in the exposure conditions (local hot-spots, non-uniform irradiation *etc*). Physical dimensions and frequency of occurrence are the parameters usually used to quantify such features, though comparison between studies is often difficult due to differences between the materials or exposure conditions used and the non-standard methods of characterisation.

Gu *et al.* (2008) showed that the roughening of weathered epoxy coatings Captured by AFM correlated to a certain extent with the gloss loss measured at 60 degrees (R^2 = 0.82), though the correlation was shown to be better with larger laser scanning confocal microscopy image based roughness measurements (R^2 = 0.93), likely due to the larger area sampled. A concise review of the development of the understanding of this general relationship is presented in the excellent review paper by Assender *et al.* (2002) which concludes that feature size relative to the wavelength of light correlates better with surface gloss than the more general roughness parameters.

2.3.4.3 Physical property modification at the surface

In addition to topography analysis, AFM can also be used to probe the mechanical properties of degraded polymer surfaces. In one of the earliest studies of its kind by Gu *et al.* (2001), force curve analysis revealed the differing surface mechanical response inside of a degraded pit feature on a degraded polyester surface, from that of the apparently undegraded remainder. A more sophisticated analysis of such force ramps and the impressions left behind by their application is known as AFM-nanoindentation. In recent polymer degradation studies, this technique has been applied mainly to crosslinked polymers and coatings - such as PVK (Bussière *et al.*, 2012), PR (Larché *et al.*, 2012), TMPC (Berthumeyrie *et al.*, 2013, Mailhot *et al.*, 2004) and most recently celluloid (Bussiere *et al.*, 2014) - where observed increases in nano-hardness have been associated with an increased crosslink density caused by UV exposure. To the author's knowledge there are no studies in the literature which have utilised this technique to study UV degraded PET.

Findings obtained by using AFM in this way are supported by other studies which have used instrumented (micro/nano) indentation tools (IIT) that also show increases in surface hardness with degradation (Larché *et al.*, 2010, Larché *et al.*, 2011, Gardette *et al.*, 2014). These findings are in turn supported by earlier observations of increased mechanical stiffness due to degradation made using the more well documented dynamic mechanical analysis (DMA) technique (Bartolomeo *et al.*, 2001, Irigoyen *et al.*, 2001).

The high force sensitivity inherent to AFM (due to the use of silicon micro-cantilevers), along with models of elastic contact enable its use to characterise sample surface mechanical properties non-destructively in the elastic regime as well

as through the analysis of plastic deformations. Robust methodologies based on these principles are still being developed and checked against IIT and DMA for various polymers (Dokukin and Sokolov, 2012, Sokolov *et al*., 2012) but it has been used with success in some few degradation studies. Lubarsky *et al.* (2004) used such methods to measure the decrease in the elastic modulus of PS samples modified by combinations of UV and ozone treatment. And using the recently developed and much more sophisticated peak-force quantitative nano-mechanical (PFQNM) AFM mode, Mertz *et al.* (2012) showed how the elastic modulus of photo-oxidised styrene butadiene rubber (SBR) varied with distance from the exposed surface. There are many other examples of depth of degradation profiles being characterised *i.e.* at varying distance from the exposed surface and this will be reviewed in detail in section 2.3.4.4.

Lastly the hydrophillicity of PET, measured by water contact angle (WCA) has been shown to increase with UV exposure (Osterhold and Glöckner, 2001), which can be explained by the increase in -COOH and -OH end groups produced as a result of UV degradation. This property has also been related to modified surface friction properties of UV degraded samples observed by friction force microscopy (Hurley and Leggett, 2009).

2.3.4.4 Depth profiling polymer degradation

As was eluded to in the previous section there is a large body of research which goes into greater detail than simply analysing surface vs. bulk degradation by examining how and why polymer degradation occurs non-uniformly through the thickness of degraded samples, particularly those degraded by exposure to UV. In the final

publication of Day and Wiles' influential series, this time led by Blais (1973), several depth profiles of PET UV degradation were presented. ATR-FTIR analysis revealed a greater concentration of carboxyl end groups (and therefore chain scissions) present at the front and rear film surfaces, than in the bulk (obtained by Transmission FTIR) and a complete degradation profile measurement was also obtained for degraded fluorescent species which showed similar behaviour. Many studies including this kind of analysis were to follow, Table 2.3 summarises prominent examples which have depth profiled polymer degradation, detailing the material examined, degradation agents and the phenomenon profiled.

Table 2.3: Studies which have included depth profiles of degradation in their analysis

Material	**Degradation agent**	**Technique/phenomenon profiled**	**Paper(s)**
PET	Acc. weathering	Carboxyl end group IR abs. and aromatic hydroxyl fluorescence (Blais *et al.* only)	(Blais *et al.*, 1973, Fechine *et al.*, 2004, Gardette *et al.*, 2014)
LDPE	Radiochemical	Carbonyl IR abs.	(Papet *et al.*, 1987)
PP	Acc. weathering	Carbonyl IR abs.	(Schoolenberg and Vink, 1991)
PBT	Acc. weathering	UV and IR abs.	(Rivaton, 1993a, Casu and Gardette, 1995)
PVC, ABS PP	Acc. weathering	UV and IR abs.	(Gardette, 1995)

PP	UVA/B radiation	Degree of crystallinity by DSC and XRD	(Rabello and White, 1997)
PET	UVA/B radiation	Molecular weight by viscosity	(Wang *et al.*, 1998)
PP/PBT blend	Acc. weathering	IR abs.	(Rivaton *et al.*, 1998)
PET copolymers	Acc. weathering	IR abs.	(Grossetête *et al.*, 2000, Fechine *et al.*, 2007)
PP	Acc. weathering	Micro-thermal analysis	(Grossetete *et al.*, 2002)
TMPC, Epoxy resin, PVK	Acc. weathering	Stiffness by AFM-nanoindentation and IR abs.	(Mailhot *et al.*, 2004, Mailhot *et al.*, 2008, Bussière *et al.*, 2012)
PET	UVC radiation and plasma	IR abs. (trans conformation, carbonyl and carboxyl areas	(Zhu and Kelley, 2005)
SBR	UVA/B radiation	IR abs. and elastic modulus by AFM	(Mertz *et al.*, 2012)
PC	Acc. weathering	IR microspectroscopy and UV abs.	(Collin *et al.*, 2012)

Within the studies listed in Table 2.3 several different methodologies have been employed to depth profile degradation. Some have prepared degraded cross-sections and studied them with high spatial resolution techniques (Nichols and Peters, 2002, Mertz *et al.*, 2012), others have employed a microtome to acquire thin slices parallel to the exposed surface, which have then been analysed (or to allow

the newly exposed surface to be investigated) (Schoolenberg and Vink, 1991, Gardette, 1995), with the process repeated as many times as is necessary to build up a profile. Another method is made possible by the use of very thin films, a stack of such films can be approximated as one continuous thicker film, and once weathered, the layers can be carefully separated and analysed individually to construct degradation depth profiles (Rivaton, 1993a, Wang *et al.*, 1998). Each of these methods has its own advantages and disadvantages and may be the most appropriate for use depending upon the sample and exposure conditions used. The methods involving a microtome require much more rigorous sample preparation and expertise, while the stack method may be considered a poor approximation as water and oxygen may ingress between the layers, which cannot be considered representative of the conditions experienced by a continuous thicker film.

There are two well recognised reasons that UV degradation may occur non-uniformly in polymers. The first reason is due to the absorbance behaviour of UV radiation by materials, for example PET strongly absorbs solar radiation in the 290-310 nm range, which is believed to be the range most detrimental to its properties. According to the Beer-Lambert law these wavelengths are strongly attenuated by the first few microns of the material and thus the degradation is most pronounced in the upper few microns. The second reason which applies beyond just UV degradation is due to changing oxygen availability for oxidative reactions within the material. In most weathering experiments oxygen is freely available at the surface but may be depleted within the material faster than it may diffuse in, a process known as diffusion limited oxidation (DLO). This can create an oxygen depleted zone within the sample inhibiting further oxidation and thus lead to relatively greater degradation near the

surfaces. DLO has been the subject of several reviews and for a much more rigorous examination the reader is referred to the following publications (Audouin *et al.*, 1994, Rivaton *et al.*, 2005, Pospíšil *et al.*, 2006, Celina, 2013). In the case of PET it is likely a combination of these two phenomena which gives rise to non-uniform UV degradation profiles however some studies indicate the effect of DLO to be negligible in comparison with the effect of radiation attenuation (Grossetête *et al*., 2000).

2.4 Chapter conclusions

In this Chapter the development and state-of-the-art in the characterisation of the UV degradation of polymers has been presented. PET environmental degradation mechanisms have been presented and discussed and polymer UV stabilisers have also been briefly discussed. Particular focus was put on the characteristic effects of polymer degradation and the state-of-the-art in polymer surface modification characterisation and depth profiling of modifications has been presented. This will have provided the reader with sufficient context to understand the research themes chosen for further exploration in this Thesis.

MATERIALS AND METHODS

3.1 Chapter introduction

In this Chapter the materials and experimental methods used in this Thesis are described. This includes the structure and material properties of the investigated PET films, the industrial film production process, the various weathering treatments which PET films were exposed to, and finally the techniques and methodologies employed to investigate PET film modification by these treatments.

3.2 DTF biaxially oriented polyethylene terephthalate film

DuPont Teijin Films (DTF) biaxially oriented polyethylene terephthalate (PET) films are formulated engineering polymer films with a broad range of material properties, principally dependent upon the film formulation, but also upon production process variables. First synthesised at Imperial Chemical Industries PLC (ICI) and soon after described in scientific literature by Whinfield (1946), PET is a thermoplastic polymer with chemical formula $(C_{10}H_8O_4)_n$ shown diagrammatically in Figure 3.1.

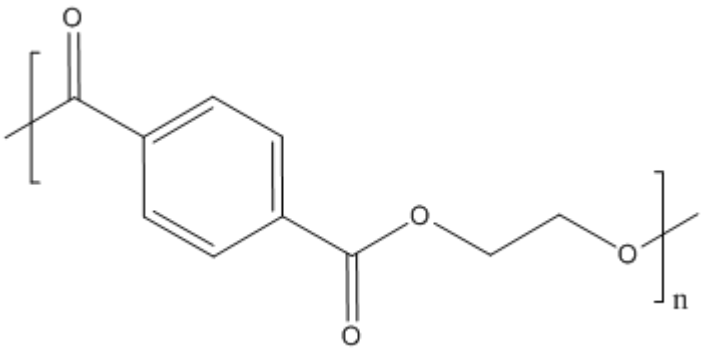

Figure 3.1: PET monomeric repeat unit

Where the ‘n’ represents the number of repeat units of the monomer present in one polymer chain, which usually has a value between one and one hundred, depending upon what is known as the degree of polymerisation of the polymer. Table 3.1 shows a list of typically quoted physical properties and their corresponding values for a nominal DTF PET film of 25 µm thickness.

Table 3.1: PET film properties, taken from MacDonald (2002)

Property	**Value**
Density (ρ)	1400 kg m^{-3}
Glass transition (T_g)	78 °C
Melting point (T_m)	258 °C
Water vapour transmission rate (WVTR)	21.3 g m^{-2} day^{-1}
Oxygen transmission rate (OTR)	55 cm^3 m^{-2} day^{-1}
Surface resistivity	6 x 10^{17} Ohms
Transmittance at 360 nm	82 %

3.2.1 PET formulation

A generic formulation for a batch of PET polymer is described in Table 3.2 which lists the components, their quantities (as a proportion of one batch) and their purpose of inclusion. The PET formulation is by majority mono ethylene glycol (MEG) and terephthalic acid (TA) which polymerise to make PET, but there are also relatively small amounts of other components included to help produce, stabilise and enhance the polymer. Inorganic fillers, such as China clay, TiO_2 and silica micro-particles, are also commonly added to tailor specific performance properties of the final film, such

as colour, gloss and micro-texture. The formulation will be discussed in more detail in the PET production process section.

Table 3.2: Generic PET film formulation

Formulation component	Proportion	Purpose of inclusion
Mono ethylene glycol (MEG)	0.33	Polymer component
Terephthalic acid (TA)	0.66	Polymer component
Campine antimony trioxide	trace	Catalyst to speed up polymerisation
Phosphoric acid	trace	Prevents melt degradation
Sodium hydroxide	trace	Softening point stabiliser

3.2.2 PET production process

There are many stages in the production of PET film products, in between the initial production of the monomer and the winding of the finished film product. A full review of the production process is beyond the scope of this Thesis, however the fundamental elements of PET film production will be described to give the reader an understanding of how the materials utilised in this project were produced and therefore how their material properties were derived. Figure 3.2 shows a diagrammatic version of a PET film production line, in the following sections each separate stage will be described, including the monomer and polymer production processes which take place prior to the filming process.

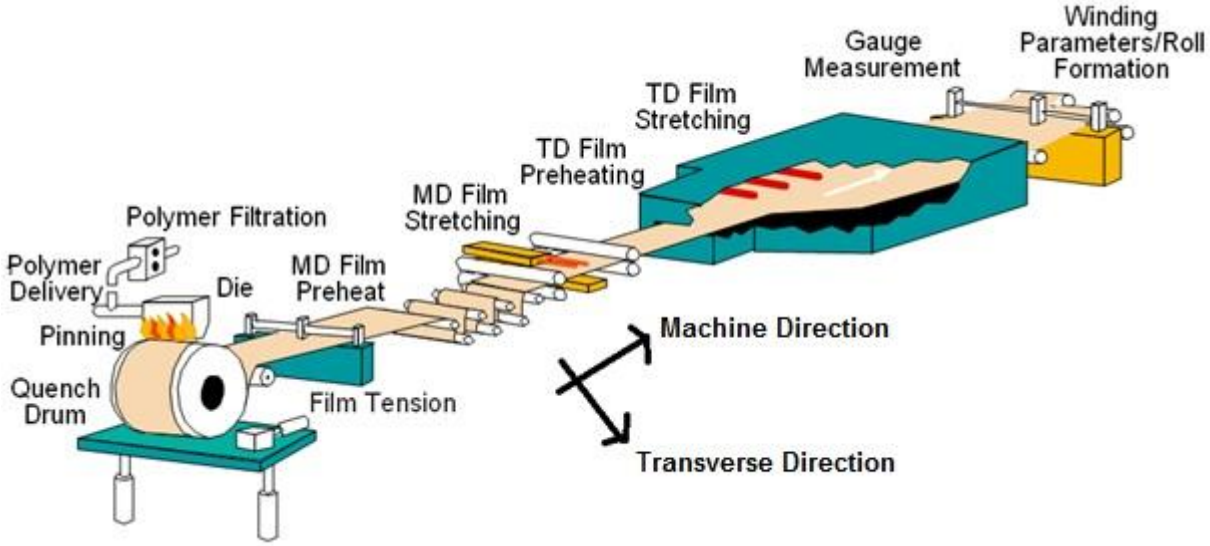

Fig 3.2: Schematic representation of a PET film production line

3.2.2.1 Monomer production

DTF produce PET monomer in a batch process by mixing MEG and TA in a stirred direct esterification vessel at a temperature of 250 - 270 °C and pressure of 270 - 290 kPa (~3 atmospheres). Under these conditions the TA dissolves in the MEG and an esterification reaction takes place to produce the monomer. Water is produced as a by-product which is allowed to boil off along with a relatively small quantity of unreacted MEG. These components are then separated by fractional distillation and the unreacted MEG is returned to the reaction vessel. The reaction is complete when no more water is collected and any excess MEG is then recovered for later use.

3.2.2.2 Polymerisation

The monomer is then transferred to a stirred polymer autoclave where the trace additives are mixed in. A catalyst, typically antimony trioxide is then added to speed up the polymerisation reaction and the mixture is heated to 290 - 300 °C. The pressure is then reduced to < 150 Pa and the polymer gradually forms through trans-esterification, the combination of the monomer units by direct addition. As the degree of polymerisation (number of repeat units per polymer molecule) of the polymer molecules gradually increases, the mixture becomes more viscous and the torque on the agitator increases. This is allowed to continue until the torque on the agitator reaches a predetermined level. The polymerisation reaction is reversible so all MEG and water must be removed to prevent a back reaction occurring. When the polymer has reached the desired viscosity it is extruded through a die in the base of the autoclave to form laces, which are quenched in water and pelletised. The PET, now in the form of small pellets, is then dried and stored, ready to be transported for use at DTF's film production lines.

3.2.2.3 Extrusion

To make PET pellets into film, they must once again be melted and fed into a film production line. This is also done by extrusion and Figure 3.3 illustrates a single screw extrusion system common to many of DTFs film lines. Due to the contained nature of single screw extrusion, PET pellets must first be dried (usually at 140 °C overnight) to remove any water present, which if left can accumulate inside the extruder and hydrolyse the PET melt. The dried PET pellets are forced down a heated barrel by a tapered screw, shearing and heating the polymer increasingly the

further it travels down the barrel. Most of the polymer heating comes from shearing it between screw and barrel (~70 %) rather than from heating the barrel itself.

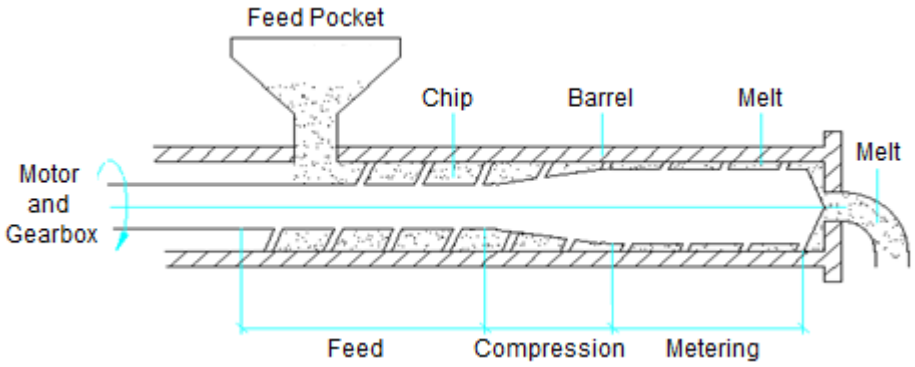

Figure 3.3: Single screw extruder cross section

DTF films may also be extruded using a co-rotating twin screw extrusion system, illustrated in Fig. 3.4, which eliminates the need to dry the polymer as water is allowed to escape by evaporation during extrusion. The twin screw system also allows for recovered PET film flake to be re-processed as it possesses a wider process window, a typical commercial film may consist of approximately 40% recycled PET flake which has been reclaimed from previous runs after edge trimming for example. A typical twin screw system can also enable up to around a 60 % greater feed rate than a single screw system which can allow faster or thicker film production.

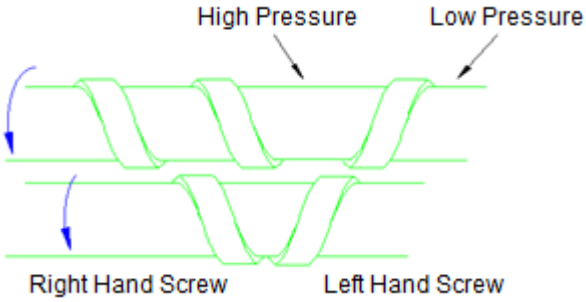

Figure 3.4: Twin screw extrusion

The now molten polymer (290 °C < T < 300 °C) then passes through the filtration section, which removes approximately 99% of any impurities and degrades present, through the melt pipe and the end fed die where it then emerges as a uniformly thick polymer melt curtain. It is then drawn onto a casting drum, which is a slow rotating, water cooled, polished chrome barrel. To ensure complete contact between polymer and drum, and to avoid air being drawn into the interface, the melt is electrostatically pinned to the drum by a high voltage wire or blade. The 15 °C casting drum rapidly cools the polymer to approximately 30 °C, well below its T_g, resulting in an entirely amorphous solid polymer film with a thickness of up to 2 mm. This rapid heat transfer ensures that the film does not crystallise at this stage which can introduce structural defects or increased haziness.

Many DTF films are made by coextrusion which utilises multiple extrusion systems feeding into the same die. These films, known as multi layer films (MLFs) are usually employed for specialised film applications which require complex structures. By bringing together multiple polymer melt flows in the injector block, films can be made with many layers allowing the cross-sectional structure to be tailored. For example a film may have an ABA structure, the A layers being filled and the B layer unfilled thereby enabling the more efficient targeted use of filler per m^2 of film produced and

reducing production costs without affecting performance. Figure 3.5 shows some typical PET MLF structures.

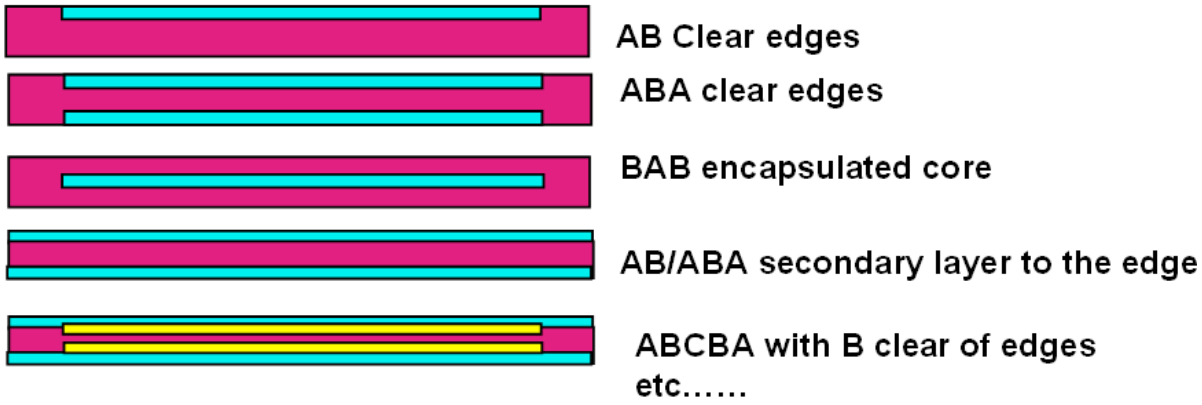

Figure 3.5: Schematic MLF film cross sectional structures

3.2.2.4 Forward draw

After casting the film soon reaches the forward draw area, which comprises of 3 consecutive sections, the heated slow nip rollers, the draw point and the chilled fast nip rollers. The slow nip rollers grip the film and are driven in the machine direction, gently pulling the film from the casting unit. The fast nip rollers are similar but are driven at several times the rate of the slow nip, this difference causes the film to be drawn in the machine direction at the point where it is hottest, the draw point, which may involve heating from infrared heaters to achieve the desired film temperature. The forward draw ratio, the amount the film has been uni-axially oriented, is then the speed of the fast nip rollers divided by the speed of the slow and is typically set to be approximately 3. This process begins to impart some of the excellent mechanical properties commonly associated with PET film. Forward drawing orients some of the polymer molecules in the machine direction, increasing both its elastic modulus and strength in this direction by a factor approximately of three (MacDonald, 2002).

3.2.2.5 Coating

After the forward draw, a coating may be applied to one or both of the films surfaces. Coatings allow for additional properties to be imparted to the film such as improved handling properties, anti-static properties or promotion of ink adhesion. Coated films are usually wet coated by a gravure process illustrated in Figure 3.6. The film is passed over an additional dipped roller which imparts the coating continuously and uniformly.

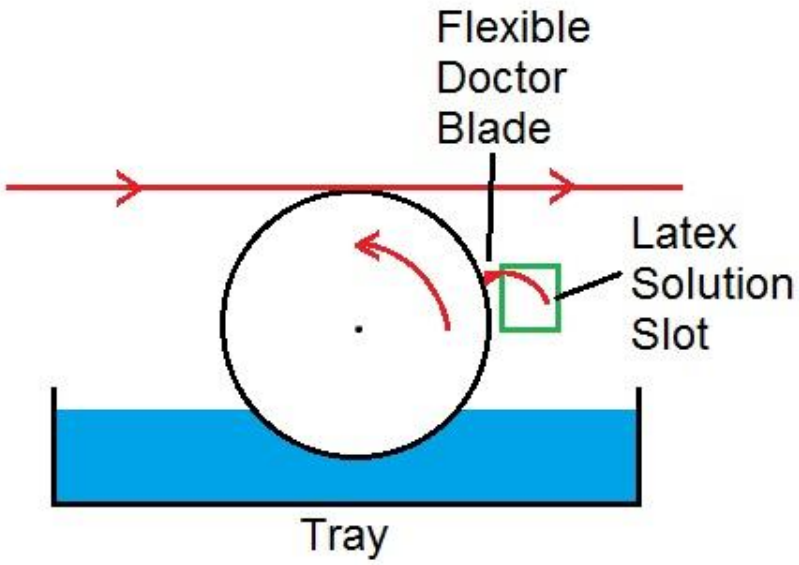

Figure 3.6: Diagram of the coating procedure

The coating of relevance in this Thesis is a multifunctional acrylic based coating which enhances windability, ink adhesion and handling properties, and shall hereafter be referred to as a slip coating. It consists mainly of demineralised water, surfactant, ammonium nitrate and latex particles, which are themselves made up of a copolymer of acrylamide, ethylacrylate, methylmethacrylate and ethylated melamine-formaldehyde.

3.2.2.6 Transverse draw

The uni-axially drawn (and coated where applicable) film then enters the stenter oven where the transverse direction drawing process takes place. The film is grasped firmly by clips at either edge as it enters the oven where it is heated to around 120 °C. The clips run along diverging rails which draw the film in the transverse direction to 3 - 4 times its original width, further orienting many of the polymer chains (and the coating), this time in the transverse direction and increasing mechanical strength by the same means as with the forward draw.

3.2.2.7 Crystallisation

The oriented film then reaches the crystalliser, a region of the stenter oven held at approximately 220 °C, this encourages the now biaxially oriented polymer chains to crystallise, making the film more resistant to shrinking when heated later during customer processing for example. Crystalline regions are also much stronger mechanically than amorphous regions and the percent crystallinity can determine much of the final behaviour of the film (Ajji *et al*., 1996). If too great a proportion of the film is crystalline, a very tough but inflexible film would be produced, if too little the film retains its amorphous quality and would yield excessively under mechanical stress, stretching and relaxing. Balance between the two phases is critical and this is achieved by temperature controlling the stenter oven precisely, effectively splitting it into multiple regions of various temperatures.

3.2.2.8 Cooling and winding

After leaving the stenter oven the film is allowed to relax slightly further, and passed over cooled rollers, the clipped edges are then trimmed off and reclaimed where possible. The film is then slit and wound onto several rolls or wound onto one large mother roll for slitting later. Depending on the individual film properties film rolls can be anything from 0.5 to 9 metres wide and from a few hundred to fifty thousand metres long. Rolls can weigh between one hundred kilos and three tonnes and on thin film units can be wound at up to three hundred metres a minute.

3.2.3 DTF PET film grades

The following sections provide information regarding the specific PET films used in this Thesis, including details of their formulations, microstructure, physical properties and why they were chosen for investigation.

3.2.3.1 Melinex 'O'

Melinex 'O' of approximately 175 µm thickness is a commercial grade of DTF biaxially oriented PET film designed to meet the demands of the optical polymer films market, which include high mechanical strength and light transmittance. Melinex 'O' is a very pure, semicrystalline, monolayer PET film (consisting of a single extruded layer), with no additional fillers or coatings. These properties make it an ideal film for investigating PET surface UV degradation as there are the minimum of additional formulation components to consider when interpreting experimental results, hence, both surface and bulk can be considered entirely PET. Thus, Melinex 'O' and it's modification by weathering treatments can also serve as the baseline when

interpreting the effects of additional formulation components on PET degradation processes.

3.2.3.2 UVA-PET

UVA-PET film of 175 µm thickness, hereafter referred to as UVA-PET, is a developmental grade of DTF UV stabilised thick PET film. It is very similar to Melinex 'O' in most regards but with the important addition of the ultraviolet absorber (UVA) Tinuvin 1577 at 1 wt% in the formulation, included to extend the outdoor performance lifetime of the film by preferentially absorbing damaging UV radiation. There is also a slip coating on one side to aid the manufacturing process (and also to enhance ink adhesion for printing). A schematic cross section of this structure is presented in Figure 3.8 to aid understanding of the film composition. The UVA is added as a powder to the formulation via a separate twin screw extrusion process known as masterbatching, usually conducted by an external converter, which is designed to provide a uniform distribution of the UVA through the PET pellets and thus, the final film matrix. UVA-PET was chosen for investigation as it is effectively a UV stabilised version of Melinex 'O', however the presence of the coating inhibits the study of the rear surface PET.

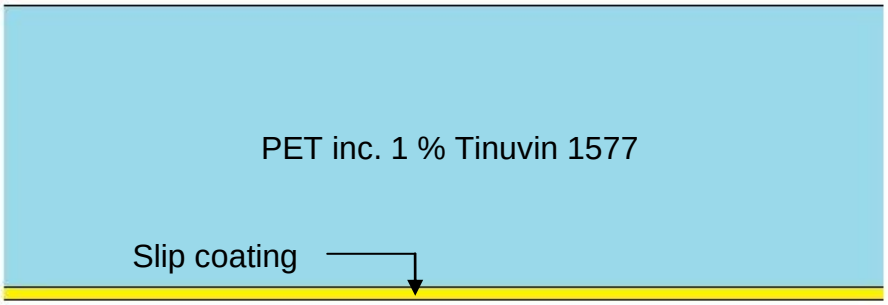

Figure 3.7: UVA-PET cross sectional structure (coating thickness not to scale)

3.3 Sample weathering procedures

The following section describes the weathering apparatus and exposure conditions employed to generate weathered samples for investigation.

3.3.1 Accelerated environmental weathering

Sample accelerated environmental weathering was performed using an Atlas Ci5000 Weather-o-meter (WOM), pictured in Figure 3.10. The WOM features a water cooled xenon arc lamp, temperature control, humidity control and a sample water spray feature. Samples are hung on wire racks in aluminium frames that are rotated around the lamp in three tiers, with room for 118 film samples in total. The top and bottom tiers are tilted towards the bulb to help ensure uniform radiant exposure of all three tiers. For consistency the sample machine direction was always aligned with the vertical axis of the sample holder.

Figure 3.8: ATLAS Ci5000 Weather-o-meter in operation at DTF (Plasticker, 2012)

DTF operate their WOMs in accordance with ISO 4892-2 (Organisation, 2013), an international standard widely adhered to by the polymer films industry when conducting weatherability tests on new polymer product developments. The standard defines the exposure periods to be 400 hours long and the conditions which samples experience during exposure are defined in Table 3.3. The radiant intensity at 340 nm is equivalent to peak terrestrial solar irradiance at sea level, hence, the acceleration arises from the synergistic effects of the other degradation agents with UV radiation, and that the instrument runs for 24 hours per day, approximately doubling the time efficiency of the WOM compared to outdoor exposure methods.

This accelerated environmental weathering procedure is designed to expose samples to more extreme conditions than would occur in polymers exposed outdoors, while not creating conditions which may enable sample degradation to

occur via unrealistic pathways. At DTF the adherence to the ISO standard is motivated by both a desire to further understand PET film weatherability and to evaluate new product development performances relative to each other and to DTF film competitor products on even terms.

Table 3.3: Degradation agents and their values defined by ISO 4892-2

Degradation agent	**Range of values during cycle**	**Set point/Frequency during cycle**
Temperature	Ambient - 68 °C	(65 ± 3) °C Black Standard Temperature
Humidity	Ambient - 100 % RH	(65 ± 5) %, rises to 100% during water spray periods
Radiation	0.5 Wm^{-2} at λ = 340 nm	Constant
Water spray	Demineralised water with conductivity below 5 µS cm^{-1}	(18 ± 0.5) minutes per 120 minutes

In general, researchers at DTF submit a number of film samples and after each 400 hour exposure period test the optical properties of all samples (Haze, total light transmittance (TLT), UV-Vis spectra) and a limited number of these samples by destructive tensile mechanical tests, before reinserting the remaining samples back into the WOM. Thus, the number of samples being exposed is reduced after each withdrawal and test interval until the last sample has either been destructively tested or has failed due to extended exposure. For this Thesis only a relatively small

number of samples could be exposed at any one time as the majority of WOM spaces were being utilised for DTF weathering experiments, which effectively ruled out the option of destructive mechanical testing. Also due to the short interval of a few days for testing between exposure intervals, the decision was made to generate a single sample for each exposure interval, thereby ensuring the best possible time resolution for observable modifications. However, it must be assumed that all samples are identical at t = 0 in order to treat results gained from each separate sample as the evolution of a parameter with exposure time. This is a reasonable assumption due to the homogeneity of most of PETs bulk properties, however this may be a factor when interpreting nanoscale inhomogeneous parameters. To help minimise variability, samples were always taken from the same source and point in the transverse direction and the surface and orientation of the sample were kept consistent throughout experimentation and testing.

There are many disadvantages of adhering to ISO standard weathering procedures from an academic research perspective. Due to the combination of degradation agents acting on samples simultaneously it may be difficult to deduce which (or what combination of) degradation agents were principally responsible for certain observed changes. This Thesis was partly motivated by the desire to investigate and address this issue and as such the high intensity solar simulator (HISS) apparatus described in the next section was applied to the task.

3.3.2 High intensity solar simulator

Samples were UV exposed using a LOT Oriel high intensity solar simulator (HISS), presented in Figure 3.11 a-c. The HISS consisted primarily of an air cooled 1200 W

xenon arc lamp, focussing optics and beam turner (to direct the bulb output onto a sample), and an AM 1.5 filter which further modified the lamp output to be more spectrally similar to terrestrial sunlight, though still many times more intense. An adjustable collimator allowed the focal point of the beam to be adjusted to provide relatively uniform sample exposure over the 40 mm diameter sample holder. Circular samples were held at the edges inside an anodised aluminium frame held at a fixed distance from the source. Thermal radiation was also generated by the bulb and transmitted by the optics, but was screened by a water filter with a 40 mm optical path length of ultra pure water, kept at constant temperature by circulating 20 °C water around its housing. To protect other lab users from UV radiation a containment chamber was built around the beam turner to contain the bulb output.

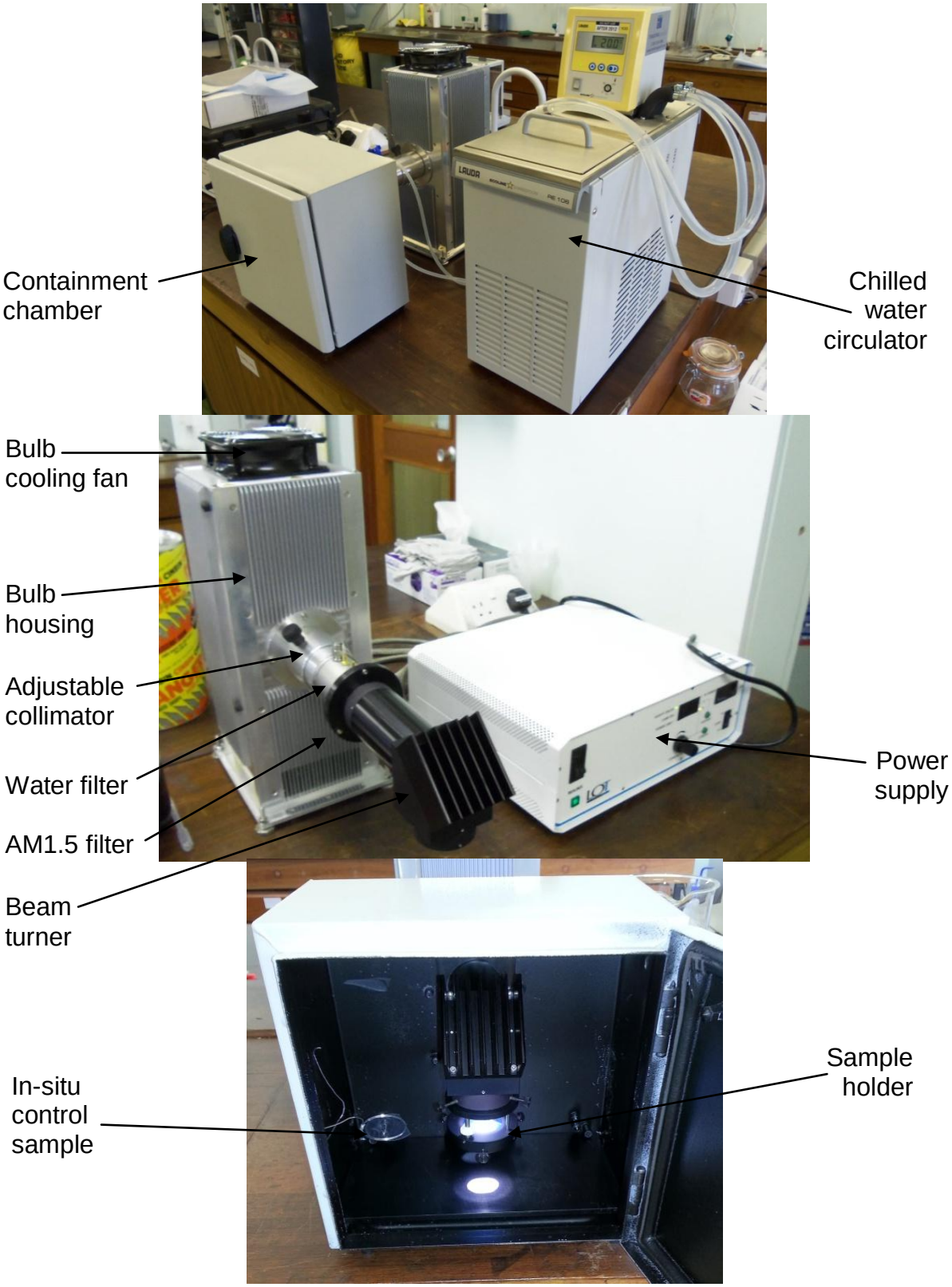

Figure 3.9 a-c: a. Full HISS setup; b. HISS bulb housing, optics and power supply; c. inside exposure chamber during operation

Each xenon arc lamp had an operational lifetime of approximately 1000 hours, over the course of which, due to anode deposition on the bulb's internal quartz surface, the UV output would deteriorate. Following the manufacturer's recommendations to ensure a consistent output over the bulb's lifetime, each bulb was operated at 80 % of its maximum power, which was increased up to 100% as necessary over the lifetime of the bulb, in order to keep the measured spectral output at 400 nm constant. A measurement of the HISS output is shown in Fig. 3.12, along with the ASTM G173 terrestrial solar spectrum (ASTM, 2012a). More precisely, that is annually averaged spectral irradiance at sea level, transmitted through 1.5 atmospheres of air, incident to a 37° hemispherically tilted sample.

Spectral irradiance measurements were performed with an ILT 950 spectroradiometer, which, due to containing only a single slit spectrometer experienced quite poor signal to noise ratio in the UVB region of the spectrum. This was countered somewhat by the fact that the signal was in this case particularly high, but still means that the measured output below 380 nm is likely an underestimate. In summary, the output from the HISS xenon arc lamps was at least equivalent to peak terrestrial solar irradiance and at most wavelengths 8-10 times as intense.

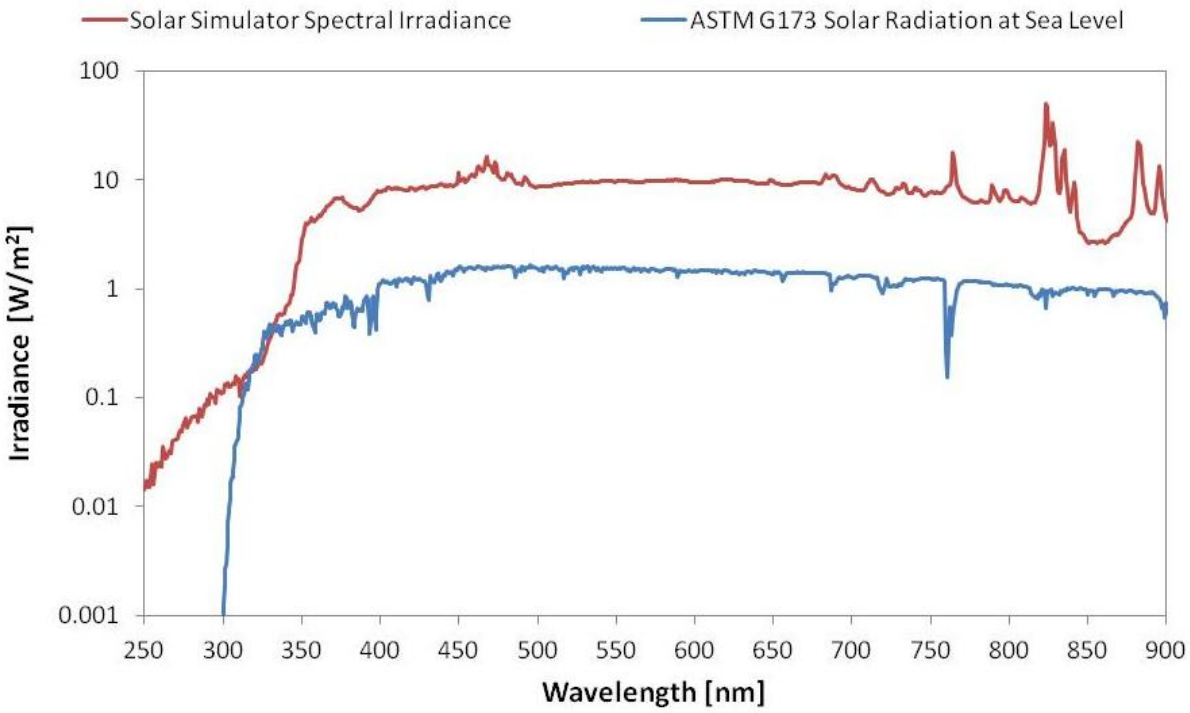

Figure 3.10: Solar simulator spectral output operating at 830 W and G173 reference solar spectrum

3.3.3 Damp heat oven

Samples were exposed to hydrolysing conditions in a Gallenkamp damp heat oven, (DHO) operated in accordance with IEC 60068 (2010). During exposure samples are continually exposed to temperature and humidity levels of 85 °C and 85% RH respectively for exposure intervals of 504 hours (3 weeks). Samples were mounted in aluminium WOM sample frames for consistency between exposure apparatus. All samples began DHO exposure at the same time, with one withdrawn after each exposure period up to a maximum exposure of 3024 hours.

3.4 Analytical toolkit

3.4.1 Optical techniques

Haze and TLT measurements were performed with a BYK Gardner haze-gard plus and yellowness (b*) measurements with a BYK Gardner color-view 9000 spectrophotometer. In both cases, single measurements encompassed a 25 mm diameter circular area and the average value of several different measured areas within a sample was used where possible. Gloss measurements were performed with a Dr Lange Refo 3-D reflectometer at a 60 degree angle of incidence, single measurements encompassed a 40 x 10 mm area and again an average value obtained from several areas was used where possible.

3.4.2 Chemical techniques

3.4.2.1 Fourier transform infra-red spectroscopy

Fourier transform infra-red (FT-IR) absorbance spectra were acquired using a Thermo Scientific Nicolet iS50 FT-IR in transmission mode. Scans were performed over a wavenumber range of 400 - 4000 cm^{-1} with resolution of 2 cm^{-1} and an average of 32 scans was used per measured area. Single measurements encompassed an approximately 2 x 2 mm sample area, but with no recommended means of holding film samples, a modified setup was constructed which enabled the measurement of samples but only in a limited region.

3.4.2.2 Absorbance spectroscopy

Absorbance and transmittance spectra were acquired using a Shimadzu UV-1800 UV spectrophotometer. Scans were performed at a medium speed over a

wavelength range of 300 - 900 nm with resolution of 1 nm. Single measurements encompassed a 2 x 2 mm area. To aid comparisons between different sample spectra, beam scatter and reflection were assumed to be zero by normalising collected transmittance spectra according to Equation 3.1, where x is wavelength and T and T_{norm} are transmittance before and after normalisation respectively.

$$T_{norm}(x) = \frac{T(x)}{T(900\ nm)} \quad ; \quad T_{norm}(900\ nm) = 100\ \% \qquad \text{Equation 3.1}$$

Where absorbance spectra were collected, these were transformed into transmittance spectra, normalised and transformed back to absorbance spectra using the absorbance-transmittance relationship shown in Equation 3.2 which is derived from the Beer-Lambert law.

$$A = Log_{10}\frac{1}{T} \qquad \text{Equation 3.2}$$

3.4.2.3 Fluorescence spectroscopy

Fluorescent emission and excitation spectra were recorded using a Horiba Jobin Yvon Fluoromax 4 spectrofluorometer. Before each set of measurements the system's spectrometers were wavelength checked to ensure that measurements were kept consistent over long periods. The excitation spectrometer calibration was checked against the peak irradiance band of the system's lamp centred at 468 nm and the emission spectrometer calibration against the Raman emission peak of water centred at 397 nm. The system had an accuracy of ±0.5 nm, resolution of 0.3 nm and

signal to noise ratio of 3000:1 at 397 nm using standard operating settings. For film samples, excitation wavelengths (λ_{ex}) of 320 and 340 nm were used where appropriate. Emission spectra were recorded over a range starting 15 nm greater than the λ_{ex} used and up to 600 nm, thereby preventing λ_{ex} scatter and its overtone at 2 times λ_{ex} from appearing in the measured emission spectra.

3.4.2.4 Gel permeation chromatography

Gel permeation chromatography (GPC) spectra were performed by Smithers Rapra of Shawbury, Shropshire. The instrument was a Malvern/Viscotek TDA 301 fitted with Agilent PL HFIPgel guard plus 2 x PL HFIPgel 300 x 7.5 mm, 9 µm columns. A refractive index detector was used with differential pressure/viscosity and right-angle light scattering. Malvern/Viscotek “OmniSec” software was used for data collection and analysis. Single sample solutions were prepared by adding 10 mL of hexafluoro-2-propanol (HFIP) to 20 mg of film sample and left overnight to dissolve. Solutions were thoroughly mixed and filtered through a 0.45 micron polytetrafluoroethylene (PTFE) membrane before insertion to autosampler vials. The nominal flow-rate of the solutions was 0.8 mL minute^{-1}, at a nominal temperature of 40 C. The system was calibrated using Agilent/Polymer Laboratories EasiVial poly(methyl methacrylate) (PMMA) calibrants of known molecular weight distribution, thus, all molecular weight results are considered PMMA equivalent molecular weights which may differ from true molecular weights. Due to the large number of samples, different calibrations were used for the initial 19 samples and the subsequent 22 samples.

3.4.3 Surface chemistry techniques

3.4.3.1 Water contact angle (WCA)

Water contact angle (WCA) measurements were performed using a Video Contact Angle Systems 2500XE. 5 µL drops of deionised water were applied to the sample surface using a motorised pipette, the drop angle on either side was measured and then averaged by the software. 5 drops were measured on each sample surface and the measurements were taken within 2 seconds of the drop hitting the surface as drops tended to wet out with time.

3.4.3.2 Attenuated total reflection FT-IR

Attenuated total reflection Fourier transform infra-red (ATR FT-IR) absorbance spectra were acquired using a Thermo Scientific Nicolet iS50 FT-IR in ATR mode. Scans were performed over a wavenumber range of 400 - 4000 cm^{-1} with resolution 2 cm^{-1} and an average of 32 scans used per measured area. Samples are held firmly on the ATR crystal during measurement using a small clamp. Samples were measured in 3 different locations with single measurements encompassing an approximately 2 x 2 mm sample area. The combination of instrument settings used, including beam angle incidence of 40° and diamond ATR crystal yielded a depth sensitivity of between 1.3 and 2.7 µm in the wavenumber regions of interest.

3.4.4 Microscopy techniques

3.4.4.1 Light microscopy

Light micrographs were collected using a Leica DMRX compound microscope operated in reflection mode in air. Objectives of 5x, 10x, 20x and 50x magnification

were used where appropriate. Image sizes (scale bars) were calibrated using a graticule to give the approximate size of a pixel obtained using each objective.

3.4.4.2 Scanning electron microscopy

Scanning electron micrographs were acquired by Intertek MSG using an FEI Quanta FEG 250 scanning electron microscope (SEM) instrument. Samples were imaged in high vac mode giving a quoted maximum resolution of 1 nm when operated at 30 kV. Energy dispersive x-ray (EDX) spectra were acquired using a Bruker AXS Quantax 200 Microanalysis System with an XFlash 5030 silicon drift detector and quoted resolution of 127 eV FWHM MnKa.

3.4.5 Surface metrology

3.4.5.1 Phase shifting interferometry

Sample areal surface topography was mapped by phase shifting interferometry (PSI) using a Bruker WYKO NT9800 white light interferometer (WLI). Generally a 50x magnification objective was used to generate surface topography maps with a field of view (FOV) of 120 x 90 microns, lateral resolution of no less than 0.4 µm and average height resolution of ± 0.5 nm (Z detector noise floor measured using an optical flat). A full review of the working principles of WLI is beyond the scope of this Thesis but can be found in Leach (2011). In short, PSI works on the principle of optical interference between 2 components of a split light source, known as the reference and sample beams. In the case of the NT9800 the light source used is a white light LED. The phase difference between these coherent light beams is set to be ¼ lambda by a Mirau interferometer. After reflection of the sample beam from the

sample surface, the modified phase difference depends upon the optical path length travelled, which itself depends on the sample surface topography. This effect is used to generate an interferrogram, where the rate of change of intensity during a scan is directly proportional to the rate of change in surface height. This information is captured by a charge coupled detector (CCD) camera and interpreted by the software for each point of the surface in view, yielding a 3-dimensional (3D) map of sample surface topography (Calatroni *et al*., 1996).

3.4.5.1.1 Large area measurements

For the large area array measurements samples were mounted on a DTF proprietary low tack gel plate which ensured that they were held firmly in place and presented the entire surface area of interest flat enough to be within the system autofocus tolerance. An automated measurement protocol was designed in the Vision software to facilitate the measurement of a 100 x 100 grid of 120 x 90 µm adjacent areas with 640 x 480 pixel resolution. To characterise an area of this size the system was set to operate as follows. First the system automatically brought the surface into focus, it then optimised the brightness and number of interference fringes which were visible by adjusting the beam intensity and stage tilt accordingly. The system then took an average of 5 PSI measurements, automatically saved the resulting image file and inputted the user chosen measured roughness parameters into a database, before moving onto the next area in the grid and repeating the procedure until all 10,000 measurements were complete.

3.4.5.2 Atomic force microscopy (AFM)

The AFM used predominantly during this research project was a Bruker Dimension 3100 (D3100) with a Nanoscope IV controller, running version 6.14 r1 software. It has a maximum FOV of 100 μm ^{2}, height (Z) range of approximately 5 μm and maximum pixel resolution of 1024^2. For tapping mode imaging, Bruker Tapping MPP-12220 antimony doped silicon cantilevers with reflective aluminium coated backs were used, their characteristic parameters are summarised in Table 3.4.

Table 3.4: Bruker Tapping MPP-12220 AFM cantilever parameters

Parameter	Value
Length	(125 ± 10) μm
Width	(30 ± 5) μm
Thickness	(2 ± 0.5) μm
Resonant frequency	(145 ± 22) kHz
Spring constant	5 N/m
Tip Radius	8 nm

Scan parameters used when imaging samples are described in Table 3.5. Where a range is given, parameters were optimised within the range to give consistently overlaid trace and retrace line scans. This is strongly dependent upon the scan size, and thus, the cantilever speed. For example when acquiring 2 μm scans a 1 Hz scan rate and 1.8 V A_{sp} are appropriate (soft tapping), whereas when acquiring 20 μm scans a 0.5 Hz scan rate and 1.6 V A_{sp} are appropriate (hard tapping).

Table 3.5: Scan parameters used when imaging PET films in tapping mode

Parameter	Value
Target amplitude	2 V
Amplitude setpoint (A_{sp})	(1.6 - 1.8) V
Scan rate	(0.5 - 1) Hz
Integral (I) gain	0.1 - 0.2
Proportional (P) gain	0.2 - 0.3

3.4.5.2.1 Image processing

All AFM images presented in this Thesis, including those summarised as roughness parameters, have been post processed in the Nanoscope software to remove any artefacts introduced by the imaging process or software, which can be considered unrepresentative of the surface analysed. This includes artefacts such as piezo wandering, streaking, parachuting and height irregularities. Such artefacts are common in AFM images due to the operational nature of AFM and specifically in this Thesis due to the PET film surface, as it often exhibits sparse and irregular features which can adversely affect the expected distribution of feature heights. The image post processing procedure was carried out in the same way for all images for consistency and that any errors unintentionally introduced were systematic. Specifically this involved the removal of up to third order polynomial spatial frequencies in the X and Y axes, followed by a background flattening process while excluding the uppermost features of the surface.

3.4.5.2.2 Peak force quantitative nano-mechanical analysis (PFQNM)

Peak force quantitative nano-mechanical (PFQNM) measurements were performed on a Bruker Multimode 8 with a Nanoscope V controller, running 2013 version Nanoscope software. It has a maximum FOV of 100 μm^2, Z range of approximately 10 µm and maximum pixel resolution of 4096^2. Bruker Tapping MPP-12220 probes were used and had their spring constant (k) calibrated using the Sader method (Sader *et al*., 1995). Cantilever deflection sensitivity (units of nm/V) was measured by performing a force ramp of calibrated Z displacement on a very stiff and clean sample, in this case freshly cleaved mica, and measuring the maximum cantilever deflection. The deflection sensitivity is the amount of real cantilever deflection (in nm) per measured unit of deflection (in volts). Assuming linear deflection behaviour and no deformation of the mica or tip (which is reasonable given their very high moduli of 70 and 169 GPa respectively (McNeil and Grimsditch, 1993, Hopcroft *et al*., 2010), the cantilever deflection equals the vertical piezo displacement. Therefore by using the gradient of this force ramp (*e.g.* 90 nm/V), the software can display all subsequent cantilever deflections in nm and the difference between Z piezo displacement and cantilever deflection when performing force ramps on samples is the sample deformation.

The final piece of information required to yield quantitative nano-mechanical information is the tip radius, which can be measured using tip calibration artefacts or deconvolution algorithms. However, since this is the property most likely to evolve over the course of any measurement routine (due to tip wear, hard contact during calibration, becoming contaminated for example) it is used more as an input parameter for controlling the outputted modulus value than as a true indication of

reality. Thus, the “relative method” was employed where the tip radius is varied up or down from the nominal 10 nm to make the mean measured modulus (calculated using the Derjaguin-Muller-Toporov (DMT) model over a few scan lines) match the known modulus of a polystyrene (PS) calibration sample. PS was used as it was the closest match to the modulus of PET available as a modulus calibrated sample. The DMT model (Derjaguin *et al*., 1975) is the model preferred by the manufacturer and is considered most appropriate for AFM measurements as it uses a fixed contact profile as in the Hertz model (Hertz, 1895), while also taking into account both tip-sample adhesion and adhesion forces outside of the area of contact, where models such as the Johnson-Kendall-Roberts (JKR) model (Johnson *et al.*, 1971) assume sample deformation to affect the contact area also. In order for PFQNM to yield quantitative and accurate sample modulus information the cantilever spring constant, deflection sensitivity and tip radius must be accurately obtained. An appropriately stiff cantilever must also be employed to give enough sample deformation for the contact mechanics models to be applicable without the peak force having to be set too high, which could cause tip wear and subsequent change in the radius and hence the contact area.

In PFQNM mode, calibrated force ramps are continuously performed at 2 kHz (significantly less than the cantilever resonant frequency) while the AFM probe is raster scanned across the surface in the same way as in tapping mode AFM. The user defines the “peak force”, the maximum force exerted by the cantilever on the sample, in order to cause a measured deformation of a few nm. At each point on the sample, once the peak force is reached the probe is moved away and the process is repeated at the next point on the sample. In this way, force curves of the same peak

force are performed at every point in the image area. The software then automatically interprets the different regions of the force curves and measurement information (height, tip-sample adhesion, deformation, modulus, dissipation) is extracted and can be displayed as colour scales in multiple AFM images illustrating the variability of each parameter over the area scanned. Figure 3.13 illustrates a typical force curve labelled to show where measurement information can be extracted from.

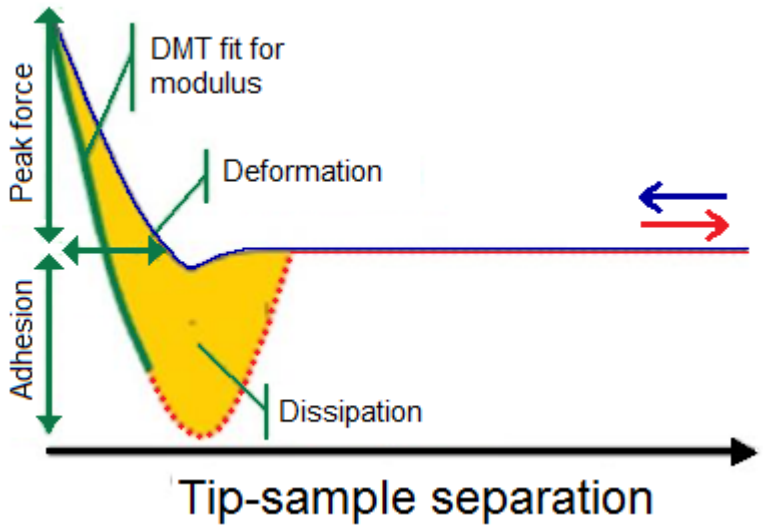

Figure 3.11: Typical AFM force curve labelled to show regions containing information

3.4.6 Mechanical testing

3.4.6.1 Instrumented indentation

Instrumented (nano)indentation (IIT) was performed at the University of Birmingham Science City Labs using a Micromaterials NanoTest Platform 3 Nanoindenter fitted with a diamond Berkovitch indenter tip. Indentations were programmed to be either 0.5 or 1 um deep and were carried out at a constant load rate of 1 mNs^{-1}, up to a maximum load of approximately 2 mN, which was then held for 30 seconds before retraction of the indenter. The instrument software calculates the material hardness

and reduced modulus (E_r) according to the Oliver-Pharr model (Oliver and Pharr, 2004) and the average values obtained from 100 indentations performed over 1 mm^2 per sample were used. The indenter itself has Poisson ratio of 0.07 and Young's modulus (E_i) of 1141 GPa which when inputted to Equation 3.2 yields a value for sample Young's modulus (E_s), which is more comparable with modulus values obtained with the other mechanical analysis techniques utilised in this Thesis.

$$\frac{1}{E_r} = \frac{1-\nu_i^2}{E_i} + \frac{1-\nu_s^2}{E_s}$$ Equation 3.3

BULK PROPERTY MODIFICATION OF ARTIFICIALLY WEATHERED PET FILM

4.1 Hypotheses

The direction of research in this Chapter was informed by the following hypotheses:

- During accelerated environmental weathering, UV radiation is the main degradation agent responsible for the deterioration of PET film bulk properties.
- Isolated exposure to high levels of UV, for long periods will result in observable modifications to film performance properties such as molecular weight parameters and optical properties.
- In addition to causing the hydrolysis of PET during accelerated environmental weathering, periodic water spraying, temperature and humidity exposure synergistically increases the rate at which PET film UV degradation takes place.

4.2 Objectives

Therefore, with these hypotheses in mind, the objectives of this Chapter are:

- To investigate the bulk property modification of plain 175 µm DTF PET film with exposure in the laboratory artificial weathering apparatus described in Chapter 3 - damp heat oven (DHO), high intensity solar simulator (HISS) and the weather-o-meter (WOM), which effectively combines the degradative effects of the DHO and HISS.

- Develop an understanding of how PET degradation processes, which occur during accelerated environmental weathering, manifest in PET films by comparing the bulk modifications of each different treatment.
- Develop an understanding of the individual and synergistic roles of the PET degradation agents - UV radiation, water and heat - in PET film bulk degradation due to accelerated environmental weathering.

4.3 Bulk property modifications

Various analytical techniques were employed to examine the modification of a broad range of PET film properties with artificial weathering and comparisons between the effects of the different exposure techniques are made. The modifications observed with artificial weathering are then related to the chemical processes known to occur during the artificial weathering of PET film. The result is a more complete picture of PET degradation processes during artificial weathering which will aid in the application of new strategies designed to prevent features of PET film degradation from inhibiting PET film application performances.

4.3.1 Macroscopic sample changes

Each exposure technique - WOM, HISS and DHO - had different effects on Melinex® ‘O’ film, hereafter referred to as PET film, which could be observed with the naked eye. These observations, though simplistic, are useful and will be referred back to later in the light of the more complex observations made using the analytical techniques described in Chapter 3.

4.3.1.1 Macroscopic sample changes after WOM exposure

After withdrawal from the WOM, there were a number of visually observable changes to the PET film samples which had taken place. The long (machine direction) edges of the rectangular samples were drawn up, normal to the exposed surface, giving the samples a mild curvature along the short (transverse direction) edges and a half cylinder like shape overall. This could be due to an increase in the exposed surface tension, caused by localised contraction of the polymer macromolecules near the exposed surface (MacKerron, 2014). The samples also became increasingly brittle with exposure; when cut with scissors, cracks would form and propagate short distances perpendicular to the cut direction. Sub millimetre sized translucent spots on the samples became increasingly prevalent with exposure, as well as what appeared to be water marks, which in some cases extended over the entire exposed surface. Many of these could be easily scraped from the sample with a scalpel, and were hence primarily surface features, and as such, these are analysed in detail in Chapter 5. However, it is important to note that such surface features can have an effect on bulk properties such as optical properties.

4.3.1.2 Macroscopic sample changes with DHO exposure

PET film samples became increasingly brittle with DHO exposure, and after 2000 hours snapped and shattered like thin glass when cut. Visually the samples also exhibited increased waviness with exposure, with centimetre scale wavelengths and mm scale amplitudes.

4.3.1.3 Macroscopic sample changes with HISS exposure

Surprisingly little appeared to have changed about the film sample exposed in the HISS, even after 2000 hours. The sample retained its original dimensions and ductile behaviour when cut, unlike the samples exposed for long periods in the WOM and DHO. The only macroscopic change reportable with HISS exposure is an increased level of discontinuous cloudy white residue on the surface of the sample, which is likely to be oligomer bloom. However, due to the low thickness of the bloom it was very difficult to say which surface was affected, or whether it was a feature of both. Surface blooming is a phenomenon seen in PET film (Perovic and Sundararajan, 1982), but also in chocolate (Cerbulis *et al*., 1957), commonly after long periods of ambient storage or heat treatment. In PET film it has been found that blooming is due to low molecular weight polymer structures, usually described as oligomers (Goodman and Nesbitt, 1960), migrating to the surface over long periods due to their incompatibility with the polymer matrix. It appears that HISS exposure has accelerated this process, while also not ablating the bloomed oligomer from the film surface. Blooming may also be occurring as a result of the slightly increased temperature of the sample due to the absorbance of the very intense UV radiation. The bloom could have been washed off with solvent and the solution analysed by absorption spectroscopy for example, however this could have affected the results of other analysis techniques, particularly surface analysis and so was not carried out.

4.3.2 Aromatic hydroxylation and yellowing behaviour

This section examines the optical property modification of environmentally weathered PET film samples, which will be shown to be related to the aromatic hydroxylation of PET due to UV exposure.

4.3.2.1 Spectral transmittance modification of PET film due to WOM exposure

Figure 4.1 shows the raw transmittance spectra of PET film which received between 0 and 4000 hours of WOM exposure. Transmittance has been used here rather than absorbance as it provides a more sensitive measure of the relative changes taking place over the full range of wavelengths analysed (300 - 900 nm). However, transmittance varies exponentially with species concentration and film thickness, and hence for quantitative analysis absorbance must be used,

The UV transmittance (300 - 400 nm) of the PET film is greatly reduced after 400 hours of WOM exposure, while transmittance in the visible region of the spectrum and beyond is only reduced after 1600 hours of exposure. The evolution of the film transmittance spectrum with increasing WOM exposure time is irregular after 1600 hours of exposure, most likely due to surface cracking and contamination adversely affecting the total transmittance. Therefore, to better understand the kinetic behaviour with exposure time, the curves were normalised using the conditions shown in Equation 3.1. For PET film, this transformation effectively assumes scattering and reflection at 900 nm to be zero and makes transmittance at all wavelengths relative to the maximum transmittance for that sample. The result of this normalisation procedure yields the sample's relative spectral transmittance (RST), which can be seen in Figure 4.2.

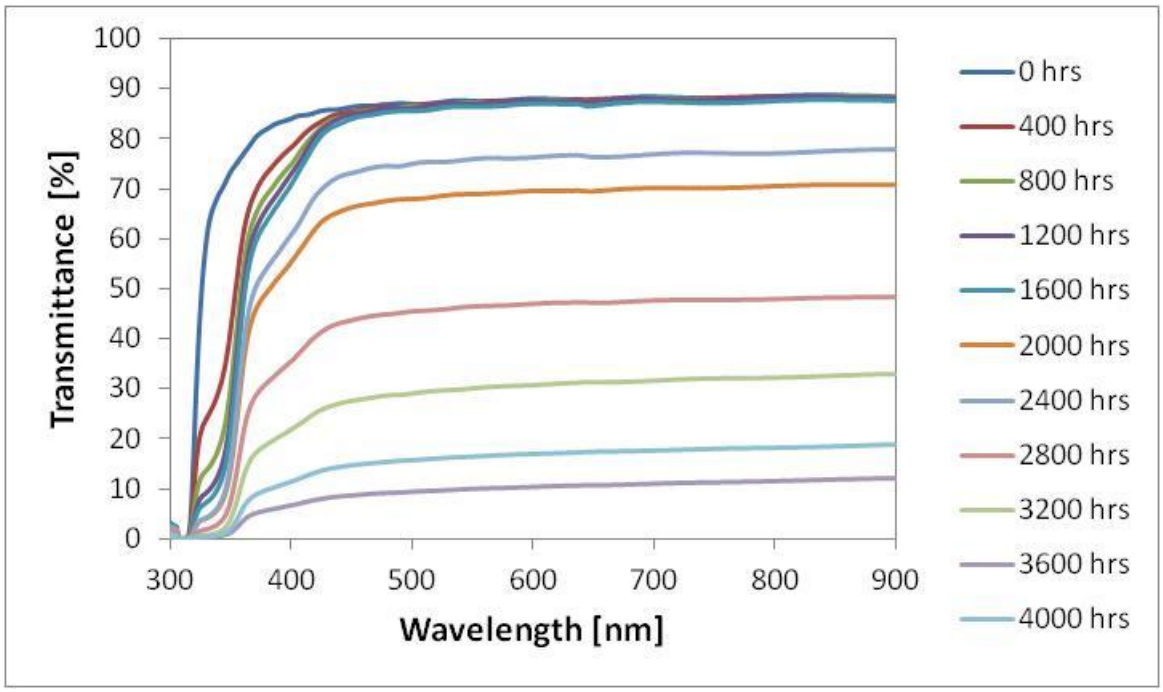

Figure 4.1: Raw transmittance spectra of PET film with 0 - 4000 hours WOM exposure

Figure 4.2 reveals that there are 3 particular wavebands where PET film RST is reduced with WOM exposure at different rates: 310 - 350 nm, 350 - 450 nm, 450 - 900 nm. RST in the 450 - 900 nm range is only minimally changed up to 2000 hours of exposure, but thereafter, there is decreasing transmittance over the entire range with exposure time (small arrow in figure), with the RST at 450 nm reduced by approximately 25 % after 4000 hours of exposure. A shoulder can be seen to grow with exposure time in the 350 - 450 nm range (middle arrow in figure), however in this case RST is reduced more rapidly by up to approximately 40 % after 4000 hours. These observations may be due to the fluorescence of liberated PET monomer and associated molecular dimer species (Allen *et al*., 1998).

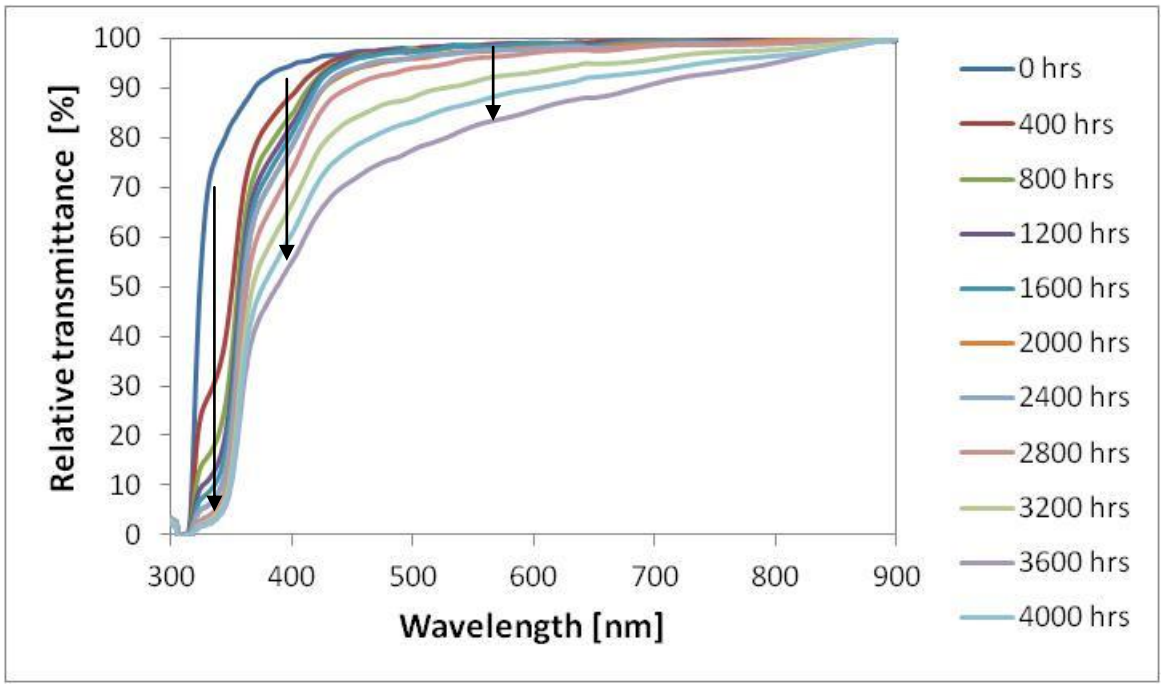

Figure 4.2: Relative transmittance spectra of PET film with 0 - 4000 hours WOM exposure

Figure 4.3 focuses in on the 310 - 400 nm wavelength range (largest arrow in Fig. 4.2) which contains the waveband known to be absorbed by mono-hydroxylated aromatic species, λ_{max} = 340 nm (Allen *et al*., 2000), commonly used as a measure of polymer yellowing (see section 8.2 Appendix 2 for reference spectra). Transmittance at this wavelength depends upon the concentration of mono-hydroxylated aromatic species present within the PET film. By presenting it as RST, the reduction with exposure time represents the increase in the amount of mono-hydroxylated aromatic species present in the sample, relative to the unmodified aromatic species. Figure 4.3 reveals a prominent shoulder in the transmittance curves with an inflection point at approximately 340 nm (arrow in figure) which forms between 0 and 400 hours of exposure, and which grows with exposure time with a decaying rate of growth.

To better examine the kinetics of the changes at each identified waveband, Figure 4.4 is presented, which shows the raw and relative transmittance modification with WOM exposure time, at a chosen wavelength from within each of the three identified regions. It reveals that sample transmittance at 380 and 500 nm are at first reduced relatively slowly with WOM exposure, however the rate of change begins to increase after 2400 hours. Conversely, the reduction in transmittance at 340 nm is initially rapid, but slows down with increasing exposure time until after 3200 hours, when further change becomes negligible. This suggests that different absorbing species, and hence different degradation products, are responsible for the changes in transmittance with exposure at 340 nm and at 380 and 500 nm.

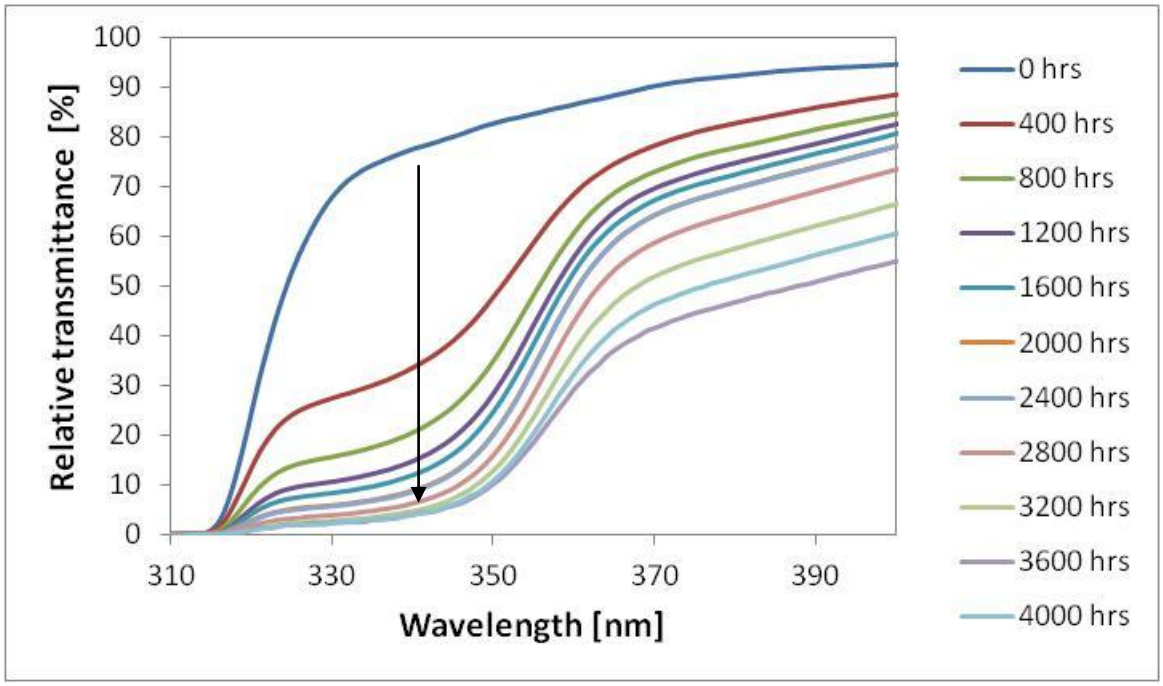

Figure 4.3: Relative transmittance spectra of PET film with 0 - 4000 hours WOM exposure over the 310 - 400 nm range

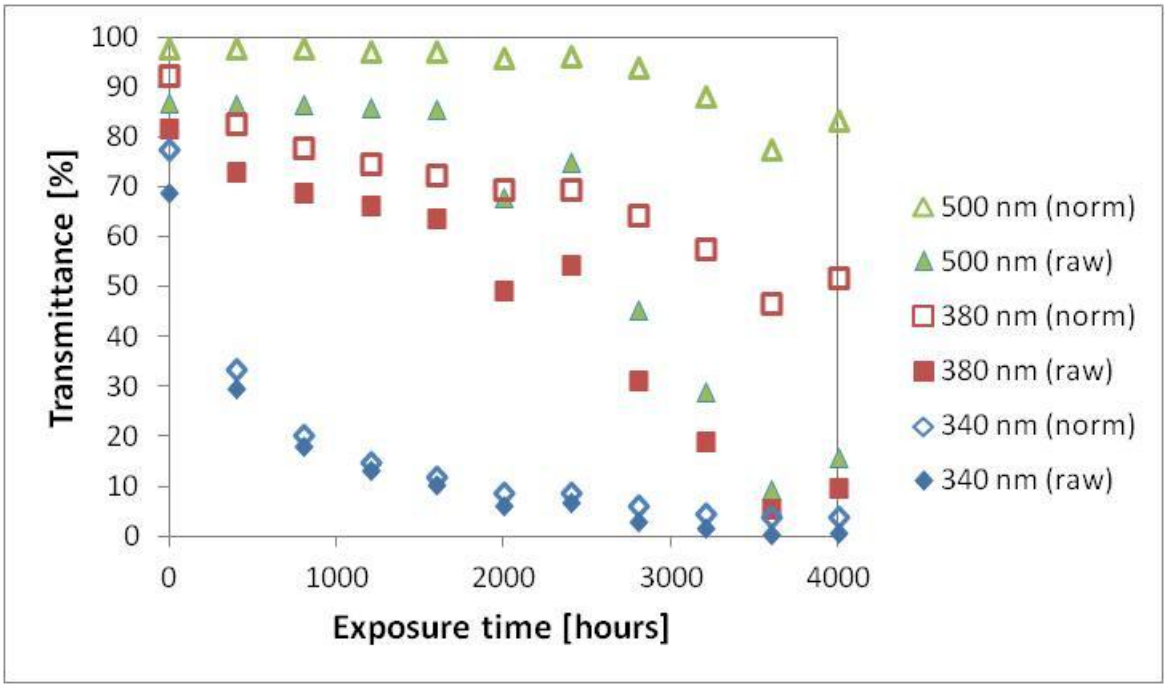

Figure 4.4: Raw and normalised PET film transmittance at three specific wavelengths vs. WOM exposure time

4.3.2.2 Spectral transmittance modification of PET film by different weathering apparatus

To evaluate the effects of different degradation agents on the formation of mono-hydroxylated aromatic species, the process of measurement and transformation of raw transmittance spectra to RST spectra was carried out for PET films exposed in the WOM, DHO and HISS. Figure 4.5 shows relative transmittance at 340 nm vs. exposure time, for plain PET film samples exposed in the WOM, DHO and HISS. Error bars are based on the manufacturer's quoted instrument uncertainty. It reveals that in the DHO, PET film relative transmittance at 340 nm is reduced linearly with exposure time, but only by a few percent. Here linearity has not been robustly confirmed due to only having three datapoints to fit to. In the HISS, relative transmittance at 340 nm is reduced with exposure time over a much greater range,

and at an exponentially decaying rate, highlighting the importance of UV in this particular modification.

A similar but more pronounced decaying rate time behaviour is displayed by the PET in WOM dataset, but in this case the exponential fit of the data is poor over the first half of the exposure duration, though much better for the second, with an overall R^2 of 0.93. Since the levels of UV present in both WOM and HISS are very similar, along with the shapes of the two curves, it is reasonable to conclude that the greater and more rapid drop in PET film relative transmittance at 340 nm with WOM exposure time is due to the action of the non-UV degradation agents present in the WOM (heat, humidity and direct water contact). Further, since the modification of PET film relative transmittance at 340 nm by these degradation agents independent of UV (in the DHO) is minor by comparison, it is reasonable to conclude that the non-UV degradation agents work synergistically with UV to enhance the rate of the UV mono-hydroxylation reaction, particularly in the early stage of the exposure duration.

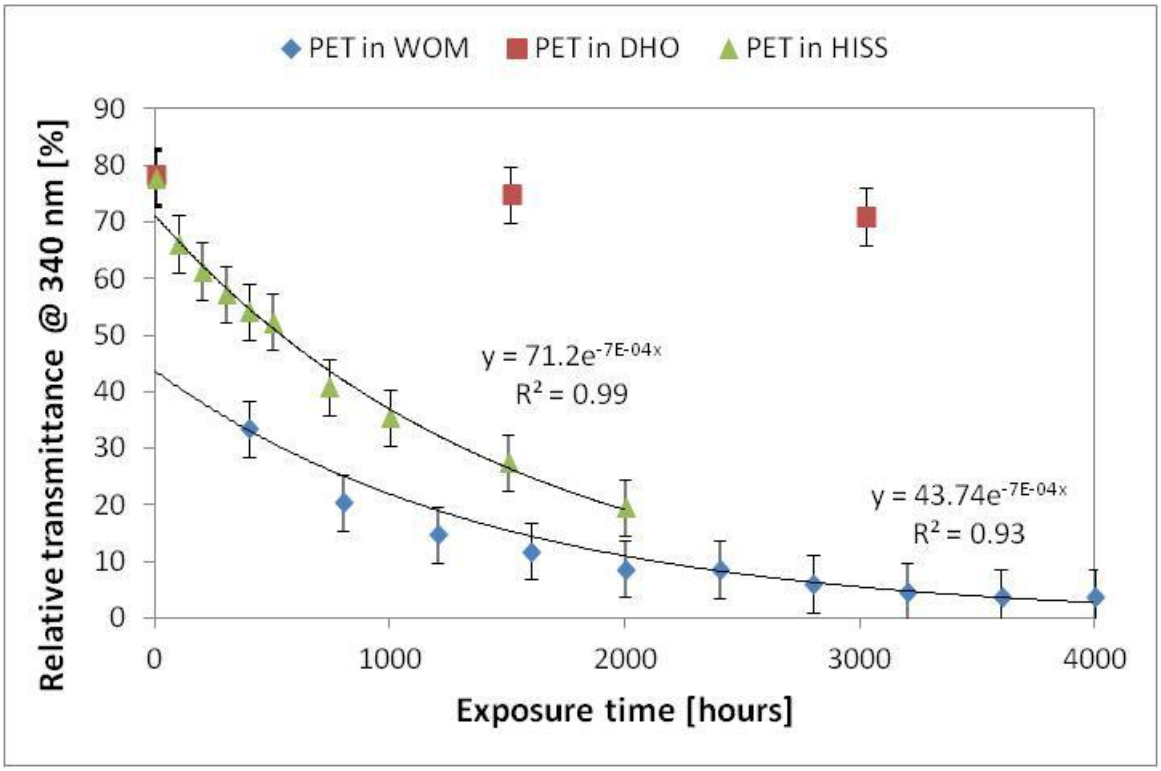

Figure 4.5: Transmittance at 340 nm vs. exposure time for PET film exposed in the WOM, DHO and HISS

Lastly, by transforming the transmittance axis of Fig. 4.5 to absorbance using the relationship given in Equation 3.1, we obtain Fig. 4.6, the relative absorbance at 340 nm vs. exposure time, in which all three datasets are well described by linear relationships, with the exception of the initial 500 hours of the PET in WOM dataset. Again the linearity of the PET in DHO data has not been robustly confirmed and the error bars are based on the manufacturer's quoted instrument uncertainty.

Figure 4.6 reveals that the rates of change of relative absorbance at 340 nm for the PET in WOM and PET in HISS datasets are the same, which suggests that the rate of mono-hydroxylation in the later stages of weathering does not depend on the action of the non-UV degradation agents present in the WOM. The linear nature of the data also suggests that the mono-hydroxylation reaction would continue to occur

at the same rate to greater exposure durations, which makes it likely that the population of unmodified PET molecules still exceeds the population of mono-hydroxylated PET, even after 4000 hours of WOM exposure.

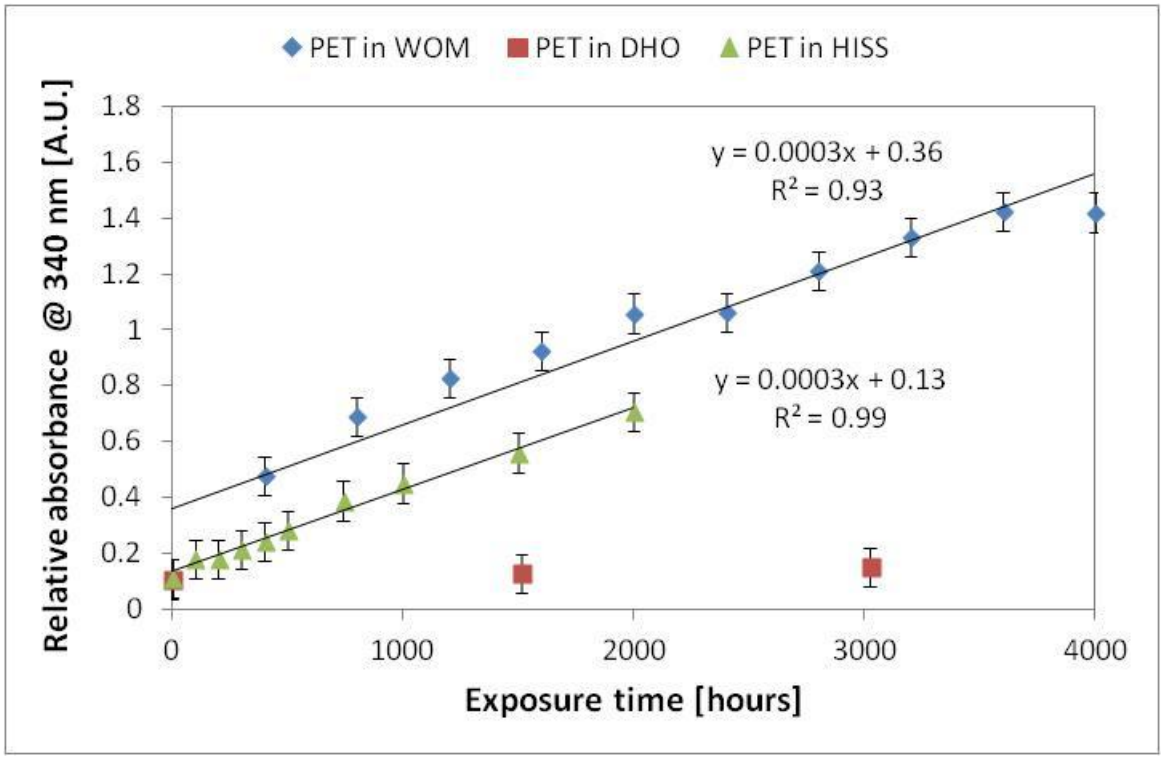

Figure 4.6: Absorbance at 340 nm vs. exposure time for PET film exposed in the WOM, DHO and HISS

4.3.2.3 Characterisation of degraded species blue fluorescence

It was shown in Chapter 2 that hydroxylated aromatic species in PET film fluoresce blue-violet light when exposed to 340 nm radiation. However, the evolution of this fluorescence with increasing UV exposure has not been previously explored, likely as it can be problematic to quantify due to the variable nature of fluorescence measurements. Nor has much work been done regarding other excitation wavelengths. These two aspects are explored in the following section.

Figure 4.7 shows the raw fluorescent emission spectra of PET film which received between 0 and 500 hours of HISS exposure, with a range of measurement between 335 and 600 nm and an excitation wavelength (λ_{ex}) of 320 nm. Pre exposure, the PET film sample fluorescence has a three pointed single peak structure, typical of bi-axially oriented PET film (Hemker *et al*., 1988), with a maximum at around 366 nm that falls to 0 at approximately 550 nm. With UV exposure, a new fluorescence peak centred at approximately 456 nm, known to be due to the production of mono-hydroxylated aromatic species (Edge *et al*., 1995), forms and grows, while the original PET film fluorescence peak appears to be suppressed.

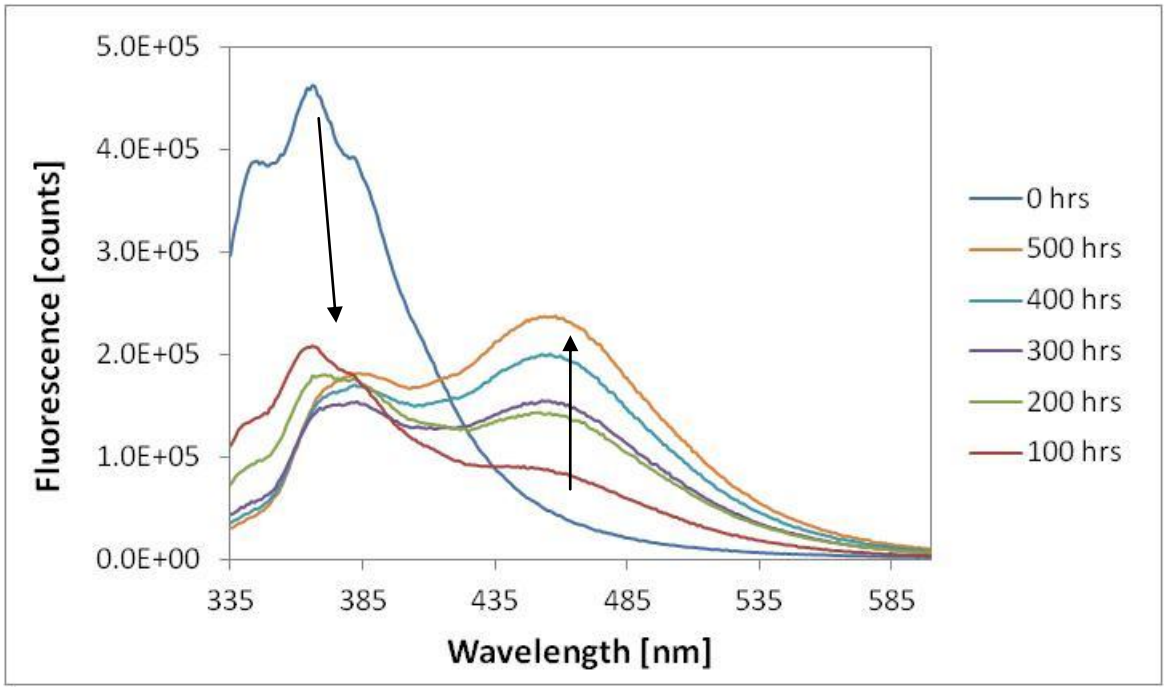

Figure 4.7: Raw fluorescent emission spectra of PET film with 0 - 500 hours HISS exposure (λ_{ex} = 320 nm)

This incremental growth with exposure of the raw fluorescence signal at around 456 nm was only observed in the early stages of sample HISS exposure. In all other

cases the fluorescence signal magnitude did not scale with exposure time. However, the difference in height between the degraded (456 nm) and un-degraded (386 nm) fluorescence peaks in the exposed sample spectra did change regularly with increasing exposure.

Therefore, the full range of data in each set was scaled using the secondary peak fluorescence at 386 nm to obtain a set of relative spectral fluorescence curves, in a manner conceptually similar to the transformation performed for the spectral transmittance data. It was then possible to quantify the degraded species fluorescence, relative to the undegraded PET film fluorescence, thereby obtaining another measure of the extent of aromatic mono-hydroxylation, which also indicated the rate of formation of these species with exposure time. Fig. 4.8 shows the result of the 386 nm curve scaling procedure for PET film which received between 0 and 4000 hours of WOM exposure. This illustrates the growth with exposure time of the degraded species fluorescence peak relative to the un-degraded PET peak, up to 2000 hours of exposure, after which the time-behaviour once again becomes irregular.

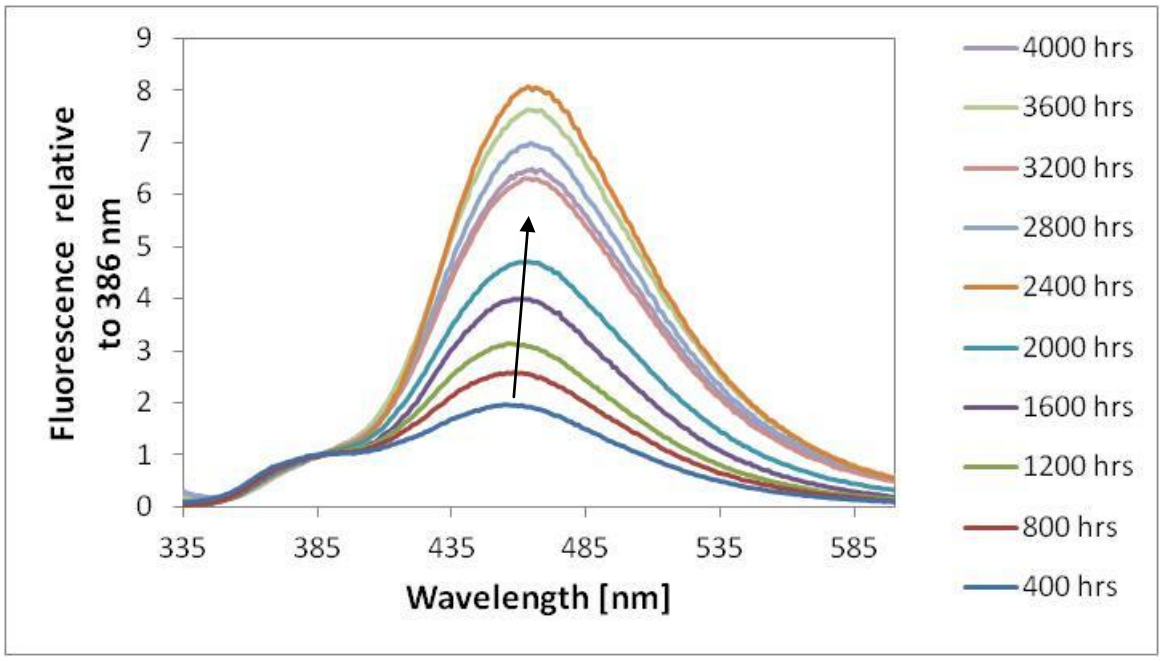

Figure 4.8: Fluorescent emission spectra of PET film with 400 - 4000 hours WOM exposure, relative to 386 nm emission (λ_{ex} = 320 nm)

4.3.2.4 Generation of blue fluorescing species by different weathering apparatus

This same scaling process has been carried out for the fluorescent emission curves of PET film samples exposed in the HISS and DHT and the relative fluorescence at 456 nm of samples exposed in all three weathering apparatus plotted against exposure time. This result is shown in Fig. 4.9 which again confirms the role of UV in the formation of mono-hydroxylated PET in environmentally weathered PET film as no change is observed for the PET in DHO dataset, while the other 2 exposure techniques do promote a modification in the fluorescent emission behaviour with exposure time. Fig. 4.9 also shows that with HISS exposure (*i.e.* isolated UV) growth of PET film relative fluorescence at 456 nm is reduced to zero after 1500 hours, which suggests that the mono-hydroxylation reaction is no longer occurring.

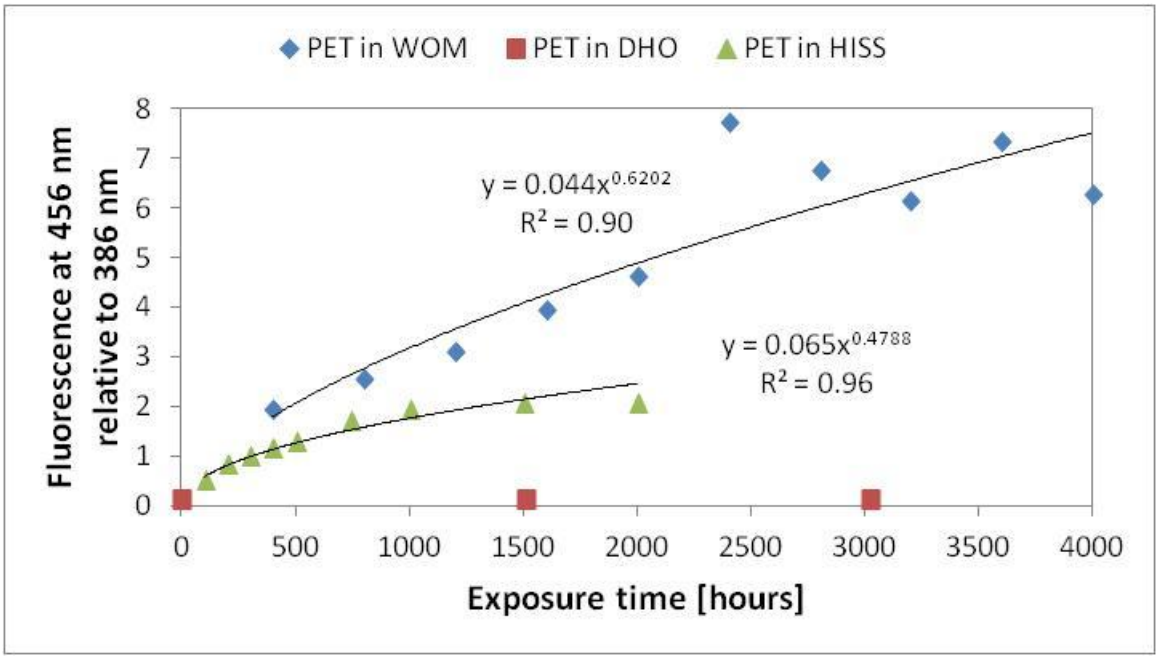

Figure 4.9: Fluorescent emission at 456 nm relative to 386 nm emission vs. exposure time for PET film exposed in the WOM, DHO and HISS (λ_{ex} = 320 nm)

4.3.2.5 Fluorescence excitation behaviour with WOM exposure

Another type of fluorescence measurement which yielded an interesting result for the WOM exposed PET film samples was the measurement of their 456 nm fluorescent excitation spectra. For comparison, Figure 4.10 shows the 386 nm fluorescence excitation spectra of unexposed PET film, where the range of measurement was between 250 and 370 nm and the emission wavelength (λ_{ex}) monitored was 386 nm. The curve reveals that 320 nm is the most effective wavelength to excite the 386 nm emission, but that any wavelength between 310 and 370 nm will also excite the 386 nm emission with varying degrees of efficacy. Commonly, the excitation spectrum of a sample is an approximate mirror image of its emission spectrum due to the relationship between fluorescent excitation and emission (Allen and McKellar, 1978). This effect can be seen by comparing the curve in Fig 4.10 with the unexposed sample curve in Fig. 4.7.

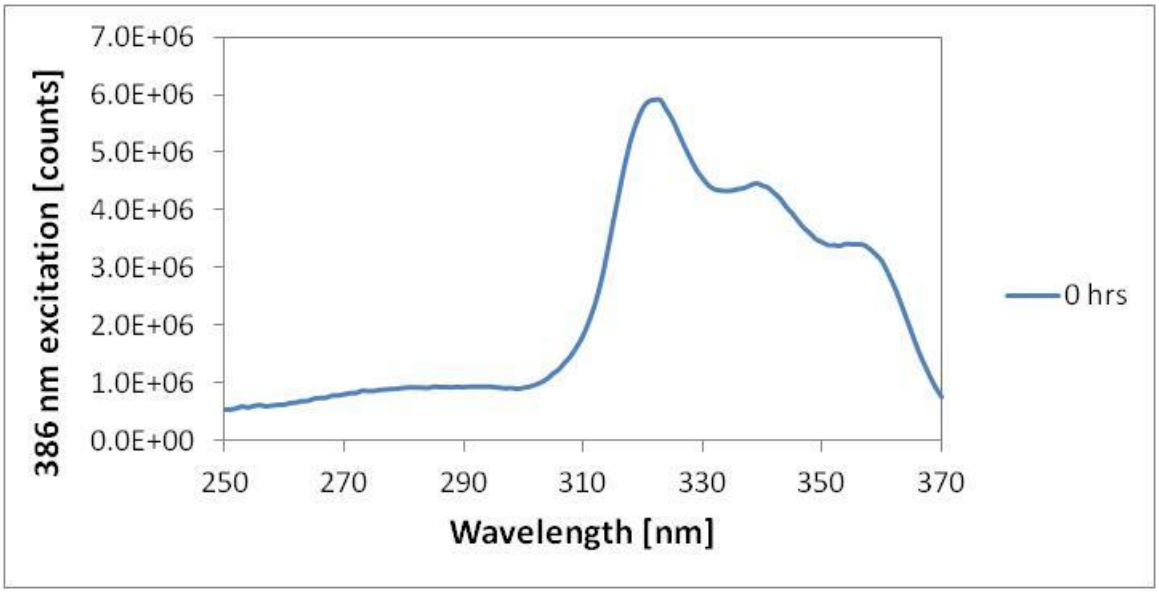

Figure 4.10: Raw fluorescent excitation spectra of unexposed PET film (λ_{em} = 386 nm)

Meaningful observations concerning PET film UV modification can be made from Figure 4.11, which shows the 463 nm fluorescence excitation spectra of PET film which received 400, 2000 and 4000 hours of WOM exposure, the range of measurement used was between 250 and 440 nm and the emission wavelength (λ_{ex}) monitored was 463 nm. The curves reveal that a waveband approximately 50 nm across and centred at 340 nm is most effective at exciting the mono-hydroxylated PET fluorescence, but also that after longer exposure times, wavelengths between 360 and 430 nm will also excite the 463 nm peak emission, albeit to a lesser effect. The position of this second excitation peak at around 385 nm is consistent with the excitation wavelengths of the model di-hydroxylated aromatic compound diethyldihydroxyterephthalate (Allen *et. al,* 2000), which suggests that after extended WOM exposure, di-hydroxylated aromatic species, whose production was first hypothesised by Pacifici and Straley (1969), may be responsible for this UV-modified fluorescence behaviour, and are hence a product of PET UV degradation.

The excitation of the 456 nm fluorescence by wavebands centred at approximately 340 and 380 nm correlates very well with the decreasing transmittance in the same wavelength regions revealed by Figure 4.2, which provides further support to the hypothesis that the production of fluorescing hydroxylated aromatic species contributes to the change in transmittance behaviour commonly observed in environmentally weathered PET film.

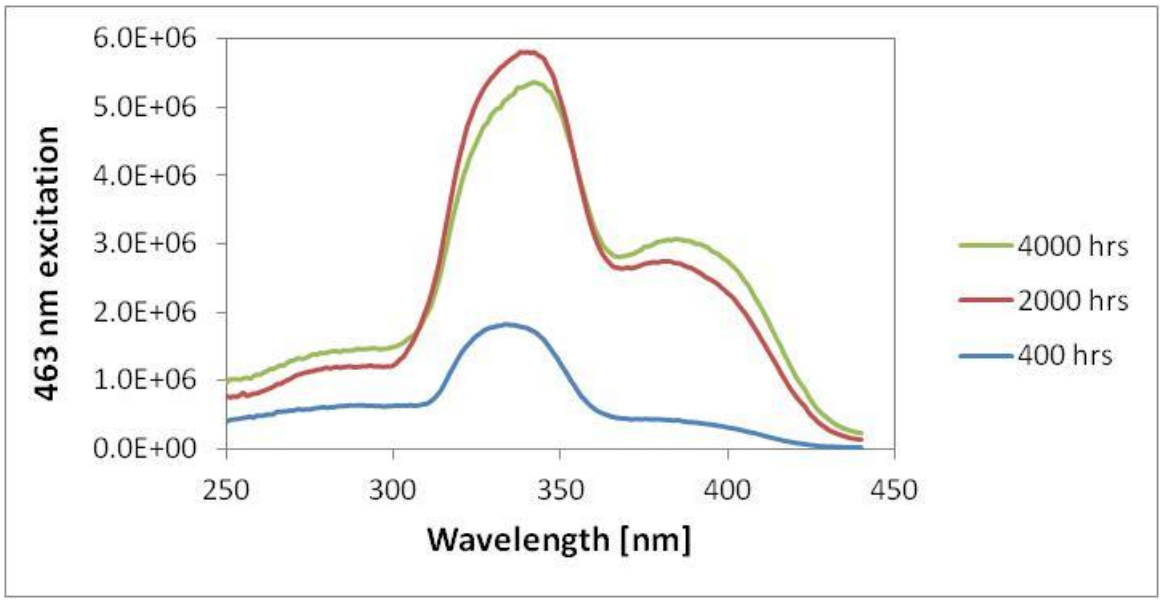

Figure 4.11: Raw fluorescent excitation spectra of PET film with 400, 2000 and 4000 hours WOM exposure (λ_{em} = 463 nm)

4.3.2.6 Optical properties discussion

There are several aspects of the presented optical data which are worthy of further discussion. In Fig. 4.4 the time-behaviour of the RST kinetic curves deviates from the emerging trend after 3200 hours, which brings the accuracy of the 3600 and 4000 hour measurements into question (to within around 10 %). Using an average of several measurements for each withdrawal time may have yielded more accurate

spectra, however, this would have increased the acquisition time and the number of samples required to be tested.

Further accuracy improvements of many of the dataset fits could be gained by employing more advanced data-fitting software than was available at the time of analysis or by increasing the time resolution of the weathering processes, as was done for the early stages of HISS exposure, where 100 hour intervals were used instead of 500 hours. However, utilising such shorter intervals may have negatively impacted other DTF weathering studies in progress in the WOM and DHO and so was ruled out.

In Fig. 4.9 after 2000 hours of WOM exposure, the change with exposure time of 456 nm fluorescence becomes erratic. This may be due to an error in the method, but was more likely due to surface microcracking affecting the quality of the measurement. As a bulk measurement, it should be possible to investigate the sample via the unexposed surface, rather than the exposed microcracked surface, while still detecting the degraded species fluorescence. Such a procedure would need to be applied to all samples to avoid introducing a results bias but may enable better comparisons between the fluorescence of microcracked and un-microcracked samples at high exposure times.

Additionally, after 1000 hours of HISS exposure there are no further increases in 456 nm fluorescence, however, the modified absorbance at 340 nm, proposed to be due to the same process, continued to grow linearly up to 2000 hours. This detracts from the hypothesis that the two observations are related to the hydroxylation of the PET aromatic ring, however, the majority of the analysis still points to this.

4.3.3 Chain scission behaviour

In Chapter 2, it was shown that UV photo-oxidation contributes greatly to the molecular chain scission (and consequent loss of performance properties) of PET films subjected to accelerated environmental weathering methods. However, many questions relevant to this Thesis remain, particularly concerning the individual contributions of elevated temperatures and humidity to degradation processes during accelerated environmental weathering, and their synergistic effects with UV radiation. This section presents results which explore these outstanding issues of interest with respect to PET film UV photo-oxidation in the bulk.

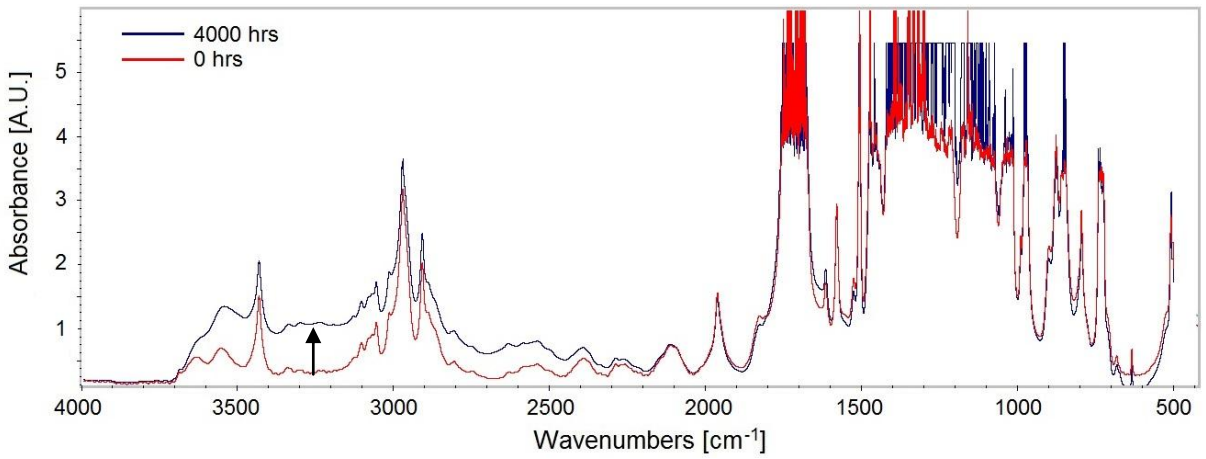

Figure 4.12: Transmission FTIR spectra of unexposed and 4000 hour WOM exposed PET film

4.3.3.1 Transmission Fourier transform infra-red spectroscopy

Figure 4.12 shows Fourier transform infra-red (FTIR) absorbance spectra collected in transmission mode between 400 and 4000 cm^{-1}, of PET film which received 0 and 4000 hours of WOM exposure. While the peak positions are unchanged, the IR absorbance is increased over a broad range of wavenumbers. This is consistent with

the findings of Day and Wiles (see section 2.2.1.2) and is indicative of an increase in the prevalence of -OH bonds in the film, in large part due to new -COOH end groups, produced as a result of photo-scission reactions. This phenomenon has been observed to varying extents in all the samples degraded for this Thesis and is formalised in Fig. 4.13 which presents the carboxyl index vs. exposure time for plain PET film samples exposed in the WOM, DHO and HISS.

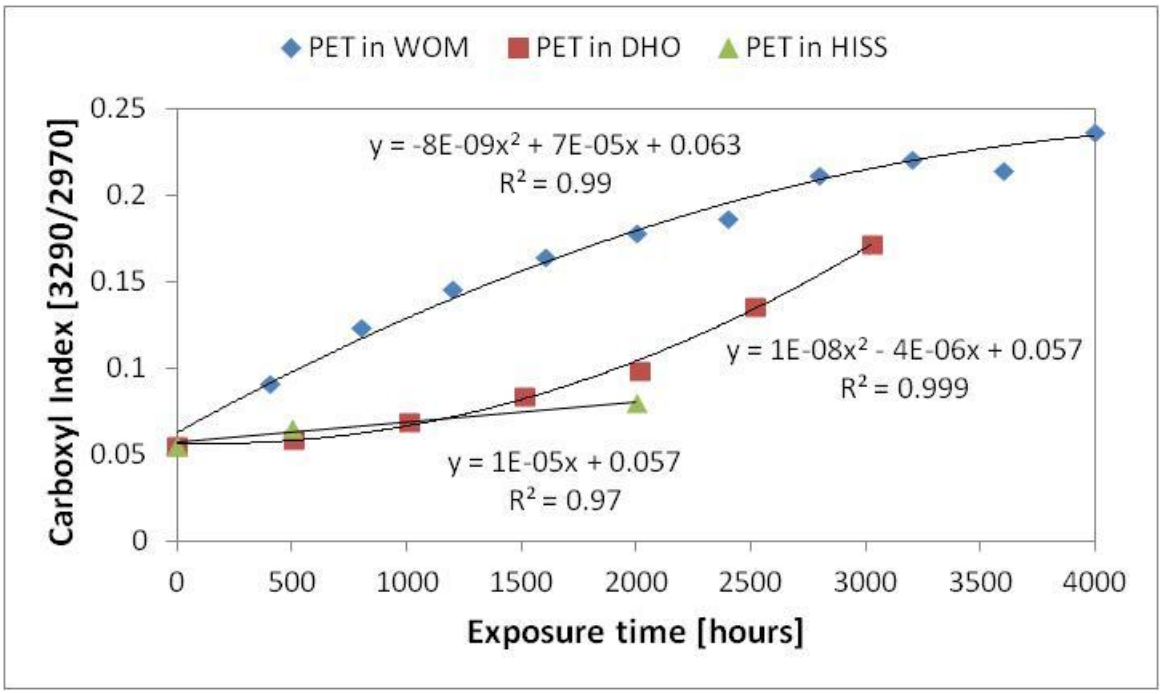

Figure 4.13: Carboxyl index vs. exposure time for PET film exposed in the WOM, DHO and HISS

The greatest overall increase in PET film carboxyl index, and therefore the largest number of chain scissions, has occurred due to WOM exposure, where the carboxyl index increases with exposure time with a rate of growth best described by a 2nd order polynomial with negative first term. The carboxyl index of PET film exposed in the DHO increases with exposure time, likely due to increasing numbers of -OH

groups produced as a result of hydrolysis at the ester linkage. It increases with a growing rate of change, up to the end of the exposure duration for that sample of 3024 hours. This difference between these two time behaviours is interesting as it suggests that in the DHO, PET film samples become more susceptible to hydrolysis chain scissions with exposure time, while in the WOM, PET film samples become less susceptible to bulk chain scission processes. PET hydrolysis is known to be a second order, auto-catalytic reaction, as -OH groups produced during hydrolysis can further catalyse the hydrolysis reaction (Ballara and Verdu, 1989, Pickett and Coyle, 2013). The degradation kinetics during accelerated environmental weathering however are much more complex, due to the simultaneous occurrence of several different degradation processes (photolysis, photo-oxidation and hydrolysis).

The far lower carboxyl index values of PET film exposed in the HISS shows that photo-scissions occur in the PET film bulk at a much slower rate due to HISS exposure than WOM exposure.

4.3.3.2 Carboxyl index discussion

There are several feasible explanations for the large discrepancy between the WOM sample carboxyl index curve, and the HISS and DHO sample carboxyl index curves:

i. Hydrolysis reactions occurring during WOM exposure are also responsible for a substantial number of chain scissions.
ii. Direct water contact due to the intermittent rain simulation cycle may have a much greater effect on the production of -COOH end groups in the bulk than previously thought.

iii. The additional presence of heat, humidity and direct water contact work synergistically with UV radiation to increase the rate at which photo-scissions occur.

Since carboxyl index (WOM) >> carboxyl index (DHO) + carboxyl index (HISS), the first point seems less likely than the latter two. The enhancing effect of direct water contact would also probably be much more pronounced after surface microcracking at 2000 hours, due to the significantly reduced barrier properties of the weathered surface, which is not observed. Therefore, the synergistic effects of heat, humidity and direct water contact with UV seem the most reasonable explanation for the greatly enhanced carboxyl index observed with WOM exposure.

More accurate results could have been obtained if water was removed from the samples by drying in an oven and/or measuring in a dry environment, however, the former was judged to be potentially damaging to the samples and the latter was not possible with the FTIR instrument used. Thus, sample water content may have lead to possible systematic and random errors.

To the author's knowledge this is the first time that the carboxyl index method of Day and Wiles has been used to monitor -COOH end groups produced as a result of hydrolysis reactions, which can also result in other forms of chain end groups, likely making the approximation of -OH end groups to chain scissions an underestimate for the DHO samples. Further, glycolysis may also occur under hydrolysing conditions which results in $-CH_2OH$ end groups (Sangalang *et al*., 2015), which also have likely not been captured by the carboxyl index.

The carboxyl index method of Day and Wiles is also utilised to great effect in the analysis of surface -COOH end group concentration and this effect is analysed in detail in the next Chapter on PET film surface degradation.

4.3.3.3 Gel permeation chromatography

Having shown differing bulk scission time-behaviours due to the three exposure techniques by the FTIR carboxyl index method, it was both desirable and logical to further explore the varying effects of the three exposure techniques on the PET film sample's molecular weight distributions (MWDs) by employing GPC. Additionally, GPC analysis can also be used to determine the molecular weight parameters of analysed samples, which allows for direct and quantifiable comparisons to be made between the various samples and hence the effects of the three exposure techniques on specific parts of the MWDs to be evaluated. In the following plots all MWDs are normalised with respect to area, the x-axis is a log scale and the y-axis is a function of weight fraction.

4.3.3.3.1 Molecular weight distributions

Figure 4.14 shows computed MWDs of PET film samples which received between 0 and 4000 hours of WOM exposure. Pre-exposure, the MWD is moderately skewed to the left; then with increasing exposure the distributions shift down and to the left while becoming broader and less skewed. The shift to the left indicates a reduction in average chain length and thus, reflects the number of chain scissions which occurred in that exposure interval. The rate at which the MWD shifts, decreasing with exposure time, suggests that the number of chain scissions occurring per unit time of exposure

is itself reduced with exposure time, which is consistent with the FTIR carboxyl index findings. The broadening of the MWD indicates that the spread of chain length values is increasing and the reduction in skewness is resulting in the PET film MWD becoming more log-normally distributed with exposure time.

Together these modifications indicate that a greater number of the above average length polymer chains are subject to chain scissions during WOM exposure, than below average length polymer chains. This suggests that longer chains are more susceptible to photo-scission than shorter length chains, which is reasonable as longer chains have a greater number of bonds available to scission than shorter chains. Notably, the distribution also broadens to the right with increasing exposure time, which is likely due to photo-crosslinking (White, 2009, Gardette *et al*., 2014). This feature of the MWD will be discussed in greater detail in section 4.3.4 Cross-linking behaviour.

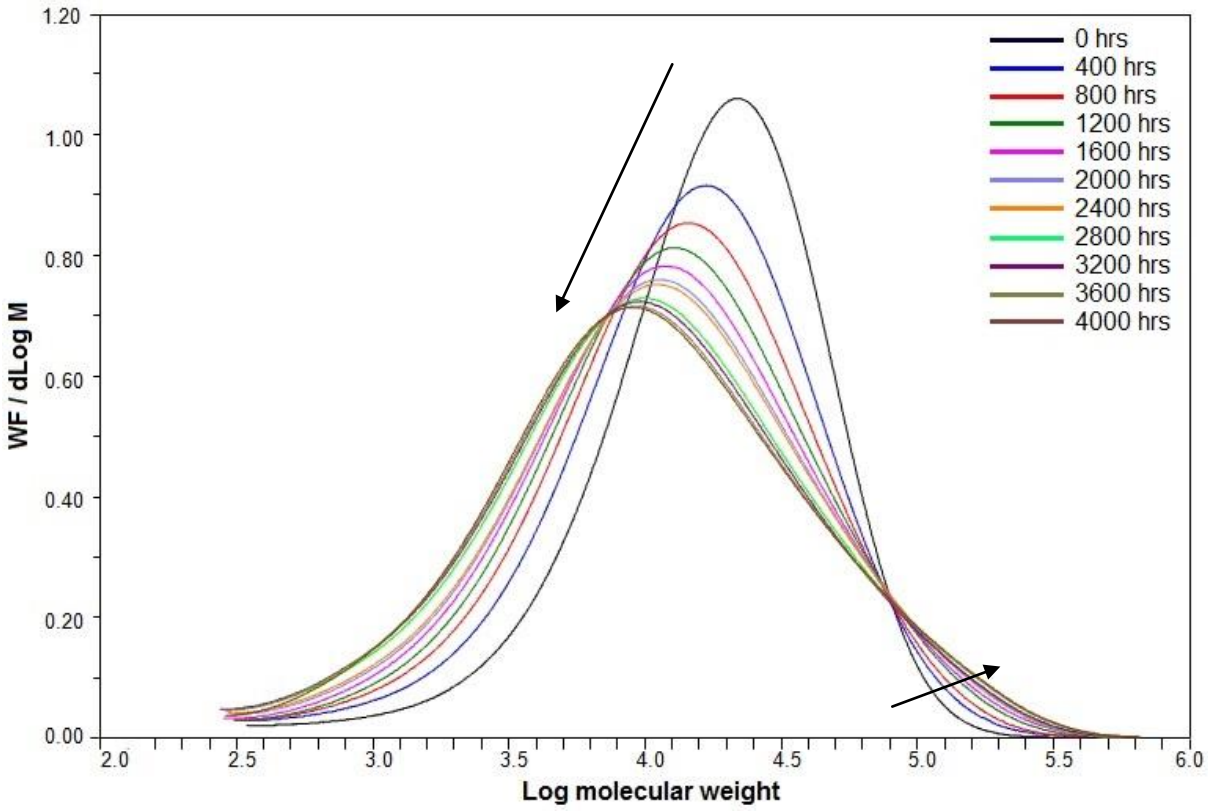

Figure 4.14: MWDs of PET film which received between 0 and 4000 hours of WOM exposure

Figure 4.15 shows computed MWDs of PET film samples which received 0, 500 and 2000 hours of HISS exposure. The modifications to the PET film MWD by HISS exposure are similar to the modifications due to WOM exposure, though lesser per unit exposure time in all respects, excepting the increase at the high molecular weight end of the distribution which appears greater after 2000 hours of HISS exposure than with 4000 hours of WOM exposure. These observations further confirm the role of UV radiation in the changes observed in the WOM PET film MWDs, and also suggest that the additional degradation agents present in the WOM (humidity, heat and direct water contact) must cause a substantial number of chain scissions, either independent of UV or synergistically, by increasing the degradative effect of UV radiation on the sample.

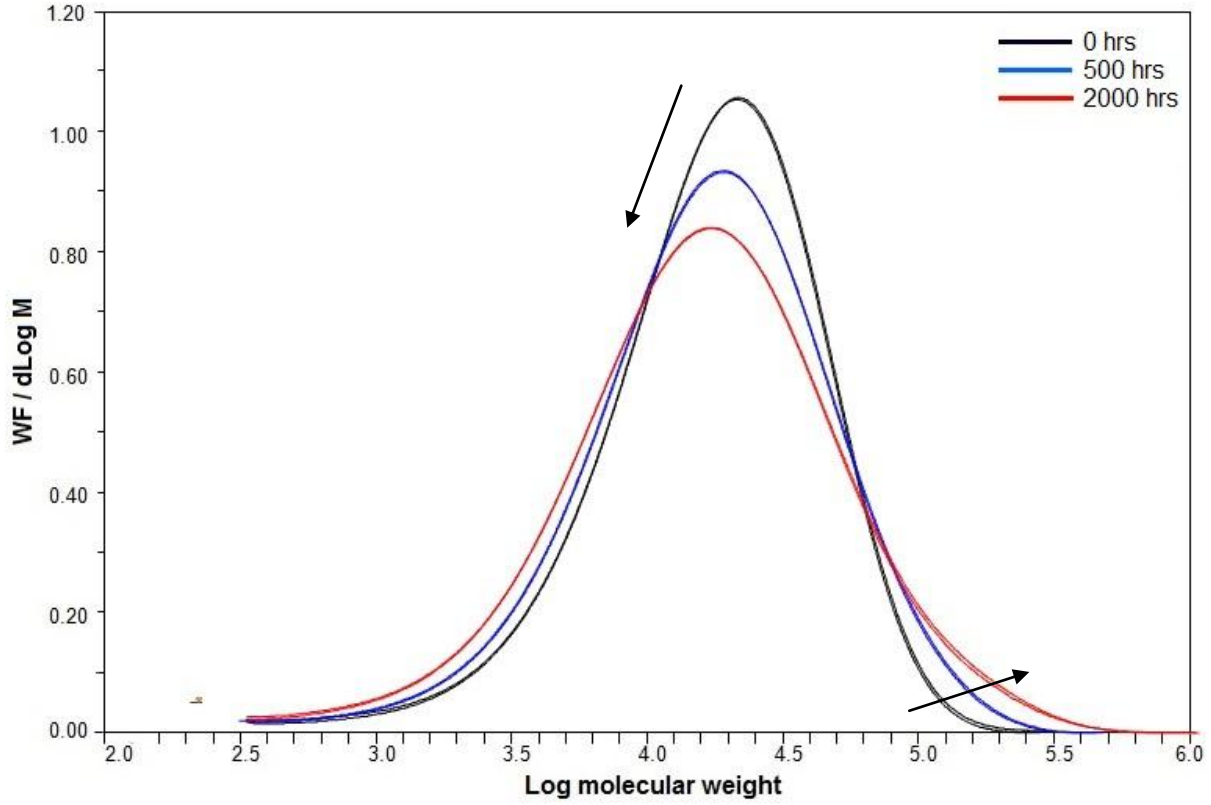

Figure 4.15: MWDs of PET film which received between 0 and 2000 hours of HISS exposure

Figure 4.16 shows computed MWDs of PET film samples which received between 0 and 3024 hours of DHO exposure. With DHO exposure the MWD is again shifting to the left as expected, but this time much more regularly than was observed with WOM and HISS exposure, which represents a consistent drop in chain lengths due to hydrolysis over the whole of the MWD. There also appears to be no change in the shape of the distribution with DHO exposure, which indicates that unlike with WOM and HISS exposure, chain length has no impact on the likelihood of chain scissions occurring in any particular length of polymer chain. The slight shift upwards of the MWD with exposure time suggests that the chain length standard deviation is being reduced with increasing exposure, although this is a relatively minor change.

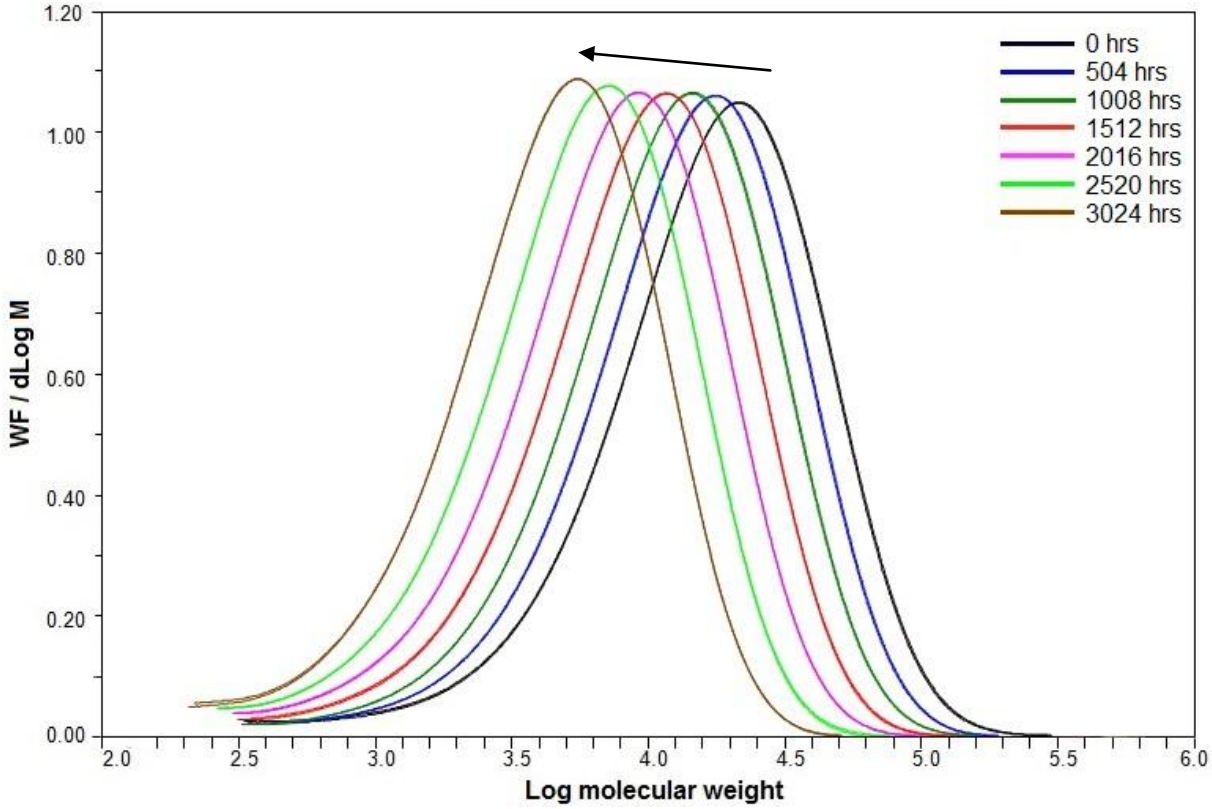

Figure 4.16: MWDs of PET film which received between 0 and 3024 hours of DHO exposure

To illustrate the differences between the effects of the three exposure techniques on the PET film MWD, Figure 4.17 is presented which shows computed MWDs of PET film samples after approximately 500 hours of DHO and HISS exposure and 400 hours of WOM exposure. It should be clear from this figure that to compare the full effects of the different exposure techniques side by side is highly impractical, due to the number of curves that would be needed in the same plot. Therefore, to quantitatively compare the effects of the three exposure techniques over the entire exposure duration, it is simpler to view the molecular weight parameters with exposure time, rather than the MWDs themselves.

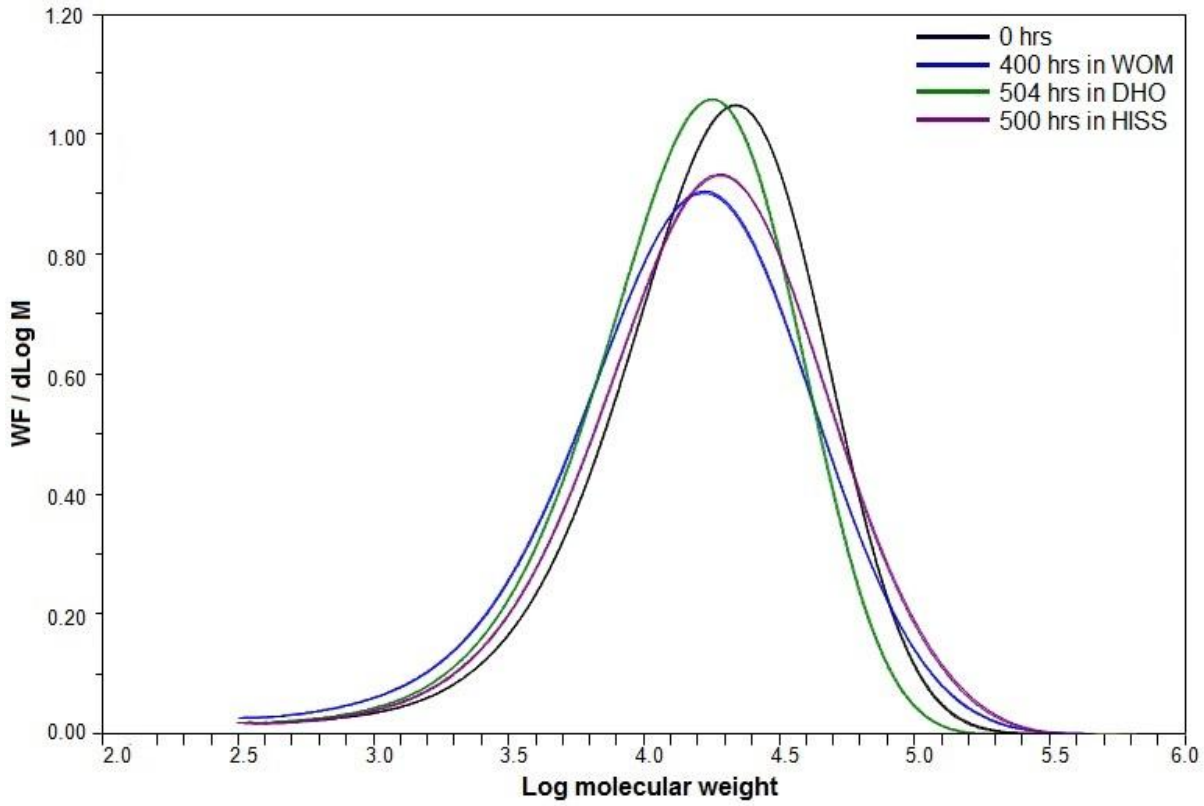

Figure 4.17: MWDs of PET film after approx. 500 hours of WOM, DHO and HISS exposure

4.3.3.3.2 Molecular weight parameters and degradation kinetics

Figure 4.18 shows a plot of number average molecular weight (M_n) vs. exposure time, for plain PET film samples exposed in the WOM, DHO and HISS. Both DHO and HISS sample M_n exhibit linear decreases with exposure time, suggesting constant rates of chain scission throughout the exposure durations. The WOM PET film M_n data exhibits a greater initial decrease with exposure time, however, it continues with a decaying rate of change, which reaches 0 at greater than 3000 hours of exposure. This suggests that the effect of the WOM on the PET film sample M_n is greatest when the sample is first exposed, and that this effect is lessened with subsequent exposure intervals, until around 3000 hours when exposure appears to

no longer have a significant effect on sample M_n, and thus, chain scissions appear to have ceased occurring.

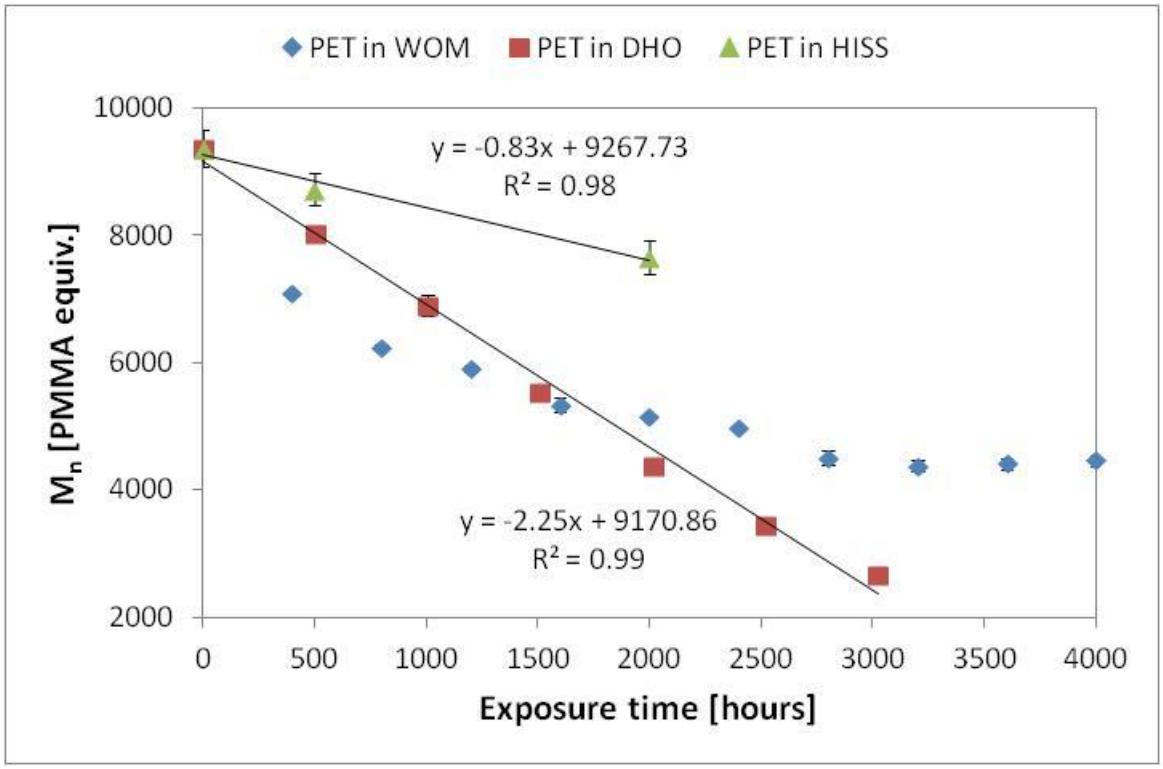

Figure 4.18: M_n vs. exposure time for PET film exposed in the WOM, DHO and HISS

Figure 4.19 shows a plot of weight average molecular weight (M_w) vs. exposure time, for plain PET film samples exposed in the WOM, DHO and HISS. M_w is a weighted average rather than number average and is therefore more greatly affected by the higher molecular weight chains of the MWD than M_n. All the M_w curves exhibit approximately linear kinetic behaviour, however, none moves in the same direction as another. The DHO sample M_w is reduced to approximately one fifth of its initial value after 3024 hours due to hydrolysis, while the HISS sample M_w increases by approximately one fifth of its initial value after 2000 hours exposure, despite the degradative action of UV radiation on PET film M_n already shown. This is likely due to

photo-crosslinking increasing the amount of high molecular weight material in the HISS sample, which in this case has had a greater effect than chain scissions on the M_w parameter. The WOM sample M_w however remains approximately constant over the entire 4000 hour exposure duration, which suggests that the greater amount of chain scissions occurring during WOM exposure has balanced the M_w increasing effects of the photo-crosslinking reaction, yielding an insignificant overall change even after 4000 hours of exposure time. However, considering that WOM exposure causes the greatest loss of material properties in PET film, this result shows that M_w does not provide a good overall measure of PET film degradation.

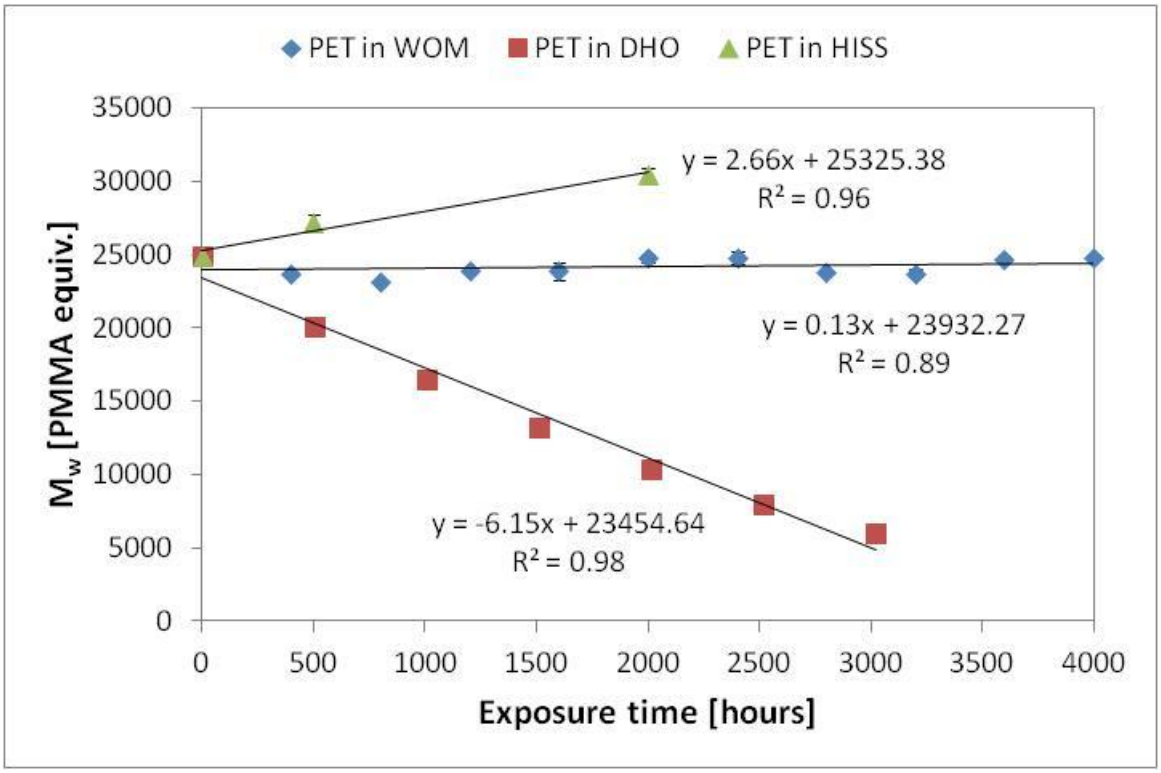

Figure 4.19: M_w vs. exposure time for PET film exposed in the WOM, DHO and HISS

Figure 4.20 shows a plot of dispersity vs. exposure time, for plain PET film samples exposed in the WOM, DHO and HISS. This plot reflects the changing breadths of the

MWDs with exposure time and is thus, a quantified measure of the change in chain length variance with exposure. As expected from the changes in shapes of the MWDs with exposure time, the DHO sample shows little change in its dispersity, while the WOM and HISS samples both show increasing dispersity with exposure time. The greater and more rapid increase is shown by the WOM exposed samples, likely due to the greater amount of chain length reduction occurring with WOM exposure than with HISS exposure. The rate of change in dispersity of the WOM exposed sample decays with exposure time, reaching zero after 3600 hours, which suggests no further change in the breadth of the MWD after this point.

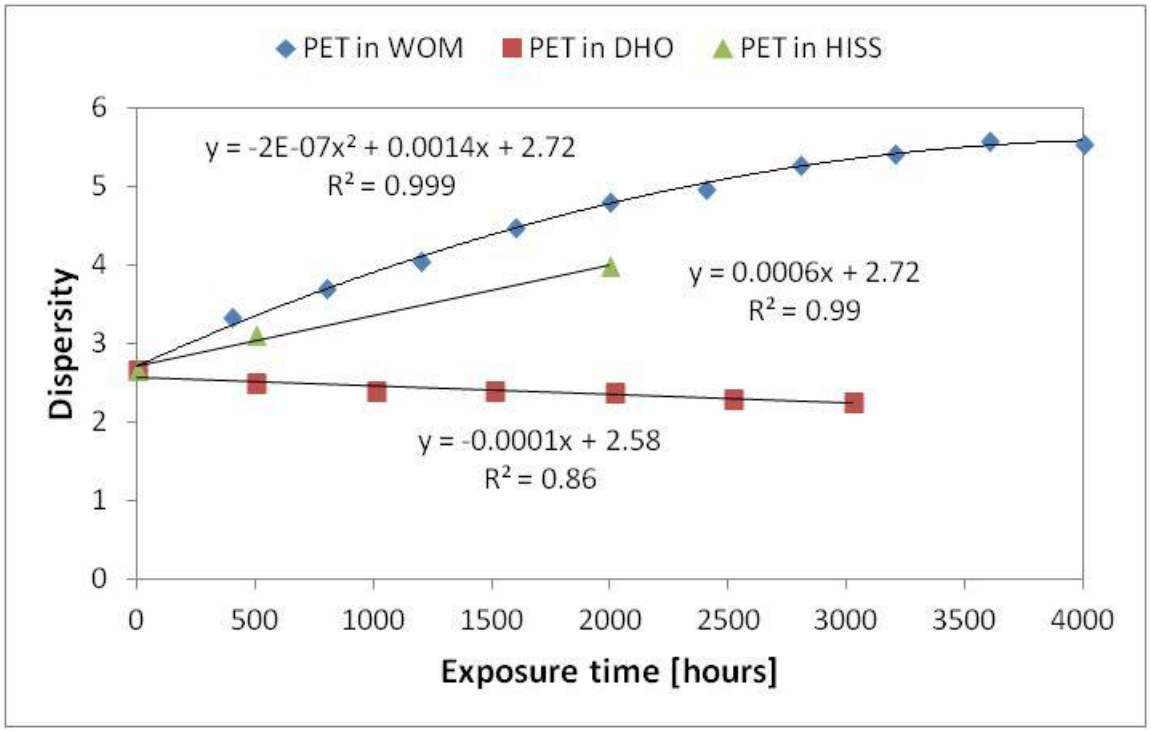

Figure 4.20: Dispersity vs. exposure time for PET film exposed in the WOM, DHO and HISS

Figure 4.21 shows the random chain scission approximation for plain PET film samples exposed in the WOM, DHO and HISS. By assuming the chain scission

processes responsible for the reduction of M_n, observed in Fig. 4.18, are random, the random chain scission approximation yields information about the kinetics of the degradation processes. Specifically, each curve represents the rate at which chain scissions were occurring in the plain PET film samples over the course of the exposure duration, via the relevant degradation pathways (hydrolysis and/or photo-scission). Thus, in the HISS, the rate at which photo-scissions were occurring increased with exposure time at a linear rate, though with only three datapoints it may be desirable to investigate this further. In the DHO, the rate at which hydrolysis chain scissions were occurring was increased with exposure time at a second order polynomial rate, which is consistent with recent PET hydrolysis literature findings (Pickett and Coyle, 2013) and further suggests that PET film samples become more susceptible to hydrolysis with increasing DHO exposure. In the WOM, the combined rate at which hydrolysis and photo-scissions were occurring decreased with exposure time, until after 2800 hours when the rate of increase fell to approximately zero.

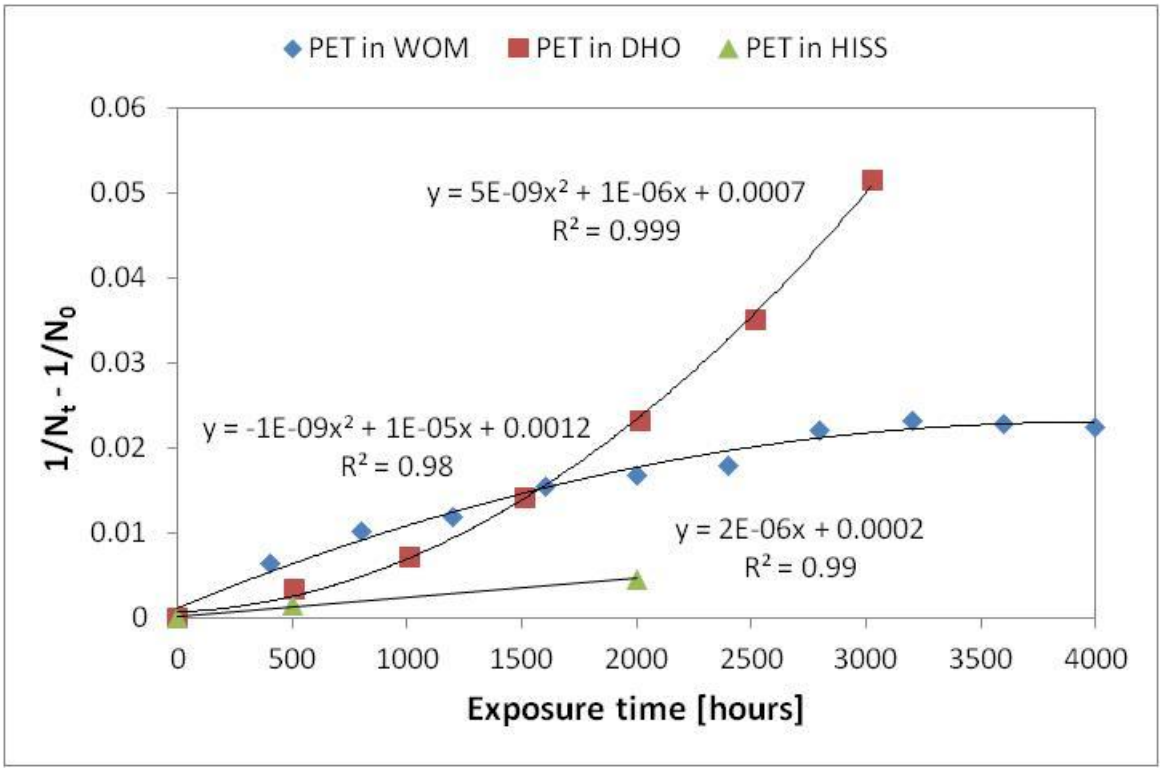

Figure 4.21: Random chain scission approximation for PET film samples exposed in the WOM, DHO and HISS

4.3.4 Cross-linking behaviour

4.3.4.1 M_z modification

Figure 4.22 shows a plot of Z average molecular weight (M_z) vs. exposure time, for plain PET film samples exposed in the WOM, DHO and HISS. M_z is the third moment of the MWD and its value is largely dependent on the above average length chains of the MWD, even more so than M_w. It can therefore be used as a quantified measure of the extent of photo-crosslinking in polymers and has been used to that effect in this Thesis. For the WOM and HISS exposed samples, the increasing M_z observed with exposure time strongly indicates that photo-crosslinking occurs with UV exposure, and with greater effect due to isolated UV exposure with the HISS. This discrepancy in M_z between WOM and HISS samples is likely to be due to the greater number of

chain scissions occurring due to WOM exposure, which could prevent the sample M_z from becoming as high as rapidly as with HISS exposure.

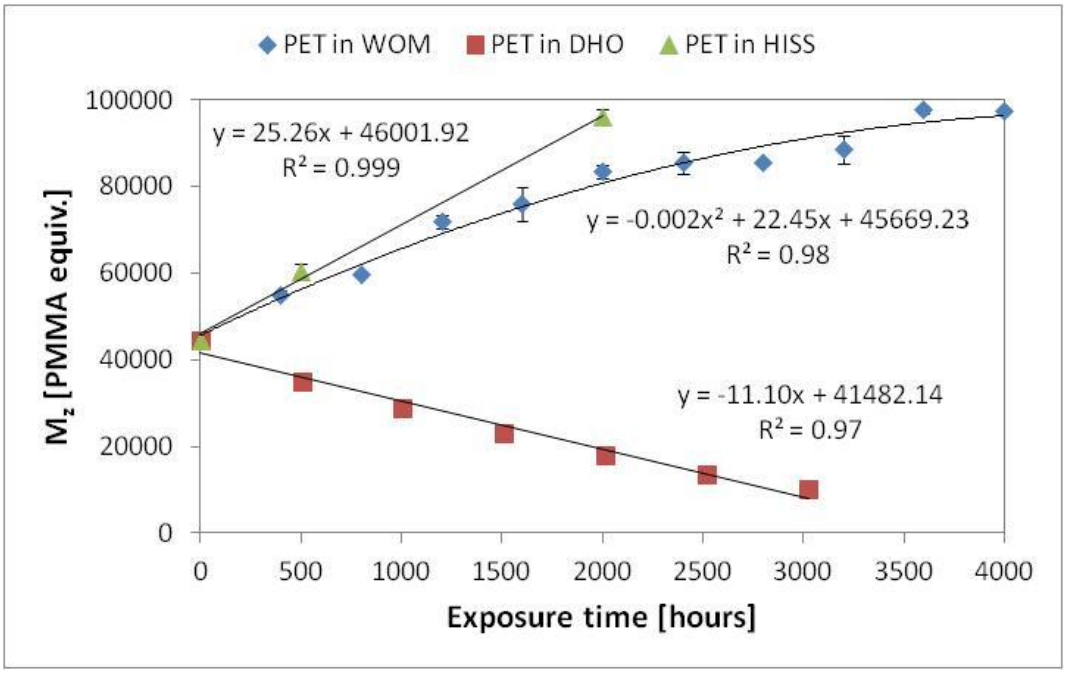

Figure 4.22: M_z vs. exposure time for PET film exposed in the WOM, DHO and HISS

4.3.5 PET MWD discussion

Several of the molecular weight parameters presented reached a lower limit (greater than zero) before the end of the sample exposure duration. In the UV exposed samples this may be related to the surface nature of PET UV degradation (~ 45 µm according to recent a recent study (Gardette *et al*., 2014)) and the thickness of the samples weathered in this Thesis (~ 175 µm). This cannot be discerned by GPC, however, it should be realised that by analysing the film in bulk, the localised effect of the photo-crosslinking reaction at the surface will have been significantly diluted by the remaining unaffected material beneath it, which for 175 micron PET film, is the majority of the sample. It is reasonable therefore, that the much less degraded bulk

of the film, below the penetration depth of damaging UV light, may prevent the parameters, which are derived from the whole of the sample, from falling below a certain level, despite the severe degradation occurring in the upper 45 microns of the PET film surface. This hypothesis will also be further explored in the next Chapter.

A further interesting observation is that the curve behaviours for each of the exposed sample types are the same in the random chain scission approximation (Fig. 4.21) as in the transmission FTIR carboxyl index plot (Fig. 4.13), which could indicate that in this case the carboxyl index reflects the reaction kinetics. This is a reasonable assessment when we consider that the carboxyl index is measuring the proportional increase in end groups produced and is thus worthy of further investigation.

4.4 Additional Chapter discussion

A common observation of several of the degradation parameters presented in this Chapter was that they exhibited decaying rates of change with increasing exposure time, which in some cases reached zero after several thousand hours of exposure. This suggests that samples became less susceptible to the applied degradation agents with increasing exposure. Possible explanations for this observation can be related to two main phenomena:

i. The decreasing amount of reaction substrate with increasing exposure.
ii. Increasing sample resistance to degradation with increasing exposure.

Unexposed samples have the greatest number of available reaction sites, and as their number is reduced, the number of reactions occurring which result in the observed changes will also be reduced.

Increased degradation resistance, or weatherability, may be achieved in the bulk as a result of photo-crosslinking generating an improved barrier against oxygen and moisture at the surface. If an improved barrier is increasing weatherability, then logically surface microcracking should substantially worsen the barrier properties of the film and the rate of degradation will increase. This hypothesis will be tested in the next Chapter, where the effects of accelerated environmental weathering on the PET film surface will be isolated for investigation and compared with bulk assessments.

Another factor which may have affected rates of UV degradation is the increasing concentrations of UV-fluorescent degraded species. With increasing concentration, more of the energetic photons which originally could be contributing to the scission of polymer chains will be being absorbed and re-emitted by the fluorescing hydroxylated aromatics, thereby dissipating some of the incident UV energy and reducing the rate at which scission reactions can occur.

Regarding the HISS exposed sample, despite the many modifications observed, which indicated the occurrence of a substantial number of photo-scissions, the film samples remained in good physical condition to the end of the exposure duration. This may be due to photo-crosslinking enhanced physical properties, or the lack of chain scissions in high enough quantities.

Due to the small exposure area of the HISS, only 40 mm diameter discs of film could be exposed at any one time. This, combined with the long exposure hours which were found to be necessary to yield observable modifications, lead to there being only 2 exposed samples available for GPC and transmission FTIR: a 2000 hour sample, exposed and non-destructively characterised every 500 hours; and a 500 hour sample exposed and non-destructively characterised every 100 hours

(commissioned to improve the time resolution in the early stages of sample modification by HISS exposure). Thus, in some cases with only three datapoints, it has not been possible to well determine the nature of the time behaviour of the HISS exposed sample degradation parameters. However, the datapoints presented still provided interesting information and informed deductions about the role of UV degradation in accelerated environmental weathering, and therefore also in general.

Another bulk film property set which would have been interesting to monitor with weathering time are bulk mechanical properties, however, due to the limited amount of sample available and the destructive nature of film mechanical property measurement this could not be attempted. To gain some understanding of the effects of degradation agents on PET film mechanical properties, surface mechanical properties have been assessed, the results of which are presented in the next chapter.

4.5 Chapter conclusions

The findings presented in this Chapter support the following conclusions:

- PET films exposed to accelerated environmental weathering exhibit modifications characteristic of both UV and humidity exposure: photo-oxidation, photo-crosslinking and hydrolysis.
- In PET film samples exposed to UV in the absence of heat, humidity and direct water contact, the effects of photo-crosslinking on bulk film properties are more prominent than those of photo-scissions.
- PET film samples exposed in the WOM exhibited greater levels of degradation than the combined levels exhibited by HISS and DHO exposed samples. This

suggests a synergistic contribution during WOM exposure of UV with humidity, heat and/or direct water contact, which has not been previously identified.

- UV exposed PET MWDs revealed that photo-scissions occurred more frequently in above average length polymer chains than in below average length chains.
- Individual molecular weight parameters do not adequately describe the multiple effects of artificial weathering on PET film, and thus, a combination of molecular weight parameters and analysis of the MWD itself is recommended for this purpose.
- Modified PET film transmittance and fluorescence behaviour appear to both be due to the production of hydroxylated aromatic species by UV radiation. Evidence for the production of both mono-hydroxylated and di-hydroxylated species has been presented.

SURFACE PROPERTY MODIFICATION OF ARTIFICIALLY WEATHERED PET FILM

5.1 Chapter introduction and objectives

The direction of research in this Chapter was informed by the following hypotheses:

i. During accelerated environmental weathering, UV radiation is the main degradation agent responsible for the surface degradation of PET film. Thus, exposure to intense UV radiation of terrestrial wavelengths for long periods will result in modifications to PET film surface properties, which lead eventually to surface microcracking.

ii. In addition to causing the hydrolysis of PET film, direct water contact and humidity coupled to heating, synergistically enhance the PET film UV degradation process.

iii. Features of PET film surface degradation will be more pronounced than bulk degradation per unit exposure time, as the film surface is the interface between the sample, the degradation agents and the oxygen in the environment, that together cause the PET photo-oxidation reaction suspected of leading to PET film surface microcracking.

Therefore, with these hypotheses in mind, the objectives of this Chapter are broadly:

- To investigate the surface property modification of plain 175 µm DTF PET film with exposure in the laboratory artificial weathering apparatus described in Chapter 3 - damp heat oven (DHO), high intensity solar simulator (HISS) and the weather-o-meter (WOM), which is effectively the combination of the other two apparatus.

- Develop an understanding of PET film surface UV degradation processes by comparing the results of each different treatment and also by comparing these effects with bulk degradation results.
- Develop an understanding of the individual and synergistic roles of the PET degradation agents - UV radiation, water and heat - in surface degradation due to accelerated environmental weathering.

5.2 Surface property modifications

Various analytical techniques have been employed to examine the modification of a broad range of PET film surface properties with artificial weathering. Comparisons are made between the effects of the different exposure regimes; and also between the weathered and rear surfaces of the exposed samples, as the majority of UV wavelengths are absorbed during transmission through the film bulk and are hence thought not to be a factor in rear surface degradation of films of greater than 50 micron thickness.

The modifications observed with artificial weathering are then related to the chemical processes known to occur due to the artificial weathering of PET film. This analysis has revealed a more complete picture of PET surface degradation processes during artificial weathering, which will aid in the application of new strategies designed to prevent features of PET film degradation from inhibiting PET film application performance.

5.2.1 Surface optical property changes

The modification of surface gloss with artificial weathering is examined in accordance with ISO 2813 (2014). Gloss is a macroscopic optical property and is of importance to DTF, and its customers, as it is one of many aesthetic film properties which can easily be judged with the naked eye. Fig. 5.1 shows the 60° gloss vs. exposure time of the weathered surface of PET film samples exposed in the WOM, DHO and HISS. It reveals that there are no significant PET film surface gloss changes with DHO and HISS exposure. The WOM exposed PET film weathered surface shows the same behaviour up to 1600 hours, however, from 2000 hours of exposure gloss has dropped substantially from approximately 170 gloss units (GU) to approximately 40 GU (black arrow in Fig. 5.1), then dropping further to almost zero after 4000 hours of exposure.

5.2.1.1 Surface optical property discussion

It should be noted that gloss values are intended to range between 0 and 100 gloss units, but polymer films often exhibit higher values due to having multiple reflecting surfaces (front and rear) and the additional contribution of internal reflections (ASTM D2457, 2013). This issue cannot be easily resolved and as such, film industry researchers often utilise values outside of the 0-100 range. Using a 20° gloss measurement can help to minimise this effect, however 60° gloss was chosen in this case to give higher instrument sensitivity on the low gloss weathered films.

PET film gloss is primarily determined by its surface roughness (Assender, 2002), or more accurately by its surface slopes (Rakos, 2014). Surface microcracking, which achieves total coverage of the weathered surface by 2000 hours of WOM exposure,

will greatly increase the film surface slopes and is likely responsible for the significant drop in gloss revealed by Fig. 5.1. Weathered PET film surface roughness and slopes will be examined directly later in this Chapter.

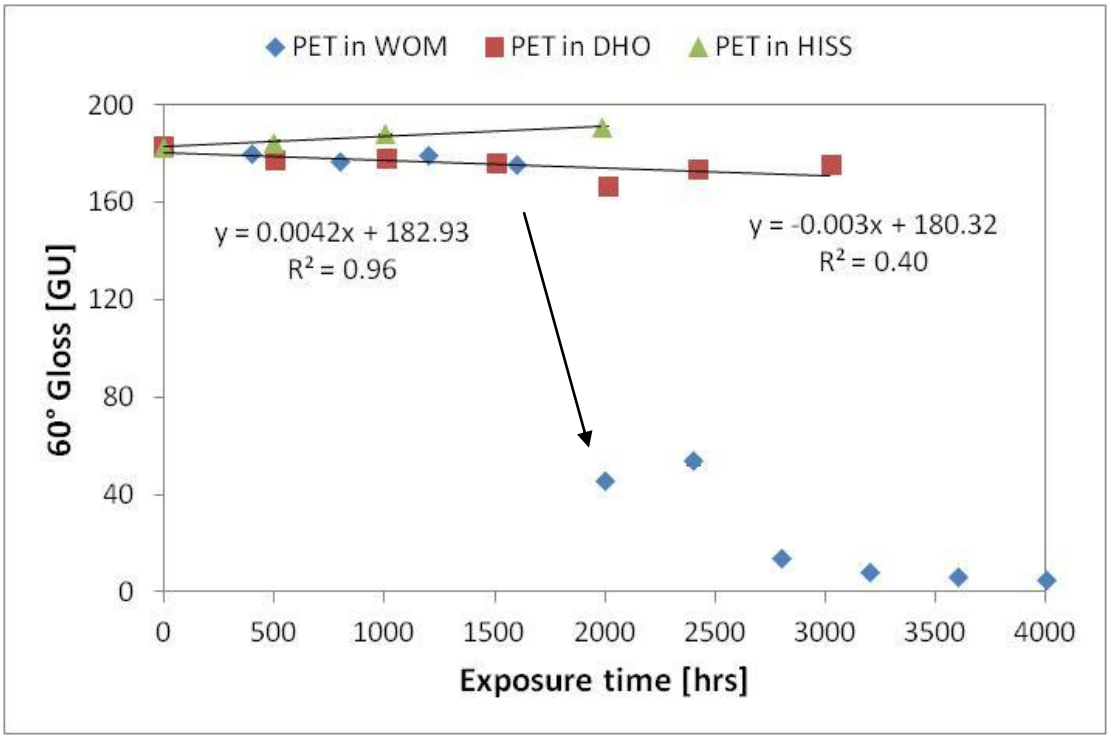

Figure 5.1: 60° gloss vs. exposure time of the weathered surface of PET film samples exposed in the WOM, DHO and HISS

5.2.2 Microscopic sample surface changes

Optical microscopy was employed to resolve the microscopic physical features of PET surface degradation due to WOM exposure. No modifications to the DHO and HISS exposed sample surfaces were observed using optical microscopy.

Figure 5.2 a-c shows reflection mode images captured by the optical microscopy of weathered PET film sample surfaces which received 0, 2000 and 3200 hours of WOM exposure. These images illustrate representative examples at this length scale, of the initial homogeneity and subsequent extreme modification of the weathered

PET film surface in the form of surface microcracking, which occurs and propagates at the intermediate and advanced stages respectively of PET film WOM exposure. Microcracks presented with both hairline structure and with wider, measurable thicknesses and efforts to quantify these properties will be presented in the following section.

After 2000 hours of WOM exposure, surface microcracks such as those shown in Fig. 5.2b extend over the entire weathered film surface and are aligned mainly with the machine direction, with fewer interconnecting cracks aligned with the transverse direction. After 3200 hours of WOM exposure (Fig. 5.2c) the microcracks perpendicular to the machine direction present with greater frequency and all microcracks are of greater width than any observed after just 2000 hours of WOM exposure. These observations suggest that further WOM exposure causes established microcracks to widen, which can be explained by the lateral shrinkage of the inter-crack PET regions, and the subsequent propagation of the microcracks.

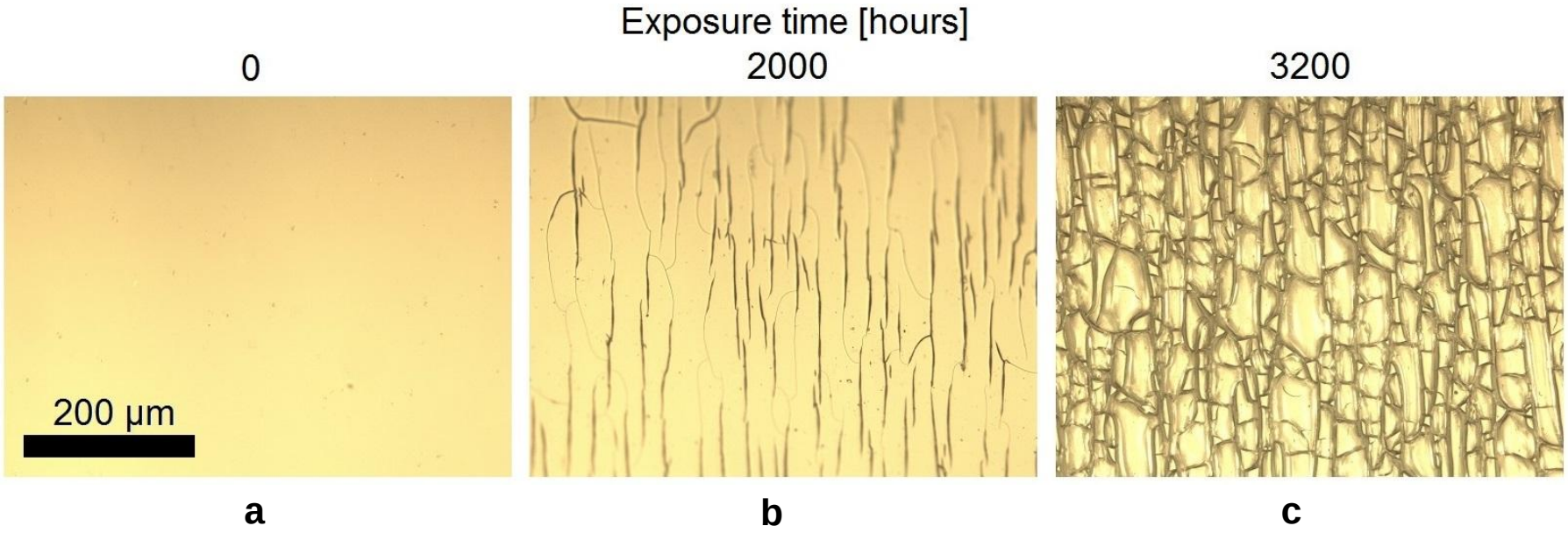

Figure 5.2 a-c: Reflection mode optical micrographs of weathered PET film surfaces which received 0 (a), 2000 (b) and 3200 (c) hours of WOM exposure - Scale bar applies to all images

5.2.2.1 Surface microcracking discussion

The direction of microcrack propagation is likely a function of the PET film drawing process and the semi-crystalline nature of PET film, briefly described in Chapter 3, and in greater detail by MacDonald (2004). PET film is bi-axially drawn to increase its mechanical strength in the machine and transverse directions by aligning the polymer molecular architecture along these axes and then encouraging these regions to crystallise. As the machine direction drawing occurs first during production, more PET molecules, and hence crystallites, are aligned with the machine direction and cracks are most likely to occur along this axis as there are the fewest number of interconnecting tie molecules aligned with the transverse direction.

PET film lateral shrinkage, which is proposed to affect microcrack propagation, normally occurs as a result of chain reorganisation due to exposure to elevated temperatures, typically above the T_g of PET. However, Allen *et al.* (1991) proposed that water can have a plasticising effect on the PET film surface, which would allow chain reorganisation, and hence shrinkage, to occur at the WOM exposure temperature, 10° C below the T_g of PET. Photo-crosslinking, which results in the densification of the film surface could also be playing a role in PET shrinkage during weathering and more will be done to verify this proposed contribution when surface mechanical properties of weathered films are examined at the end of this Chapter.

Further evidence is required to answer the following questions related to surface microcracking:

i. What processes are initiating surface microcracking?
ii. Do processes other than photo-oxidation play a significant role?
iii. Do material properties such as crystallinity and roughness contribute?

Optical microscopy yields a limited amount of lateral information and no height information at all regarding surface microcracking. Thus, more advanced surface analysis techniques must be employed to better characterise surface microcracking and the early stages of PET film surface modification due to artificial weathering if we are to better the understanding of PET film surface degradation and microcrack formation.

5.2.3 Surface chemistry changes

In Chapter 4, chain scission behaviour was characterised with artificial weathering exposure time in the PET film bulk, using transmission FTIR spectroscopy and the carboxyl index method of Day and Wiles (1972a). This technique can also be applied to the PET film surface using the attenuated total reflection (ATR) function of an infra-red spectrometer. This section will present results which utilised this function to investigate the modification of PET film surface chemistry with artificial weathering, as well as water contact angle (WCA) modification, which illustrates the surface's changing affinity with water with increasing exposure time.

5.2.3.1 Attenuated total reflection (ATR) FTIR

ATR-FTIR spectroscopy has been utilised to analyse the chain scission behaviour of the weathered PET film surfaces. More accurately, of the uppermost 1.3-2.7 microns of the inspected samples, as this is the approximate penetration depth of the technique into PET film, due to the angle of incidence of the beam and the refractive indices of the materials at the interface (Harrick and du Pré, 1966).

Figure 5.3 shows the ATR carboxyl index vs. exposure time of the weathered surfaces of plain PET film samples exposed in the WOM, DHO and HISS. It reveals that exposure each of the three weathering apparatus caused the surface carboxyl index to increase. This represents an increase in the concentration of in-chain -OH end groups, which are in this case produced by chain scission reactions occurring in the uppermost 1-2 microns of the PET film samples. The WOM exposed PET film weathered surface displays by far the greatest change in carboxyl index, reaching a maximum of approximately 0.6 after 1600 hours. The flattening off of the increase at 0.6 suggests that chain scissions are no longer occurring in significant numbers in the uppermost 1-2 microns of the samples after 1600 hours. This is an unexpected finding as from the optical microscopy observations it is evident that surface microcracks, thought to occur as a result of surface chain scissions, continue to develop up to the end of the 4000 hour exposure duration. Therefore, together these results suggest that chain scissions at the film surface do not contribute significantly to the continued development of PET film surface microcracks, however, they likely still do contribute to their nucleation.

The PET in DHO and HISS curves exhibit much smaller changes with exposure time than the PET in WOM curve, which suggests that the conditions experienced by these samples causes surface chain scissions to occur in far fewer numbers than WOM exposure. This, in conjunction with the comparable levels of UV in the HISS and WOM, and with the comparable levels of temperature and humidity in the DHO and WOM, suggests that the effects of elevated temperature, water spraying and synergistic effects with UV radiation cause substantially more chain scissions to

occur at the PET film weathered surface than UV alone, or temperature and humidity in the absence of UV radiation.

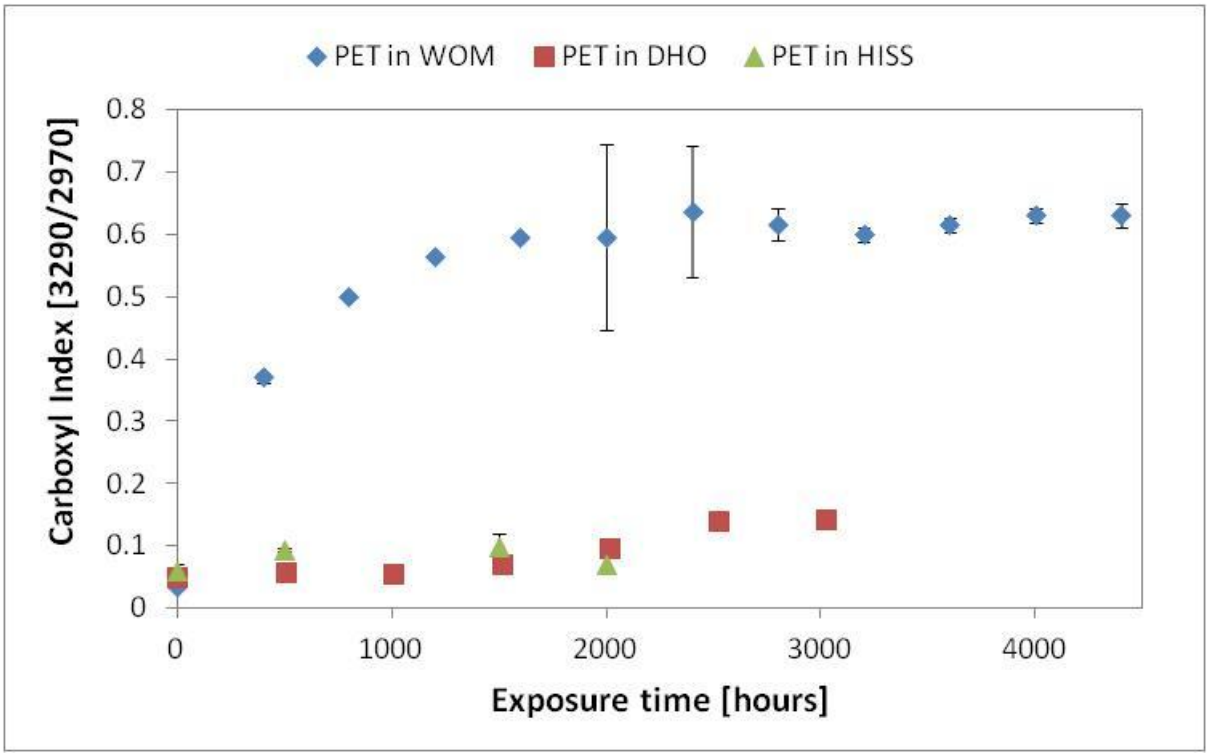

Figure 5.3: ATR carboxyl index vs. exposure time of the weathered surface of PET film samples exposed in WOM, DHO and HISS

Figure 5.4 shows carboxyl index vs. exposure time for WOM exposed PET film sample weathered surfaces, rear surfaces and in the bulk. All three curves exhibit growth with exposure time, which decays to a minimum after 1600 hours. The curves indicate that in WOM exposed PET film, the rate of chain scissions is greatest at the weathered surface, while the rear surface and bulk experience relatively lower rates of chain scissions. This is consistent with similar findings presented in the literature (Blais *et al.*, 1973, Papet *et al.*, 1987, Audouin *et al.*, 1994, Fechine *et al.*, 2004, Gardette *et al.*, 2014) which indicate that the UV absorbance properties of PET and diffusion limited oxidation (DLO) both likely contribute to the disparity between front,

rear surface and bulk chain scissions. However, UV absorbance is likely to be the more critical factor in this case, as the UVB photons associated with the photo-scission of PET are mostly absorbed by the uppermost 45 µm of film (Gardette *et al.*, 2014), and therefore cannot propagate through the 175 µm thick film sample to reach the rear surface PET molecules in significant numbers. Finally, unlike at the weathered surface, the rear surface and bulk carboxyl index curves do not reach an upper limit, which indicates that scission reactions were still occurring up to 4400 hours of exposure. This is likely to be since scissions were occurring in much lower numbers per exposure interval and did not reach a saturation point, as was observed at the weathered surface.

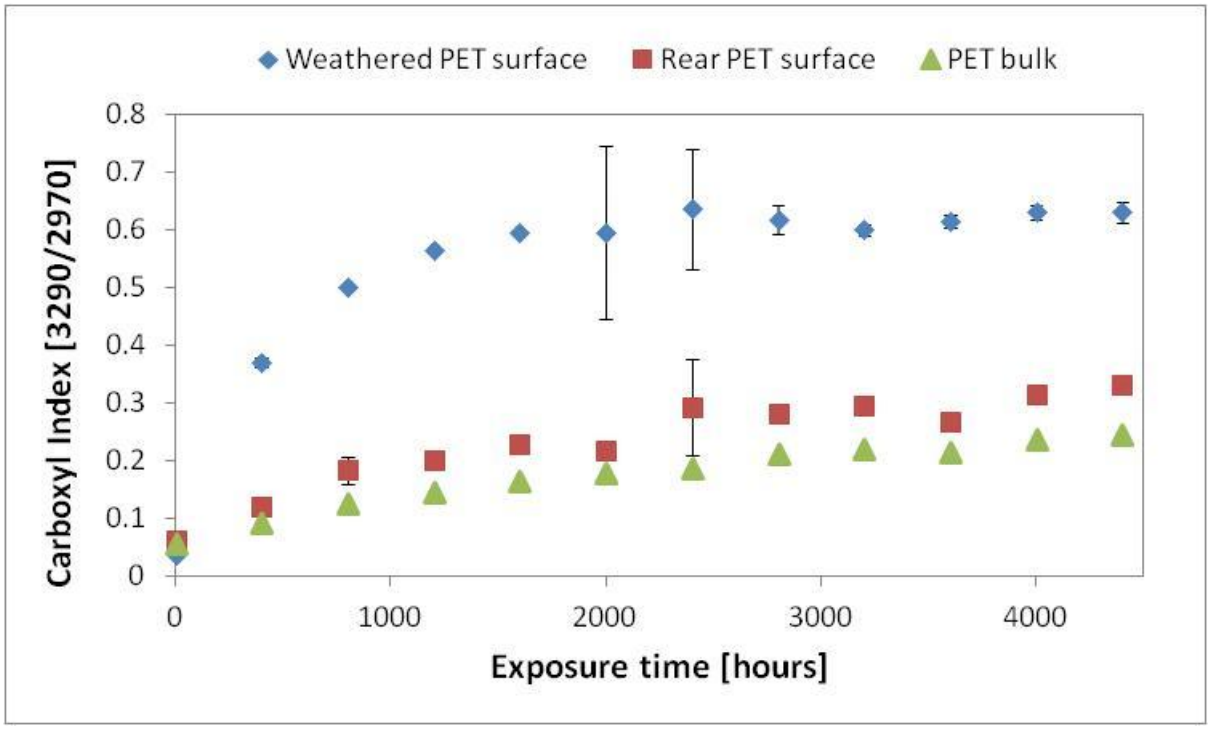

Figure 5.4: Carboxyl index vs. exposure time for WOM exposed PET film sample weathered surfaces, rear surfaces and bulk

Figure 5.5 shows the carboxyl index vs. exposure time for both the bulk and weathered surfaces of samples exposed in the DHO and HISS. In both cases the difference between the bulk and weathered surface carboxyl index values are minor, which suggests that surface and bulk chain scissions of PET film occur at similar rates due to DHO and HISS exposure. The magnitudes are also much smaller than those of the WOM exposed film sample carboxyl index measurements. These findings serve to further emphasise the importance of the synergistic effects of elevated temperature and water spraying with UV radiation, to the surface scission reactions occurring at the weathered surface of samples exposed in the WOM.

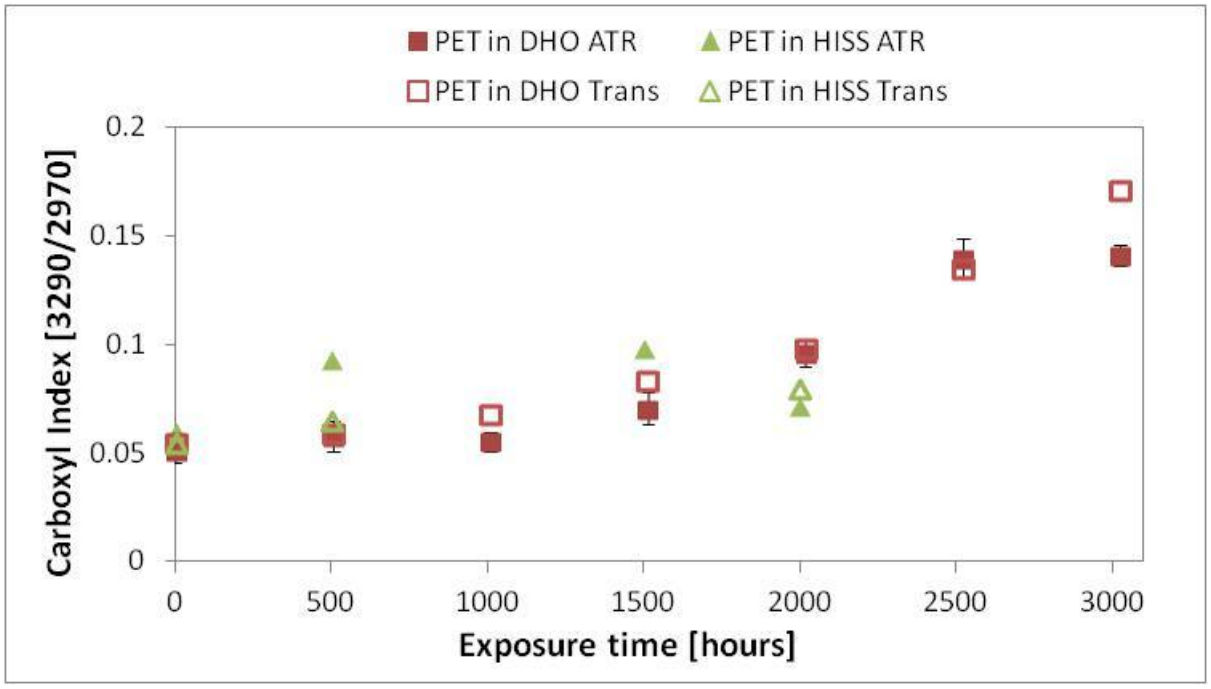

Figure 5.5: Carboxyl index vs. exposure time of both the bulk and weathered surfaces of samples exposed in the WOM, DHO and HISS

5.2.3.2 Surface chain scissions discussion

In this analysis, some samples presented much greater variance in measured carboxyl index over the areas sampled than the rest of the data set, which resulted in the larger confidence intervals seen at around 2400 hours in the weathered PET surface dataset. It may be that surface microcracking has in these cases affected the quality of contact between the film sample surface and the ATR crystal. However, if surface microcracking were solely responsible, we would reasonably expect to see similarly large uncertainties in the other carboxyl index measurements of microcracked surfaces (weathered surface 2000 hours and beyond). Therefore, it is more likely that surface contamination is responsible for the occasional greater carboxyl index value variance observed in these locations, an investigation of which will be presented later in this Chapter.

Another factor which may contribute to the enhanced weathered surface degradation due to WOM exposure is periodic water spraying, which coupled with heat, will likely cause additional hydrolysis reactions to occur here. The water spraying feature will also cause the weathered surface temperature to fluctuate more rapidly and over a greater temperature range than at the rear surface. This will result in thermal expansions and contractions of relatively greater magnitude, inducing larger stresses which may also contribute to the disparity in degradation between the weathered and rear surfaces, in particular surface microcracking.

Despite the absence of the additional factors present at the weathered surface, the magnitudes of the bulk and rear surface carboxyl index values are larger than was initially expected. This is unlikely to be entirely due to hydrolysis, considering the low magnitude of the PET in DHO carboxyl index values observed in Fig. 5.3. Possible

explanations for this include the rear surface being incident to some reflected UVB radiation, the effects of more deeply penetrating UVA radiation, or a combination of these effects.

5.2.3.3 Surface crystallinity measurement

Several researchers have assigned FTIR absorbance bands to either the trans or gauche conformations of PET molecules, which are found in the crystalline and amorphous regions of PET respectively (Ward and Wilding, 1977, Chen *et al.*, 2012). By taking a ratio of the peak absorbance values at the wavenumbers 1122 cm^{-1} and 1097 cm^{-1} it is possible to obtain a measure of the ratio of crystalline to amorphous material, which is termed the crystallinity index (Donelli *et al.*, 2010). Figure 5.6 shows crystallinity index vs. exposure time of the weathered and rear surfaces of plain PET film samples which received up to 4400 hours of WOM exposure, as well as the weathered surface of plain PET film samples which received up to 3024 hours of DHO exposure. Fig. 5.6 indicates that surface crystallinity has increased with exposure time for all three surfaces, with the largest and fastest increase occurring at the WOM weathered surface in the first 1600 hours of exposure, after which point the values decrease slightly and fluctuate between 1 and 1.1.

The crystallinity index curves of the WOM exposed sample rear surface and the DHO exposed sample surface both display a slow linear evolution with exposure time. It is likely that in both cases some combination of elevated temperature and humidity are responsible for this change, which is reasonable considering the close conditions the two surfaces experience during exposure, 65 °C, 65 % RH vs. 85 °C, 85 % RH respectively. In addition, this indicates that PET film surface crystallinity can increase

at temperatures below the T_g of PET, but that UV radiation and direct water contact have a much greater effect on surface crystallinity than heat and humidity in the absence of UV.

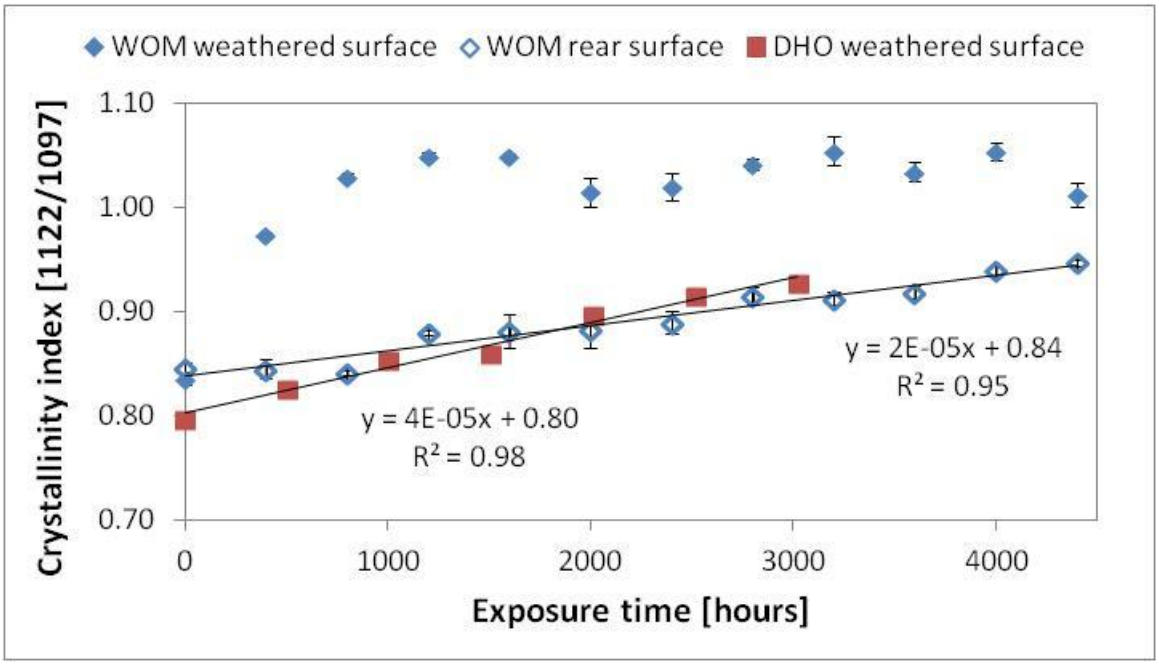

Figure 5.6: Crystallinity index vs. exposure time for weathered and rear film sample surfaces exposed in the WOM and DHO

5.2.3.4 Water contact angle

Figure 5.7 shows the mean water contact angle (WCA) vs. exposure time of the weathered surfaces of plain PET film samples exposed in the WOM, DHO and HISS. It shows that PET film surface WCA is not reduced significantly by DHO exposure up to 2500 hours, however, after 3000 hours it has fallen by approximately 5°. PET film surface WCA is reduced much more quickly when exposed to UV radiation, having been reduced by 10° after 1500 hours of both HISS and WOM exposure. The similar kinetic behaviour of these two curves suggests that the additional degradation agents

present in the WOM have relatively little additional effect on the PET film surface WCA, and hence that UV radiation exposure is the primary cause of this modification.

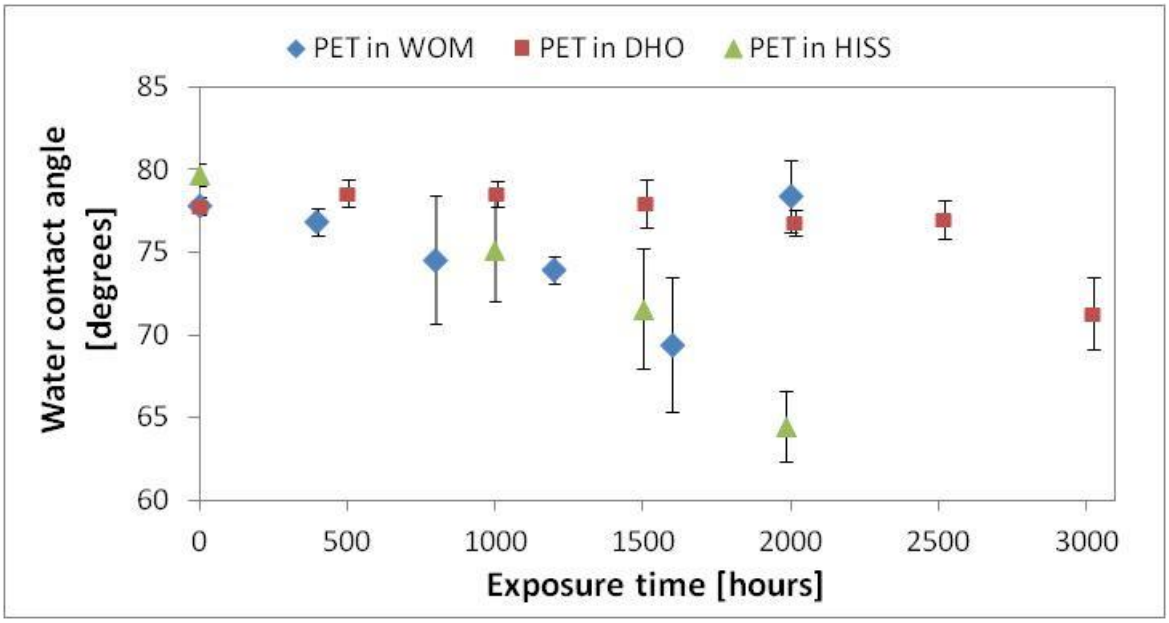

Figure 5.7: Water contact angle vs. exposure time of the weathered surface of PET film samples exposed in the WOM, DHO and HISS

5.2.3.5 Water contact angle discussion

Increased PET film surface WCA can be explained by an increase in the amount of hydrophilic -OH groups, which are formed by both aromatic hydroxylation and photo-scissions. Since hydrolysis reactions occurring in the DHO results in a substantial number of chain scissions, yet the PET film surface WCA has not decreased until relatively late in the exposure duration, it appears more likely that aromatic hydroxylation is primarily responsible for the significant change in PET film surface WCA with UV exposure in the WOM and HISS samples.

Interestingly, after complete surface microcracking (PET in WOM samples after 2000 hours exposure) there is a full recovery of PET film surface WCA to approximately

80°. Thus, surface microcracking has apparently increased the hydrophobicity of the degraded film surface, possibly due to the greatly increased surface roughness caused by microcracking. This result makes observation of WCA unsuitable for monitoring surface degradation in WOM exposed PET film samples after the onset of microcracking.

5.2.4 Surface contamination effects

During this investigation, several different observations have indicated that the weathered surfaces of the WOM exposed samples became contaminated at some point during the WOM exposure process, and that these contaminants have affected PET degradation processes. Subsequently, several surface analysis techniques have been employed to investigate the properties of the contaminants in order to develop the understanding of the effects that they may be having on PET degradation processes.

5.2.4.1 Physical characterisation

Optical microscopy, scanning electron microscopy (SEM) and elemental dispersive x-ray spectroscopy (EDX) mapping have been employed together to investigate the physical properties of the observed surface contaminants. Figure 5.8 a-d shows optical micrographs and corresponding EDX maps of contamination features representative of those frequently observed on the weathered surface of a PET film sample which received 800 hours of WOM exposure.

The contamination features commonly consisted of a central sub-millimetre sized “island” and surrounding larger “halo”, which is a formation consistent with deposits

left by evaporated droplets of water containing dissolved inorganic particulates (Marsh, 2013). EDX mapping of the features and their surrounding areas reveals a strong silicon signature (represented by red) from both the islands and halos, from which we can conclude that the contamination features are composed mainly of silica, a common water-borne particulate, but one that should not be present in the WOM water at concentrations high enough to leave deposits after evaporation, as it is both demineralised and filtered upon delivery.

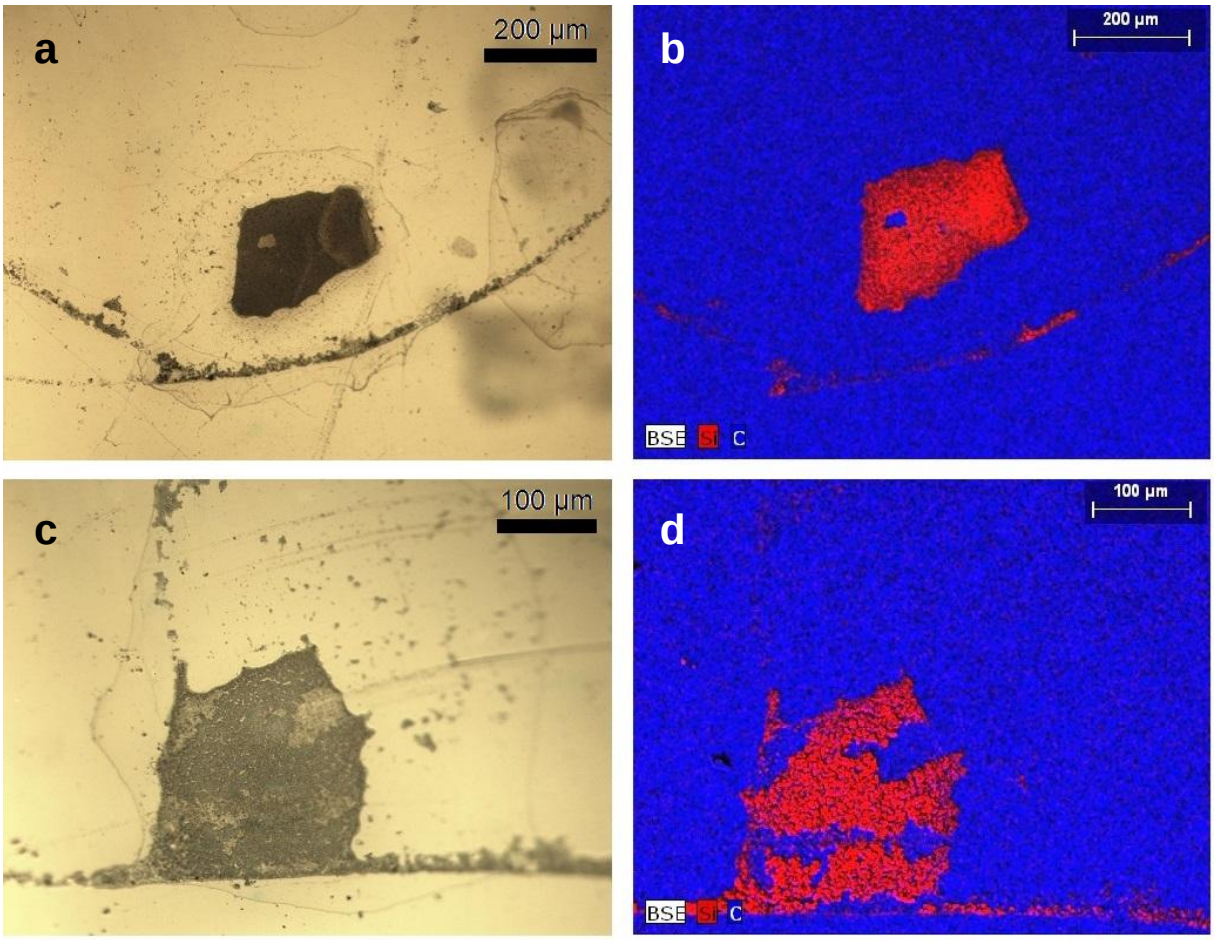

Figure 5.8 a-d: Optical micrographs (a and c) and corresponding EDX maps (b and d) of surface features of a sample which received 800 hours WOM exposure - In b and d blue and red represent carbon and silicon respectively

Figure 5.9 a-d shows optical micrographs and corresponding EDX maps of contamination features representative of those frequently observed on the weathered surface of a PET film sample which received 1600 hours of WOM exposure. The same structures and compositions as those described of the 800 hour WOM exposed sample have been observed, however, in these cases the images also reveal the additional presence of surface microcracking, both within and in close proximity to the contamination features, which in conjunction with the lack of microcracking elsewhere on the weathered sample surface, strongly suggests that the presence of surface silica deposits has influenced the local surface degradation behaviour of the PET film sample and lead prematurely to surface microcracking. It can also be seen that the deposits themselves have been microcracked during WOM exposure and in some cases, platelets thus formed have dissociated from the film surface. This behaviour has lead to further interesting observations which are best viewed after further WOM exposure.

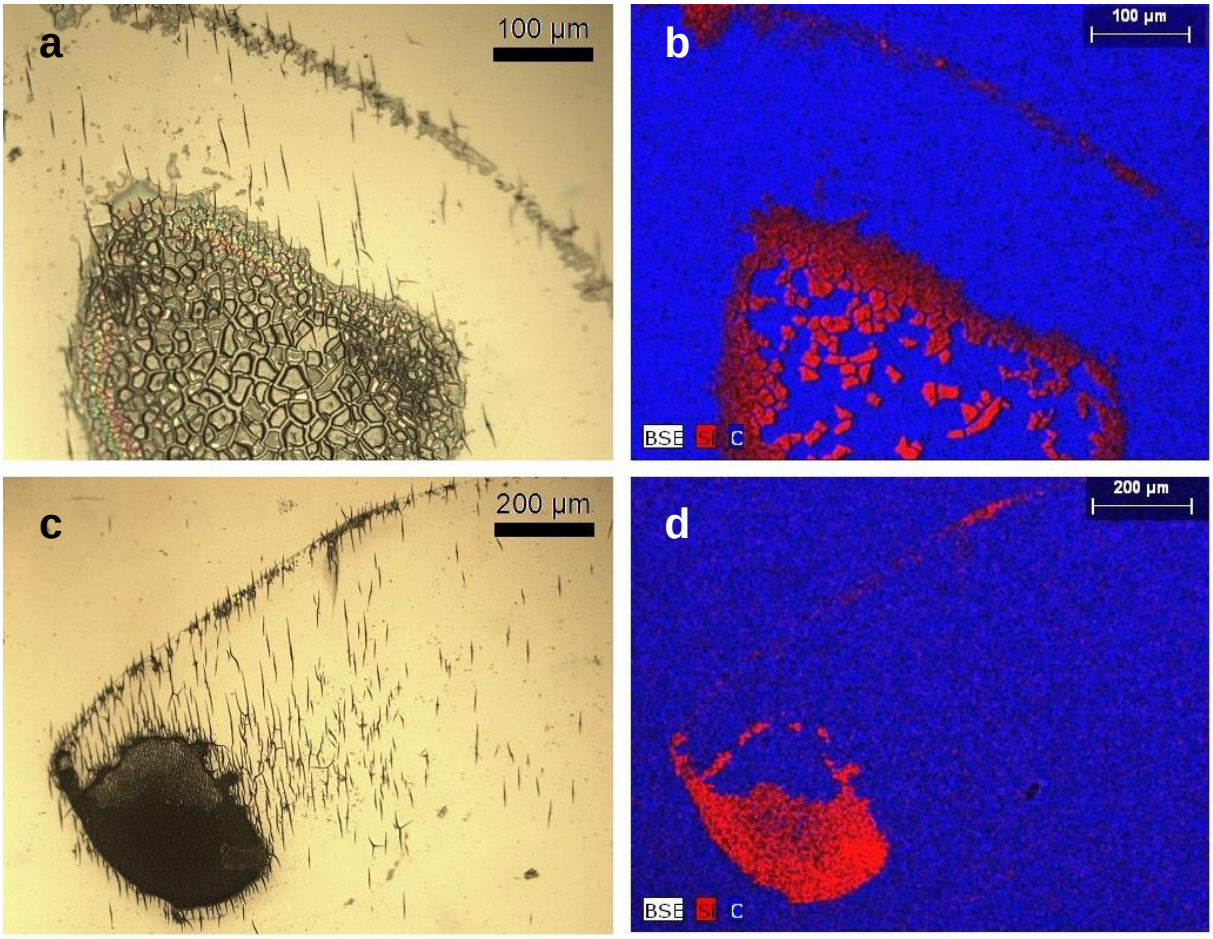

Figure 5.9 a-d: Optical micrographs (a and c) and corresponding EDX maps (b and d) of surface features of a sample which received 1600 hours WOM exposure - In b and d blue and red represent carbon and silicon respectively

Figure 5.10 a-d shows optical micrographs and corresponding EDX maps of contamination features representative of those frequently observed on the weathered surface of a PET film sample which received 2000 hours of WOM exposure. These images lend further support to the proposed role of silica deposits locally enhancing the surface microcracking of the WOM exposed PET film sample surfaces. Fig. 5.10b shows a silica deposit which has microcracked and been partially ablated prior to observation. The absence of silica in the centre of this contamination feature reveals

the underlying PET film surface, which exhibits visibly denser microcracking than that of the PET more than a few microns away from the silica deposit.

Fig. 5.10c shows an optical microscope image of a millimetre sized dark region on the exposed film surface, the edge of which is inspected more closely with EDX mapping in Fig. 5.10d. This image reveals the feature to be a region of abnormally high density surface microcracking with associated silica particulates. Here the contrast is very clear between the “normal” surface microcracking of the PET film with little associated silica and the “enhanced” microcracking of the PET film where silica particles are present.

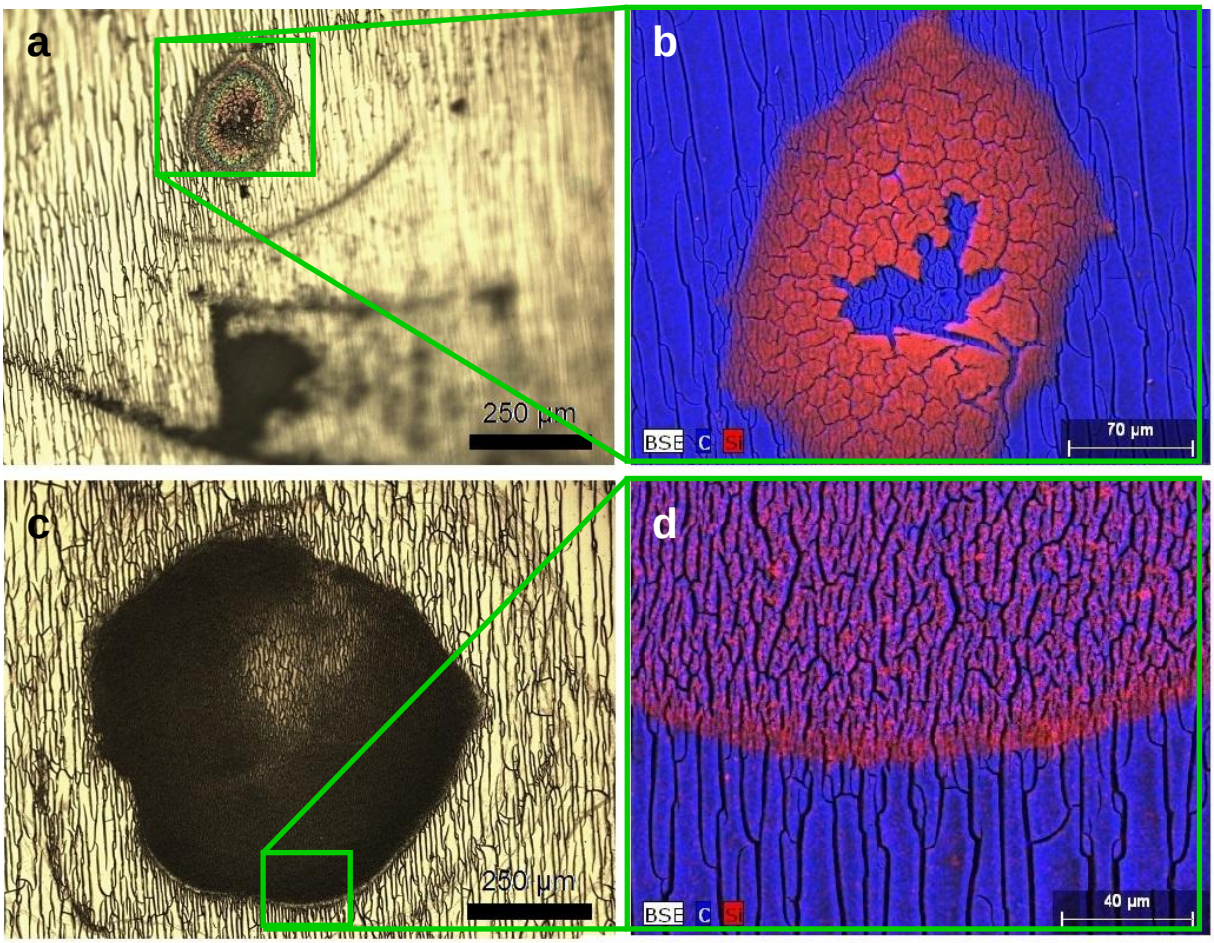

Figure 5.10 a-d: Optical micrographs (a and c) and EDX maps corresponding to the green boxed areas (b and d) of surface features of a sample which received 2000 hours WOM exposure - In b and d blue and red represent carbon and silicon respectively

5.2.4.2 Topographic characterisation

Figure 5.11 a-d shows a selection of backscatter SEM images of weathered PET film surfaces exposed for varying lengths of time in the WOM. These images further illustrate the varied morphologies and effects of the surface silica associated with PET film surface microcracking.

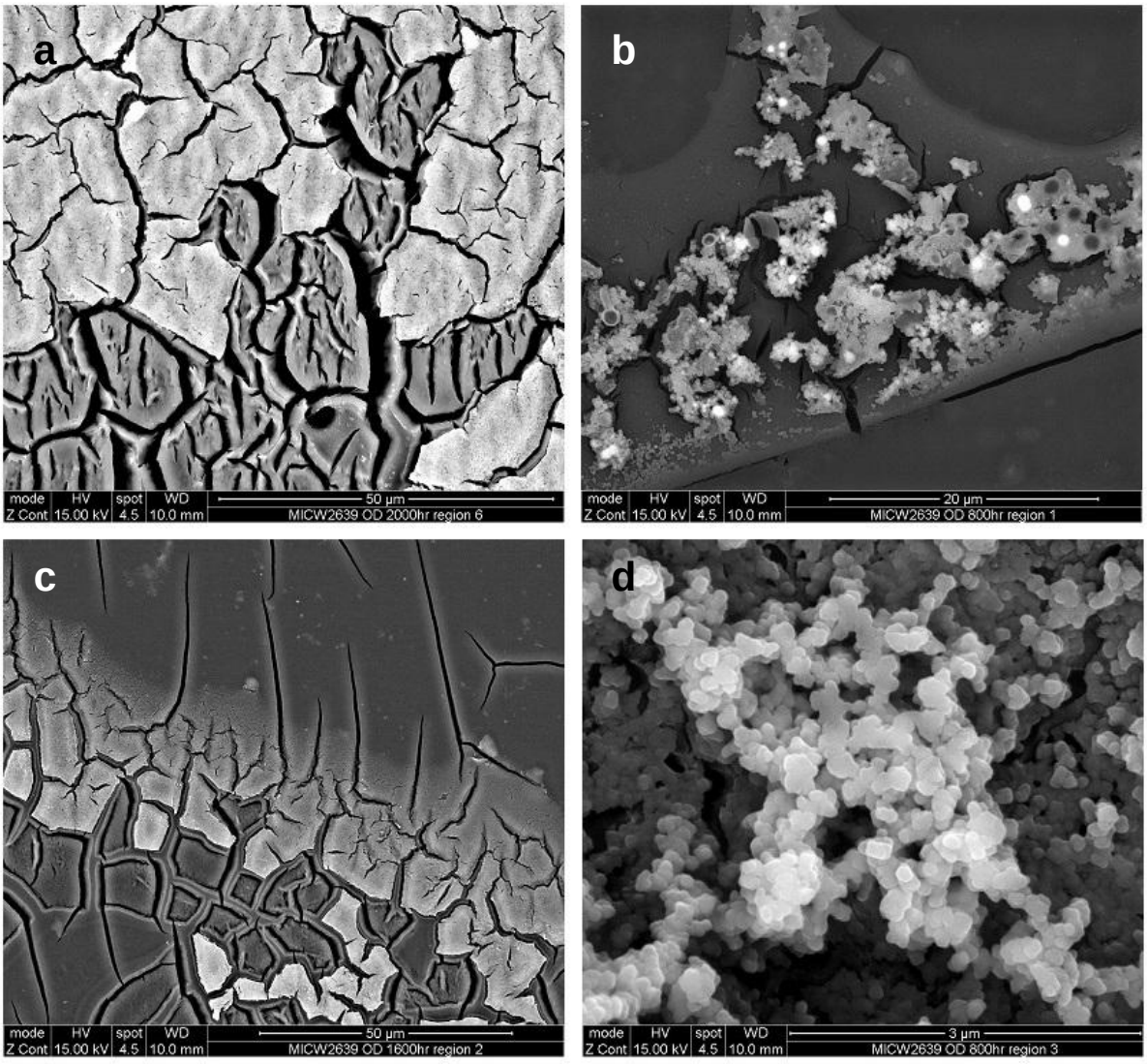

Figure 5.11 a-d: Backscatter SEM images of WOM exposed PET film sample weathered surface regions with associated silica deposits

Fig. 5.11a shows a closer view of the contamination feature in Fig. 5.10b, revealing in greater detail the microcrack structures of both the silica deposit (light grey regions) and the underlying PET film exposed by its removal (darker grey regions). The largest microcracks in the PET film appear to align with edges of the silica platelets, while the smaller and denser PET film microcracks present where the body of the now absent silica platelets would have been. This suggests that the cracking of the

PET has cracked the silica in contact with it and that the silica has continued to influence the local degradation of the PET after this point.

The feature topography in Fig. 5.11b suggests that the surface silica has both continuous and particulate phases. Here the continuous phase has microcracked in places, again likely due to the microcracking of the underlying PET film. The majority of the microcracks in this area are also in close proximity to the agglomerated particulates, which suggests that they have a greater effect on the microcracking of the PET film surface than the continuous phase, most likely due to the greater amount of silica present at these locations.

Fig. 5.11c shows the outer edge of a contamination feature, where the PET film microcracks are propagating away from the contaminated region. It is evident from this image that the presence of the silica deposit has influenced the local microcracking behaviour of the PET film surface, but that once these cracks begin to extend beyond the edge of the deposit, normal PET film microcrack behaviour resumes. This strongly suggests that surface microcracks are nucleating within the contaminated region and spreading outwards from there.

Fig. 5.11d shows a close up of the nanostructure of the particulate phase of a silica deposit which reveals the particles to be sub-micron sized. If this is representative of the nanostructure of the population of deposits, it could explain why the “pure” water utilised in the WOM contains these silica particles, as such small particles would be very difficult to detect and filter by normal means. Additionally, the narrow size distribution of these silica particles suggests that they are likely of manufactured origin (MacKerron, 2014), rather than naturally occurring, which would display a much broader distribution of particle sizes. Sub-micron silica particles are regularly

used as filler particles in DTF filled film grades. Thus, it is feasible that the contaminants may have been introduced to the WOM water system by the degradation of filled film samples within the WOM and the subsequent loss of their filler particles.

Figure 5.12 shows two additional SEM images of PET film surface microcracks which have a central feature upon which it is likely that they nucleated. Due to the topographies of the features it is possible that the central feature shown in Fig. 5.12b formed as a result of a feature such as that shown by Fig. 5.12a being removed from the surface due to some aspect of the WOM exposure process. However, it is also possible that the features are related only by their affinity with microcrack centres, which would imply that features of positive or negative height with respect to the surface can act as nucleation sites for surface microcracks. Further investigation of microcrack centres is required to substantiate either one of these claims.

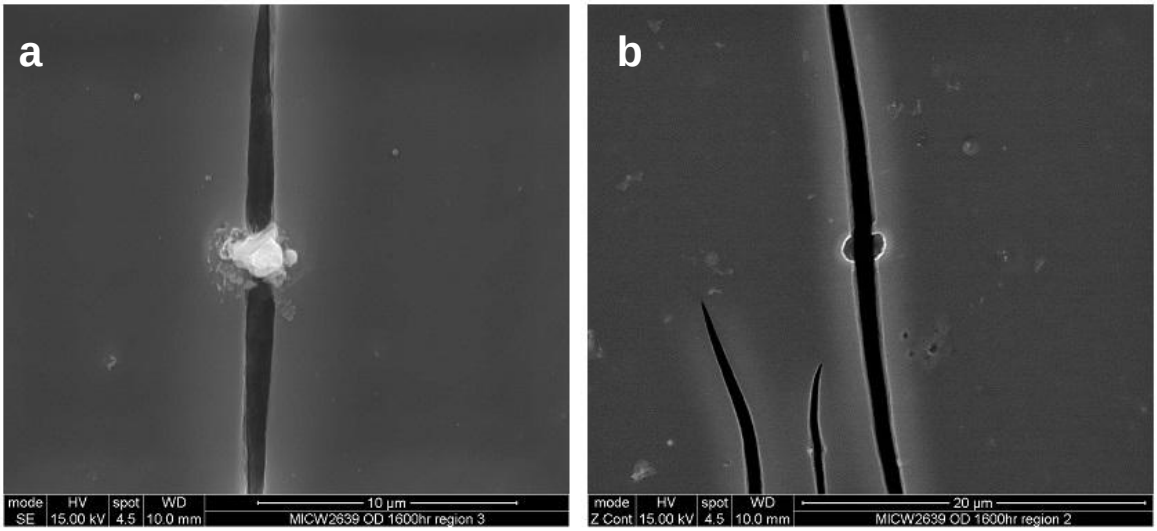

Figure 5.12 a-b: Electron micrographs showing microcracks which appear to have nucleated at surface defects. (a) at a feature of positive height and (b) around a feature of negative height (wrt. to the film surface)

5.2.4.3 Surface contamination discussion

From the surface analysis images presented in Figs 5.2a and 5.8 - 5.12 it appears that silica deposits originating from the WOM exposure process have greatly enhanced the rate of UV degradation of the PET film surface local to the areas with which they made intimate contact, causing microcracks to form in the PET film surface, earlier and with greater density than is usual due to WOM exposure.

It is possible that the water storage unit or circulating pipes were contaminated, thereby introducing the contaminants into the system. However, if the water used was up to specification upon entry to the WOM, it means that the contaminants must have been picked up by the water either after it made contact with contaminated components inside of the exposure chamber, or contact with other industrial samples present at the time of exposure. Testing of the water for particulates at key locations within the WOM may help to narrow down the range of possible particle sources. Where the silica deposits appear continuous they have also cracked, which suggests that the material is brittle and strongly adhered to the PET film. Silica occurs naturally in many crystalline forms but is commonly encountered as a desiccant in the form of silica gel. It has a high specific surface area which gives it a high affinity for water (Wiegmann, 1980).

As to the possible mechanisms of sub-micron thickness silica deposits locally enhancing PET surface microcracking, it is most likely that the deposits contributed to one or more of the factors associated with the surface microcracking of PET film - UV radiation, oxygen, temperature and pH. Hence, there are several reasonable scenarios that could locally enhance the effect of one or more of these factors, which will now be discussed.

- The deposits would readily adsorb water and thereby hold it close to the film surface after it has evaporated from the uncontaminated regions of the film surface. This may have locally increased the number of hydrolysis reactions occurring, however hydrolysis is not normally associated with surface microcracking.
- Prolonged intimate contact with water could also supply dissolved oxygen, which could increase the amount of oxygen available for photo-oxidation reactions.
- Silica and water can combine by hydration to produce silicilic acid (Wiegmann, 1980), the presence of which would reduce the local pH at the deposit-film interface. Acidic conditions are known to accelerate PET degradation reactions (Venkatachalam *et al.*, 2012).
- The micron scale thickness of the deposits, verified by AFM, would be unlikely to impede UV radiation, however, they may act to increase the local temperature of the PET film surface, which would speed up the chemical reactions occurring in the underlying PET film and hence, reduce the time until surface microcracking.
- The deposits may also have a microlensing effect, which may act to concentrate UV into smaller regions within the deposits, increasing the rate of degradation and decreasing the time until microcracking takes place.

Due to the presence of the observed contaminants, PET film samples are degrading faster due to WOM exposure than they would otherwise. This has the knock on effect of reducing the test performance of developmental films and weakens claims of greater photo-stability required to differentiate films from competitors.

The contaminants are also an additional source of uncertainty that is not being taken into account. If it is deemed that they will be a persistent feature of WOM exposure, then they should ideally be factor informing features of new product developments. *i.e.* there is a greater need for surface stabilisation, surface cleanliness, self cleaning properties, or barrier film properties. Surface degradation behaviour also has implications for any PET PV front sheet applications, as such contamination could occur regularly during outdoor device service lifetimes. Contact with sand for example may prove similarly detrimental to PET film surface performance.

As such this evidence forms the basis for a whole new research area, investigating the potential effects of a whole host of other common materials which may be of concern to outdoor applications.

5.2.5 Surface topography changes

5.2.5.1 HISS exposed sample AFM

In order to assess the effect of UV radiation on the surface topography of PET film at various AFM length scales, a plain PET film sample surface was imaged at 5 specified locations using TM-AFM, with scan sizes of between 1 and 100 µm. The calibrated motorised stage was then used in conjunction with the optical microscope of the AFM to precisely relocate these same 5 points on the sample surface after each HISS exposure period. To do this, one corner of the round HISS sample was cut away which gave a corner feature that could be centred in the AFMs optics FOV and set to be the origin of the calibrated stage. The orientation of the cut new edge was then set to be 45° relative to the vertical axis of the optical microscope FOV, so that when the stage was moved diagonally, the centre of the optics FOV travelled

along the cut edge. Then, having set an origin and orientation, specific coordinates were inputted to the software to move the AFM FOV to the 5 chosen locations, which were then imaged as described.

Fig 5.13 shows 1 μm^2 TM-AFM topography images of one specified location on the weathered PET film surface after 0, 500 and 1000 hours of HISS exposure. The surface roughness and observed nano-structures are typical of biaxially oriented PET film at 1 micron length scales (Gould *et al.*, 1997, Dinelli *et al.*, 2000). Analysis of such AFM images suggests that HISS exposure of up to 1000 hours caused no significant modification to the nano-structure of the weathered PET film surface. At the location shown in Fig. 5.13, after 1000 hours exposure, slight reductions in the average surface roughness (Ra) and root mean squared surface roughness (Rq) were observed, as well as reduced imaging resolution. However, these observations are most likely both functions of imaging the 1000 hour exposed surface with a slightly less sharp AFM tip.

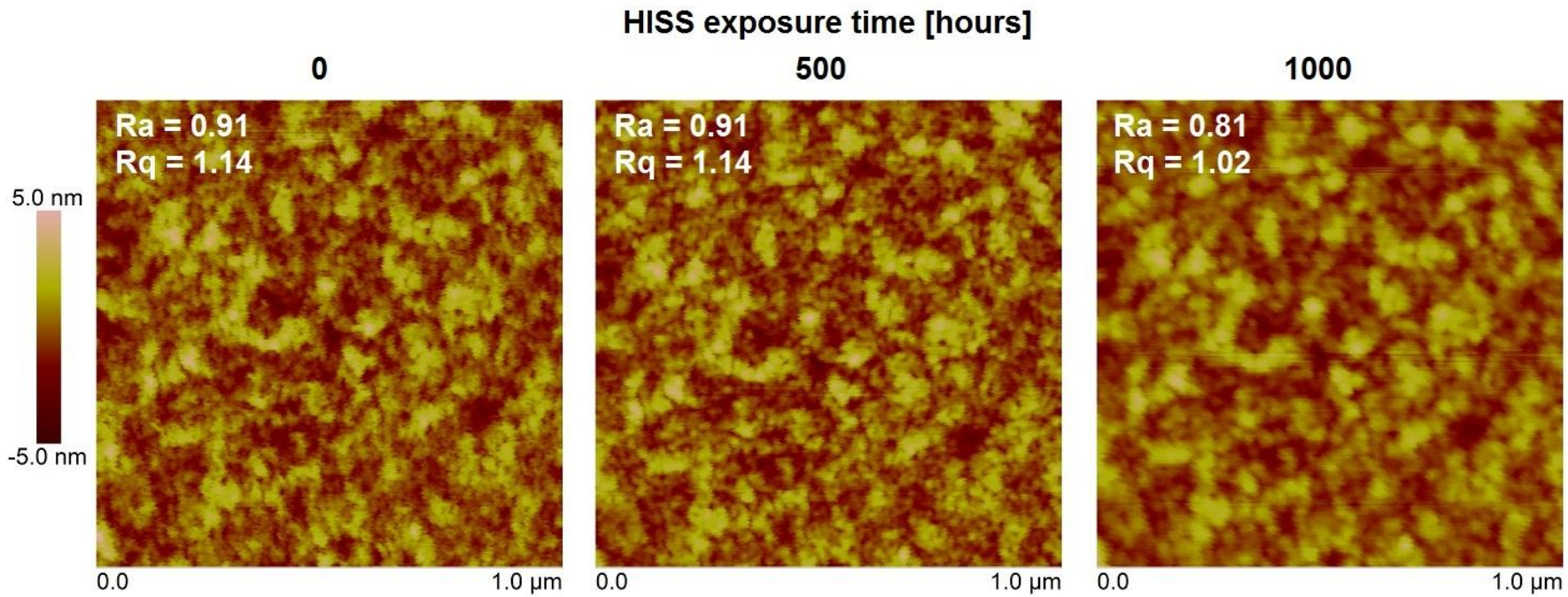

Figure 5.13: 1 µm^2 AFM topography images of a specified location on the weathered PET film surface after 0, 500 and 1000 hours of HISS exposure. Z range of 10 nm applies to all images

Negating tip effects, AFM monitoring of the HISS exposed weathered suggests that exposure to UV irradiation under lab conditions, even when as intense as in the HISS experiment, is not enough to modify the nanoscale surface topography of PET film. This provides evidence against the initial hypothesis that an overall surface roughening and nanoscale feature development would both be observed after isolated UV exposure and suggests that the surface modifications which preclude UV radiation induced microcracking require the additional presence of one or more of the non-UV PET degradation agents present in the WOM.

Owing to these findings the HISS exposed sample AFM surface monitoring experiment was discontinued in favour of AFM analysis of WOM exposed sample AFM analysis presented in the following section.

5.2.5.2 HISS sample AFM discussion

In practice, the above procedure was time intensive and to some extent unreliable, as it often resulted in AFM scans which were many microns away from the desired location due to imprecise repositioning of the sample on the AFM stage. For the UV exposed sample it was possible to make fine movements within the 100 µm FOV of the AFM using the piezo scanner, to reproduce images of the same locations with nanometre precision, however, with a control sample no common features could be identified between the initial images and the subsequent ones, which meant that re-imaging the same areas after removal and re-insertion to the AFM could not be performed.

Further, tip sharpness variations are practically unavoidable when AFM is used in this way, as it is very difficult to completely preserve the tip apex over the course of

many AFM scans, due to high frequency surface tapping gradually eroding the tip apex. Changing the cantilever to utilise a fresh tip was impractical however, as it resulted in a changed tip position, and hence scan location, requiring the lengthy site relocation procedure to be started over.

5.2.5.3 WOM exposed sample AFM

After completing the AFM analysis of the HISS exposed weathered sample surface, it was decided not to attempt to use AFM to monitor the same precise surface areas with increasing WOM exposure time. The three main reasons for this being:

i. The difficulties in mounting the relatively larger WOM samples for AFM imaging without damaging them
ii. The inflexibility of the sample withdrawal and reinsertion times to the WOM
iii. The time consuming nature of the AFM surface monitoring procedure

Instead, 6 different areas of each of the WOM exposed sample surfaces were analysed with 2, 5 and 20 μm FOVs. The statistical parameters were then averaged to yield a representative analysis of the modification of PET film surface topography with WOM exposure. Fig. 5.14 is a TM-AFM image montage of representative examples of the PET film weathered surface after increasing amounts of WOM exposure. It reveals that some aspects of the PET film weathered surface are being modified by WOM exposure, while others are being introduced. By keeping the height scale constant over the 2400 hour exposure duration, an increase in surface roughness can be interpreted from the increasing amount of light and dark regions developing in the images with increasing exposure time.

New features, both above and below the mean plane of the surface are developing and increasing in size and number with exposure time. For example, sporadic nanoscale pit features can be seen after exposure in the 5 μm^2 images, two of which have been imaged in greater detail in the 1200 and 1600 hour 2 μm^2 images. AFM imaging also captured some micron and above sized pit features, although these were much less commonly observed than the nanoscale ones.

The 20 µm images have captured the spatial distribution of a growing number of isolated surface peaks. These are most likely oligomers which have migrated from within the film bulk to the surface and then agglomerated to form soft gel-like peaks, which are deformed by the AFM tip when it contacts them during imaging.

The 2 µm images reveal changes to the PET film weathered surface nanostructure with WOM exposure. With increasing WOM exposure, the nodules which give the film surface its nanoscale roughness, grow in size and become increasingly sharp edged, while protruding a greater distance from the surface.

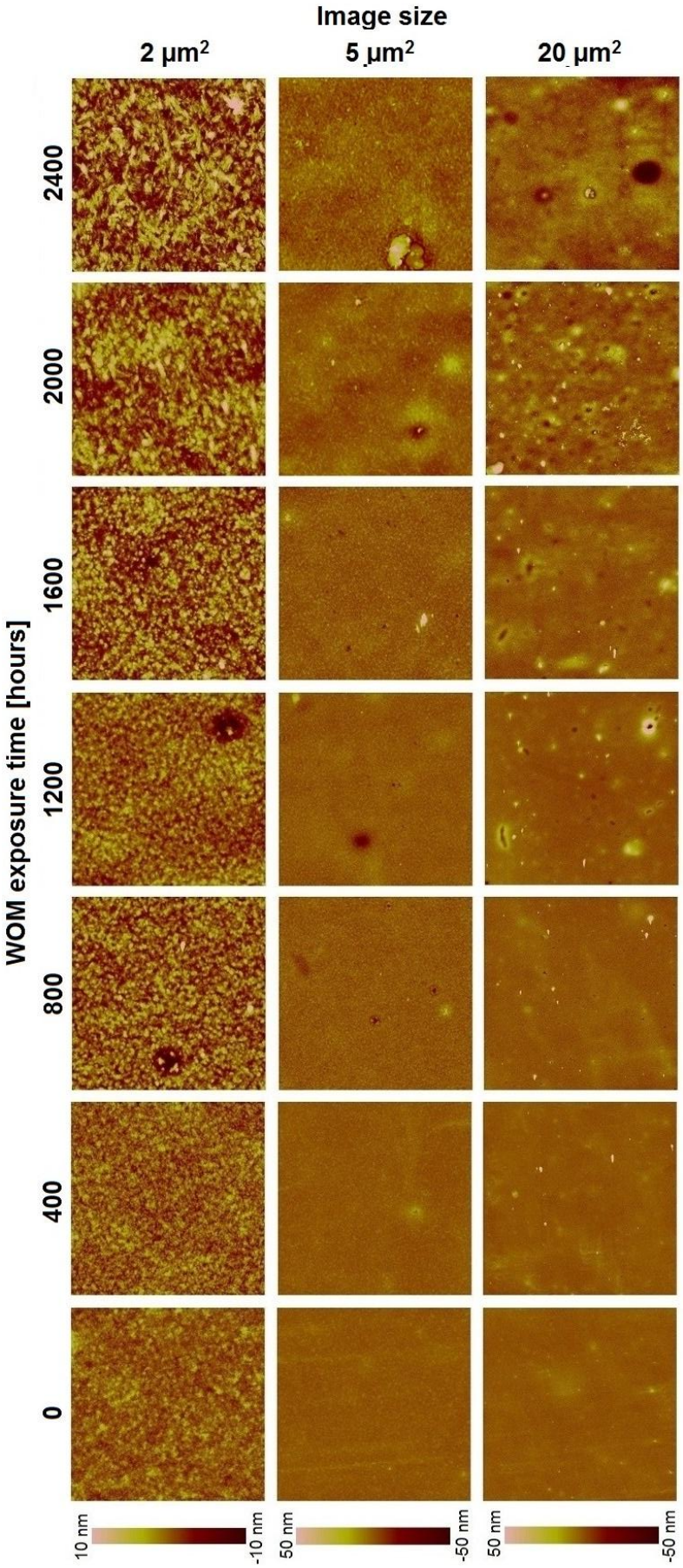

Figure 5.14: AFM topography images of the weathered PET film surface with increasing WOM exposure time up to 2400 hours. Z range of 20 nm applies to the 2 µm images while a Z range of 100 nm applies to the 5 and 20 µm images.

The observed surface roughening effect is formalised in Fig. 5.15 which shows mean Ra vs. exposure time for the 2, 5 and 20 µm images of the WOM exposed PET film weathered surface. At each point in the exposure duration, the following condition was obeyed: 2 µm Ra < 5 µm Ra < 20 µm Ra. Such scale variance is usual when analysing the surface topography of PET film, as larger scan sizes better capture the overall micro-roughness of the heterogeneous film surface, rather than just the local nanoscale topography often observed in smaller scan sizes, which may not be representative of the entire film surface.

At all three measured length scales Ra increased linearly with WOM exposure, with the rate of roughening fastest at the 20 µm scan size and slowest for the 2 µm scan size. The coefficient of variation R^2 approaches 1 with increasing scan size, which strongly suggests that surface roughening due to weathering is a linear process at AFM length scales. Notably confidence intervals were also widening on average with increasing scan size, indicating greater sample heterogeneity at larger scan sizes as expected.

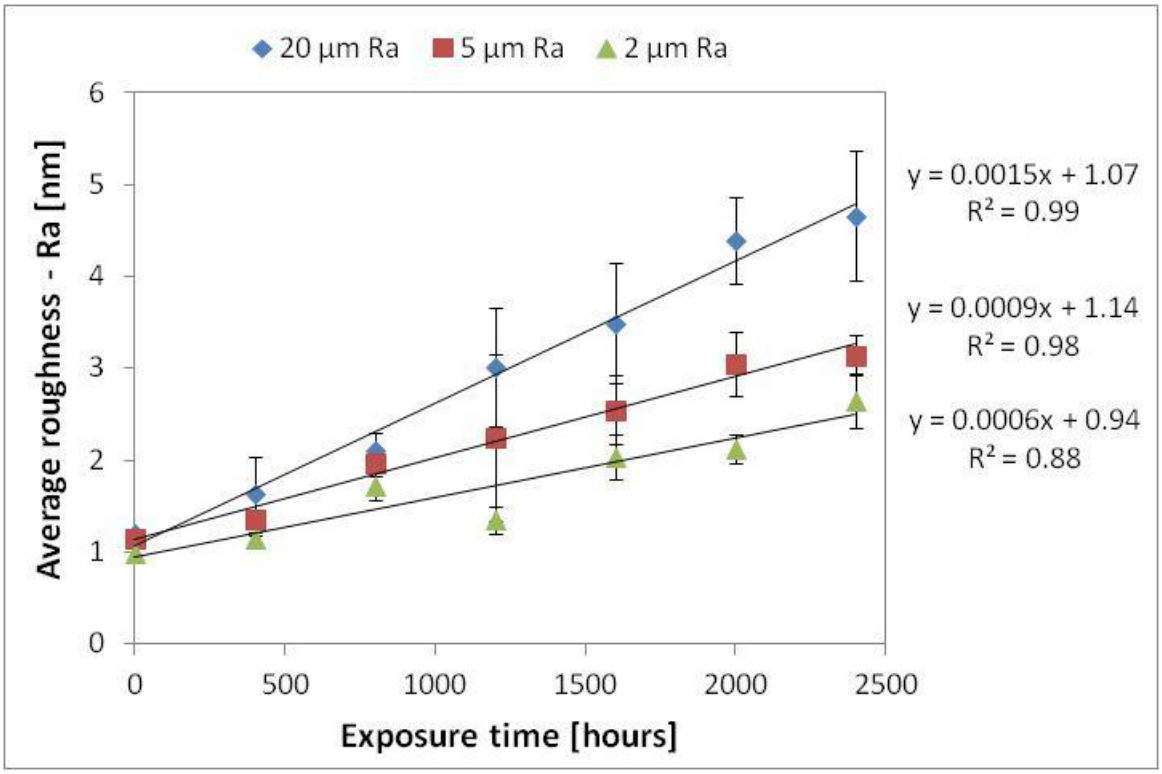

Figure 5.15: Ra vs. exposure time at 2, 5 and 20 um AFM length scales for the weathered surface of WOM exposed PET film

5.2.5.4 WOM sample AFM discussion

Ra was chosen for this analysis as it is describes the average surface roughness and is hence, not strongly affected by sporadic changes, but is affected by significant changes to the surface overall *i.e.* surface roughening. The root mean square roughness Rq, which better reflects the extremes of a surface height distribution also increased with WOM exposure time, however, it was subject to much larger confidence intervals and poorer linear fits with exposure time and hence has not been included. There are several other common statistical parameters which can be extracted from the AFM image data such as the maximum roughness (Rz), skewness and kurtosis (ISO 25718-2, 2012), however, these parameters did not display evolutionary behaviour with exposure time as did Ra and Rq. Recently, some in the

metrology community are encouraging the adoption of newer ‘S’ parameters, which are based on 3D surface integrals rather than 2D statistical calculations (ISO 25718-2, 2012). To see if the use of these newer parameters had any impact on the findings the AFM data was converted to Bruker Vision file formats and the Sa values extracted. However, these were not significantly different to the corresponding Ra values, and as such the data is not presented here. Additionally there are many other S parameters such as the spatial and functional parameters which it is possible could yield further interesting insights into the surface roughening process. Analysis of such parameters is recommended future work in this area.

It must also be noted here that all the areas represented in the above AFM figures are within intact regions of the weathered PET film surface, *i.e.* in between surface microcracks where they were present after 1600 hours WOM exposure. Thus, the images and the statistical parameters extracted from them are representative of the uncracked regions of the weathered PET film surface, and are not representative of the surface as a whole after microcracking. To incorporate the substantial contribution of microcracks into such statistical surface analysis requires metrological tools which can measure over much larger lateral and vertical regimes. An attempt was made to do this with WLI and is the focus of the next section.

5.2.5.5 WOM exposed sample optical metrology

Fig. 5.16 shows the 3 parameter log-logistic fits of the Ra distributions of WOM exposed PET film sample weathered surfaces. Ra on the x-axis is a log scale and data density on the y-axis reflects the relative number of individual areas which have the corresponding Ra. Each distribution was constructed by collating and fitting the

Ra values of 10,000 adjacent 120 x 90 µm areas, in 100 x 100 grids, totalling an area of approximately 1 cm^2 per sample. An example of the raw data acquired, Ra distributions and fit process can be found in Appendix 2. Attempts to measure sample surfaces WOM exposed for up to 2400 hours were made, however, PSI proved unable to well capture the topography of severely microcracked areas and hence no data past 1600 hours (when the surface is only partially microcracked) is presented.

The 3 parameter log-logistic fits illustrate the distributions approximately, but were found to be the best way of comparing multiple roughness distributions due to the very high number of data points which each original Ra distribution consists of. Initially, the PET film surface Ra distribution is relatively narrow, centred around a modal value of approximately 1 nm, has a lower limit of approximately 0.7 nm and a heavy tail that reaches well beyond the 50 nm limit of the x-axis due to occasional outlying high Ra areas containing surface scratches and other such manufacturing defects, which greatly affect the local surface roughness.

With increasing WOM exposure the Ra distributions shift to the right, which signifies the roughening of all parts of the sample surface. The minimum (distribution cut-on) and modal (distribution peak) Ra values are both increasing at a growing rate, which suggests the roughening process speeds up with increasing exposure time. The Ra distribution also becomes much broader, indicating that the spread of Ra values is increasing and the surface is becoming more heterogeneous. The shape of the distribution is becoming more log-normal with exposure time, however, as roughness distributions have not been previously explored the significance of this finding is as of yet uncertain.

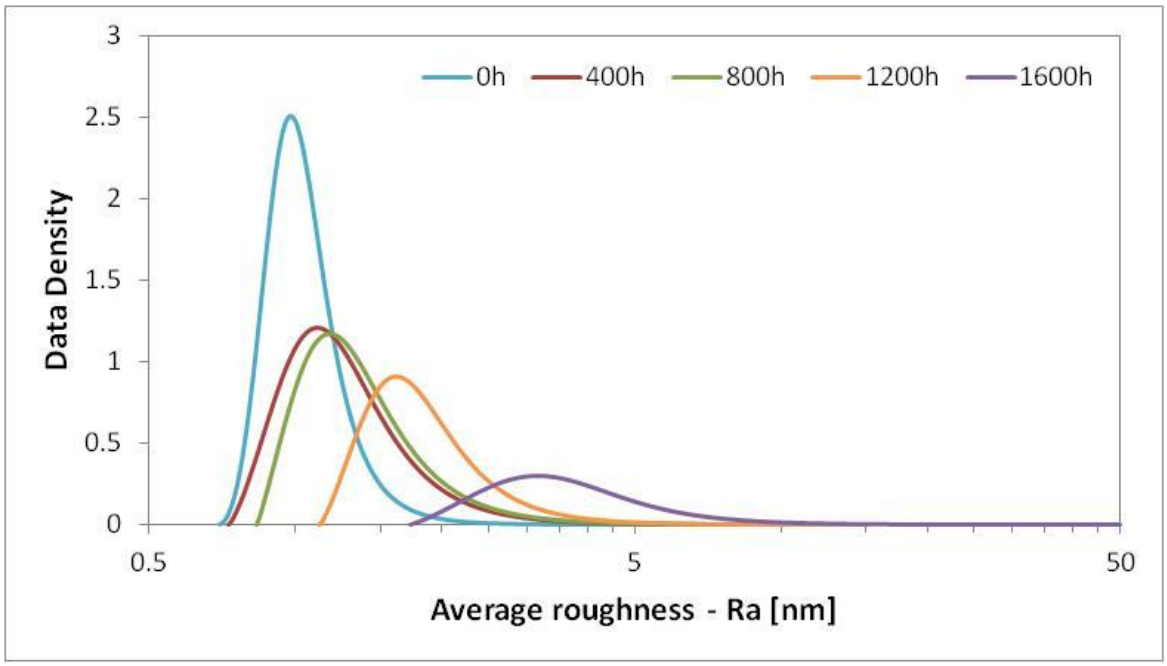

Figure 5.16: 3 parameter log-logistic fits of Ra distributions obtained from 1 cm^2 areas of the weathered surfaces of PET film samples WOM exposed for up to 1600 hours

Fig. 5.17 shows the modal and minimum values of the Ra distributions with WOM exposure time, which represent two distinct qualities of the film surfaces: the most commonly occurring roughness and the smoothest regions. This figure better highlights the increasing rate of roughening with increasing WOM exposure and reveals a much larger increase in modal roughness between 1200 and 1600 hours, which is likely due to contributions from the initial stages of surface microcracking. The disparity between modal and minimum values at 1600 hours exposure indicates that despite the more substantial modification of some surface areas, there are still areas which remain relatively smooth. These areas are most likely away from and in between microcracked regions and are similar to the areas observed using AFM.

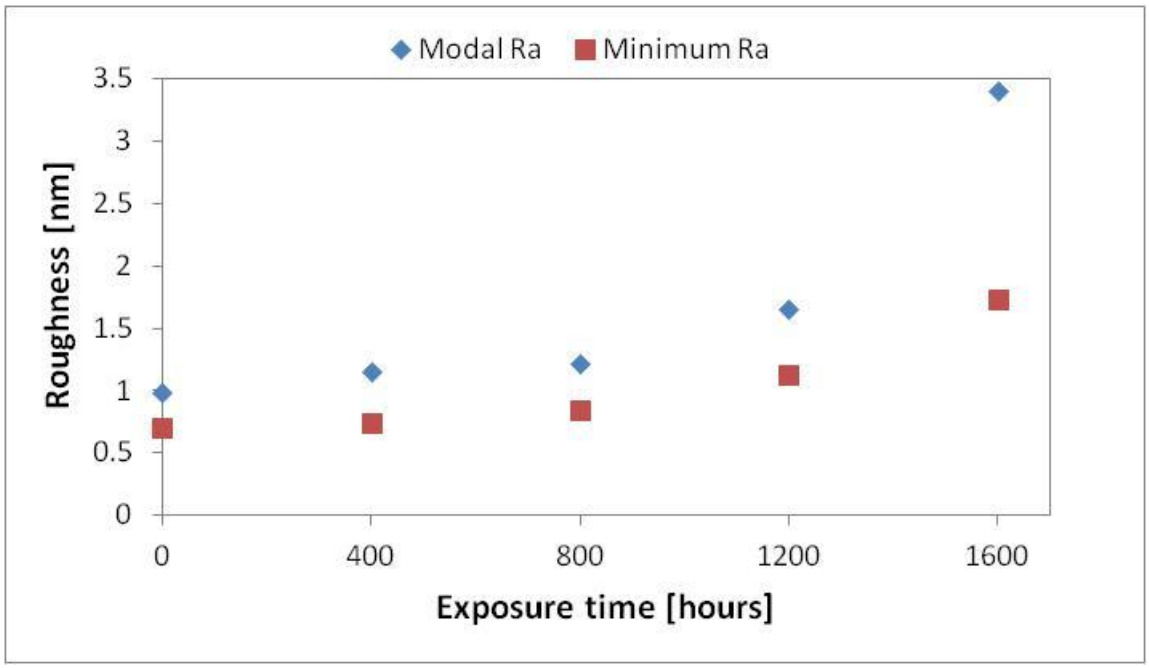

Figure 5.17: Modal Ra vs. exposure time for the weathered surface of WOM exposed PET film

5.2.5.6 Surface roughening discussion

There are many studies in the scientific literature which have characterised polymer surface roughening due to various treatments. However, the polymers studied, research methods and degree of rigour have all varied considerably over the years. As such, several firsts have been achieved in this Thesis:

i. AFM has been used to monitor the topography development of multiple micron scale locations on a PET film surface with up to 1000 hours of high intensity UV exposure.

ii. And thereby it has been shown that exposure to high intensity UV radiation in the absence of heat, humidity and direct water contact does not modify surface topography.

iii. The surface roughening of PET film due to accelerated environmental weathering has been shown to be a linear process with exposure time.

iv. PET film surface topography has been quantified with accelerated environmental weathering over a range of 7 orders of magnitude in size, from 10's of nanometres up to centimetres.

Of the two surface metrology techniques each presented its own advantages and disadvantages when applied to artificially weathered PET films. AFM yielded images with better lateral resolution, but could only reasonably be used to characterise a relatively small area. Conversely, WLI yielded images with much lower lateral resolution but enabled the sampling of a much larger, macroscopic area.

The rate of surface roughening due to WOM exposure increases with increasing scan size (scale variance), which is likely influenced by microcracking and larger scale modifications not observed at the lower end of AFM scan length scales. Similarly, some surface features and effects were only observed by AFM, however these appear to have had a lesser effect on the roughness parameters used to formalise the surface modifications.

The automation feature of the WLI and its much faster measurement capability meant that it was far more easily utilised than AFM to monitor sample surface roughness with WOM exposure time, once methods were developed to analyse the large amounts of data generated.

In summary, the AFM is well suited to the nanoscale analysis of a few areas, giving the user an insight into the small scale morphological changes occurring due to weathering; while WLI is better suited to large scale statistical analysis of the surface, however the techniques are complementary and are best utilised together. The large area WLI analysis method has shown great promise in comprehensively

characterising weathered PET film surfaces, but could also be readily applied to a broad range of other research and product development projects.

5.2.6 Surface mechanical property changes

Weathered PET film surface mechanical properties have been investigated in order to further test the relationship between chemical and physical sample modifications. Surface crystallinity and crosslink density are linked to PET film surface mechanical properties and can hence be evaluated using indentation testing in conjunction with the analyses presented earlier.

5.2.6.1 Instrumented nanoindentation

Figure 5.18 shows surface Young's modulus acquired by instrumented nanoindentation (IIT) vs. exposure time for plain PET film samples exposed in the WOM, DHO and HISS. The numerous indentations performed to generate these values were each approximately 1 µm in depth, and therefore reflect the Young's modulus of the uppermost few microns of the surface in which they were performed.

Fig. 5.18 reveals that the plain PET film weathered surface Young's modulus is increased after exposure to each of the artificial weathering techniques. With DHO exposure PET film surface Young's modulus increases linearly, at a rate of approximately 1 GPa per 1000 hours. With HISS exposure, approximately the same increase in surface Young's modulus is seen after 2000 hours, but with non-linear growth behaviour, characterised by a greater initial increase between 0 and 500 hours than between 500 and 2000 hours.

PET film surface Young's modulus has also increased non-linearly with WOM exposure, however, in this case it peaked at over 7 GPa after 1200 hours, then fell linearly to approximately 6 GPa up to 2400 hours, after which point surface Young's modulus was reduced dramatically to around 1 GPa, a quarter of its initial value. It is interesting that a relatively high surface Young's modulus was retained up until 2400 hours of WOM exposure, as microcracking of the weathered surface is well established by this time. Surface Young's modulus also starts dropping at around the time microcracking starts significantly spreading, which suggests that the surface becomes gradually weaker as microcracking spreads, before reaching its mechanical failure point between 2400 and 2800 hours.

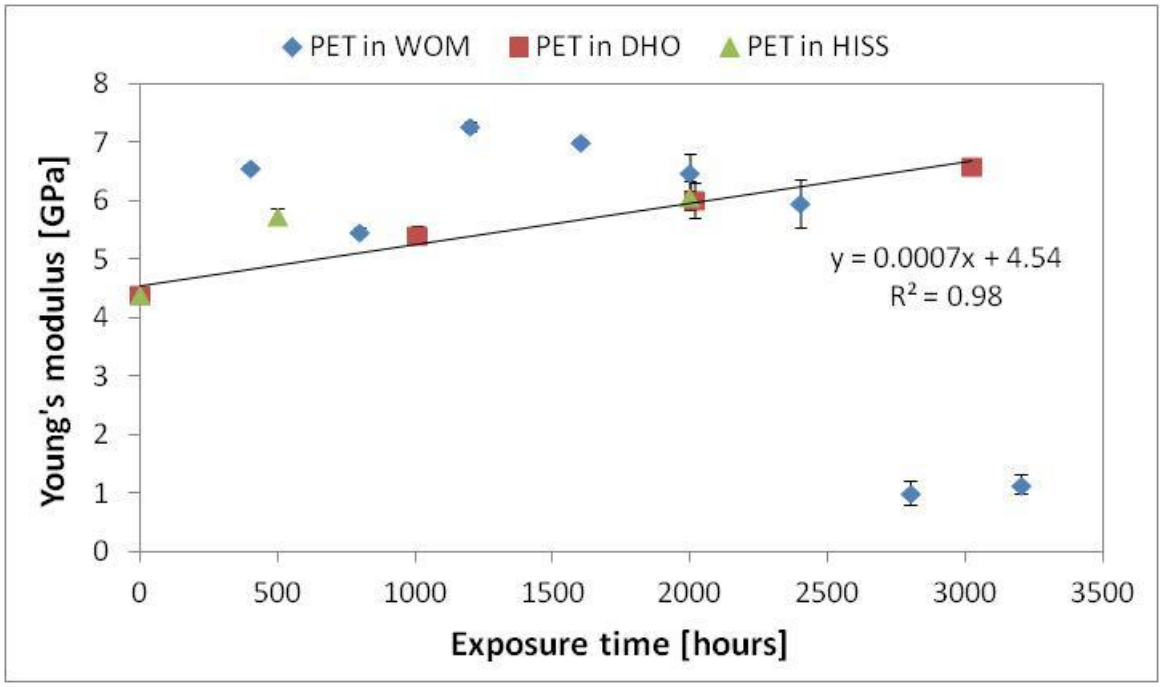

Figure 5.18: Surface Young's modulus vs. exposure time of PET film weathered surfaces exposed in the WOM, DHO and HISS

Figure 5.19 shows the Young's modulus vs. exposure time of the weathered and rear surfaces for plain PET film samples exposed in the WOM and HISS. It reveals an increase in the surface Young's modulus of the rear surfaces of the WOM and HISS exposed PET film samples but one that is lesser in magnitude than the corresponding increases in the weathered surface moduli. After 3200 hours of WOM exposure the film rear surface modulus is still increasing, unlike the weathered surface modulus which fell to below 1 GPa. These changes are extremely similar to those observed of surface crystallinity, providing evidence that the two observations are linked in this case. This result also quite clearly demonstrates that mechanical properties of the two surfaces are independent of each other and that the IIT testing is surface specific for 175 micron thick films.

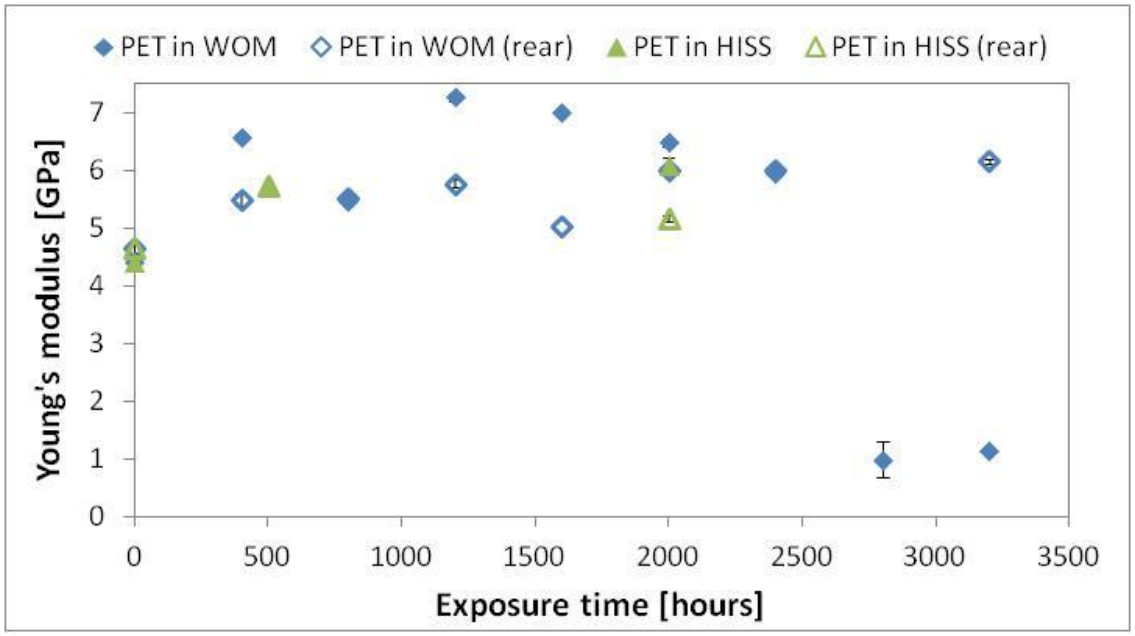

Figure 5.19: Young's modulus vs. exposure time of PET film sample surfaces (weathered and rear) exposed in the WOM and HISS

5.2.6.2 PFQNM

Fig. 5.20 is a PFQNM-AFM image montage of 1 μm^2 topography and DMT modulus images representative of the PET film weathered surface areas analysed after 0 and 2000 hours of WOM exposure. The PFQNM topography images display the same changes with WOM exposure as already evidenced by TM-AFM, which further validates the surface roughening findings. The DMT modulus images illustrate the spatial distribution of modulus values, which are calculated from the deformation depths achieved by the AFM tip at each point in the image. The range and distribution of modulus values suggests nanoscale heterogeneities in surface mechanical properties.

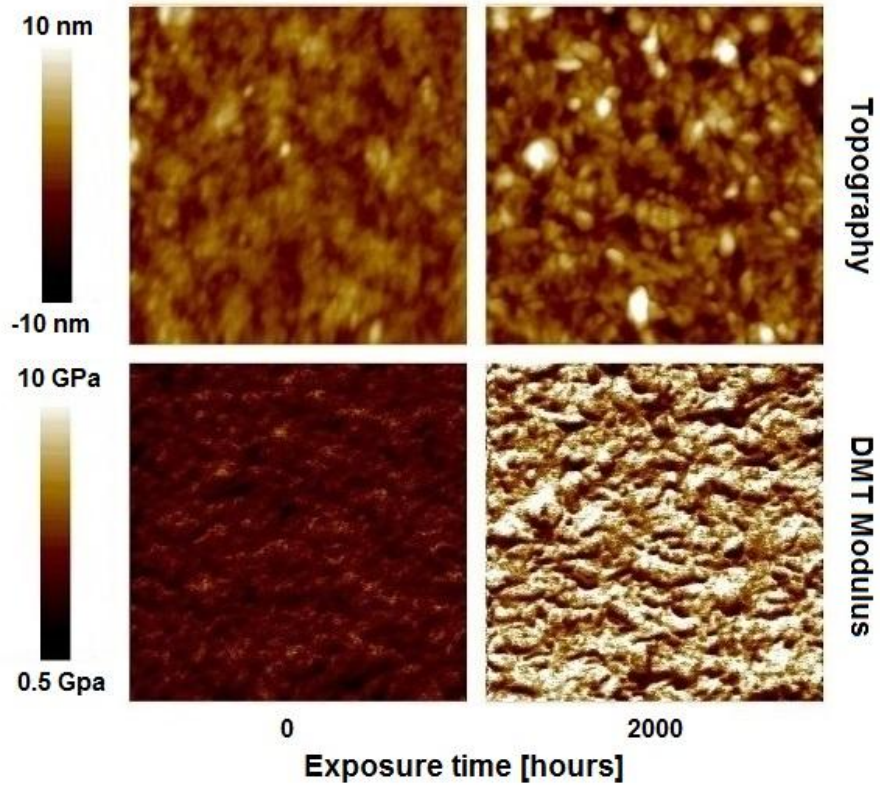

Figure 5.20: PFQNM-AFM image montage of 1 μm^2 topography and DMT modulus images taken from 0 and 2000 hour WOM exposed PET weathered surfaces

The modulus image mean values can be extracted using the Nanoscope software and represent the arithmetic means of the modulus values that make up each image. Fig. 5.21 shows a comparison of the average surface modulus results obtained via IIT and PFQNM of the weathered surface of plain PET film after 0 and 2000 hours of WOM exposure. It reveals that both techniques measured an increase in surface Young's modulus. The PFQNM DMT modulus rose from approximately 3 GPa initially to 7 GPa after 2000 hours WOM exposure. While IIT surface Young's modulus rose from approximately 4 GPa initially to 7 GPa after 2000 hours WOM exposure. PFQNM is an emerging analysis technique and as such the data obtained should not be accepted without scrutiny. However, in this case it appears that the measured values are close to those found by IIT, and are the same within error for the 2000 hours exposed sample. Thus, it has been demonstrated that PFQNM is capable of accurately determining the surface Young's modulus of both unweathered and weathered PET films. This result also suggests that for PET film, the nanomechanical and micromechanical moduli are approximately equivalent.

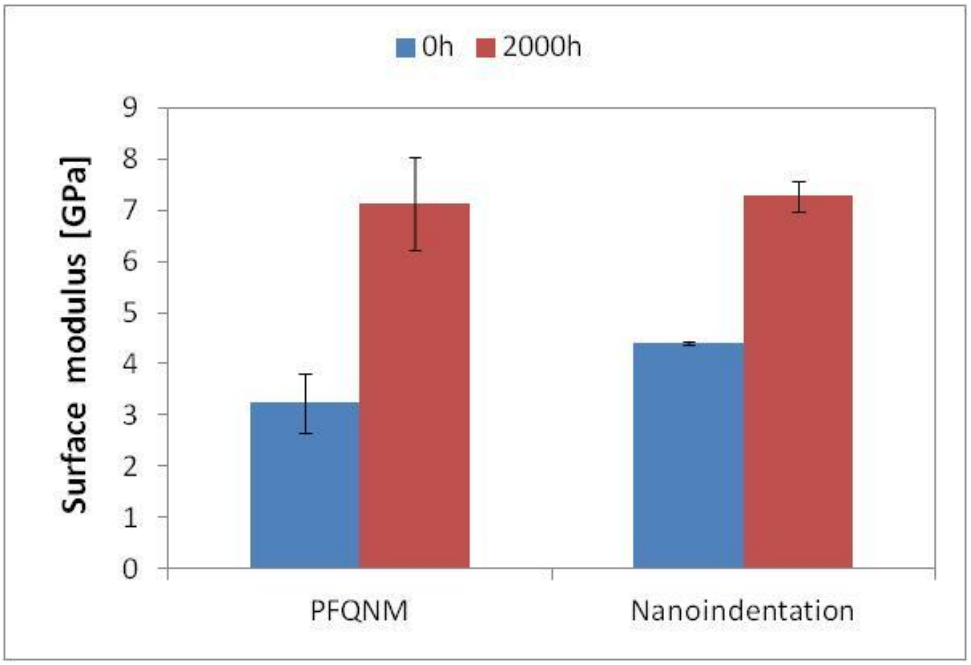

Figure 5.21: Average surface modulus values of an unexposed and 2000 hour WOM exposed sample obtained via PFQNM and IIT respectively

5.2.6.3 Surface mechanical properties discussion

In the IIT data the PET in WOM 800 hour data point did not appear to fit with the emerging trend and so was repeated at another location on the weathered surface of the same sample. The result was approximately the same, which raises further questions about the development of PET film surface mechanical properties with WOM exposure, particularly in the relatively early stages of WOM exposure. In order to better test if the 800 hour sample results are representative of the population, the measurement should be repeated on a new 800 hour exposed film sample, however there was not sufficient time to do this in the course of this investigation.

An increase in the surface Young's modulus of weathered PET films could potentially be caused by increased surface crystallinity, which has already been characterised by ATR-IR measurements. Due to their more closely packed molecular arrangement, PET crystallites have higher mechanical strength than amorphous PET regions of

similar size and shape (Cruz *et al.*, 1991), thus, an increase in the proportion of crystalline material at the surface results in an increased surface Young's modulus.

Another potential explanation for an increasing surface Young's modulus with UV exposure is photo-crosslinking. It has been proposed that photo-crosslinking can account for the increased indentation hardness of a weathered PET film surface due to the greater number of chain links generated by the UV photo-crosslinking reaction (Gardette *et al.*, 2014). Increases in both PET film crystallinity and crosslink density have been presented in this Thesis, however the evidence for photo-crosslinking being the mechanism behind surface hardening is far more compelling than increased crystallinity.

Since the spectral distributions of UV radiation in the WOM and HISS are approximately the same, there must be an additional factor responsible for the discrepancy between the surface Young's modulus of the two sample sets. Thus, it appears that the one or more of the additional degradation agents present in the WOM (elevated temperature and/or humidity) are responsible for this effect. Most likely, the increased temperature has increased the rate at which chemi-crystallisation and photo-crosslinking reactions have occurred.

The indentations caused by PFQNM imaging are on the order of nm and thus, the DMT modulus reflects the Young's modulus of the uppermost few nm of the weathered surface. While the indentations caused by IIT are on the order of 1 micron, and so reflects the Young's modulus of the uppermost few microns of the weathered surface. This difference in the surface sensitivity of the two techniques is reason for caution when comparing values generated by each technique. It may be that the modulus of the uppermost few nm varies considerably from the uppermost

few microns. Therefore, further investigation of these aspects of the analysis is recommended.

5.3 Conclusions

The findings presented in this Chapter support the following conclusions:

- PET film surface properties are more greatly modified by the applied artificial weathering techniques than bulk properties, with WOM exposure causing the most severe modifications overall, due to the synergistic effects of UV radiation with heat, humidity and direct water contact.
- Film rear surface modifications were observed on artificially weathered samples and also showed consistently greater degradation than in the sample bulk, further highlighting the greater sensitivity of film surfaces to weathering degradation processes than the film bulk.
- Of the modifications observed, PET film surface roughening is of particular note as it has previously only been sparsely reported in the literature:
    - It has been shown that at AFM length scales surface roughness increases linearly with WOM exposure time, but remains approximately unchanged with exposure to UV irradiation alone.
    - Several discrete changes were also observed, such as the sharpening of the nodular nanostructure of PET and the introduction of nanoscale pit-features.
    - The concept of surface roughness parameter distributions has been introduced and shown to give a more complete picture of surface

modification due to artificial weathering than has been possible using more traditional roughness analysis methods.

  - PET film samples were shown to have 3 parameter log-logistic shaped Ra distributions, which shifted to the right with accelerated environmental weathering, indicating the observed surface roughening of PET films to affect areas of different initial roughness equally.

- PET film surface mechanical properties have been shown to increase with artificial weathering exposure, due to a combination of photo-crosslinking and chemi-crystallisation. This highlights the scale variance of polymer mechanical properties, which predominantly decrease with degradation processes in macroscopic mechanical tests such as tensile tests.
- Of the samples analysed, surface microcracking only presented at the weathered surface of WOM exposed samples, highlighting the importance of synergistic effects to this modification.
- Surface silica contamination has been shown to locally enhance surface microcracking, which has serious implications for the measurement accuracy of degradation indicators and their kinetic behaviours.

EFFECTS OF UV STABILISATION ON PET FILM MODIFICATIONS DUE TO ACCERLERATED ENVIRONMENTAL WEATHERING

6.1 Chapter introduction and objectives

The direction of research in this Chapter was informed by the following hypotheses:

- Bulk UV stabilised PET film (UVA-PET) *bulk* performance properties will be well preserved after accelerated environmental weathering compared with plain PET film.
- UVA-PET film *surface* properties will be similarly affected to plain PET film by accelerated environmental weathering due to the lack of surface protection provided by bulk UV stabilisation.
- Thus, the prevention of surface degradation should be a priority for further enhancing the weatherability of bulk UV-stabilised PET film grades.

With these hypotheses in mind, the main objective of this Chapter is to investigate the efficacy of bulk UV stabilisation in preventing PET film bulk and surface degradation due to accelerated environmental weathering. To quantify the various stabilising effects of the inclusion of UVAs on PET film degradation phenomena, the most informative methods of degradation characterisation utilised in the previous Chapters have been applied to WOM exposed bulk UV-stabilised samples. These results will be compared with those obtained from WOM exposed plain PET film samples to give a measure of the stabilising effect of the UVA against the accelerated environmental weathering of 175 micron thick PET film.

The work in this Chapter will also further demonstrate which degradation phenomena occurring during accelerated environmental weathering are most greatly influenced by UV radiation, as these phenomena will be those most reduced in effect by the presence of the UVA. Due to the limited amount of sample degradation induced in plain PET film samples by the HISS apparatus, it was decided not to HISS expose UVA-PET samples, as these would in theory need extremely long exposure times to exhibit significant modifications, which was not deemed to be practical for this Thesis. Additionally there was also judged to be no need to DHO expose UVA-PET film samples, as there ought to be little difference in the hydrolysis performance of the two film types, and thus, little to be gained from conducting the lengthy exposure and analysis procedures.

6.2 PET film property modifications

The following sections present analysis of WOM exposed plain PET and UVA-PET film bulk and surface properties, grouped by analysis type and instrument.

6.2.1 Macroscopic sample changes after WOM exposure

There were a number of differences between the visually observable changes that occurred in the WOM exposed plain PET films and the WOM exposed UVA-PET films. With WOM exposure, the UVA-PET film samples exhibited less transverse direction curvature than WOM exposed plain PET film samples. This indicates that morphological modifications occurred in the samples to a lesser extent than in the plain PET samples, which will be explored in greater detail in the following sections. The UVA-PET film samples retained their ductile behaviour when cut with scissors,

even after thousands of hours of exposure. This suggests that the UVA has protected the film samples molecular architecture from degradation processes, which is what primarily gives PET its relatively high mechanical strength among polymer films.

The UVA-PET film samples also showed little evidence of surface contamination, which suggests that the contamination which presented on the plain PET film samples does not affect all WOM samples equally. Further, since the majority of the film properties of the two sample types are the same, it is more likely that unusual WOM chamber conditions caused the plain PET films to become contaminated than some difference between the two sample sets.

6.2.2 UV-Vis Spectroscopy

Using the same data processing methodology described in Section 4.3.2.1, Fig. 6.1 shows the relative transmission spectra of UVA-PET films exposed for up to 4000 hours in the WOM. The presence of the UVA has modified the PET film transmittance spectrum to cut on at approximately 390 nm instead of 310 nm. Therefore, incident photons with wavelengths between these values will be predominantly absorbed by the UVA, while incident photons with wavelengths between 290 nm and 310 nm may be absorbed by either the PET or the UVA. Fig 6.1 reveals that there is no significant change in UVA-PET film relative spectral transmittance (RST) with exposure time at any wavelength in the range plotted. Thus, it appears that the UVA has prevented the modification of PET via aromatic hydroxylation, which led to the modified light transmittance properties of the WOM exposed plain PET film samples presented in Section 4.3.2.

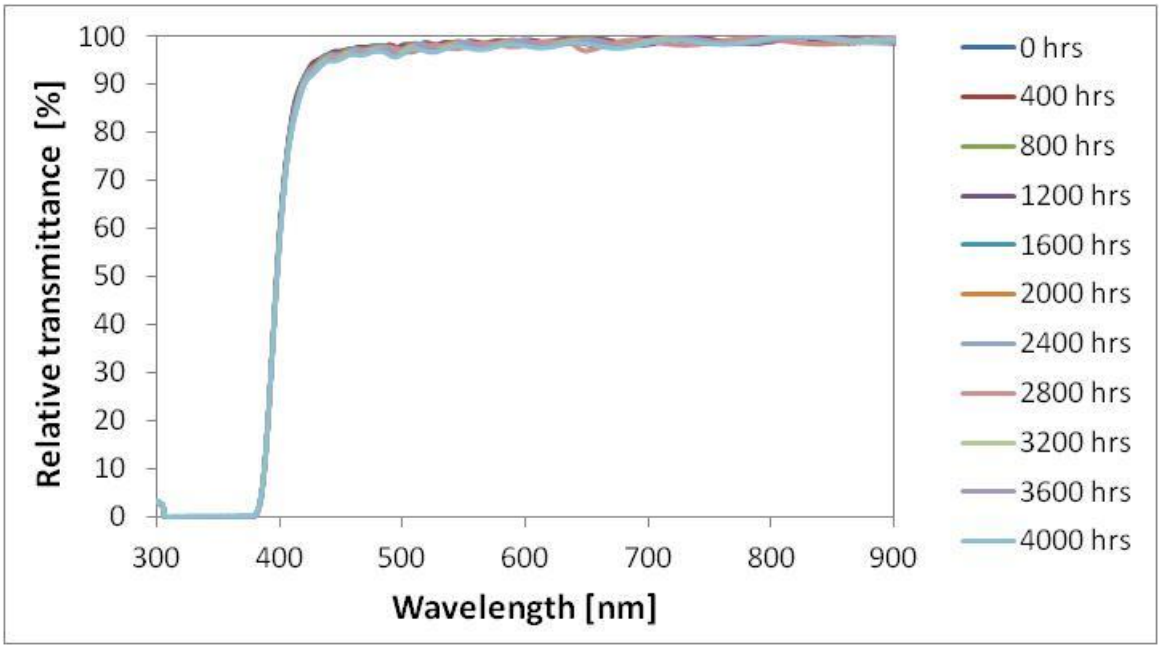

Figure 6.1: Relative transmittance spectra of UVA-PET film with 0 - 4000 hours WOM exposure

6.2.3 Fluorescence spectroscopy

Fig. 6.2 shows the fluorescent emission spectra of UVA-PET films exposed in the WOM for up to 4000 hours. Despite the apparent protection against optical modifications imparted by the UVA shown in Fig. 6.1, UV light of wavelength 320 nm was able to excite the same degraded PET fluorescence emission spectra in the WOM exposed UVA-PET film samples as was presented in Section 4.4 for plain PET film samples. With the exception of one sample, the newly formed peak centred at 456 nm increases in height with exposure time. A much smaller peak centred at 386 nm is also growing with exposure time. In the plain PET film samples this peak appeared to be due to the natural fluorescence of the PET molecules, however, in these samples the peak displays a different growth behaviour. This may simply be as a secondary result of the large fluorescence growth centred at 456 nm, but further investigation is required to validate this.

Unlike with the WOM exposed plain PET samples, no additional data processing was required to yield increasing fluorescence intensity with increasing exposure time for the UVA-PET samples. This may be because the whole sample set was tested in a single session, once the degraded PET film fluorescence spectroscopy analysis procedure had been developed using the WOM exposed plain PET samples. This provided consistent instrument parameters (bulb intensity, detector sensitivity, lab temperature, *etc*) throughout the analysis process which likely lead to the stable growth behaviour observed.

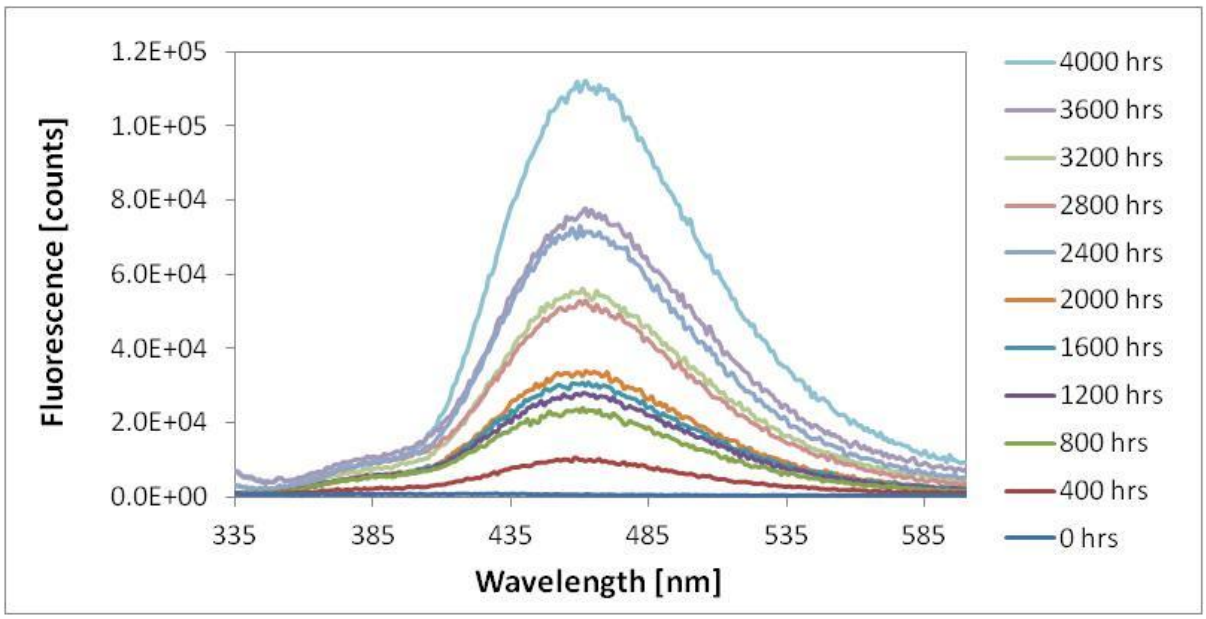

Figure 6.2: Raw fluorescent emission spectra of UVA-PET film with 0 - 4000 hours WOM exposure (λ_{ex} = 320 nm)

To compare the degraded fluorescence of the UVA-PET film with the plain PET film, the values at 456 nm were once again weighted using the values at 386 nm, which yielded Fig. 6.3. For WOM exposed UVA-PET, peak fluorescence jumps by over 4 units between 400 and 800 hours, after which point it gradually increases by

approximately 3 units over the remainder of the exposure duration. The fluorescence values of both sample sets in the late stages of exposure have similar values; the main differences are at low exposure times, where there is no initial jump observed in weathered plain PET 456 nm fluorescence, but it does increase with exposure time at a greater rate.

Thus, it appears that hydroxylated aromatic species are still being produced with WOM exposure in the UVA-PET film samples in substantial numbers, despite the presence of the UVA. However, in this case they do not appear to be contributing to the transmittance spectra of the exposed samples. This may be due to the modification occurring primarily at the UVA-PET film weathered surface, as fluorescence spectroscopy measurements are more sensitive to surface conditions than UV-Vis spectroscopy as they are conducted in reflectance mode rather than transmission (Eveson, 2013).

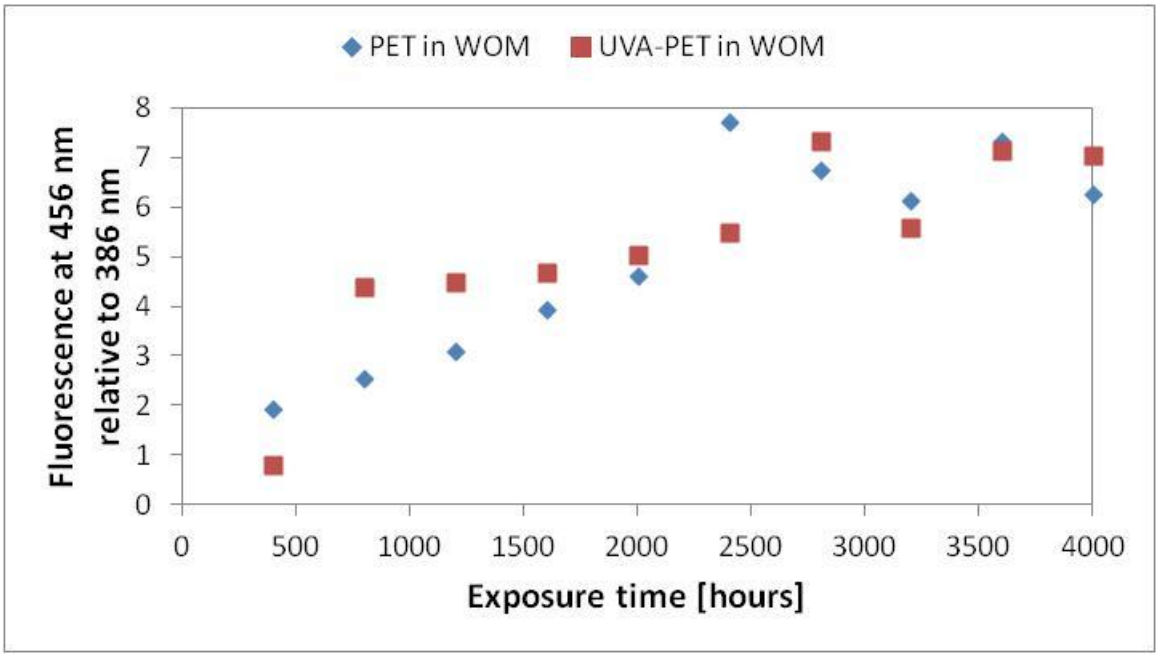

Figure 6.3: Fluorescent emission at 456 nm relative to 386 nm emission vs. exposure time for plain PET and UVA-PET film exposed in the WOM (λ_{ex} = 320 nm)

6.2.4 Optical microscopy

Figure 6.4 a-f shows reflection mode images captured by optical microscopy, of weathered PET film and UVA-PET film sample surfaces, which received 0, 2000 and 3200 hours of WOM exposure. The images illustrate several differences in surface microcrack development which have most likely been influenced by the inclusion of the UVA in the film formulation.

Pre-exposure, both film samples display homogenous surfaces at the length scale presented. After 2000 hours of WOM exposure, the plain PET film surface exhibits significant microcracking, while the UVA-PET film shows only sporadic black specks. After 3200 hours of WOM exposure, the UVA-PET film has also become microcracked, however, relative to the plain PET film microcracks these cracks are shorter, finer and present at a much lower density. Optical microscopy suggests that the UVA has reduced the impact of accelerated environmental weathering on PET

film surface microcracking. However, to understand the mechanisms responsible for this observation we must consider it in alongside the results from the other techniques successfully utilised in Chapters 4 and 5.

Interestingly, the UVA-PET film surface microcracks are not propagating in the film machine direction, as was observed of the majority of the plain PET film surface microcracks. This is most likely due to the differences in bow angle between the two films. When manufactured, biaxially oriented film at the outer edges of the production line can experience greater transverse drawing than film at the centre, commonly referred to as the bow angle of a film sample (Hodgson, 2015). Thus, in the case of films taken from the edges of a production mill roll, such as the UVA-PET film, the film molecular architecture will be tangential to the machine direction. It is proposed that this effect is responsible for the primary direction of the microcracks.

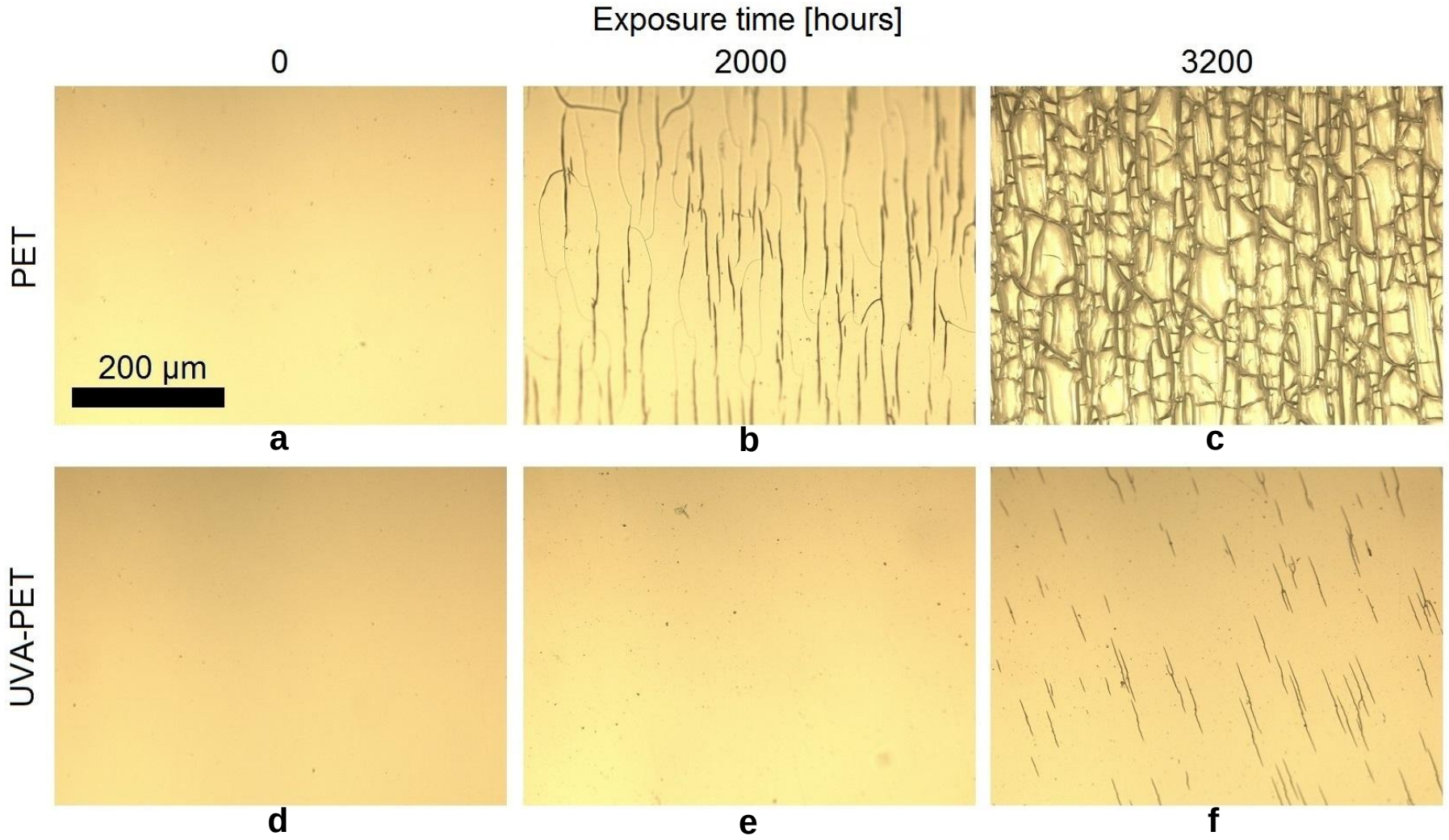

Figure 6.4 a-f: Optical micrographs of weathered PET film surfaces (a-c) and UVA-PET film surfaces (d-f) which received 0, 2000 and 3200 hours of WOM exposure - Scale bar applies to all images

6.2.5 Gel permeation chromatography

Figure 6.5 shows computed MWDs of UVA-PET film samples which received between 0 and 4000 hours of WOM exposure. The shape of the MWDs is consistent with the pre-exposure plain PET film MWD already described in Chapter 4, which indicates that the inclusion of the UVA has not affected the film MWD. With increasing exposure time, the distributions broaden to the left, but to a much lesser extent than was observed with the WOM exposed plain PET samples. Thus, it appears that far fewer photo-scissions have occurred in the UVA-PET film samples than in the plain PET film samples due to the inclusion of the UVA in the film formulation. There also appears to be no change with WOM exposure at the high molecular weight end of the distribution, which suggests that the UVA has also prevented photo-crosslinking from occurring at levels detectable by GPC.

It was expected that the UVA-PET film MWDs would have shifted less with WOM exposure than the plain PET film MWDs, however it was not expected that the shift would be so much less, as the UVA should not prevent sample hydrolysis, which was thought to be partly responsible for the discrepancy in degradation observed between the HISS and WOM exposed plain PET film samples in Chapter 4. Thus, the very small changes observed in the WOM exposed UVA-PET samples suggests that the contribution to WOM induced PET degradation by hydrolysis is in this case very small, adding further weight to the theory that the synergistic effects of UV with heat, humidity and direct water contact play a significant role in PET film degradation during accelerated environmental weathering.

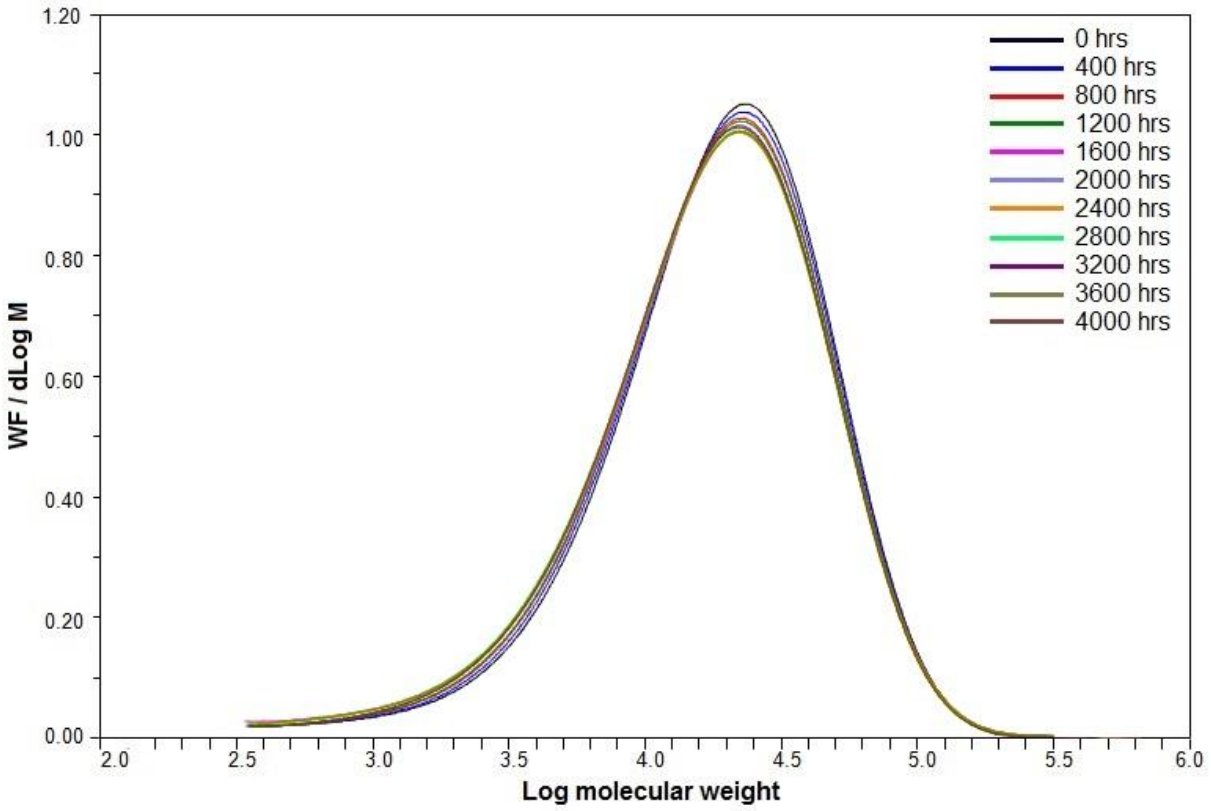

Figure 6.5: MWDs of UVA-PET film which received between 0 and 4000 hours of WOM exposure

Figure 6.6 shows a plot of number average molecular weight (M_n) vs. exposure time, for plain PET and UVA-PET film samples exposed in the WOM. It reveals a significant difference in M_n reduction with WOM exposure between the two samples, and hence the stabilising effect of the UVA against photo-scissions. While the plain PET film M_n is reduced by approximately 5000 units after 4000 hours of exposure, the UVA-PET sample M_n is only reduced by around 500 units up to 1600 hours, a stabilisation effect equivalent to one order of magnitude. Additionally, after 1600 hours there is no further appreciable change in the UVA-PET film sample M_n, this may be because the M_n represents the average chain length of molecules over the entire film thickness. If the degradation of the UVA-PET film is occurring only in a

relatively thin layer at the surface, due to the presence of the UVA in the bulk, then the sample M_n may not fall beyond a certain minimum point.

Possible reasons that chain scissions may still be occurring in the UVA-PET film during WOM exposure include: the UVA not fully preventing photo-scissions, sample hydrolysis and/or synergistic degradation effects. With further analysis of degradation parameters it may be possible to rule one or more of these factors out.

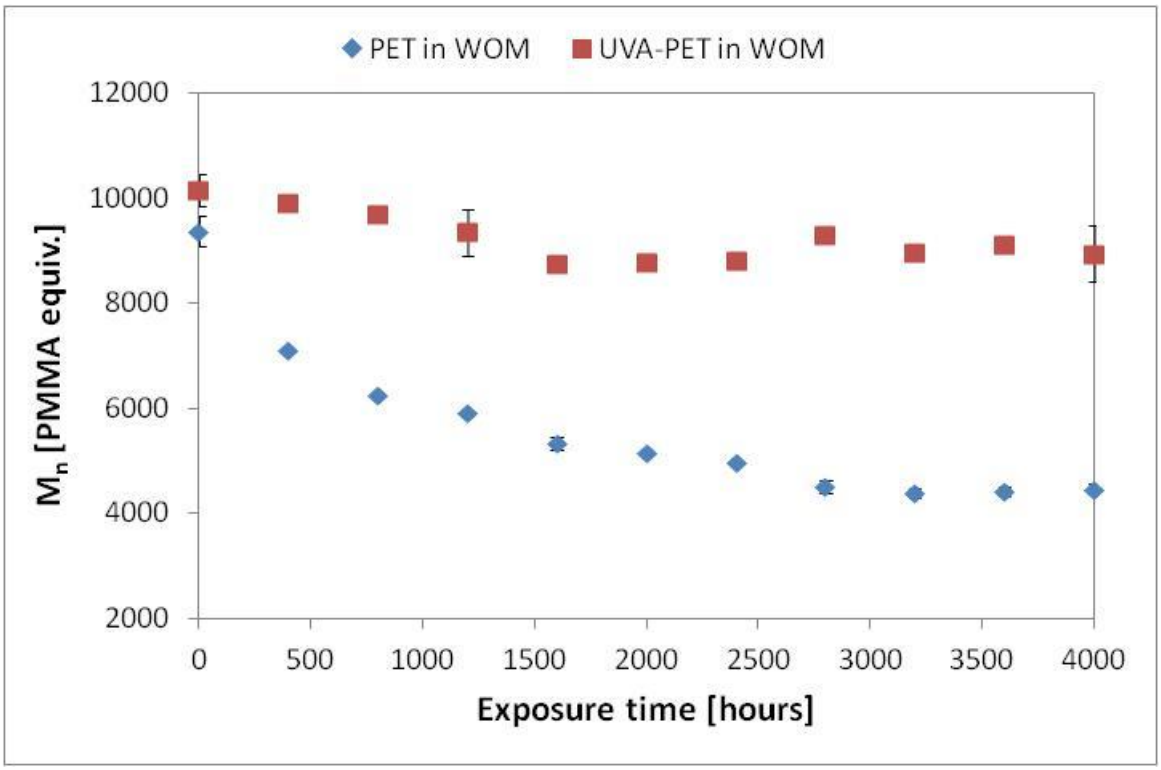

Figure 6.6: M_n vs. exposure time for plain PET and UVA-PET films exposed in the WOM

Figure 6.7 shows a plot of weight average molecular weight (M_w) vs. exposure time, for plain PET and UVA-PET film samples exposed in the WOM. UVA-PET film M_w exhibits a similar pattern of change to the M_n, however it does continue to decrease with WOM exposure after 1600 hours exposure, albeit at a slower rate. This

reduction is much more stable than the reduction shown by plain PET, which is probably due to the lack of high molecular weight molecules generated by photo-crosslinking affecting the parameter, which is more sensitive to high molecular weight material than M_n. The stable reduction in the UVA-PET film samples, which showed no photo-crosslinking, further strengthens this hypothesis.

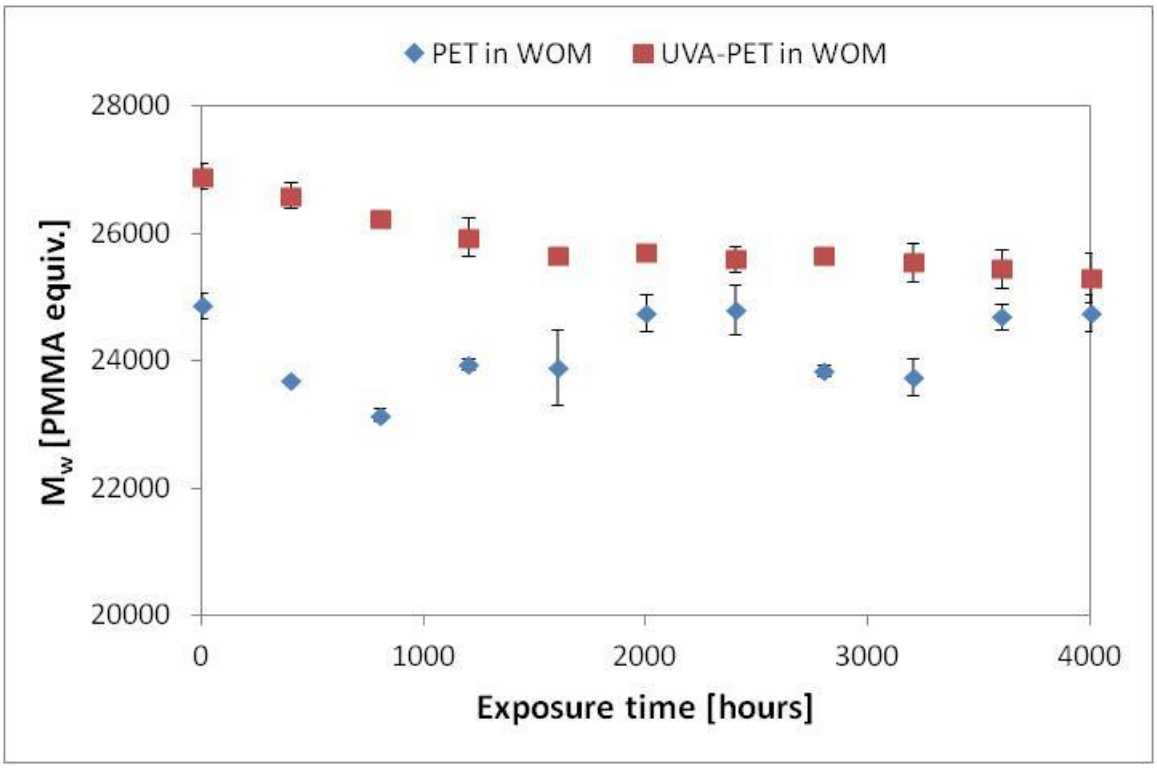

Figure 6.7: M_w vs. exposure time for plain PET and UVA-PET films exposed in the WOM

Figure 6.8 shows a plot of Z average molecular weight (M_z) vs. exposure time, for plain PET and UVA-PET film samples exposed in the WOM. It reveals that the UVA-PET film M_z is decreased by approximately 2000 units over 4000 hours of WOM exposure, which is in stark contrast to the doubling of M_z which occurred in the plain PET film samples over the same exposure period. Together with the other molecular

weight parameter results, these findings strongly suggest that while the number of chain scissions occurring has been reduced by the inclusion of UVA in the film formulation, photo-crosslinking has been effectively eliminated. However, it is possible that it may still be occurring in a very thin layer at the weathered surface, in numbers below the detection limit of GPC in thick polymer films.

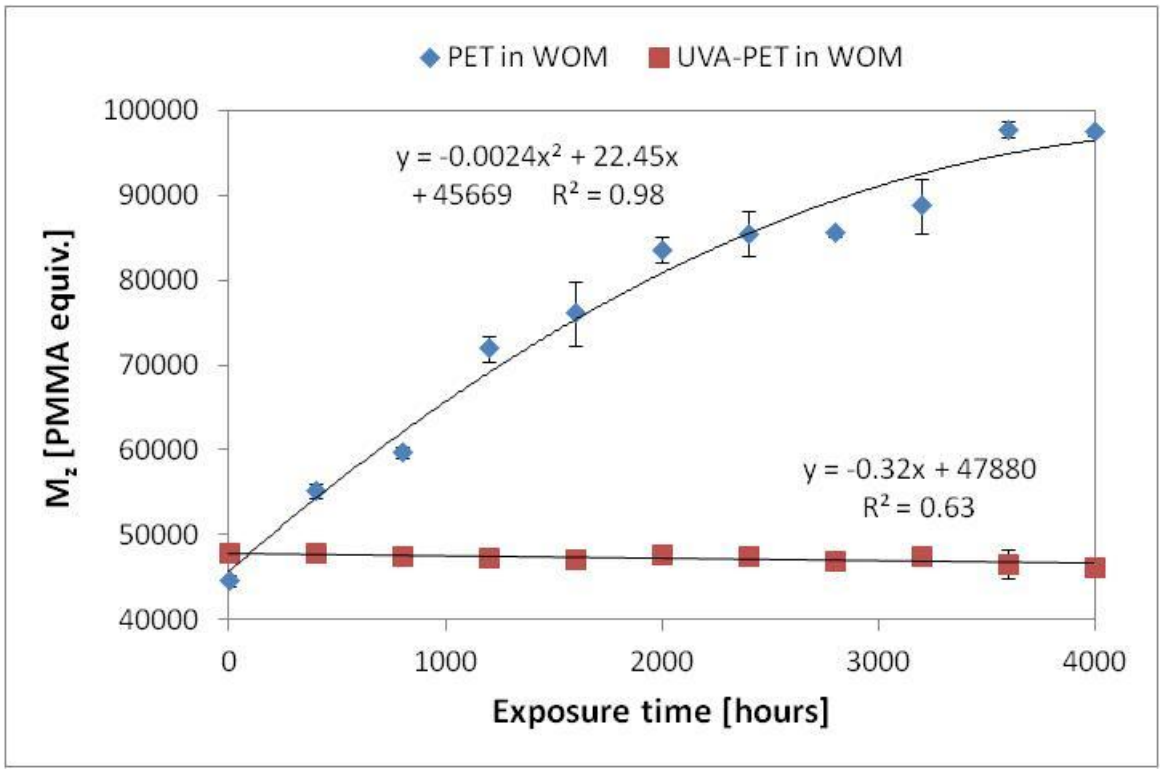

Figure 6.8: M_z vs. exposure time for plain PET and UVA-PET films exposed in the WOM

Figure 6.9 shows a plot of dispersity vs. exposure time, for plain PET and UVA-PET film samples exposed in the WOM. It shows that dispersity in the UVA-PET film samples is relatively unchanged over 4000 hours of WOM exposure compared with the plain PET film samples in which dispersity is approximately doubled. This indicates that the UVA is allowing the film to retain the shape of its MWD, even after

4000 hours of exposure, and is thus providing protection against degradation to polymer chains of all lengths. It also implies that photo-crosslinking is likely to be a significant factor in the increase in dispersity observed in the WOM exposed plain PET film samples.

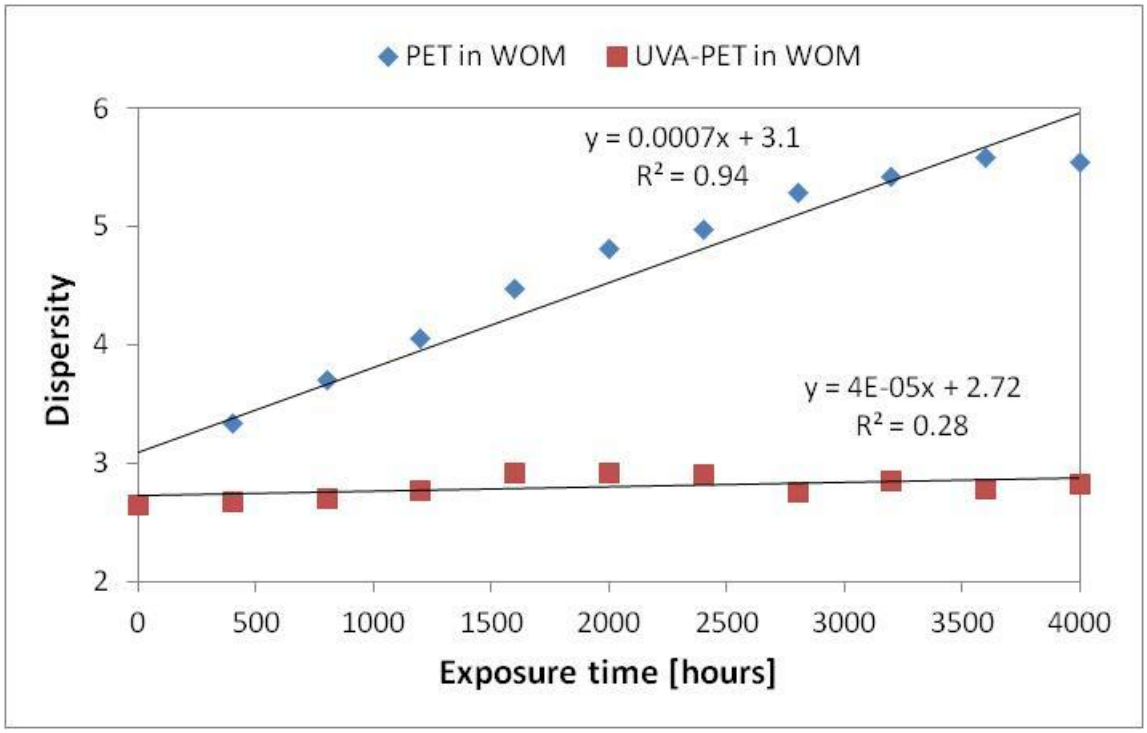

Figure 6.9: Dispersity vs. exposure time for plain PET and UVA-PET films exposed in the WOM

Figure 6.10 reveals the random chain scission approximation for plain PET and UVA-PET film samples exposed in the WOM. It shows that the rate at which scissions occur in the UVA-PET film samples increases slightly with exposure time, but is far lower than in the plain PET film samples. The rate of scissions in the UVA-PET film samples peaks between 1600 and 2400 hours of WOM exposure, but from 2800 hours returns to its former linear pattern of increase. A physical explanation for the behaviour of these central points is lacking, however that all three are above the

linear line of increase makes random data fluctuations less likely. Further investigation is required to understand this aspect of the data.

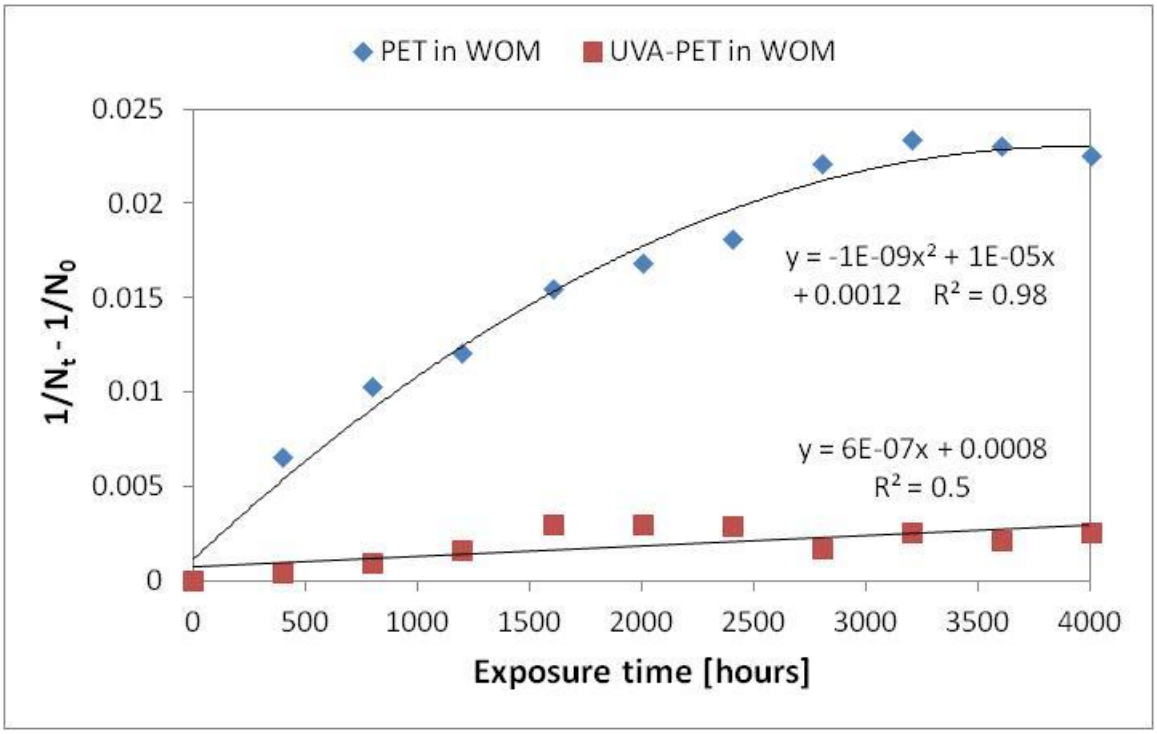

Figure 6.10: Random chain scission approximation for plain PET and UVA-PET film samples exposed in the WOM

6.2.6 FTIR Spectroscopy

6.2.6.1 Carboxyl index

In order to compare sample scission kinetics in the bulk to that of the surface region, the carboxyl index method of Day and Wiles has been used. Figure 6.11 shows a plot of carboxyl index vs. exposure time from transmission FTIR spectra, obtained from plain PET and UVA-PET samples exposed for increasing lengths of time in the WOM. After an initially rapid increase between 0 and 800 hours exposure, plain PET carboxyl index increases linearly, at rate of approximately 0.1 units per 400 hours. The UVA-PET film carboxyl index also increases linearly with exposure time, but at a

rate one order of magnitude lower than in the plain PET samples. This suggests that the UVA has not altered the mechanisms of degradation, but has substantially reduced the rate at which scissions occur, which is in agreement with the GPC findings presented in Section 6.2.5.

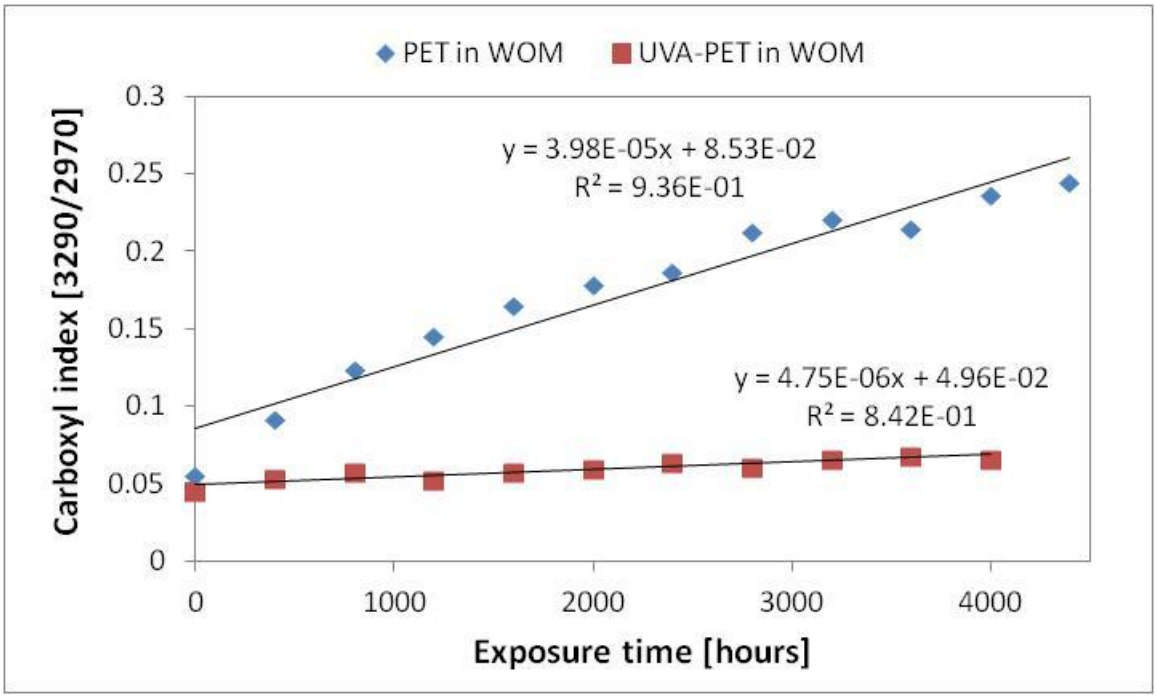

Figure 6.11: Carboxyl index vs. exposure time for plain PET and UVA-PET film samples exposed in the WOM

ATR-FTIR spectroscopy has been utilised to compare the chain scission behaviours in the uppermost 1.3-2.7 microns of the plain PET and UVA-PET film surfaces (Harrick and du Pré, 1966). Figure 6.12 shows the ATR carboxyl index vs. exposure time of the weathered surfaces of plain PET film and UVA-PET film samples exposed in the WOM. The ATR carboxyl index curves of the two sample types are much more similar than the corresponding sample transmission carboxyl index curves. However, the UVA-PET film carboxyl index is still slightly lower after each exposure interval,

indicating that the UVA has provided a small amount of stabilisation against photo-scissions at the exposed surface. Both curves increase with decaying growth rates up to 1600 hours, after which point there are no further significant developments. Thus, when compared with the film bulk it appears that there are similar numbers of chain scissions occurring at the exposed surfaces of both film samples with WOM exposure, which shows that the UVA molecules are not protecting the polymer surface as effectively against chain scissions as they do in the film bulk. This is reasonable as UV radiation intensity will decay exponentially according to the Beer-Lambert law as it travels through the UV absorbing film. Therefore, the radiation intensity reaching the film bulk will be considerably less than at the film surface.

These findings are of particular interest when we consider the substantial differences in surface microcracking displayed in Fig. 6.4. The minor differences observed between the surface carboxyl indices, together with the substantial differences in surface microcrack density, suggests that there must be additional factors to surface chain scissions which influence the surface microcracking of PET film. Other factors which may be influencing microcracking include chemi-crystallisation, photo-crosslinking and bulk scission. Further, these ATR-FTIR findings also point to the potential role of bulk property modifications in surface microcrack development.

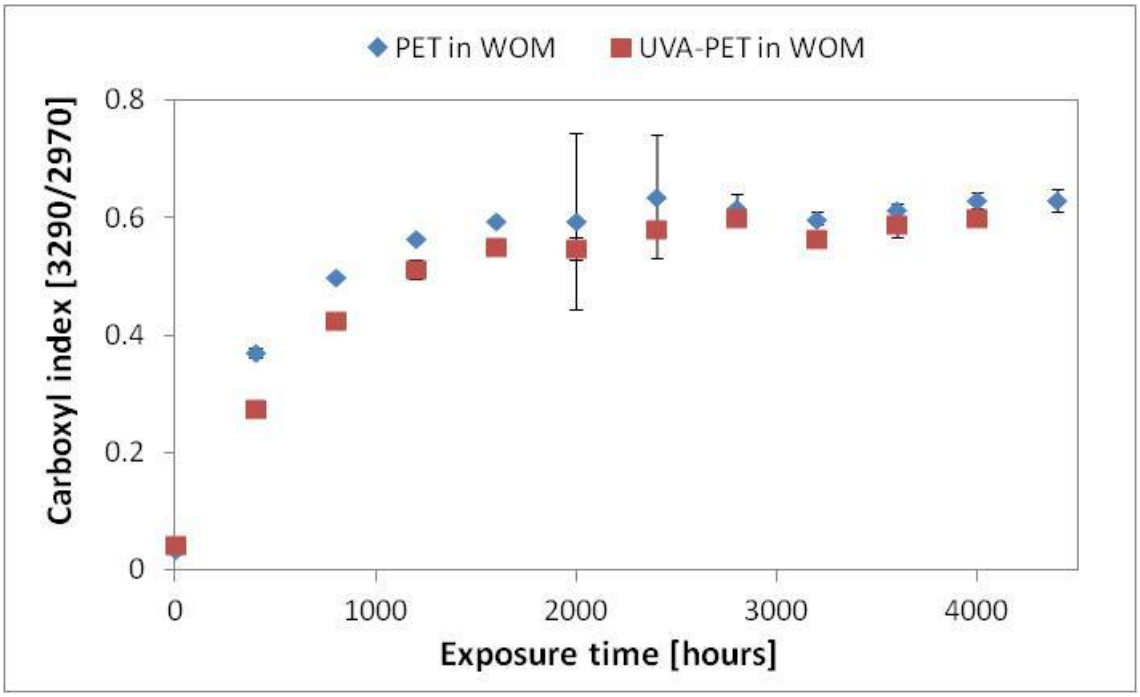

Figure 6.12: ATR carboxyl index vs. exposure time of the weathered surfaces of plain PET and UVA-PET film samples exposed in the WOM

6.2.6.2 Surface crystallinity measurement

Figure 6.13 shows crystallinity index vs. exposure time of the weathered surfaces of plain PET and UVA-PET film samples which received up to 4000 hours of WOM exposure. Fig. 6.13 reveals a similar trend in surface crystallinity development in both samples to surface carboxyl index, which suggests that the UVA is not preventing chemi-crystallisation from occurring at the surface, but is providing a small amount of protection against its occurrence. Thus, chemi-crystallisation may be a factor in the different microcrack behaviours exhibited by the plain PET and UVA-PET films, however it may only have a minor role.

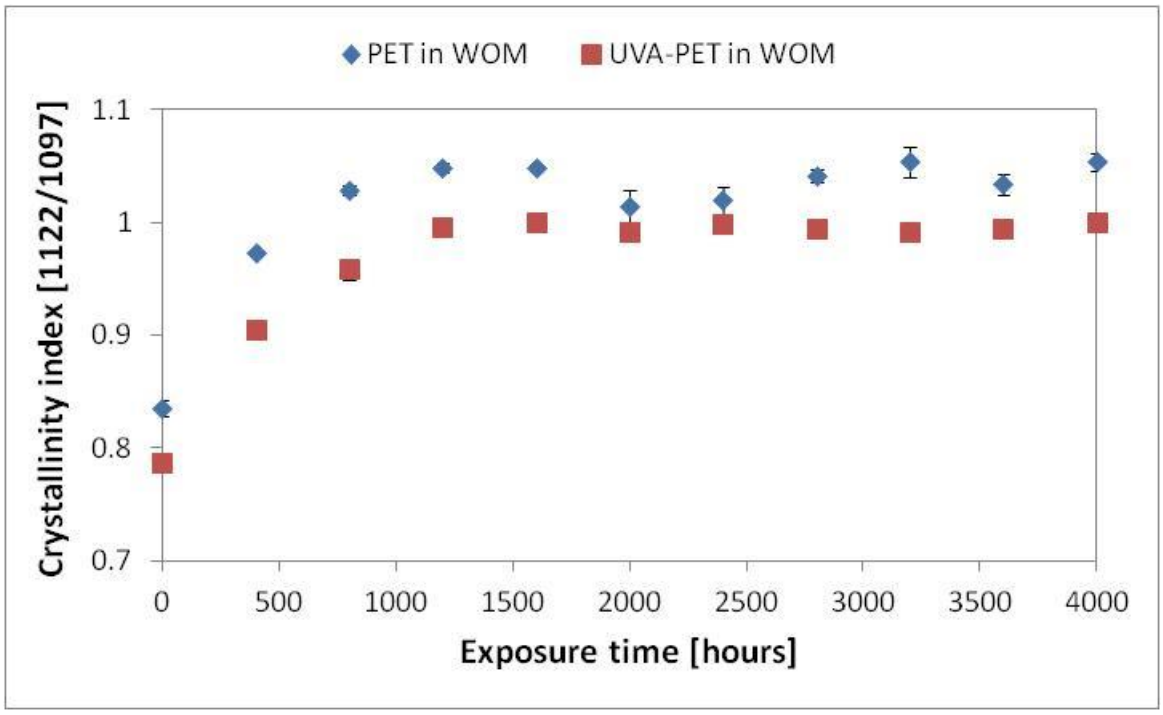

Figure 6.13: Crystallinity index vs. exposure time of the weathered surfaces of plain PET and UVA-PET film samples exposed in the WOM

6.2.7 Water contact angle

Figure 6.14 shows the mean water contact angle (WCA) vs. WOM exposure time, of the weathered surfaces of plain PET film and UVA-PET film samples. It reveals that UVA-PET film has an initially higher WCA than plain PET, but that it is reduced with WOM exposure at a similar rate to the WCA of plain PET up to 1600 hours. This indicates that the UVA is offering very little protection against -OH group formation at the film weathered surface. As surface microcracking did not occur until much later in the weathering process for the UVA-PET film, meaningful WCA values for this sample were recorded up to 4000 hours of WOM exposure, revealing a continuation of the linear trend up to the end of the exposure duration. This suggests that the number of surface -OH end groups can reach much higher levels before the onset of surface microcracking and therefore seems not to be a significant factor in

microcrack occurrence. It also strongly suggests that -OH group production continues on the plain PET film surface after the onset of microcracking, which caused the artificial recovery of the WOM exposed plain PET film WCA. Finally, much smaller WCA variances were seen on the UVA-PET film samples, suggesting more uniform levels of modification across the UVA-PET sample surfaces, though this may also be due to lesser levels of surface contamination for these samples.

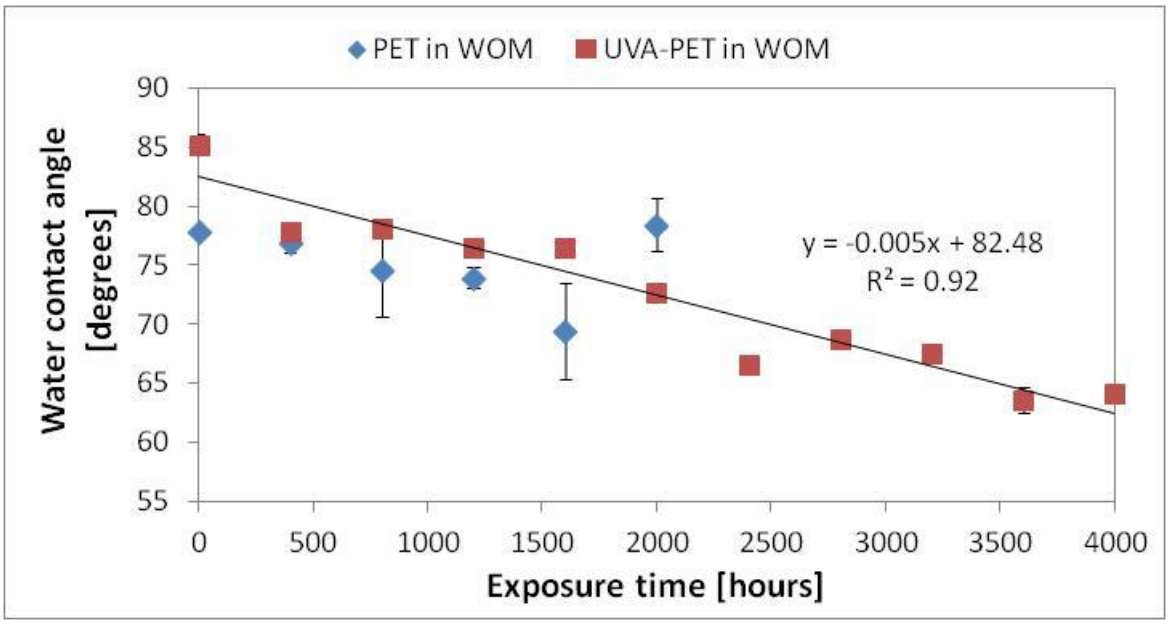

Figure 6.14: Water contact angle vs. exposure time of the weathered surfaces of plain PET and UVA-PET film samples exposed in the WOM

6.2.8 Atomic force microscopy

As for the WOM exposed plain PET film samples, 6 different areas of each of the WOM exposed UVA-PET sample weathered surfaces were analysed by AFM, with 2, 5 and 20 µm FOVs. The Ra values obtained from each image were then averaged to yield a representative analysis of the modification of UVA-PET film surface roughness with WOM exposure. Fig. 6.15 is a TM-AFM image montage of

representative examples of the imaged areas of the UVA-PET film weathered surface after increasing amounts of WOM exposure. In the areas imaged, there was little evidence of surface modification until after 1200 hours of WOM exposure, when changes similar to those observed on the WOM exposed plain PET film surface were observed at all three length scales. In addition to overall surface roughening, in the 5 µm images, many new valleys were observed, and in the 20 µm images new surface peaks were also observed, hypothesised already to be oligomers. Notably, in the 20 µm images, after 2000 hours of exposure the surface does appear significantly modified, exhibiting much deeper valleys than were initially observed. Thus, it appears that the existing surface topography has effectively been exaggerated by the weathering process. New nanoscale pit-features and sharpening of the surface nodules with exposure time were also observed, which suggests that these are common features of the accelerated environmental weathering of PET film surfaces.

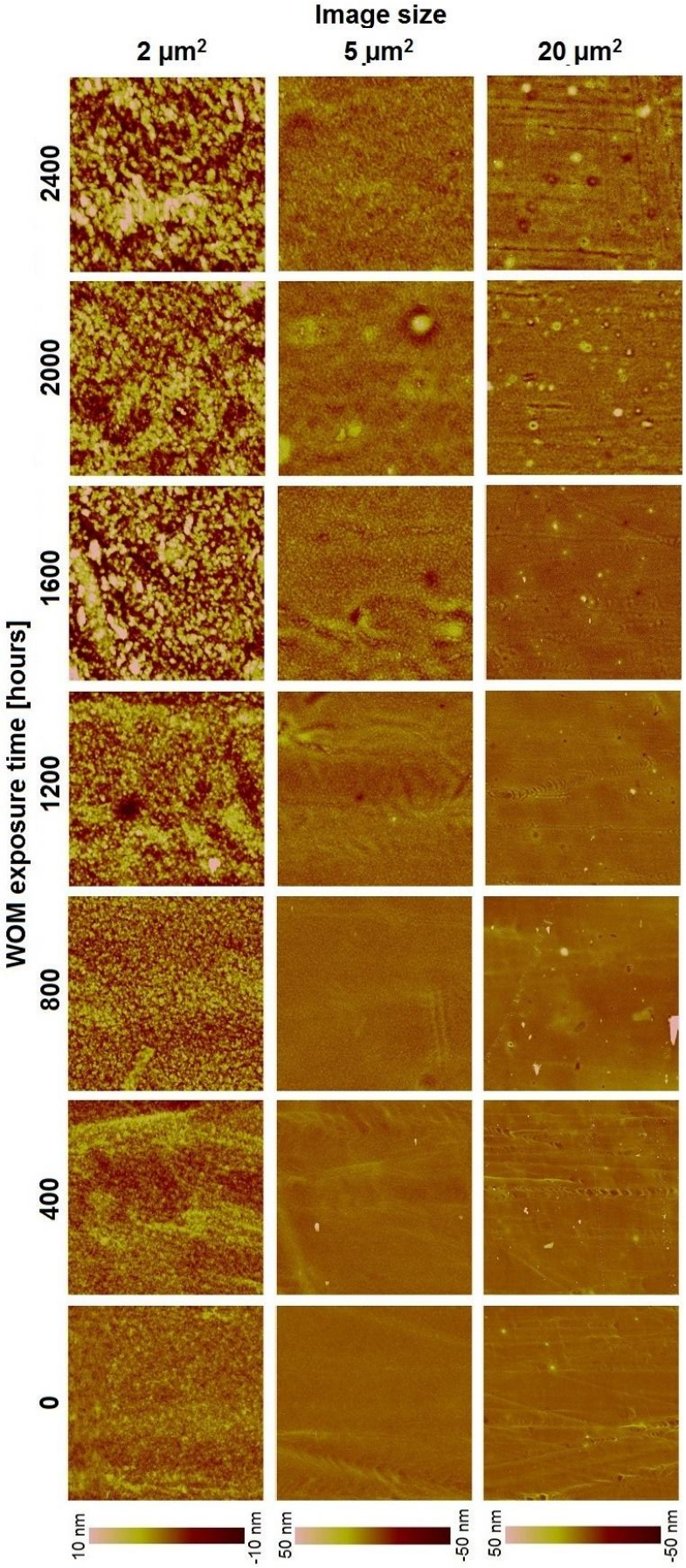

Figure 6.15: AFM topography images of the weathered UVA-PET film surface with increasing WOM exposure time up to 2400 hours. Z range of 20 nm applies to the 2 µm images while a Z range of 100 nm applies to the 5 and 20 µm images.

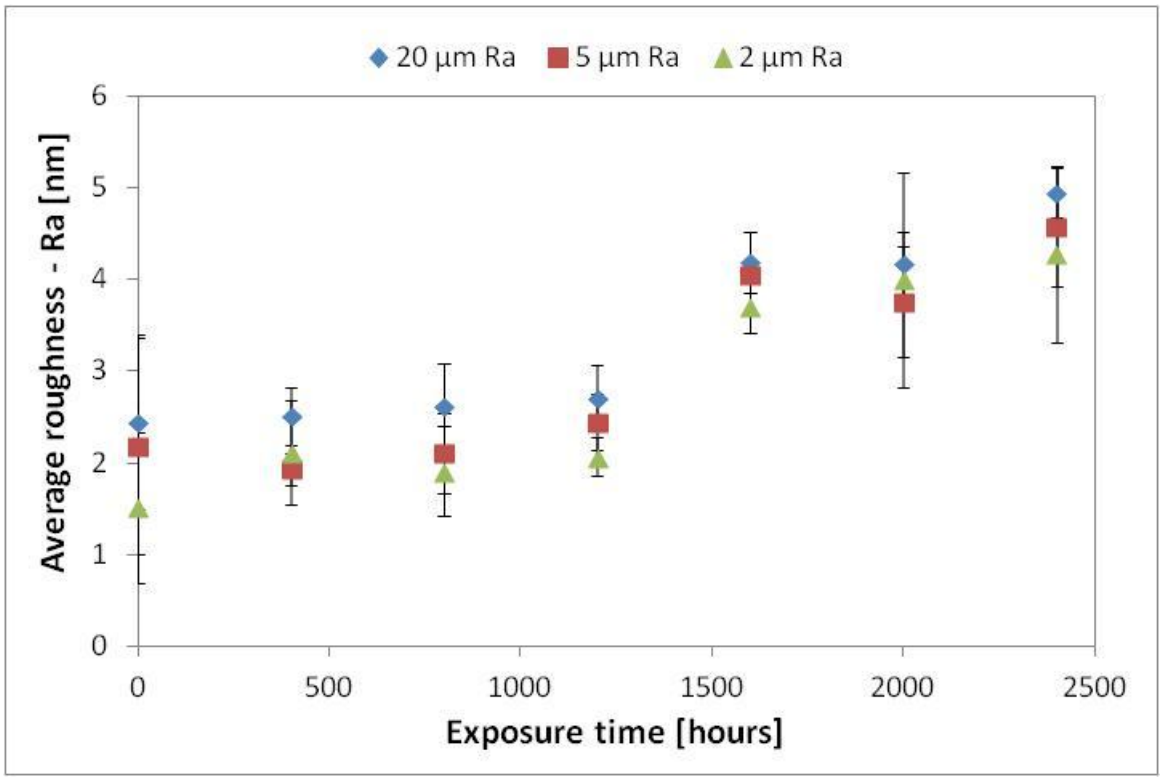

Figure 6.16: Ra vs. exposure time at 2, 5 and 20 um AFM length scales for the weathered surface of WOM exposed UVA-PET film

Fig. 6.16 shows mean Ra vs. exposure time for the 2, 5 and 20 µm TM-AFM images of the WOM exposed UVA-PET film weathered surface. At all three measured length scales Ra remains approximately the same within error until 1200 hours of WOM exposure, supporting the observation made from the images and the hypothesis that UV is the primary factor associated with PET film surface roughening due to WOM exposure. After 1600 hours, the Ra has increased by approximately 2 nm, which suggests that at some point between 1200 and 1600 hours, the UVA was no longer able to inhibit UV-induced surface roughening. There are several possible reasons that the UVA stopped preventing surface roughening, but the most logical are that it may have become depleted from the surface, or been de-activated after degrading

itself. Confidence intervals widened with exposure time which suggests that the film surface is becoming more heterogeneous with increasing exposure.

6.2.9 White light interferometry

Fig. 6.17 shows the 3 parameter log-logistic fits of the Ra distributions of WOM exposed UVA-PET sample weathered surfaces, generated by curve fitting the WLI Ra distributions of the weathered sample surfaces. The weathered UVA-PET film surface exhibits approximately the same Ra distribution profile as plain PET, log-logistic shape, heavy high end tail, left-skewed, *etc*. The distribution shapes and heights are in this case relatively unchanged with WOM exposure, unlike the plain PET film Ra distribution which was both widened and reduced in height with exposure time. Small changes in distribution position are observed until 2000 hours of exposure, at which point the whole distribution has shifted to the right by approximately 0.5 nm, which is followed by a further shift of approximately 1 nm between 2000 and 2800 hours. That the whole distribution is shifting to the right indicates that the initial surface roughness of an area does not affect the rate of roughening and that it is, in this case, a uniformly occurring process.

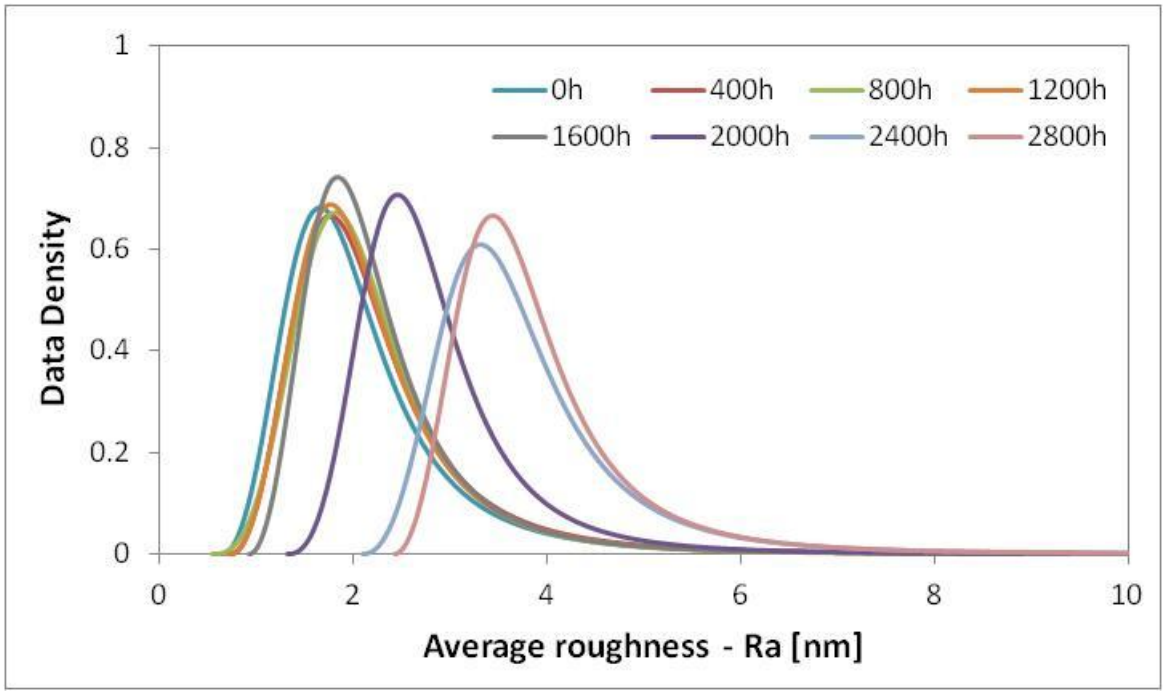

Figure 6.17: 3 parameter log-logistic fits of Ra distributions obtained from 1 cm^2 areas of the weathered surfaces of UVA-PET film samples WOM exposed for up to 2800 hours

To better compare the surface roughening effect of WOM exposure on the plain and UVA stabilised film samples, in Fig. 6.18 the modal Ra values of each distribution have been plotted against exposure time. This reveals that the UVA-PET sample surface reaches a similar modal Ra value to the plain PET film, but only after 2400 hours of exposure, and having started with a 0.5 nm greater initial modal Ra. There is also only a small increase in the UVA-PET film surface modal Ra between 2400 and 2800 hours exposure, whereas for the plain PET samples, the rate of roughening has continued to increase with exposure time. Without analysis of further weathered samples however, it is unclear whether this is due to sample variance or is in fact a physical effect.

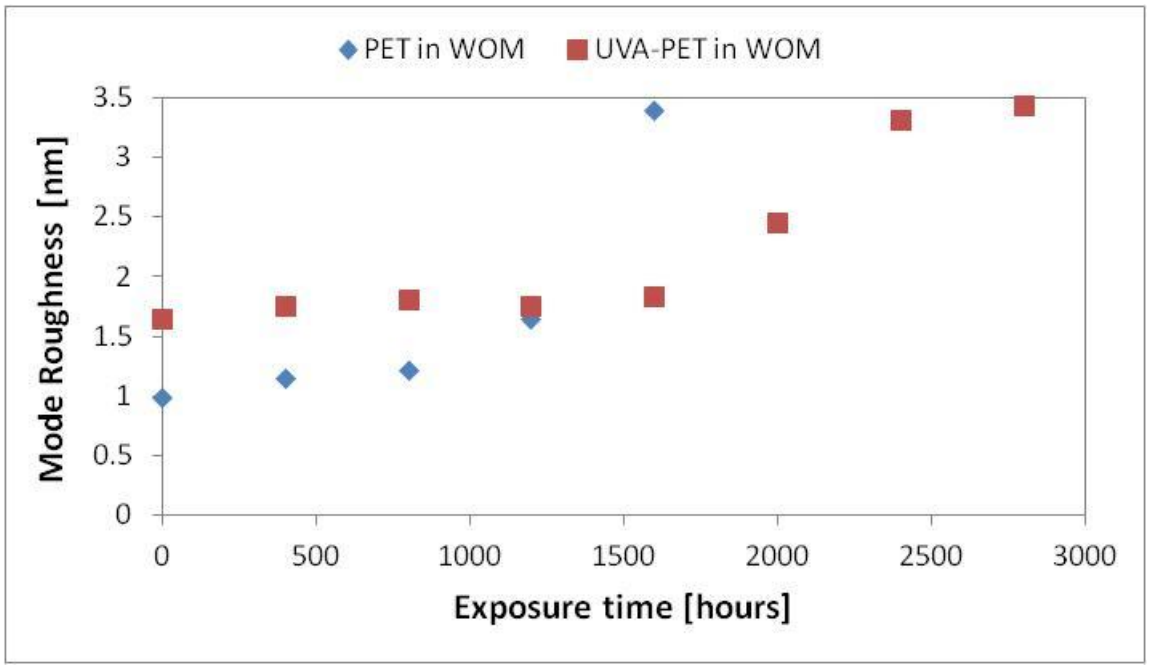

Figure 6.18: Weathered plain PET and UVA-PET film surface modal Ra value evolution with WOM exposure time

To enable the best comparison of the surface roughening processes of the plain and UVA containing samples, the change (Δ) in sample modal Ra after each exposure interval has been plotted. This reveals that on average, the plain PET is roughened by WOM exposure sooner, at a faster rate, and to a greater extent than the UVA-PET samples.

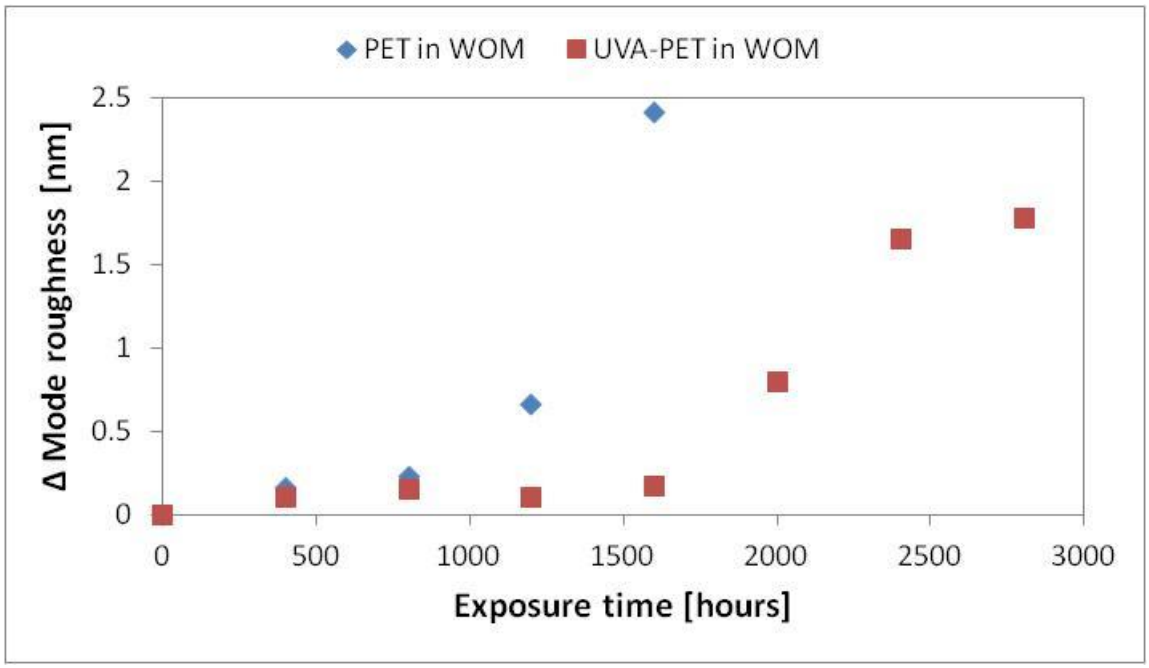

Figure 6.19: Change in modal Ra vs. exposure time for the weathered surface of WOM exposed PET film

6.2.9.1 Surface topography modification summary

By including a UVA stabilised film grade in this Thesis, several more aspects of the UV induced surface modification of PET films due to accelerated environmental weathering have been observed, which are summarised below:

- The inclusion of a UVA in the PET film formulation does not change the shape of the average surface roughness distribution, probably due to the low wt. % present in the samples and hence at the surface.
- Bulk UV stabilisation has prevented PET film surface roughening due to accelerated environmental weathering from occurring for at least 1200 hours at AFM length scales, and 1600 hours at WLI lengths scales. This indicates that AFM is able to detect PET film surface roughening earlier, due to its greater resolving power.

- The mechanism of the surface roughening process also appears unchanged by including UVA in the film formulation.
- That the other surface properties of the plain and UV stabilised films are affected similarly by the weathering process, the disparity in surface roughening rates suggests that PET film surface roughness may to some extent depend upon the integrity of the film bulk.

6.2.10 Instrumented nanoindentation

Figure 6.20 shows surface Young's modulus values acquired by instrumented nanoindentation (IIT) vs. exposure time, for plain PET and UVA-PET film samples exposed in the WOM. It reveals that the Young's moduli of both film sample weathered surfaces increase with WOM exposure, suggesting that the UVA does little to prevent this surface modification. After an initial larger increase, the UVA-PET surface modulus gradually increases up until the end of the exposure duration, but unlike for plain PET, does not fall to a fraction of its initial value after 2800 hours. Thus, the UVA does not appear to have prevented the hardening of the film surface after accelerated environmental weathering, which has thus far been theorised to be due to a combination of photo-crosslinking and chemi-crystallisation. That the surface Young's modulus of the UVA-PET film samples did not fall dramatically as it did in the plain PET samples, indicates that the surface retained its ductile mechanical properties up to the end of the 4000 hour exposure duration, despite surface microcracking. After 1200 hours the UVA-PET film surface modulus fell by 1 GPa which appears to be due to local sample variation.

Unfortunately it has not been possible to gain strong evidence to convincingly rule one way or another on this phenomenon, due to the lack of a surface sensitive test for crosslinked material. GPC analysis of the WOM exposed UVA-PET film samples showed photo-crosslinking to have been eliminated in the bulk, while ATR-FTIR analysis showed surface crystallinity to have increased. However, since IIT cannot determine the mechanism responsible for the surface hardening process, it can only be concluded that both photo-crosslinking and chemi-crystallisation are likely to play a role in increasing PET film surface modulus, but that the evidence suggests that chemi-crystallisation likely plays a greater role, as photo-crosslinking was eliminated in the film bulk by the addition of the UVA to the film formulation.

Once more, if photo-crosslinking was occurring only in a very thin surface layer, it is possible that it would not be detected by GPC but still affect the film surface modulus. To test this hypothesis, a surface specific test for polymer crosslinking must be utilised, or a sample resistant to chemi-crystallisation employed; PET polymer or co-polymer with an increased T_g for example.

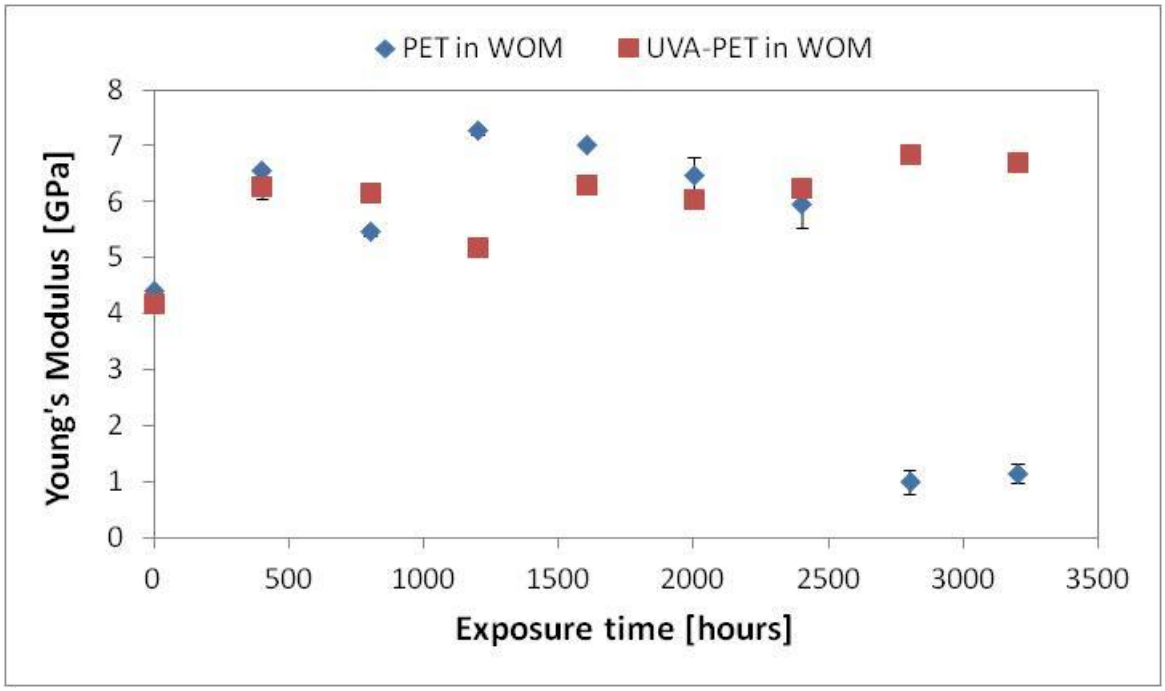

Figure 6.20: Surface Young's modulus vs. exposure time of plain PET and UVA-PET film sample weathered surfaces exposed in the WOM

6.2.11 PeakForce QNM-AFM

Fig. 6.21 shows a comparison of the average surface modulus results obtained via IIT and PFQNM of the weathered surfaces of plain PET and UVA-PET films after 0 and 2000 hours of WOM exposure. The mean surface modulus values of the UVA-PET film samples obtained by PFQNM are 1 GPa both before and after 2000 hours of WOM exposure. Unlike for the plain PET film samples, these values do not correspond well with the Young's modulus values measured by IIT. Thus, it appears that the PFQNM analysis has not yielded accurate surface modulus values for the UVA-PET film samples. This may be due to miscalibration of one of the instrument parameters prior to data capture, however, all instrument parameters were kept constant throughout the analysis process and therefore, even though some values

may have been incorrect, the fact that the mean modulus values were unchanged by WOM exposure may still have some value.

However, this was not the case with IIT, where a modulus increase was observed after 2000 hours of WOM exposure for the UVA-PET film sample. Thus, if this is a physical effect it would indicate that in the top few nm of the surface, mechanical properties are unchanged by WOM exposure. However, this is not consistent with the theorised mechanisms of surface hardening, for which evidence has already been presented. Overall, this result suggests that the PFQNM technique requires further refinement before it can be successfully applied to artificial weathering studies with various differing samples, as well as control and test samples.

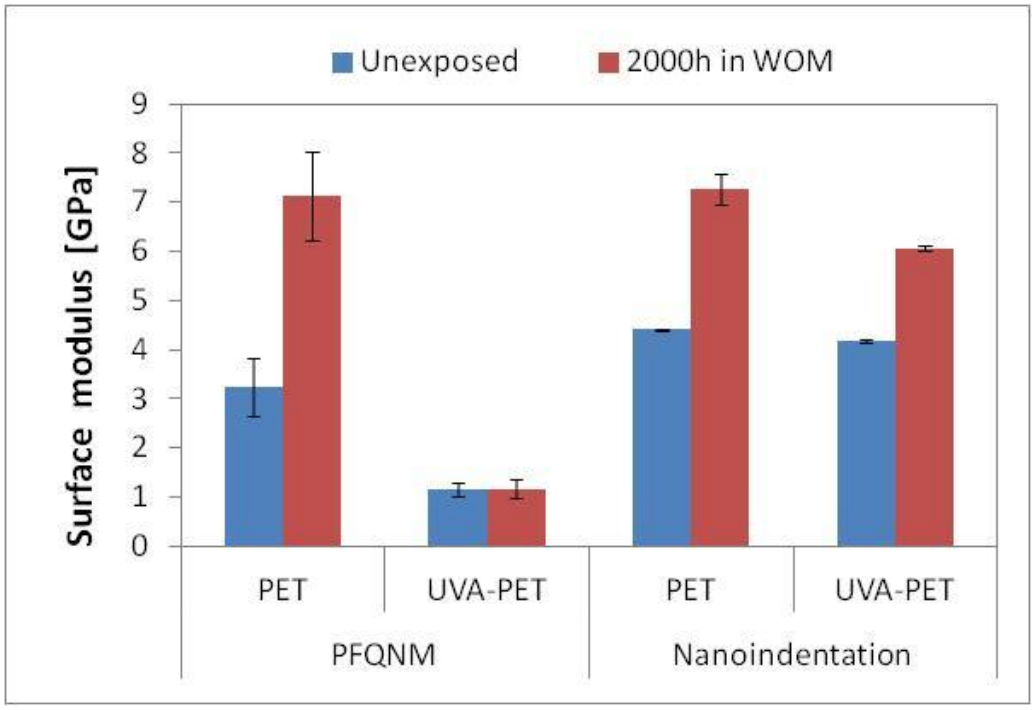

Figure 6.21: Mean surface modulus values of unexposed and 2000 hour WOM exposed plain PET and UVA-PET film samples obtained via PFQNM and IIT respectively

6.3 Chapter conclusions

The findings presented in this Chapter support the following conclusions. The presence of the UVA in the PET film formulation appears to have:

- Protected PET film bulk properties such as M_n, and spectral transmittance from modification much more effectively than surface properties, most likely due to the exponential decay in UV intensity as the radiation penetrates deeper into the film bulk.
- However, it also appears to have delayed the occurrence of surface roughening until 1200-1600 hours of exposure, and surface microcracking until 2800-3200 hours, despite the various property degradations observed at the surface. This suggests that surface properties are a poor predictor for surface microcracking, and that film bulk properties also play a significant role.
- Lessened the severity of several other modifications uniformly over the entire exposure duration, which suggests that the mechanisms of degradation are unchanged, but have been slowed down by interaction with the UVA.
- Reduced photo-crosslinking to levels below the detection limit for GPC, suggesting that the modification has been effectively eliminated. Thus, photo-crosslinking also appears to have a strong influence on surface microcrack severity.
- Despite the lack of photo-crosslinking, surface hardness was still significantly increased by WOM exposure. Therefore, it appears likely that in this case chemi-crystallisation has played the greater role.

The work herein has also provided quantitative values from a broad range of analysis instruments which can be referred to by DTF researchers when modifying and assessing future PET film UV stabilisation strategies.

FINAL CONCLUSIONS AND FUTURE WORK

This Chapter presents the main conclusions drawn from each experimental Chapter, as well as conclusions which have been derived from the Thesis as a whole. This Chapter also highlights the commercial implications of the research such as suggestions for improving PET film outdoor performance. Suggestions for potential future work in related research areas are also presented.

7.1 Overall conclusions

The aims set out at the start of this Thesis were:

- To investigate the degradation of PET films caused by prolonged exposure to accelerated UV weathering.
- To comprehensively characterise this degradation in novel ways using techniques including AFM, infra-red spectroscopy (FTIR) and nano-indentation.
- To develop the limited understanding of the relationship between chemical degradation and surface modification.
- Ultimately, to generate new knowledge to inform existing strategies for preventing UV degradation from occurring in outdoor applications of PET film.

These aims have been achieved and notably, several potential ways to improve PET film weatherability were found, which will be presented shortly. The research conducted in this Thesis has explored the modifications of PET films due to artificial weathering, and where possible attempted to correlate modifications with well understood degradation mechanisms. There remains a great deal of work to be done

before any formal relationships can be established, however the results presented in this Thesis may help to guide future investigations in exploring this expansive subject.

7.2 PET film bulk modifications

In Chapter Four, the modifications to PET film *bulk* properties by the various artificial weathering techniques employed were characterised and compared, which supported the following main conclusions:

- PET films exposed to accelerated environmental weathering exhibit modifications characteristic of both UV and humidity exposure: photo-oxidation, photo-crosslinking and hydrolysis.
- In PET film samples exposed to UV in the absence of heat, humidity and direct water contact, the effects of photo-crosslinking on bulk film properties are more prominent than those of photo-scissions.
- PET film samples exposed in the WOM exhibited greater levels of degradation than the combined levels exhibited by HISS and DHO exposed samples. This suggests a synergistic contribution during WOM exposure of UV with humidity, heat and/or direct water contact, which has not been previously identified.
- UV exposed PET MWDs revealed that photo-scissions occurred more frequently in above average length polymer chains than in below average length chains.
- Modified PET film transmittance and fluorescence behaviour appear to both be due to the production of hydroxylated aromatic species by UV radiation.

Evidence for the production of both mono-hydroxylated and di-hydroxylated species has been presented.

7.3 PET film surface modifications

In Chapter Five, the modifications to PET film *surface* properties by the various artificial weathering techniques employed were characterised and compared, which supported the following main conclusions:

- PET film surface properties are more greatly modified by the applied artificial weathering techniques than bulk properties, with WOM exposure causing the most severe modifications overall, due to the synergistic effects of UV radiation with heat, humidity and direct water contact.
- Film rear surface modifications were observed on artificially weathered samples and also showed consistently greater degradation than in the sample bulk, further highlighting the greater sensitivity of film surfaces to weathering degradation processes than the film bulk.
- Of the modifications observed, PET film surface roughening is of particular note as it has previously only been sparsely reported in the literature:
    - It has been shown that at AFM length scales surface roughness increases linearly with WOM exposure time, but remains approximately unchanged with exposure to UV irradiation alone.
    - Several discrete changes were also observed, such as the sharpening of the nodular nanostructure of PET and the introduction of nanoscale pit-features.

  - The concept of surface roughness parameter distributions has been introduced and shown to give a more complete picture of surface modification due to artificial weathering than has been possible using more traditional roughness analysis methods.
  - PET film samples were shown to have 3 parameter log-logistic shaped Ra distributions, which shifted to the right with accelerated environmental weathering, indicating the observed surface roughening of PET films to affect areas of different initial roughness equally.
- PET film surface mechanical properties have been shown to increase with artificial weathering exposure, due to a combination of photo-crosslinking and chemi-crystallisation. This highlights the scale variance of polymer mechanical properties, which predominantly decrease with degradation processes in macroscopic mechanical tests such as tensile tests.
- Of the samples analysed, surface microcracking only presented at the weathered surface of WOM exposed samples, highlighting the importance of synergistic effects to this modification.
- Surface silica contamination has been shown to locally enhance surface microcracking, which has serious implications for the measurement accuracy of degradation indicators and their kinetic behaviours.

7.4 Stabilising effects of the UVA

In Chapter Six, the techniques employed to characterise both *bulk* and *surface* modifications of artificially weathered plain PET film were utilised to assess the stabilising effects against accelerated environmental weathering of including the UVA

Tinuvin 1577 in the PET film formulation. It was concluded that the presence of the UVA in the PET film formulation appeared to have:

- Protected PET film bulk properties such as M_n, and spectral transmittance from modification much more effectively than surface properties, most likely due to the exponential decay in UV intensity as the radiation penetrates deeper into the film bulk.
- However, it also appears to have delayed the occurrence of surface roughening until 1200-1600 hours of exposure, and surface microcracking until 2800-3200 hours, despite the various property degradations observed at the surface. This suggests that surface properties are a poor predictor for surface microcracking, and that film bulk properties also play a significant role.
- Lessened the severity of several other modifications uniformly over the entire exposure duration, which suggests that the mechanisms of degradation are unchanged, but have been slowed down by interaction with the UVA.
- Reduced photo-crosslinking to levels below the detection limit for GPC, suggesting that the modification has been effectively eliminated. Thus, photo-crosslinking also appears to have a strong influence on surface microcrack severity.
- Despite the lack of photo-crosslinking, surface hardness was still significantly increased by WOM exposure. Therefore, it appears likely that in this case chemi-crystallisation has played the greater role.

7.5 Commercial implications of findings

The findings presented in this Thesis have several implications for DTF and the development of new PET films for outdoor applications. The evidence herein supports the mainstream view in the literature that the UV degradation of the PET film surface is a critical factor in the overall weatherability of PET films during exposure to environmental degradation agents. Hence, by better protecting the film surface from the effects of UV radiation it should be possible to extend the outdoor service lifetimes of PET film products.

Ways in which this may be achieved include the development of a UV absorbing or reflecting coating, which could inhibit surface degradation, or prevent microcracks from nucleating at the surface and penetrating into the film bulk. Imparting self cleaning properties to the exposed surface, *e.g.* by modifying the surface structures to change the hydrophilicity of the film, could help to discourage surface contamination and hence mitigate the degradative effects observed in the presence of surface silica deposits.

Unfortunately, due to the longer than anticipated sample generation times encountered during the research, there was not sufficient time to practically test any of the hypothesised means of improving PET film weatherability, by manufacturing new films in accordance with one or more of the proposed modifications. Such efforts must be consigned to future work, further ideas for which will be presented shortly:

- The work herein has provided up to date quantitative values from a broad range of analysis instruments, which can be referred to by DTF researchers when modifying and assessing future PET film UV stabilisation strategies.

- DTF's advanced surface metrology capabilities enable them to further differentiate their films performance from that of competitor films, in terms of representative surface roughening rates.
- The discovery of DTF film physical stability with isolated high intensity UV exposure is also important, as DTF may now more confidently supply films for applications where UV radiation may be present in the absence of extreme heat and humidity, such as solar window applications and indoor advertising.
- The effects of silica contamination on the surface degradation of PET films are an important discovery, as PET film performance lifetimes may be significantly lengthened simply by improving the hygiene standards of weather testing programmes.
- Samples with an exposed rear surface during weathering, a factor which likely contributed to the rear surface degradation observed with WOM exposure, are not representative of films that would be degrading in application in a multilayer device. Therefore, it would be beneficial to film performance, and more representative of true device conditions, to weather films which are laminated to glass or aluminium, instead of the current system of using open backed sample holders.

7.6 Future work

This Thesis has highlighted a number of areas in which it would be desirable to conduct further research, while also revealing a number of potential new research themes, which are likely to be of interest to DTF and the wider academic community.

The impact of silica on film surface microcracking is one such new research theme which could be beneficially explored. It is possible that other commonplace contaminants may also negatively impact PET film outdoor performance. Such investigations may also present further potential opportunities to mitigate the negative effects of surface contamination experienced by films in application.

Of the analytical techniques utilised in this Thesis, nano-indentation demonstrated particular promise as a means of non-destructively testing weathered film mechanical properties. With refinement it is possible that this technique could complement existing destructive tensile mechanical testing (which requires the weathering of far greater amounts of PET film) allowing for a reduction in the number of samples required for weathering, and hence for efficiency improvements to be made in film weather testing programs. PFQNM analysis also showed great potential as a technique for analysing nanoscale film surface mechanical properties, however, due to the high cost and technical expertise required to conduct and interpret the measurements, it seems far less likely than nano-indentation to have any potential commercial impact.

GPC provided new insights into the modification of polymer molecular weight distributions by artificial weathering and as such will likely prove useful in further investigations into UVA efficacy and more fundamental studies such as surface microcrack investigations. Further research is required to understand the mechanism responsible for the observed surface hardening of weathered PET films. Ideally, this would help determine the relative contributions of chemi-crystallisation and photo-crosslinking to this process, which could then be used to inform future film

stabilisation investigations. The development of a methodology for surface sensitive measurement of crosslinking would aid this investigation considerably.

In terms of the weathering apparatus used for this Thesis, a relatively simple modification to the HISS apparatus would be to add sample heating and chamber humidity control, thereby allowing each environmental degradation agent to be individually controlled. This would allow for a designed experiment type approach to be implemented, whereby the individual and synergistic effects of UV radiation, heat and humidity exposure could be much more precisely determined and investigated. In particular, this would help in determining how large of an effect increased temperature has on UV-modifications and would enable further deductions to be made about the role of water (both as humidity and as a surface spray) in UV modifications during WOM exposure, helping to narrow down the list of potential synergistic effects.

APPENDICES

8.1 Appendix 1 - Polymer molecular weight

To properly describe polymer properties, several terms potentially unfamiliar to non-polymer experts must be used. These will be explained in the following section to aid the readers understanding of the molecular weight findings and interpretations presented in this thesis.

8.1.1 Degree of polymerisation

A simple polymer molecule such as PET is made up of a single unit repeated many times. The degree of polymerisation of a polymer chain describes the number of repeat units which make up that chain. For biaxially oriented PET film, made up of millions of polymer molecules, the typical degree of polymerisation of a molecule in the film is approximately 100.

8.1.2 Molecular weight parameters

The molecular weight of a molecule is the sum of the atomic weights of its constituent atoms. For a polymer chain, made up of many repeat units, the molecular weight of the chain is the molecular weight of the repeat unit, multiplied by the degree of polymerisation. Polymer systems are polydisperse and hence their molecular weight exists as a distribution of many different chain lengths around an average value. To more easily describe the molecular weight of a polymer there are several parameters which describe meaningful points within the molecular weight distribution (MWD), these are described below.

8.1.2.1 Number average molecular weight (M_n)

The number average molecular weight (M_n) is the arithmetic mean of a polymers molecular weights and for a symmetric MWD falls exactly at the centre of the distribution. It is defined in Equation 8.1 below, where M_i is the molecular weight of a chain and N_i is the number of chains of that molecular weight.

$$\bar{M}_n = \frac{\sum_i M_i N_i}{\sum_i N_i} \qquad \text{Equation 8.1}$$

8.1.2.2 Weight average molecular weight (M_w)

The weight average molecular weight (M_w) is the weighted mean of the molecular weight values and for a symmetric MWD falls slightly to the right of the distribution centre. M_w takes into account the weight of each molecule and hence larger molecules have a larger contribution to the M_w than smaller molecules. It is defined in Equation 8.2 below, where M_i is the molecular weight of a chain and N_i is the number of chains of that molecular weight.

$$\bar{M}_w = \frac{\sum_i M_i^2 N_i}{\sum_i M_i N_i} \qquad \text{Equation 8.2}$$

8.1.2.3 Z average molecular weight (M_z)

The Z average molecular weight is the third moment of the MWD and is even more sensitive to larger molecules than M_w It is commonly measured by centrifugation but serves as a good measurement of very high molecular weight material in a sample. It is defined in Equation 8.3.

$$\bar{M}_z = \frac{\sum_i M_i^3 N_i}{\sum_i M_i^2 N_i}$$ Equation 8.3

8.1.2.4 Polydispersity

Polydispersity describes the breadth of a MWD and is simply the M_w over the M_n. The larger the polydispersity, the broader the MWD. It is defined in Equation 8.4.

$$D_M = \frac{M_w}{M_n}$$ Equation 8.4

8.2 Appendix 2 - Additional figures relating to PET hydroxylation processes

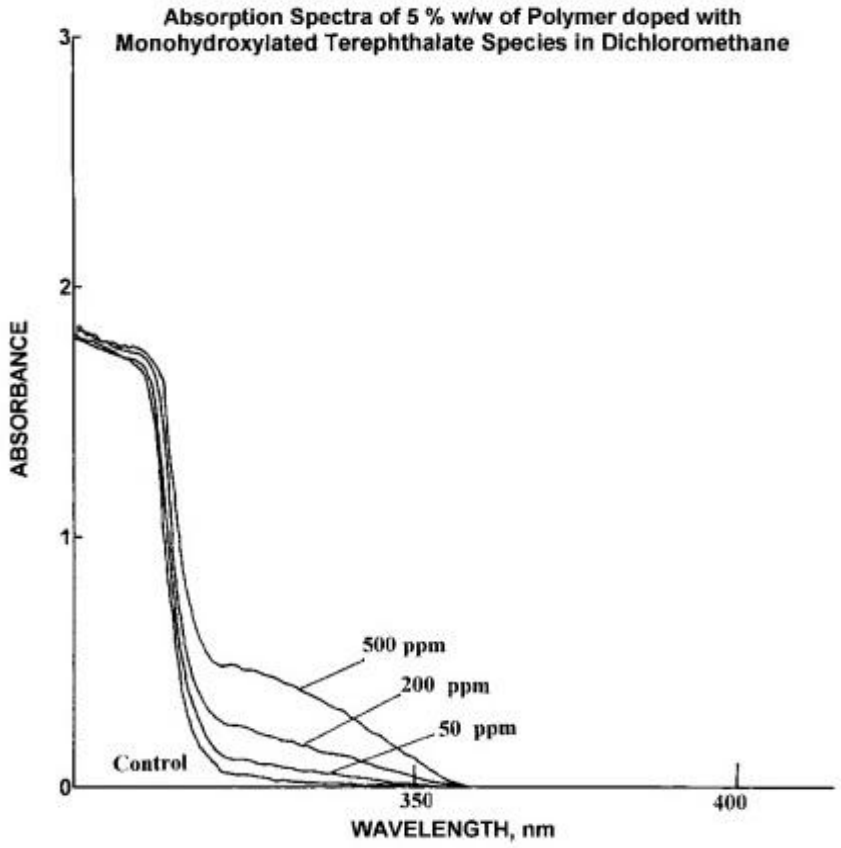

Figure 8.1: Absorption spectra of PECT with increasing diethyl-2-mono-hydroxyterephthalate in dichloromethane (reproduced from (Allen et al., 2000).

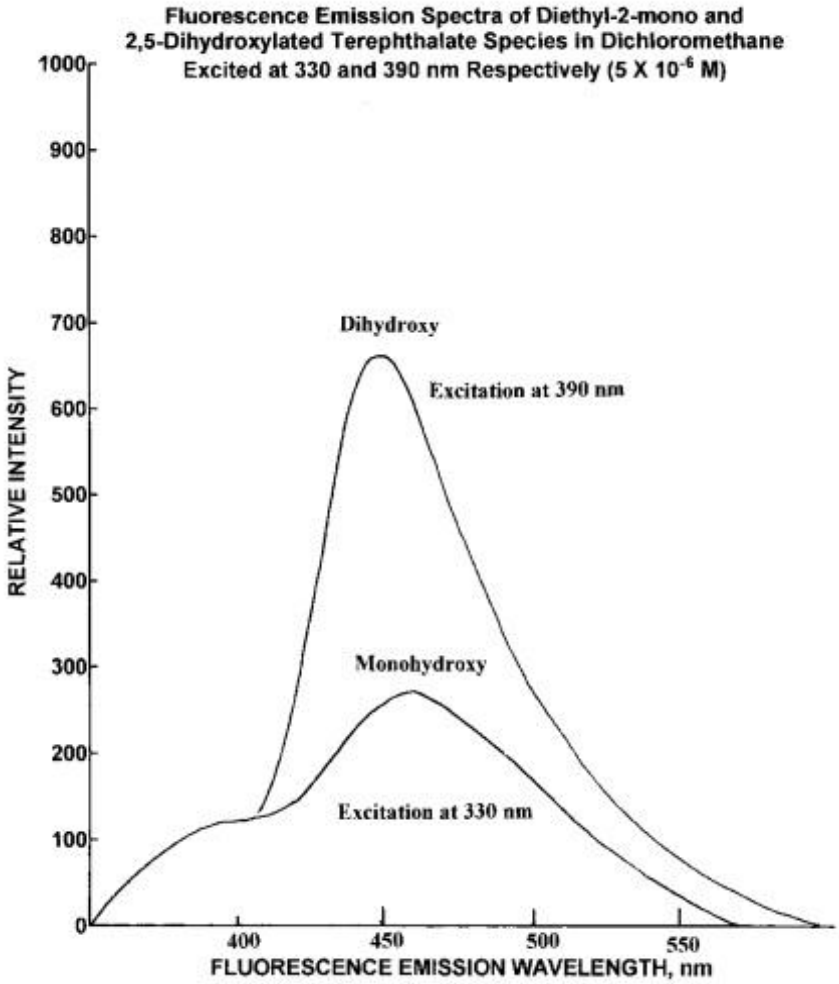

Figure 8.2: Fluorescence emission spectra of the diethyl-2-mono-hydroxterephthalate and 2,5-dihydroxyterephthalate models at 5 x 10^{-6} M concentration in dichloromethane (reproduced from (Allen et al., 2000).

8.3 Appendix 3 - 3 Parameter log-logistic distribution function

The 3 parameter log-logistic distribution function was used to fit the large area WLI Ra datasets as this function type was the best available function to fit the shape of the Ra distributions. The 3 parameter log-logistic probability density function is shown in Equation 8.5 below.

$$F(x;\mu,\sigma,\xi) = \frac{\left(1+\frac{\xi(x-\mu)}{\sigma}\right)^{-(1/\xi+1)}}{\sigma\left[1+\left(1+\frac{\xi(x-\mu)}{\sigma}\right)^{-1/\xi}\right]^2} \qquad \text{Equation 8.5}$$

For $1+\xi(x-\mu)/\sigma \geq 0$. Where x is the continuous variable, μ = the location parameter, σ = the scale parameter and ξ = the shape parameter.

8.4 Appendix 3 - Large area WLI additional figures

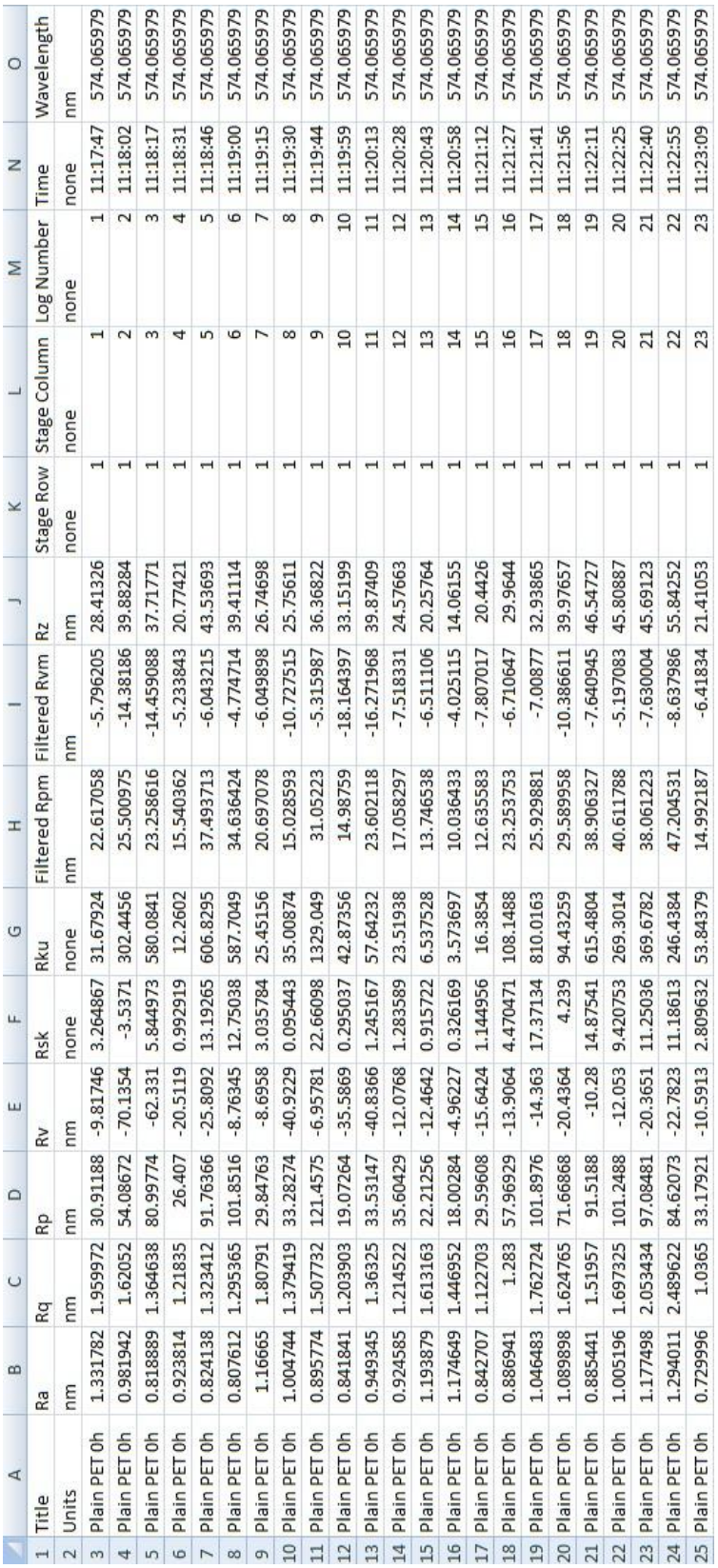

	A	B	C	D	E	F	G	H	I	J	K	L	M	N	O
1	Title	Ra	Rq	Rp	Rv	Rsk	Rku	Filtered Rpm	Filtered Rvm	Rz	Stage Row	Stage Column	Log Number	Time	Wavelength
2	Units	nm	nm	nm	nm	none	none	nm	nm	nm	none	none	none	none	nm
3	Plain PET 0h	1.331782	1.959972	30.91188	-9.81746	3.264867	31.67924	22.617058	-5.796205	28.41326	1	1	1	11:17:47	574.065979
4	Plain PET 0h	0.981942	1.62052	54.08672	-70.1354	-3.5371	302.4456	25.500975	-14.38186	39.88284	1	2	2	11:18:02	574.065979
5	Plain PET 0h	0.818889	1.364638	80.99774	-62.331	5.844973	580.0841	23.258616	-14.459088	37.71771	1	3	3	11:18:17	574.065979
6	Plain PET 0h	0.923814	1.21835	26.407	-20.5119	0.992919	12.2602	15.540362	-5.233843	20.77421	1	4	4	11:18:31	574.065979
7	Plain PET 0h	0.824138	1.323412	91.76366	-25.8092	13.19265	606.8295	37.493713	-6.043215	43.53693	1	5	5	11:18:46	574.065979
8	Plain PET 0h	0.807612	1.295365	101.8516	-8.76345	12.75038	587.7049	34.636424	-4.774714	39.41114	1	6	6	11:19:00	574.065979
9	Plain PET 0h	1.16665	1.80791	29.84763	-8.6958	3.035784	25.45156	20.697078	-6.049898	26.74698	1	7	7	11:19:15	574.065979
10	Plain PET 0h	1.004744	1.379419	33.28274	-40.9229	0.095443	35.00874	15.028593	-10.727515	25.75611	1	8	8	11:19:30	574.065979
11	Plain PET 0h	0.895774	1.507732	121.4575	-6.95781	22.66098	1329.049	31.05223	-5.315987	36.36822	1	9	9	11:19:44	574.065979
12	Plain PET 0h	0.841841	1.203903	19.07264	-35.5869	0.295037	42.87356	14.98759	-18.164397	33.15199	1	10	10	11:19:59	574.065979
13	Plain PET 0h	0.949345	1.36325	33.53147	-40.8366	1.245167	57.64232	23.602118	-16.271968	39.87409	1	11	11	11:20:13	574.065979
14	Plain PET 0h	0.924585	1.214522	35.60429	-12.0768	1.283589	23.51938	17.058297	-7.518331	24.57663	1	12	12	11:20:28	574.065979
15	Plain PET 0h	1.193879	1.613163	22.21256	-12.4642	0.915722	6.537528	13.746538	-6.511106	20.25764	1	13	13	11:20:43	574.065979
16	Plain PET 0h	1.174649	1.446952	18.00284	-4.96227	0.326169	3.573697	10.036433	-4.025115	14.06155	1	14	14	11:20:58	574.065979
17	Plain PET 0h	0.842707	1.122703	29.59608	-15.6424	1.144956	16.3854	12.635583	-7.807017	20.4426	1	15	15	11:21:12	574.065979
18	Plain PET 0h	0.886941	1.283	57.96929	-13.9064	4.470471	108.1488	23.253753	-6.710647	29.9644	1	16	16	11:21:27	574.065979
19	Plain PET 0h	1.046483	1.762724	101.8976	-14.363	17.37134	810.0163	25.929881	-7.00877	32.93865	1	17	17	11:21:41	574.065979
20	Plain PET 0h	1.089898	1.624765	71.66868	-20.4364	4.239	94.43259	29.589958	-10.386611	39.97657	1	18	18	11:21:56	574.065979
21	Plain PET 0h	0.885441	1.51957	91.5188	-10.28	14.87541	615.4804	38.906327	-7.640945	46.54727	1	19	19	11:22:11	574.065979
22	Plain PET 0h	1.005196	1.697325	101.2488	-12.053	9.420753	269.3014	40.611788	-5.197083	45.80887	1	20	20	11:22:25	574.065979
23	Plain PET 0h	1.177498	2.053434	97.08481	-20.3651	11.25036	369.6782	38.061223	-7.630004	45.69123	1	21	21	11:22:40	574.065979
24	Plain PET 0h	1.294011	2.489622	84.62073	-22.7823	11.18613	246.4384	47.204531	-8.637986	55.84252	1	22	22	11:22:55	574.065979
25	Plain PET 0h	0.729996	1.0365	33.17921	-10.5913	2.809632	53.84379	14.992187	-6.41834	21.41053	1	23	23	11:23:09	574.065979

Figure 8.3: One page example of the roughness and log data captured during the large area WLI analysis procedure. These particular examples correspond to the pre WOM exposure plain PET film sample, areas 1 -23 of 10,000

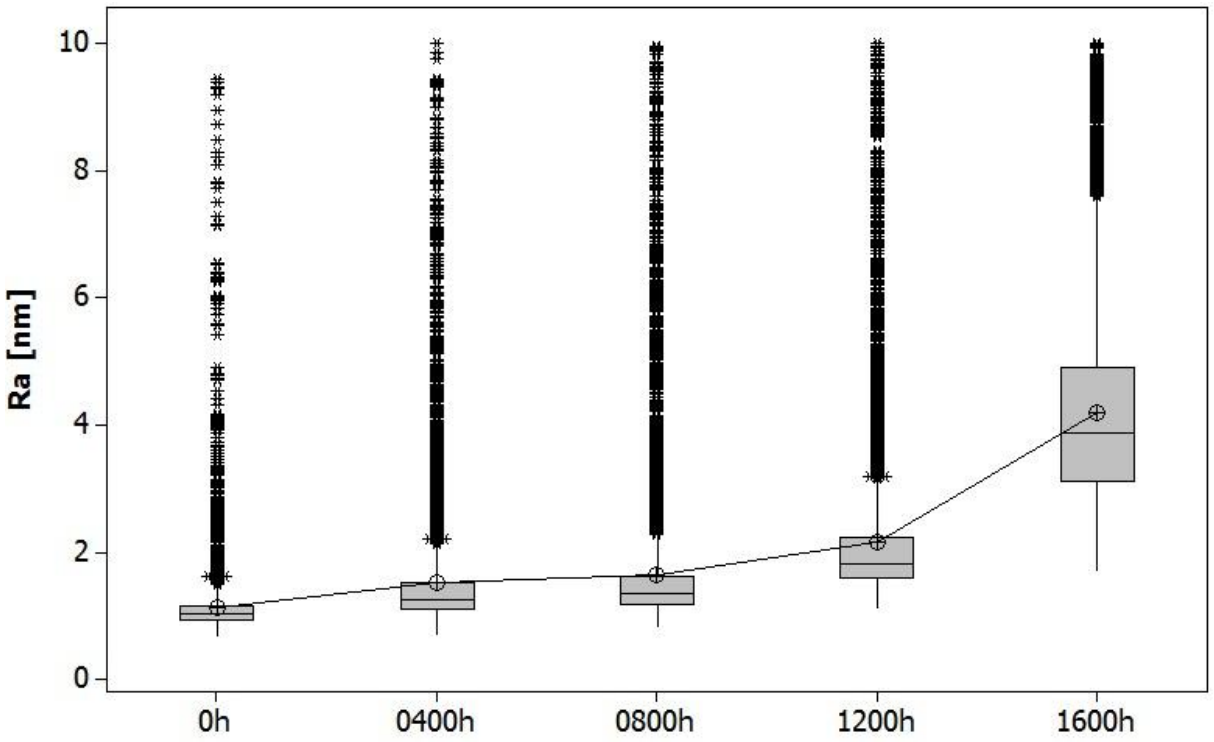

Figure 8.4: Box-plots of plain PET Ra values with increasing WOM exposure. Data limited to < 10 nm Ra to allow visualisation of interquartile range and mean-median differences

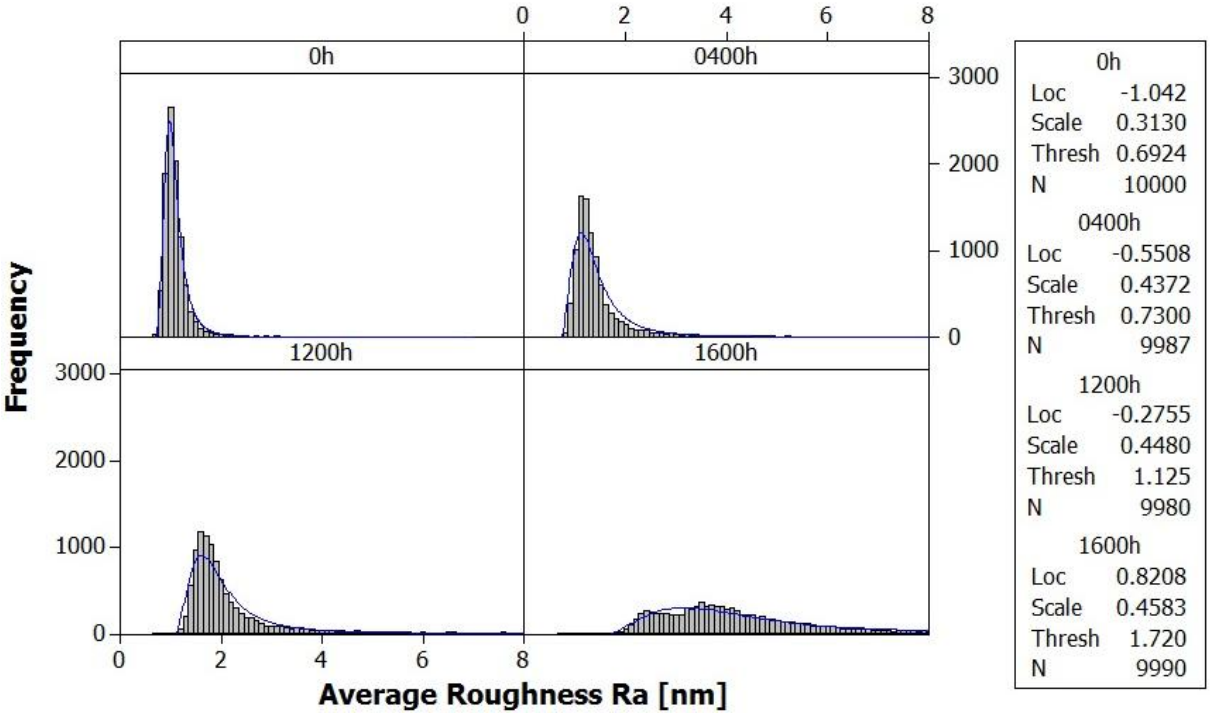

Figure 8.5: Ra distributions of plain PET with increasing WOM exposure of up to 1600 hours. Included to illustrate the quality of the fits over the actual data

REFERENCES

AJJI, A., GUÈVREMONT, J., COLE, K. C. & DUMOULIN, M. M. 1996. Orientation and structure of drawn poly(ethylene terephthalate). *Polymer,* 37**,** 3707-3714.

ALLEN, N. S., EDGE, M., DANIELS, J. & ROYALL, D. 1998. Spectroscopic analysis of organic contaminants in terephthalic acid: colour implications in poly(ethylene terephthalate) manufacture. *Polymer Degradation and Stability,* 62**,** 373-383.

ALLEN, N. S., EDGE, M., MOHAMMADIAN, M. & JONES, K. 1991. Hydrolytic degradation of poly(ethylene terephthalate): Importance of chain scission versus crystallinity. *European Polymer Journal,* 27**,** 1373-1378.

ALLEN, N. S. & MCKELLAR, J. F. 1978. Luminescent species in poly(ethylene terephthalate). *Die Makromolekulare Chemie,* 179**,** 523-526.

ALLEN, N. S., RIVALLE, G., EDGE, M., CORRALES, T. & CATALINA, F. 2002. Chemiluminescence processes in thermal and photochemically oxidised poly(ethylene-co-1,4-cyclohexanedimethylene terephthalate) (PECT): influence of stabilisers. *Polymer Degradation and Stability,* 75**,** 237-246.

ALLEN, N. S., RIVALLE, G., EDGE, M., ROBERTS, I. & FAGERBURG, D. R. 2000. Characterisation and identification of fluorescent hydroxylated terephthalate species in the thermal and UV degradation of poly(ethylene-co-1,4-cyclohexanedimethylene terephthalate) (PECT). *Polymer Degradation and Stability,* 67**,** 325-334.

ANDRADY, A. L. 2007. Ultraviolet Radiation and Polymers

Physical Properties of Polymers Handbook. *In:* MARK, J. E. (ed.). Springer New York.

ANDRADY, A. L., HAMID, S. H., HU, X. & TORIKAI, A. 1998. Effects of increased solar ultraviolet radiation on materials. *Journal of Photochemistry and Photobiology B: Biology,* 46**,** 96-103.

ASSENDER, H. 2002. How Surface Topography Relates to Materials' Properties. *Science,* 297**,** 973-976.

ASTM 2012a. "ASTM Standard G173 Standard Tables for Reference Solar Spectral Irradiances". West Conshohocken, PA: ASTM International.

ASTM 2012b. D882-12, Standard Test Method for Tensile Properties of Thin Plastic Sheeting. ASTM International, West Conshohocken, PA.

ASTM 2013. D2457, Standard Test Method for Specular Gloss of Plastic Films and Solid Plastics. ASTM International, West Conshohocken, PA.

AUDOUIN, L., LANGLOIS, V., VERDU, J. & DE BRUIJN, J. C. M. 1994. Role of oxygen diffusion in polymer ageing: kinetic and mechanical aspects. *Journal of Materials Science,* 29**,** 569-583.

AWASTHI, K., KULSHRESTHA, V., AVASTHI, D. K. & VIJAY, Y. K. 2010. Optical, chemical and structural modification of oxygen irradiated PET. *Radiation Measurements,* 45**,** 850-855.

BALLARA, A. & VERDU, J. 1989. Physical aspects of the hydrolysis of polyethylene terephthalate. *Polymer Degradation and Stability,* 26**,** 361-374.

BARTOLOMEO, P., IRIGOYEN, M., ARAGON, E., FRIZZI, M. A. & PERRIN, F. X. 2001. Dynamic mechanical analysis and Vickers micro hardness correlation

for polymer coating UV ageing characterisation. *Polymer Degradation and Stability,* 72**,** 63-68.

BEDIA, E. L., PAGLICAWAN, M. A., BERNAS, C. V., BERNARDO, S. T., TOSAKA, M. & KOHJIYA, S. 2003. Natural weathering of polypropylene in a tropical zone. *Journal of Applied Polymer Science,* 87**,** 931-938.

BERTHUMEYRIE, S., COLIN, A., ESPARCIEUX, C., BABA, M., CATALINA, F., BUSSIERE, P.-O. & THERIAS, S. 2013. Photodegradation of tetramethylpolycarbonate (TMPC): Correlation of properties with chemical modifications. *Polymer Degradation and Stability,* 98**,** 2081-2088.

BIGGS, S., LUKEY, C. A., SPINKS, G. M. & YAU, S.-T. 2001. An atomic force microscopy study of weathering of polyester/melamine paint surfaces. *Progress in Organic Coatings,* 42**,** 49-58.

BILLINGHAM, N. C. 2000. Degradation and Stabilization of Polymers. *Materials Science and Technology: A Comprehensive Treatment.* Wiley-VCH Verlag GmbH.

BINNIG, G. & QUATE, C. F. 1986. Atomic Force Microscope. *Physical Review Letters,* 56**,** 930-933.

BLAIS, P., DAY, M. & WILES, D. M. 1973. Photochemical degradation of poly(ethylene terephthalate). IV. Surface changes. *Journal of Applied Polymer Science,* 17**,** 1895-1907.

BLUMTHALER, M. 1993. Solar UV measurements. *Environmental effects of UV (ultraviolet) radiation. Lewis Publisher, Boca Raton, Florida***,** 17-79.

BOURBAN, C., MERGAERT, J., RUFFIEUX, K., SWINGS, J. & WINTERMANTEL, E. 1998. Atomic Force-, Confocal Laser Scanning-, and Scanning Electron

Microscopy Characterization of the Surface Degradation of a Polymer. 694**,** 194-202.

BRABEC, C. J. 2004. Organic photovoltaics: technology and market. *Solar Energy Materials and Solar Cells,* 83**,** 273-292.

BUSSIERE, P.-O., GARDETTE, J.-L. & THERIAS, S. 2014. Photodegradation of celluloid used in museum artifacts. *Polymer Degradation and Stability*.

BUSSIÈRE, P.-O., RIVATON, A., THÉRIAS, S. & GARDETTE, J.-L. 2012. Multiscale Investigation of the Poly(N-vinylcarbazole) Photoageing Mechanism. *The Journal of Physical Chemistry B,* 116**,** 802-812.

BUXBAUM, L. H. 1968. The Degradation of Poly(ethylene terephthalate). *Angewandte Chemie International Edition in English,* 7**,** 182-190.

CALATRONI, J., GUERRERO, A. L., SÁINZ, C. & ESCALONA, R. 1996. Spectrally-resolved white-light interferometry as a profilometry tool. *Optics & Laser Technology,* 28**,** 485-489.

CAMPBELL, D. & TURNER, D. T. 1968. Photo-induced post-irradiation free-radical conversion in poly(ethylene terephthalate): An ESR study. *Journal of Polymer Science Part B: Polymer Letters,* 6**,** 1-4.

CASU, A. & GARDETTE, J.-L. 1995. Photolysis and photooxidation of poly(butylene terephthalate)-fibre glass systems. *Polymer,* 36**,** 4005-4009.

CELINA, M. C. 2013. Review of polymer oxidation and its relationship with materials performance and lifetime prediction. *Polymer Degradation and Stability,* 98**,** 2419-2429.

CERBULIS, J., CLAY, C. & MACK, C. H. 1957. The composition of bloom fat in chocolate. *Journal of the American Oil Chemists Society,* 34**,** 533-537.

CHEN, Z., HAY, J. N. & JENKINS, M. J. 2012. FTIR spectroscopic analysis of poly(ethylene terephthalate) on crystallization. *European Polymer Journal,* 48**,** 1586-1610.

COLLIN, S., BUSSIÈRE, P. O., THÉRIAS, S., LAMBERT, J. M., PERDEREAU, J. & GARDETTE, J. L. 2012. Physicochemical and mechanical impacts of photo-ageing on bisphenol a polycarbonate. *Polymer Degradation and Stability,* 97**,** 2284-2293.

IEC 60068, 2010, International Electrotechnical Commission - Environmental testing.

CRUZ, C. S., CALLEJA, F. J. B., ZACHMANN, H. G., STRIBECK, N. & ASANO, T. 1991. Relating microhardness of poly(ethylene terephthalate) to microstructure. *Journal of Polymer Science Part B: Polymer Physics,* 29**,** 819-824.

DAY, M. & WILES, D. M. 1972a. Photochemical degradation of poly(ethylene terephthalate). I. Irradiation experiments with the xenon and carbon arc. *Journal of Applied Polymer Science,* 16**,** 175-189.

DAY, M. & WILES, D. M. 1972b. Photochemical degradation of poly(ethylene terephthalate). II. Effect of wavelength and environment on the decomposition process. *Journal of Applied Polymer Science,* 16**,** 191-202.

DAY, M. & WILES, D. M. 1972c. Photochemical degradation of poly(ethylene terephthalate). III. Determination of decomposition products and reaction mechanism. *Journal of Applied Polymer Science,* 16**,** 203-215.

DEBLIECK, R. A. C., VAN BEEK, D. J. M., REMERIE, K. & WARD, I. M. 2011. Failure mechanisms in polyolefines: The role of crazing, shear yielding and the entanglement network. *Polymer,* 52**,** 2979-2990.

DERJAGUIN, B. V., MULLER, V. M. & TOPOROV, Y. P. 1975. Effect of contact deformations on the adhesion of particles. *Journal of Colloid and Interface Science,* 53**,** 314-326.

DINELLI, F., ASSENDER, H. E., KIROV, K. & KOLOSOV, O. V. 2000. Surface morphology and crystallinity of biaxially stretched PET films on the nanoscale. *Polymer,* 41**,** 4285-4289.

DOKUKIN, M. E. & SOKOLOV, I. 2012. On the Measurements of Rigidity Modulus of Soft Materials in Nanoindentation Experiments at Small Depth. *Macromolecules,* 45**,** 4277-4288.

DONELLI, I., FREDDI, G., NIERSTRASZ, V. A. & TADDEI, P. 2010. Surface structure and properties of poly-(ethylene terephthalate) hydrolyzed by alkali and cutinase. *Polymer Degradation and Stability,* 95**,** 1542-1550.

DUPONT TEIJIN FILMS UK LTD, 2013. DuPont Teijin Films Internal Corporate Presentation.

EDGE, M., ALLEN, N., HE, J., DERHAM, M. & SHINAGAWA, Y. 1994. Physical aspects of the thermal and hydrolytic ageing of polyester, polysulphone and polycarbonate films. *Polymer Degradation and Stability,* 44**,** 193-200.

EDGE, M., ALLEN, N. S., WILES, R., MCDONALD, W. & MORTLOCK, S. V. 1995. Identification of luminescent species contributing to the yellowing of poly(ethyleneterephthalate) on degradation. *Polymer,* 36**,** 227-234.

EDGE, M., HAYES, M., MOHAMMADIAN, M., ALLEN, N. S., JEWITT, T. S., BREMS, K. & JONES, K. 1991. Aspects of poly(ethylene terephthalate) degradation for archival life and environmental degradation. *Polymer Degradation and Stability,* 32**,** 131-153.

EVESON, R. 2013. Personal Communication with Robert Eveson, DuPont Teijin Films Senior Research Scientist.

FECHINE, G. J. M., CHRISTENSEN, P. A., EGERTON, T. A. & WHITE, J. R. 2009. Evaluation of poly(ethylene terephthalate) photostabilisation using FTIR spectrometry of evolved carbon dioxide. *Polymer Degradation and Stability,* 94**,** 234-239.

FECHINE, G. J. M., RABELLO, M. S., MAIOR, R. M. S. & CATALANI, L. H. 2004. Surface characterization of photodegraded poly(ethylene terephthalate). The effect of ultraviolet absorbers. *Polymer,* 45**,** 2303-2308.

FECHINE, G. J. M., RABELLO, M. S. & SOUTO-MAIOR, R. M. 2002a. The effect of ultraviolet stabilizers on the photodegradation of poly(ethylene terephthalate). *Polymer Degradation and Stability,* 75**,** 153-159.

FECHINE, G. J. M., SOUTO-MAIOR, R. M. & RABELLO, M. S. 2002b. Structural changes during photodegradation of poly(ethylene terephthalate). *Journal of Materials Science,* 37**,** 4979-4984.

FECHINE, G. J. M., SOUTO-MAIOR, R. M. & RABELLO, M. S. 2007. Photodegradation of multilayer films based on PET copolymers. *Journal of Applied Polymer Science,* 104**,** 51-57.

FERNANDO, S. S., CHRISTENSEN, P. A., EGERTON, T. A. & WHITE, J. R. 2007. Carbon dioxide evolution and carbonyl group development during photodegradation of polyethylene and polypropylene. *Polymer Degradation and Stability,* 92**,** 2163-2172.

GARDETTE, J.-L. 1995. Heterogeneous photooxidation of solid polymers. *Die Angewandte Makromolekulare Chemie,* 232**,** 85-103.

GARDETTE, J.-L., COLIN, A., TRIVIS, S., GERMAN, S. & THERIAS, S. 2014. Impact of photooxidative degradation on the oxygen permeability of poly(ethyleneterephthalate). *Polymer Degradation and Stability,* 103**,** 35-41.

GOODMAN, I. & NESBITT, B. F. 1960. The structures and reversible polymerization of cyclic oligomers from poly(ethylene terephthalate). *Journal of Polymer Science,* 48**,** 423-433.

GOULD, S. A. C., SCHIRALDI, D. A. & OCCELLI, M. L. 1997. Analysis of poly(ethylene terephthalate) (PET) films by atomic force microscopy. *Journal of Applied Polymer Science,* 65**,** 1237-1243.

GROSSETETE, T., GONON, L. & VERNEY, V. 2002. Submicrometric characterization of the heterogeneous photooxidation of polypropylene by microthermal analysis. *Polymer Degradation and Stability,* 78**,** 203-210.

GROSSETÊTE, T., RIVATON, A., GARDETTE, J. L., HOYLE, C. E., ZIEMER, M., FAGERBURG, D. R. & CLAUBERG, H. 2000. Photochemical degradation of poly(ethylene terephthalate)-modified copolymer. *Polymer,* 41**,** 3541-3554.

GROSSIORD, N., KROON, J. M., ANDRIESSEN, R. & BLOM, P. W. M. 2012. Degradation mechanisms in organic photovoltaic devices. *Organic Electronics,* 13**,** 432-456.

GU, X., RAGHAVAN, D., NGUYEN, T., VANLANDINGHAM, M. R. & YEBASSA, D. 2001. Characterization of polyester degradation using tapping mode atomic force microscopy: exposure to alkaline solution at room temperature. *Polymer Degradation and Stability,* 74**,** 139-149.

GU, X., SUNG, L., KIDAH, B., OUDINA, M., CLERICI, C., HU, H., STANLEY, D., BYRD, W. E., JEAN, J. Y. C., NGUYEN, T. & MARTIN, J. W. 2008. Multiscale

physical characterization of an outdoor-exposed polymeric coating system. *Journal of Coatings Technology and Research,* 6**,** 67-79.

GUPTA, B., HILBORN, J., HOLLENSTEIN, C., PLUMMER, C. J. G., HOURIET, R. & XANTHOPOULOS, N. 2000. Surface modification of polyester films by RF plasma. *Journal of Applied Polymer Science,* 78**,** 1083-1091.

HARRICK, N. J. & DU PRÉ, F. K. 1966. Effective Thickness of Bulk Materials and of Thin Films for Internal Reflection Spectroscopy. *Applied Optics,* 5**,** 1739-1743.

HEMKER, D. J., FRANK, C. W. & THOMAS, J. W. 1988. Photophysical studies of amorphous orientation in poly(ethylene terephthalate) films. *Polymer,* 29**,** 437-447.

HERTZ, H. R. 1895. Ueber die beruehrung elastischer koerper (On contact between elastic bodies). *Gesammelte werke (Collected works)*.

HODGSON, M. 2015. Personal Communication with Mark Hodgson, DuPont Teijin Films Senior Research Scientist.

HOPCROFT, M. A., NIX, W. D. & KENNY, T. W. 2010. What is the Young's Modulus of Silicon? *Microelectromechanical Systems, Journal of,* 19**,** 229-238.

HURLEY, C. R. & LEGGETT, G. J. 2009. Quantitative Investigation of the Photodegradation of Polyethylene Terephthalate Film by Friction Force Microscopy, Contact-Angle Goniometry, and X-ray Photoelectron Spectroscopy. *ACS Applied Materials & Interfaces,* 1**,** 1688-1697.

IRIGOYEN, M., BARTOLOMEO, P., PERRIN, F. X., ARAGON, E. & VERNET, J. L. 2001. UV ageing characterisation of organic anticorrosion coatings by dynamic mechanical analysis, Vickers microhardness, and infra-red analysis. *Polymer Degradation and Stability,* 74**,** 59-67.

JANG, J. & JEONG, Y. 2006. Nano roughening of PET and PTT fabrics via continuous UV/O3 irradiation. *Dyes and Pigments,* 69**,** 137-143.

JOHNSON, K. L., KENDALL, K. & ROBERTS, A. D. 1971. Surface Energy and the Contact of Elastic Solids. *Proceedings of the Royal Society of London. A. Mathematical and Physical Sciences,* 324**,** 301-313.

JOHNSON, M. & COTE, P. 2003. Detrended fluctuation analysis of UV degradation in a polyurethane coating. *Journal of Coatings Technology,* 75**,** 51-57.

JORGENSEN, G., TERWILLIGER, K., DELCUETO, J., GLICK, S., KEMPE, M., PANKOW, J., PERN, F. & MCMAHON, T. 2006. Moisture transport, adhesion, and corrosion protection of PV module packaging materials. *Solar Energy Materials and Solar Cells,* 90**,** 2739-2775.

KEMPE, M. 2006. Modeling of rates of moisture ingress into photovoltaic modules. *Solar Energy Materials and Solar Cells,* 90**,** 2720-2738.

KIMBALL, W. H. & MUNIR, Z. A. 1978. The effect of accelerated weathering on the degradation of polymeric films. *Polymer Engineering & Science,* 18**,** 230-237.

LARCHÉ, J. F., BUSSIÈRE, P. O. & GARDETTE, J. L. 2010. How to reveal latent degradation of coatings provoked by UV-light. *Polymer Degradation and Stability,* 95**,** 1810-1817.

LARCHÉ, J. F., BUSSIÈRE, P. O. & GARDETTE, J. L. 2011. Photo-oxidation of acrylic-urethane thermoset networks. Relating materials properties to changes of chemical structure. *Polymer Degradation and Stability,* 96**,** 1438-1444.

LARCHÉ, J. F., BUSSIÈRE, P. O., THÉRIAS, S. & GARDETTE, J. L. 2012. Photooxidation of polymers: Relating material properties to chemical changes. *Polymer Degradation and Stability,* 97**,** 25-34.

LEACH, R. 2011. *Optical measurement of surface topography*, Springer.

LIU, M., HORROCKS, A. R. & HALL, M. E. 1995. Correlation of physicochemical changes in UV-exposed low density polyethylene films containing various UV stabilisers. *Polymer Degradation and Stability,* 49**,** 151-161.

LUBARSKY, G. V., DAVIDSON, M. R. & BRADLEY, R. H. 2004. Elastic modulus, oxidation depth and adhesion force of surface modified polystyrene studied by AFM and XPS. *Surface Science,* 558**,** 135-144.

MACDONALD, W. A. 2002. Polyester Films. *Encyclopedia of Polymer Science and Technology.* John Wiley & Sons, Inc.

MACDONALD, W. A. 2004. Engineered films for display technologies. *Journal of Materials Chemistry,* 14**,** 4.

MACKERRON, D. 2014. Personal Communication with Duncan MacKerron, DuPont Teijin Films Senior Research Scientist, 2014.

MAILHOT, B., BUSSIÈRE, P.-O., RIVATON, A., MORLAT-THÉRIAS, S. & GARDETTE, J.-L. 2004. Depth Profiling by AFM Nanoindentations and Micro-FTIR Spectroscopy for the Study of Polymer Ageing. *Macromolecular Rapid Communications,* 25**,** 436-440.

MAILHOT, B., MORLAT-THÉRIAS, S., BUSSIÈRE, P.-O., LE PLUART, L., DUCHET, J., SAUTEREAU, H., GÉRARD, J.-F. & GARDETTE, J.-L. 2008. Photoageing behaviour of epoxy nanocomposites: Comparison between spherical and lamellar nanofillers. *Polymer Degradation and Stability,* 93**,** 1786-1792.

MAILHOT, B., MORLAT, S. & GARDETTE, J. L. 2000. Photooxidation of blends of polystyrene and poly(vinyl methyl ether): FTIR and AFM studies. *Polymer,* 41**,** 1981-1988.

MANLEY, T. R. & WILLIAMS, D. A. 1969. Polarized Far-Infrared Spectra of Oriented Poly(ethylene Terephthalate). *Journal of Polymer Science Part C: Polymer Symposia,* 22**,** 1009-1018.

MARCOTTE, F. B., CAMPBELL, D., CLEAVELAND, J. A. & TURNER, D. T. 1967. Photolysis of poly(ethylene terephthalate). *Journal of Polymer Science Part A-1: Polymer Chemistry,* 5**,** 481-501.

MARSH, P. 2013. Personal Communication with Paul Marsh, Intertek Senior Research Scientist, 2013.

MCMAHON, W., BIRDSALL, H. A., JOHNSON, G. R. & CAMILLI, C. T. 1959. Degradation Studies of Polyethylene Terephthalate. *Journal of Chemical & Engineering Data,* 4**,** 57-79.

MCNEIL, L. E. & GRIMSDITCH, M. 1993. Elastic moduli of muscovite mica. *Journal of Physics: Condensed Matter,* 5**,** 1681.

MERTZ, G., HASSOUNA, F., LECLÈRE, P., DAHOUN, A., TONIAZZO, V. & RUCH, D. 2012. Correlation between (nano)-mechanical and chemical changes occurring during photo-oxidation of filled vulcanised styrene butadiene rubber (SBR). *Polymer Degradation and Stability,* 97**,** 2195-2201.

NGUYEN, T., GU, X., VANLANDINGHAM, M., BYRD, E., RYNTZ, R. & MARTIN, J. W. 2012. Degradation modes of crosslinked coatings exposed to photolytic environment. *Journal of Coatings Technology and Research,* 10**,** 1-14.

NICHOLS, M. E. & PETERS, C. A. 2002. The effect of weathering on the fracture energy of hardcoats over polycarbonate. *Polymer Degradation and Stability,* 75**,** 439-446.

OLIVER, W. C. & PHARR, G. M. 2004. Measurement of hardness and elastic modulus by instrumented indentation: Advances in understanding and refinements to methodology. *Journal of Materials Research,* 19**,** 3-20.

OSBORN, K. R. 1959. The photolysis of polyethylene terephthalate. *Journal of Polymer Science,* 38**,** 357-367.

OSTERHOLD, M. & GLÖCKNER, P. 2001. Influence of weathering on physical properties of clearcoats. *Progress in Organic Coatings,* 41**,** 177-182.

PACIFICI, J. G. & STRALEY, J. M. 1969. Photolysis of terephthalate polyesters: Hydroxylation of the aromatic nuclei. *Journal of Polymer Science Part B: Polymer Letters,* 7**,** 7-9.

PAPET, G., JIRACKOVA-AUDOUIN, L. & VERDU, J. 1987. Diffusion controlled radiochemical oxidation of low density polyethylene—I: Depth dependence of morphological changes. *International Journal of Radiation Applications and Instrumentation. Part C. Radiation Physics and Chemistry,* 29**,** 65-69.

PEEVOR, M. 2015. Personal Communication with Martin Peevor, DuPont Teijin Films Photovoltaics Market Manager.

PEROVIC, A. & SUNDARARAJAN, P. R. 1982. Crystallization of cyclic oligomers in commercial poly(ethyleneterephthalate) films. *Polymer Bulletin,* 6**,** 277-283.

PICKETT, J. E. & COYLE, D. J. 2013. Hydrolysis kinetics of condensation polymers under humidity aging conditions. *Polymer Degradation and Stability,* 98**,** 1311-1320.

PLASTICKER. 2012. *Plasticker.de*: http://plasticker.de/Kunstsoff_News [Accessed 30/5/14].

POSPÍŠIL, J., PILAŘ, J., BILLINGHAM, N. C., MAREK, A., HORÁK, Z. & NEŠPŮREK, S. 2006. Factors affecting accelerated testing of polymer photostability. *Polymer Degradation and Stability,* 91**,** 417-422.

POULINGUE, M., IGNAT, M. & DIJON, J. 1999. The effects of particle pollution on the mechanical behaviour of multilayered systems. *Thin Solid Films,* 348**,** 215-221.

PRISMARK, 2014. Discovery Series - Photovoltaics Review and Outlook.

RAAB, M., KOTULAK, L., KOLAŘÍK, J. & POSPÍŠIL, J. 1982. The effect of ultraviolet light on the mechanical properties of polyethylene and polypropylene films. *Journal of Applied Polymer Science,* 27**,** 2457-2466.

RABELLO, M. S. & WHITE, J. R. 1997. Crystallization and melting behaviour of photodegraded polypropylene — I. Chemi-crystallization. *Polymer,* 38**,** 6379-6387.

RAKOS, K. 2014. Personal Communication with Karl Rakos, DuPont Teijin Films Senior Applications Scientist.

RIVATON, A. 1993a. Photochemistry of poly(butyleneterephthalate): 1—Identification of the IR-absorbing photolysis products. *Polymer Degradation and Stability,* 41**,** 283-296.

RIVATON, A. 1993b. Photochemistry of poly(butyleneterephthalate): 2—Identification of the IR-absorbing photooxidation products. *Polymer Degradation and Stability,* 41**,** 297-310.

RIVATON, A., GARDETTE, J.-L., MAILHOT, B. & MORLAT-THERLAS, S. 2005. Basic Aspects of Polymer Degradation. *Macromolecular Symposia,* 225**,** 129-146.

RIVATON, A., SERRE, F. & GARDETTE, J. L. 1998. Oxidative and photooxidative degradations of PP/PBT blends. *Polymer Degradation and Stability,* 62**,** 127-143.

SADER, J. E., LARSON, I., MULVANEY, P. & WHITE, L. R. 1995. Method for the calibration of atomic force microscope cantilevers. *Review of Scientific Instruments,* 66**,** 3789-3798.

SAMMON, C., YARWOOD, J. & EVERALL, N. 2000. An FT–IR study of the effect of hydrolytic degradation on the structure of thin PET films. *Polymer Degradation and Stability,* 67**,** 149-158.

SANGALANG, A., BARTOLOME, L. & KIM, D. H. 2015. Generalized kinetic analysis of heterogeneous PET glycolysis: Nucleation-controlled depolymerization. *Polymer Degradation and Stability,* 115**,** 45-53.

SCHOOLENBERG, G. E. & MEIJER, H. D. F. 1991. Ultra-violet degradation of polypropylene: 2. Residual strength and failure mode in relation to the degraded surface layer. *Polymer,* 32**,** 438-444.

SCHOOLENBERG, G. E. & VINK, P. 1991. Ultra-violet degradation of polypropylene: 1. Degradation profile and thickness of the embrittled surface layer. *Polymer,* 32**,** 432-437.

SHAKESHEFF, K. M., DAVIES, M. C., DOMB, A., JACKSON, D. E., ROBERTS, C. J., TENDLER, S. J. B. & WILLIAMS, P. M. 1995. In Situ Atomic Force Microscopy Visualization of the Degradation of Melt-Crystallized Poly(sebacic anhydride). *Macromolecules,* 28**,** 1108-1114.

SOKOLOV, I., KALAPARTHI, V., KRESHCHUK, M. & DOKUKIN, M. E. 2012. On averaging force curves over heterogeneous surfaces in atomic force microscopy. *Ultramicroscopy,* 121**,** 16-24.

SPANGGAARD, H. & KREBS, F. C. 2004. A brief history of the development of organic and polymeric photovoltaics. *Solar Energy Materials and Solar Cells,* 83**,** 125-146.

STANDARDIZATION, I. O. F. 2012. ISO 25178-2: Geometrical Product Specifications (GPS) -- Surface Texture: Areal -- Part 2: Terms, Definitions and Surface Texture Parameters. International Organization for Standardization.

STANDARDIZATION, I. O. F. 2013. ISO 4892-2: Plastics - Methods of exposure to laboratory light sources - Part 2: Xenon-arc lamps.

STANDARDIZATION, I. O. F. 2014. ISO 2813: Paints and Varnishes -- Determination of Gloss Value at 20 Degrees, 60 Degrees and 85 Degrees. International Organization for Standardization.

STEPHENSON, C. V., MOSES, B. C. & WILCOX, W. S. 1961a. Ultraviolet irradiation of plastics. I. Degradation of physical properties. *Journal of Polymer Science,* 55**,** 451-464.

STEPHENSON, C. V., MOSES, B. C., BURKS, R. E., COBURN, W. C. & WILCOX, W. S. 1961b. Ultraviolet irradiation of plastics. II. Crosslinking and scission. *Journal of Polymer Science,* 55**,** 465-475.

STEPHENSON, C. V., LACEY, J. C. & WILCOX, W. S. 1961c. Ultraviolet irradiation of plastics III. Decomposition products and mechanisms. *Journal of Polymer Science,* 55**,** 477-488.

STEPHENSON, C. V. & WILCOX, W. S. 1963. Ultraviolet irradiation of plastics. IV. Further studies of environmental effects on films and fibers. *Journal of Polymer Science Part A: General Papers,* 1**,** 2741-2752.

TABANKIA, M. H. & GARDETTE, J.-L. 1986. Photo-chemical degradation of polybutyleneterephthalate: Part 1—Photo-oxidation and photolysis at long wavelengths. *Polymer Degradation and Stability,* 14**,** 351-365.

TABANKIA, M. H. & GARDETTE, J.-L. 1987. Photo-oxidation of block copoly(ether-ester) thermoplastic elastomers: Part 2—Origins of the photo-yellowing. *Polymer Degradation and Stability,* 19**,** 113-123.

TERSELIUS, B., GEDDE, U. W. & JANSSON, J. F. 1982. Structure and morphology of thermally oxidized high density polyethylene pipes. *Polymer Engineering & Science,* 22**,** 422-431.

VANLANDINGHAM, M., NGUYEN, T., BYRD, W. E. & MARTIN, J. 2001. On the use of the atomic force microscope to monitor physical degradation of polymeric coating surfaces. *Journal of Coatings Technology,* 73**,** 43-50.

VENKATACHALAM, S., NAYAK, S. G., LABDE, J. V., GHARAL, P. R., RAO, K. & KELKAR, A. K. 2012. Degradation and Recyclability of Poly (Ethylene Terephthalate). *Edited by Hosam El-Din M. Saleh***,** 107.

VINK, H. 1963. Degradation of some polymers in aqueous solutions. *Die Makromolekulare Chemie,* 67**,** 105-123.

WANG, W., TANIGUCHI, A., FUKUHARA, M. & OKADA, T. 1998. Surface nature of UV deterioration in properties of solid poly(ethylene terephthalate). *Journal of Applied Polymer Science,* 67**,** 705-714.

WANG, W., TANIGUCHI, A., FUKUHARA, M. & OKADA, T. 1999. Two-step photodegradation process of poly(ethylene terephthalate). *Journal of Applied Polymer Science,* 74**,** 306-310.

WARD, I. M. & WILDING, M. A. 1977. Infra-red and Raman spectra of poly(m-methylene terephthalate) polymers. *Polymer,* 18**,** 327-335.

WHINFIELD, J. R. 1946. Chemistry of 'terylene'. *Nature,* 158**,** 930-931.

WHITE, J. R. 2009. A Critical Assessment of Techniques for Monitoring Polymer Photodegradation

Service Life Prediction of Polymeric Materials. *In:* MARTIN, J. W., RYNTZ, R. A., CHIN, J. & DICKIE, R. A. (eds.). Springer US.

WIEGMANN, J. 1980. The chemistry of silica. Solubility, polymerization, colloid and surface properties, and biochemistry. Von RALPH K. ILER. New York/Chichester/Brisbane/Toronto: John Wiley & Sons 1979. XXIV, 866 S., Lwd., £ 39.50. *Acta Polymerica,* 31**,** 406-406.

WILES, D. M. 1973. The effect of light on some commercially important polymers. *Polymer Engineering & Science,* 13**,** 74-77.

WILES, D. M. & CARLSSON, D. J. 1980. Photostabilisation mechanisms in polymers: A review. *Polymer Degradation and Stability,* 3**,** 61-72.

YADAV, P., VERMA, U., SHRIVASTAVA, A. K., SEMWAL, R. P., YADAV, B. S. & CHAUHAN, R. S. 2011. Tensile Properties of Photoexposed Poly(ethylene-terephthalate) Films. *Journal of Polymer Materials,* 28**,** 587-598.

YANG, J., XIA, Z., KONG, F. & MA, X. 2010. The effect of metal catalyst on the discoloration of poly(ethylene terephthalate) in thermo-oxidative degradation. *Polymer Degradation and Stability,* 95**,** 53-58.

ZHAO, H. & LI, R. K. Y. 2006. A study on the photo-degradation of zinc oxide (ZnO) filled polypropylene nanocomposites. *Polymer,* 47**,** 3207-3217.

ZHU, Z. & KELLEY, M. J. 2005. IR spectroscopic investigation of the effect of deep UV irradiation on PET films. *Polymer,* 46**,** 8883-8891.

ZWEIFEL, H. 1999. Stabilization of polymeric materials. *Annales de Chimie Science des Matériaux,* 24**,** 401-401.